Title
Studies on the Organometallic Reactivity of Gold(III)

Author
Wolf, William James

Publication Date
2016

Peer reviewed|Thesis/dissertation

Studies on the Organometallic Reactivity of Gold(III)

by

William Wolf

A Dissertation submitted in partial fulfillment of the

requirements for the degree of

Doctor of Philosophy

in

Chemistry

in the

Graduate Division

of the

University of California, Berkeley

Committee in charge:

Professor F. Dean Toste, Chair
Professor John F. Hartwig
Professor Wenjun Zhang

Spring 2016

Abstract

Studies on the Organometallic Reactivity of Gold(III)

by

William Wolf

Doctor of Philosophy in Chemistry

University of California, Berkeley

Prof. F. Dean Toste, Chair

The work contained in thesis represents our efforts towards a fundamental understanding of gold in the context of redox cycling. The use of late transition metals in catalysis typically relies on two or more readily accessible oxidation states for bond breaking and bond forming events. However, the heaviest coinage metal does not enjoy such a wealth of reactivity and has been comparatively unexplored.

Chapter 1 summarizes the research by our group and others in advancing the concept of redox active gold catalysis. Two strategies that differ on the use sacrificial oxidants to affect catalysis are described, as well as our efforts to improve on the performance of bimetallic gold catalysts through a ligand design approach. A brief survey of fundamental reactivity of Au(I) towards oxidative addition is also presented, to provide context for our studies as described in the subsequent chapters.

Chapter 2 describes our studies on the C(sp^2)–C(sp^2) reductive elimination of biaryls from Au(III). Low temperature NMR studies revealed and characterized an unexpectedly rapid process that is mechanistically distinct from previous studies on C(sp^3)–C(sp^3) reductive elimination from Au(III). In addition, our preliminary efforts towards the development of a gold-catalyzed biaryl cross-coupling were informed by these studies on reductive elimination.

Chapter 3 focuses on our investigations of a photochemical oxidative addition of CF_3I to Au(I) complexes. This type of transformation was initially described for the oxidation of phosphine-supported Au(I) alkyl complexes; however the use of phosphine-supported Au(I) aryl complexes allows for the isolation and characterization of organometallic Au(III) complexes containing the $–CF_3$ moiety. These complexes are also capable of C(sp^2)–CF_3 bond forming reductive elimination upon halide abstraction at low temperature and represent a unique class of compound in this regard.

Chapter 4 builds on the results from chapter 3 and focuses on the effects of halide ligands on the C(sp^2)–CF_3 reductive elimination from Au(III) at elevated temperature. A series of Au(III) complexes containing each member of the halide family (I, Br, Cl, and F) were prepared and the effects of these ancillary ligands on the selectivity of C(sp^2)–CF_3 vs. C(sp^2)–X (X = halide) elimination from Au(III) were characterized. The selectivity can be tuned by choice of halide ligand, and this phenomenon is attributed to increasing Au–X bond strengths which correlate with an increase in selectivity for C(sp^2)–CF_3 elimination.

Table of Contents

Acknowledgements

I wouldn't be writing this thing if it weren't for the generous support and encouragement from a great number of people. To everyone who has had a positive impact on my life: thank you.

I am grateful to Professor Dean Toste for giving me the opportunity to explore. The chemistry hardly ever went according to plan, but I know that my growth as a scientist has benefitted greatly because Dean gave me room to discover. I made plenty of mistakes and learned lots of lessons the hard way, but Dean was there when I needed his advice and he always trusted me and treated me as an equal and for that, I thank him. I must also thank Professors Andy Harned and John Ellis for letting me join their groups as an undergraduate and starting me along my path to graduate school. Andy gave me my first chance to try research, and I'm truly grateful for that opportunity. I'm grateful to John for showing me that chemistry is fun ("Think good thoughts about chemistry!") and for sparking my interest in the transition metals (gold counts!).

None of the work that I've done thus far would have been possible without Dr. Matt Winston, and I thank him for joining me to study gold chemistry. Matt was a phenomenal mentor and co-worker and I learned pretty much everything from him (I hope he learned a few things from me, too). He is also a wonderful dude, and I am particularly thankful for his friendship.

I am extremely grateful to my classmates (in alphabetical order) Dimitri Khrakovsky, Dillon Miles, Andrew Neel, and Jigar Patel for both their friendship and camaraderie over the past 5 years. We've had too many adventures to count (and I hope for many more), but I know that we always had good times together, both in and out of the lab, and I couldn't have asked for a better group of guys to learn with.

The Toste Group is a wild and crazy place and I have been lucky to work alongside a long list of exceptional people. In particular, I am grateful to the older members in the Toste group: Dr. Aaron Lackner, Dr. Yiming Wang, Dr. Miles Johnson, Professor Neal Mankad, and Dr. Jane Wang for showing me the ropes when I was young and eager and I didn't know any better. I should also thank them for enduring my lame jokes. I must also thank the more youthful members of the group: Mark Levin, Drew Samant, Rebecca Triano, Dave Kaphan, Cindy Hong, Richard Thornbury, John T. Lee, Suhong Kim, Patrick Bohan, and Alec Christian for making the 6th floor of Latimer a fun place to work (and play: sorry Neel!) and for all the fun times out on the town. I've also been lucky to get to know Drs. John Brantley, Hosea Nelson, Rake Wu, and Derek Dalton, and I thank them for their advice throughout the years. I am extraordinarily proud to be a member of the 2015 Chemistry League Championship Softball Team.

I am grateful to Professor Ken Raymond for letting me teach his X-ray crystallography course. It was an honor and a privilege to work and learn alongside one of the masters. I must also thank Dr. Antonio DiPasquale for showing me the practical art of crystallography.

I cannot begin to describe how fortunate I am to have such a great family and I extend my deepest thanks to them. To my mom and dad, Mary and Marty, my brothers, John and Kevin, my grandparents, my aunts and uncles, and my cousins: thank you all for your support and encouragement in every aspect of my life, from when I was just a little guy until now and into the future. I know that I couldn't have made it this far without you all, and I am proud to be on your team. I am also grateful to Louise, Red, and Rosie for being steadfast companions.

Chapter 1: Studies Towards the Development of Redox Active Gold Catalysis

Abstract: Gold catalysis has been largely characterized by the Lewis acidity of the metal. The large majority of transformations are mediated by the Au(I) cation as the metal possesses a high oxidation potential that prevents it from undergoing facile redox cycling. However, the use of sacrificial oxidants can overcome this inherent limitation and provide access to a new manifold of redox-active gold catalysis. Described herein are the current methods available in this realm of gold catalysis and our efforts towards designing new, efficient gold complexes for this type of catalysis.

Introduction: Transition metal catalysis is an invaluable synthetic tool for the construction of a broad variety of compounds ranging from small-molecules such as therapeutics and pesticides to macromolecules like synthetic polymers. The development and maturation of transition metal catalysis has relied on the study of the fundamental steps (oxidative addition, migratory insertion, transmetallation, and reductive elimination) involved in such transformations. The metal center must undergo a specific sequence of these steps and it must do so with high fidelity and selectivity for the desired products in order to ensure a highly efficient process. The study of the factors that affect these elementary organometallic steps is critical in designing and improving new metal-catalyzed transformations. An example of the palladium-catalyzed Suzuki-Miyaura reaction is shown in Figure 1.1, where several fundamental organometallic reactions must occur in the proper sequence in order to furnish the desired organic product in high yield and efficiency.

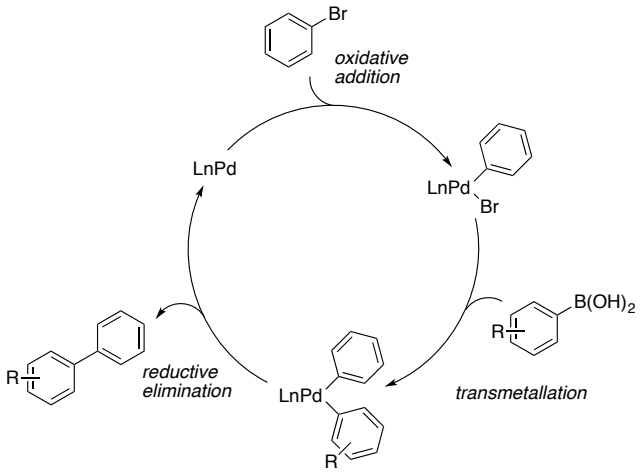

Figure 1.1. Generally accepted mechanism of the palladium-catalyzed Suzuki-Miyaura coupling composed of oxidative addition, transmetallation, and reductive elimination steps.

The synthetic utility of the Suzuki-Miyaura coupling, and that of many other metal-catalyzed transformations, lies in its efficiency and breadth of scope. Extensive studies on the effects of ligands, solvents, bases, organoboron reagents, and aryl halides have turned this reaction into one of the mostly widely used and powerful methods in modern organic chemistry.[1,2] Similar progress has also been made in other catalytic methods, including olefin metathesis,[3,4] asymmetric hydrogenation,[5,6] asymmetric oxidation,[7] and the Buchwald-Hartwig amination.[8–10] The investigation of the basic organometallic steps involved in each of these

reactions is a powerful means of development that has driven the growth of these methods, and others, to the ubiquitous and powerful tools that they are today.

In contrast to the wealth of well-establish organometallic chemistry of the other late metals, gold and its compounds are relatively unexplored. The recent interest in homogeneous gold catalysis has led to a number of unique transformations, but the primary mode of reactivity exploits the carbophilic Lewis acidity of the metal center. The metal catalyst activates a C–C π-bond towards nucleophilic attack, enabling a variety of rearrangements and cyclizations (Figure **1.2**). The gold center is almost invariably active in the +1 oxidation state, which stands in contrast to the established redox chemistry of other late metals; particularly the group 10 metals. While several early reports explored the reductive elimination[11–16] and oxidative addition[13,17,18] of gold complexes, these steps have rarely found use in catalytic transformations.

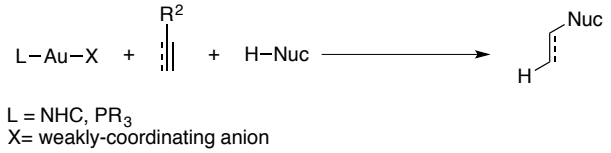

Figure 1.2. Activation of π-bonds towards nucleophilic attack.

Discussion: One of the main differences between gold and other late metals are the relativistic effects that control the electronic structure of the metal and its behavior towards redox events. The large nuclear charge of gold (Z = 79) causes significant Coulombic attraction between the nucleus and the core *s*- and *p*-electrons. As a result, a significant contraction of these orbitals occurs which effectively shields the valence d-orbitals from Z, which in turn causes them to expand, both energetically and spatially, allowing extensive mixing of the 6*s* and 6*p* with the 5*d* orbitals.[19] Gold has the highest electronegativity of the transition metals, and its ionization potential (9.225 eV) and electron affinity (2.308 eV) are consistent with a highly contracted 6*s* orbital. Gold metal and its complexes are easily reduced, which has acted to limit its study as a redox active metal center.

Nevertheless, progress has been made in the area of redox active gold catalysis using two mechanistically distinct strategies. The first uses a sacrificial oxidant to achieve the redox cycling of the gold center. The second approach is analogous to the Suzuki-Miyaura cross-coupling and relies on the substrates to act as oxidants. These methods represent an important bridge between the known π-acidity of gold and its comparatively unexplored redox chemistry. Early efforts used Selectfluor® as a stoichiometric oxidant with the goal of extending the scope of a gold-catalyzed rearrangement/iodination of propargylic acetates to include a fluorine electrophile, as shown in Figure 1.3.

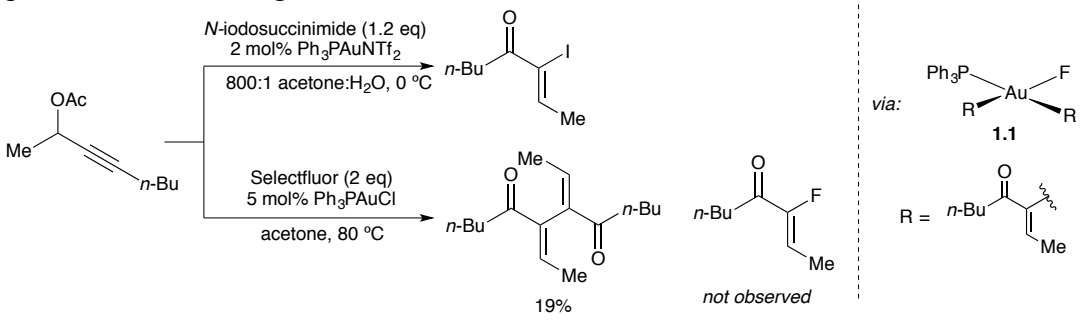

Figure 1.3. Evolution of a gold-catalyzed halogenation using Selectfluor leads to oxidative dimerization.

The dimeric product was proposed to be the product of an oxidative coupling.[20] The authors hypothesized that Selectfluor was serving as an oxidant to access a Au(III) intermediate

1.1. In the presence of arylboronic acids, the dimerization is minimized and instead, α-arylated enones are formed (eq 1.1) as the boronic acid intercepts a Au(III) fluoride leading to the arylated product.[21] This type of gold-catalyzed oxidative functionalization was expanded to include an intramolecular aminoarylation and an intermolecular alkoxyarylation of monosubstituted alkenes (eq 1.2).[22–24] Our group proposed an alternative mechanism for the key C–C bond forming step and introduced a bimetallic gold catalyst (dppm(AuBr)$_2$; dppm = 1,1-bis-(diphenylphosphino)methane) that showed improved reactivity (eq 1.3).

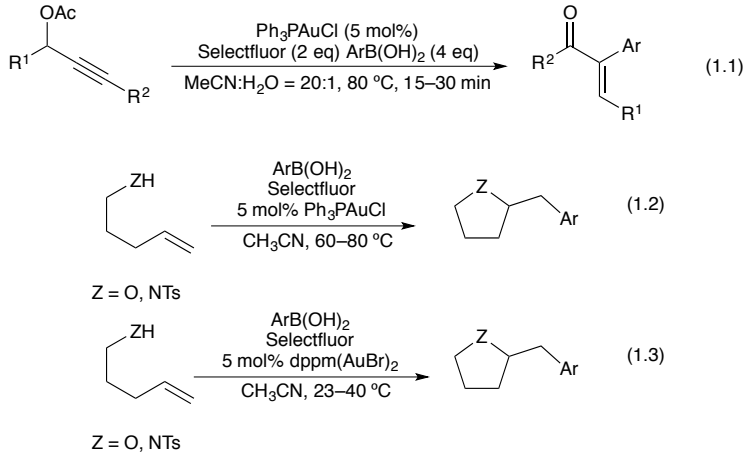

Mechanistic studies suggested that a unique step was involved in the key C–C bond forming event: a bimolecular reductive elimination that proceeds through the transition state shown in Figure 1.4.[24] A putative Au(III)–F intermediate attacks the boronic acid as it transfers the aryl group directly to the α-carbon of the alkyl Au(III) species **1.2**.

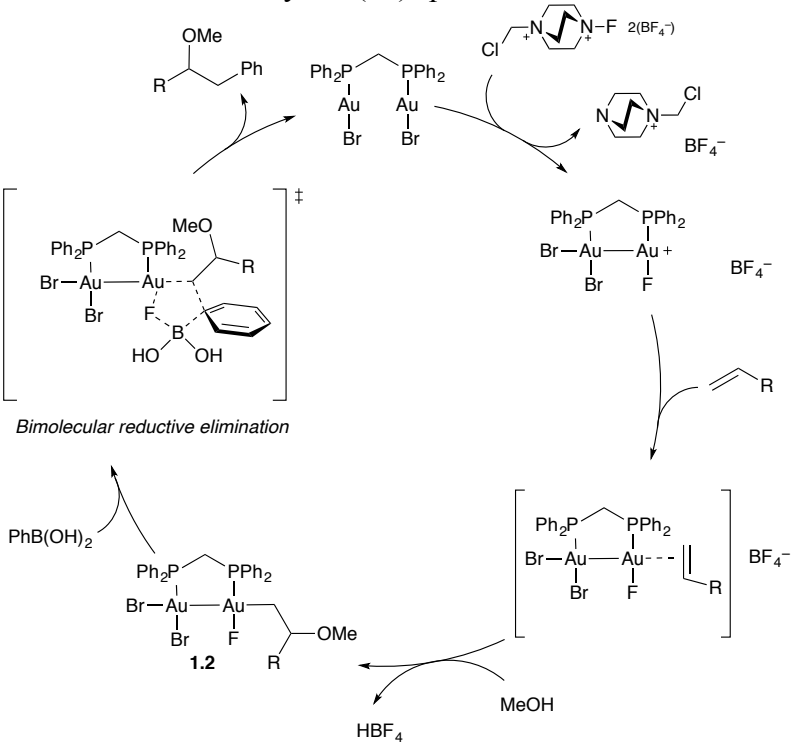

Figure 1.4. Proposed mechanism of gold-catalyzed alkoxyarylation of olefins using a bimetallic catalyst.

The use of a bimetallic catalyst was initially hypothesized to stabilize the oxidized Au(III) center, *via* electron donation from the adjacent Au(I) center. Computations then

suggested that an oxidation to a metal–metal bonded Au(II)–Au(II) species was energetically more favorable, and provided further support for a bimetallic reductive elimination pathway as the means of C–C bond formation.[25]

The scope of this transformation was extended to an intermolecular alkoxyarylation of unactivated olefins under similar conditions (eq 1.4).[23] Alcoholic cosolvents were used in attempt to improve the solubility of aryl boronic acids, but they were instead incorporated into the products. In addition to boronic acids, aryl silanes[26,27] (eq 1.5) are also competent nucleophiles; the strength of the Si–F bond is presumed to be a thermodynamic driving force.

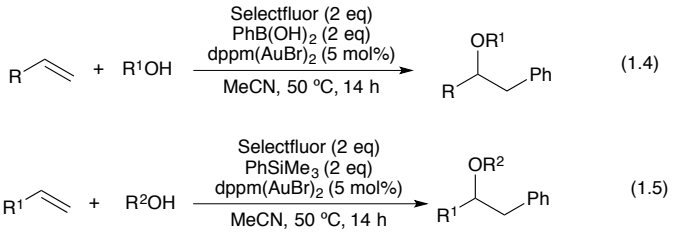

The bimetallic system provided a platform for further optimization, and our initial efforts were focused on improving the performance of the bimetallic catalysts. To exploit the purported gold-gold interactions, a bis(phosphino)amine was chosen as a more rigid scaffold for two gold centers.[28] These complexes proved to be competent catalysts for the alkoxyarylation (Figure 1.5). The reaction profile for the alkoxyarylation of monosubstituted alkene **1.3** using the bimetallic complex **1.4** to give the ether **1.6** is shown in Figure 1.5.

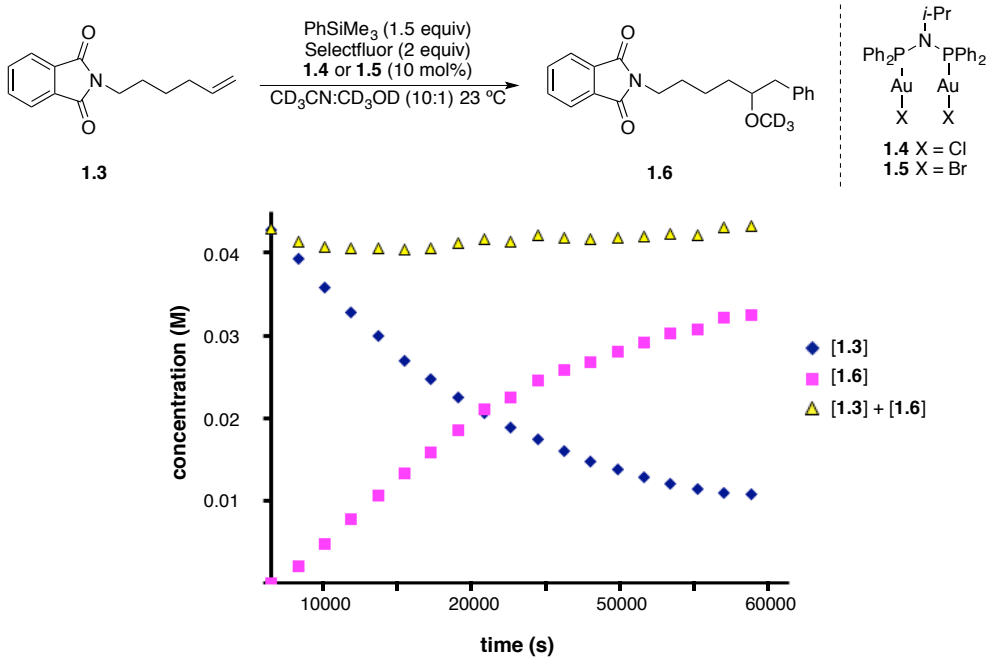

Figure 1.5. Reaction of **1.3** with $PhSiMe_3$ and CD_3OD in the presence of **1.4** and Selectfluor® under N_2 where ◆ = [**1.3**], ■ = [**1.6**] and Δ = [**1.3**] + [**1.6**].

We attempted to further modify this ligand platform by using more electron-rich alkylphosphines. We hypothesized that a more electron-rich gold center may be more readily oxidized by other, milder oxidants to overcome limitations of substrate compatibility and

solubility encountered with Selectfluor®. To this end, ligand **1.7** was prepared and metallated yielding **1.8** (Figure 1.6).

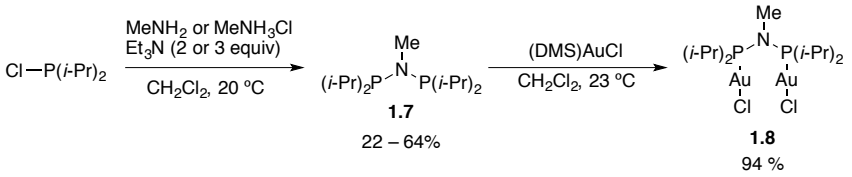

Figure 1.6. Preparation of a bimetallic bis(alkylphosphino)amine gold complex.

Unfortunately, **1.8** readily decomposed to gold nanoparticles under the reaction conditions, and low yields of **1.6** were observed (20%). We believe that **1.8** was more susceptible to oxidative degradation than **1.4** or **1.5** due to the increased electron-donating ability of the alkylphosphine moiety. Additionally, Selectfluor proved to be the only viable oxidant for this transformation using these bimetallic complexes as precatalysts.

A chiral bis(alkylphosphino)amine ligand was also prepared in an attempt to render the three-component coupling reactions (eq 1.5) enantioselective. We were inspired by the DuPhos ligand and incorporated a chiral phospholane element using **1.9** into the bis(phosphino)amine **1.10** as shown in Figure 1.7.

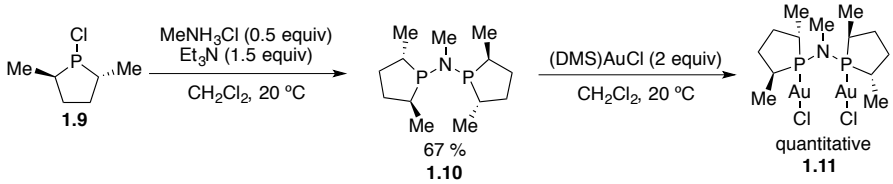

Figure 1.7. Prepartion of chiral bimetallic bis(phosphino)amine gold complex.

Metallation of **1.10** afforded the chiral gold complex **1.11** in quantitative yield: the absolute configuration of the ligand was confirmed using X-ray diffraction. However, given the poor performance of **1.8**, it was unsurprising that **1.11** was also prone to degradation under the reaction conditions and required higher catalyst loading (15 mol%) to give low yields of **1.6** (30% within 12 h). For the alkoxyarylation of **1.3** (eq 1.5), using **1.11** as a precatalyst gave **1.6** with a poor, but measurable level of enantioselectivity (12% ee). In spite of this, the bis(phosphino)amine ligand platform was promising when compared to other chiral bidentate phosphines (BINAP, SEGPhos, BINAPHANE) which only gave racemic product. We attempted to prepare the phenyl-substituted bis(phospholano)amine **1.12** to increase the steric bulk of the chiral element but were unsuccessful (eq 1.6).

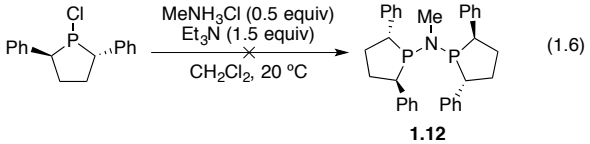

While the bimetallic bis(phosphino)amine system offers a slight improvement over the dppm system, it offers some validation to the hypothesis that a more rigid ligand could promote bimetallic cooperativity in these types of gold-catalyzed functionalizations.

In addition to olefin functionalization, several other reactions have been developed that mimic the venerable palladium-catalyzed cross-coupling methods. Lloyd-Jones recently disclosed a gold-catalyzed coupling of aryl silanes and arenes using $PhI(OAc)_2$ as the oxidant (eq 1.6).[29,30] This transformation relies on the electrophilicity of Au(III) to activate the arene

coupling partners and to drive the product forming reductive elimination. Mechanistic studies showed that the catalyst resting state is an aryl aurate $[Au(Ar)X_4]^-$ (X = halide, sulfate, alkoxide), and that a precatalyst activiation step was required when phosphine-ligated Au(I) precatalysts were used. Under the oxidizing conditions of the reaction, the phosphine ligands were oxidized to liberate the active Au(III) catalyst.

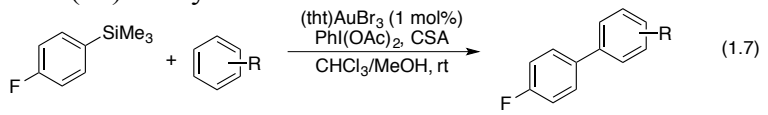

(1.7)

Another cross-coupling method was developed by Larrosa that operates *via* a double C–H functionalization.[31,32] Electron-poor and electron-rich arenes could be selectively coupled by exploiting two selective C–H functionalization events. The selectivity was imparted by the oxidation state of the gold catalyst: the Au(I) state functionalized the electron-poor arene and the Au(III) state functionalized the electron-rich arene, leading to selective cross-coupling following reductive elimination. An example is shown in Figure 1.8; the additive DMSO was proposed to solubilize the silver salt. This scope of this method was limited to two extremes of the electronic spectrum: the coupling partners must be highly electron-poor or electron-rich.

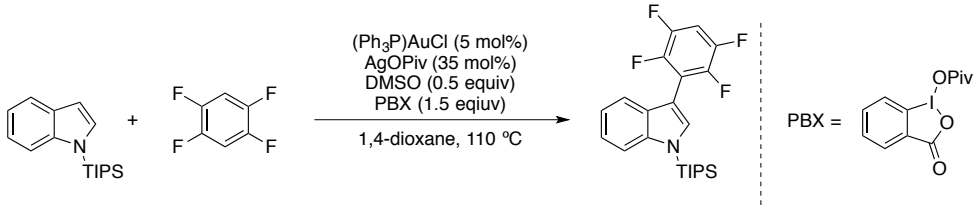

Figure 1.8. Gold catalyzed dual C–H functionalization to achieve cross-coupling of electronically dissimilar arenes.

In addition to the methods that require a sacrificial oxidant, there are also several examples of oxidant-free couplings. Our group reported this type of catalysis to couple aryl boronic acids with allyl bromide using **1.4** as a precatalyst (eq 1.8).[33] The bimetallic complexes offered superior performance compared to monometallic complexes, and the proposed mechanism proceeds through a Au(II)–Au(II) intermediate that was formed upon oxidative addition of a bimetallic complex to allyl bromide. This method is highly selective for the coupling of allyl bromide and tolerates aryl halides, offering an approach that is orthogonal to palladium catalysis.

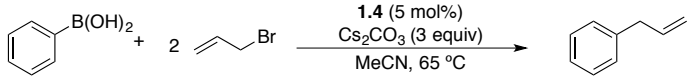

(1.8)

Shi has also developed a gold-catalyzed arylation of alkynes using aryl diazonium salts. There are also several examples of dual gold-catalyzed transformations that use photoredox catalysts to promote the formation of aryl radicals to oxidize the gold center: these transformations are briefly summarized in Figure 1.9.[34–37] The mechanism was monitored by time resolved FT-IR spectroscopy which supported a mechanism involving oxidation of the Au(I) catalyst *via* aryl radicals generated from photoredox catalyzed decomposition of the aryl diazonium coupling partners.[38]

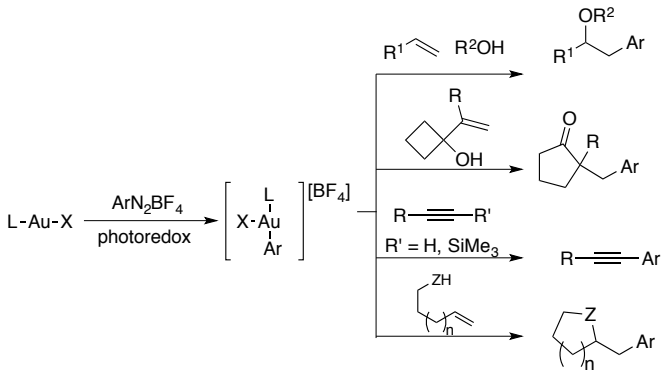

Figure 1.9. Photoredox/gold dual catalysis for cross-coupling.

An oxidant-free gold-catalyzed halogen exchange was recently reported by Ribas and co-workers, shown in eq 1.9.[39] In the presence of either sodium iodide or sodium phenoxide salts, either halogen exchange or C(sp)^2–O coupling can be achieved. Computations supported a mechanism involving oxidative addition into the aryl bromide and reductive elimination from a Au(III) intermediate.

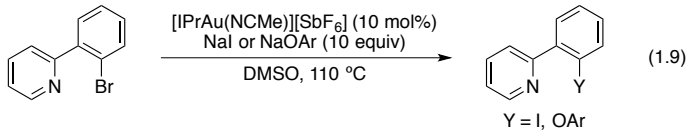

(1.9)

Though these catalytic transformations are proposed to proceed though oxidative addition, this elementary step remains a very rare transformation for Au(I), unlike other late metals.[40] Kochi's studies on the gold-catalyzed coupling of alkyl iodides implicated oxidative addition as a key step to access Au(III) intermediates. Linear, two-coordinate Au(I) complexes underwent oxidative addition of alkyl iodides to give the corresponding Au(III) complexes (Figure 1.9).[13,14,18] Oxidative addition was also achieved with the dialkylaurates (Figure 1.10, bottom).

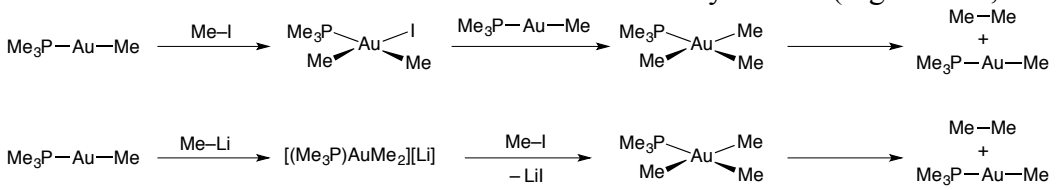

Figure 1.10. Oxidative addition of methyl iodide to neutral phosphine-supported Au(I) (top) or anionic aurates (bottom).

The N-heterocyclic carbene (NHC) supported Au(I) aryls displayed similar reactivity. When (IMes)AuPh was heated with methyl iodide, a mixture of biphenyl and toluene was produced, presumably as a result of oxidative addition and reductive elimination (eq 1.10).[41] Similar reactivity was observed when methyl triflate was used as the electrophile, as shown in eq 1.11. Computations supported an S_N2 mechanism of oxidative addition, similar to that observed for Au(I) alkyls. In comparison, when phenyl iodide was heated with (IMes)AuPh, biphenyl was the sole organic product, but the computed barriers for a concerted oxidative addition of Ph–I to Au(I) were prohibitively high ($\Delta G^{\ddagger}$ = 40.4 kcal/mol) and the participation of gold nanoparticles was not discounted as an explanation for the formation of biphenyl in eq 1.12. A computational study by Echavarren[42] reached the same conclusion and suggested that the high kinetic barrier for oxidative addition to two-coordinate gold complexes is a result of deforming the linear coordination geometry. Despite this, there are a number of examples of oxidative addition to Au(I) centers.

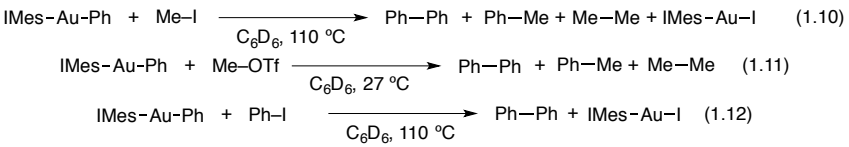

Several examples exist of oxidative addition of chelating aryl iodides and bromides to Au(I), as shown in Figure 1.11.[43] Aryl iodides were more reactive than aryl bromides, and chlorides were unreactive, even after prolonged heating. The use of chelating phosphines to promote oxidative addition is a strategy that was initially used for activating Si–Si and Sn–Sn bonds.

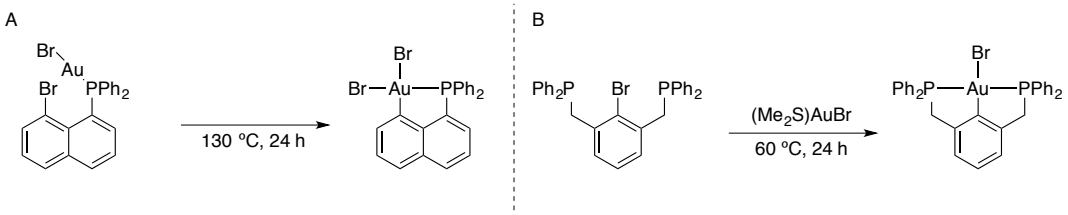

Figure 1.11. A) Insertion of Au(I) into a C–Br bond using a chelating phosphine. B) insertion of Au(I) into a C–Br bond using a chelating bisphosphine.

At low temperatures (–80 ºC) monocoordinate Au(I) cations were readily oxidized by disilanes, both inter- and intramolecularly. The phosphine ligands **1.13** or **1.15** were chosen so that the gold center would be in direct proximity to the relatively weak Si–Si bond. This proved effective and stable, cyclometallated Au(III) silyl cations **1.14** and **1.16** were synthesized at low temperature (–80 ºC; eq 1.13 and eq 1.14). However, the coordination of a disilane to the gold center *via* phosphine coordination was not required to access this type of reactivity, as the intermolecular insertion of $(Cy_3P)AuCl$ or $(Ph_3P)AuCl$ into a Si–Si bond was also observed using low temperature NMR techniques (eq 1.15). This process is extremely rapid at low temperature, and no intermediate species were observed. The disilyl cation is thermally unstable and decomposes upon warming.

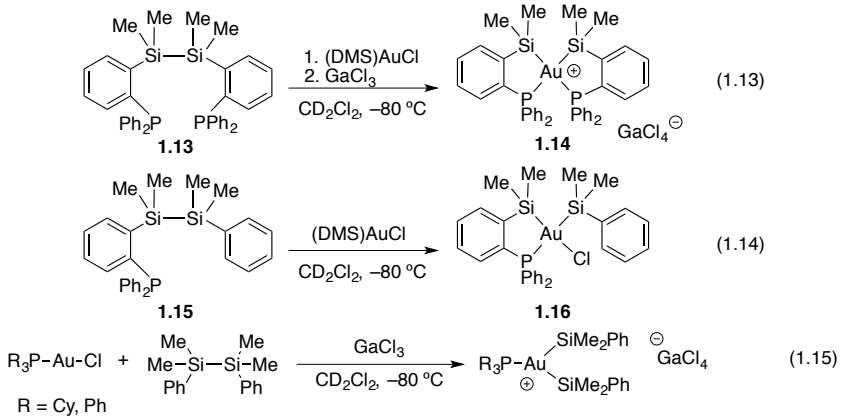

These examples are part of a growing number of oxidative addition at Au(I) centers. Bourissou also recently showed that a bent Au(I) cation or into the C–I bond of aryl iodides,[44] a key step in many cross-coupling reactions. The use of bis(phosphino)carborane ligand was crucial for accessing a strained geometry at the gold center given that Au(I) strongly prefers a linear geometry.[45] The geometry of the metal center destabilizes the M–L antibonding orbital of the metal center and makes it more available to backbond to the C–C or C–I σ bond.[46] A similar

effect has been observed in palladium systems, where bent L_2Pd complexes exhibit faster rates of oxidative addition than their linear analogues.[47–49]

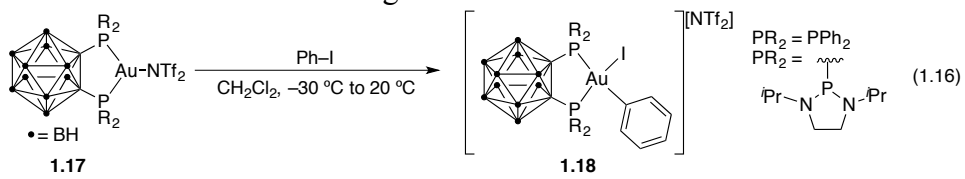

(1.16)

The carborane-based phosphines are unique in that they are able to enforce a bent geometry on the metal center of **1.17**, which is unlike other commonly employed chelating bisphosphines like dppf[50,51] or BINAP.[52,53] This transformation is also an important conceptual advance as it bridges the gap between traditional gold coordination chemistry and the elements of catalyst design that are commonly employed in palladium catalysis i.e. that changing the coordination geometry of the metal center can enable or improve the rate of oxidative addition.

Gold(I) is also capable of insertion into highly strained C–C bonds. Several other transition metals have been shown to insert into biphenylene, and the overall transformation is thermodynamically favorable, since two strong M–C bonds are formed and a weak C–C bond is broken in addition to the relief of the strain of the carbocycle.[54,55] The cation $[IPrAu][SbF_6]$ readily inserted in the C–C bond of biphenylene[56] and the resulting Au(III) cation **1.18** was a highly active Lewis acid catalyst for Mukaiyama aldol reactions and Diels-Alder cycloadditions, shown in Figure 1.12. Interestingly, the oxidative addition of biphenylene to Au(I) was not predicated on accessing a bent geometry at the gold center.

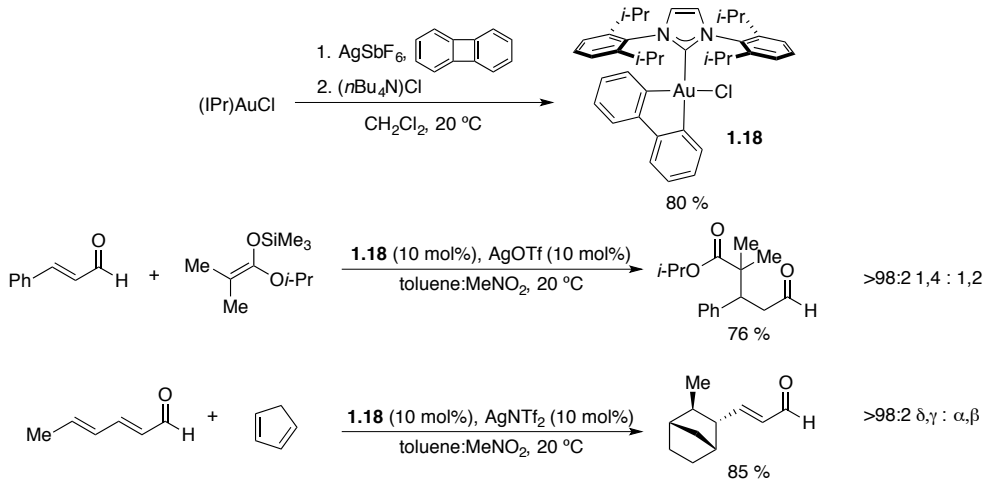

Figure 1.12. Oxidative addition of biphenylene to $[(IPr)Au][SbF_6]$ and Lewis acid catalysis of the resulting Au(III) cation.

Abstraction of the chloride from **1.18** generated a catalyst that activated conjugate aldehydes towards highly selective conjugate additions and Diels-Alder cycloadditions. The 'hard' Lewis acidity of the Au(III) cation was proposed to activate the carbonyl *via* coordination to the oxygen. The IPr ligand defined and binding pocket and provided steric shielding of the carbonyl, preventing 1,2 addition or α,β cycloadditions.

In comparison, Bourissou's bent Au(I) complex was also capable of inserting into the strained C–C bond of biphenylene or benzocyclobutanone, as shown in Figure 1.13.[57]

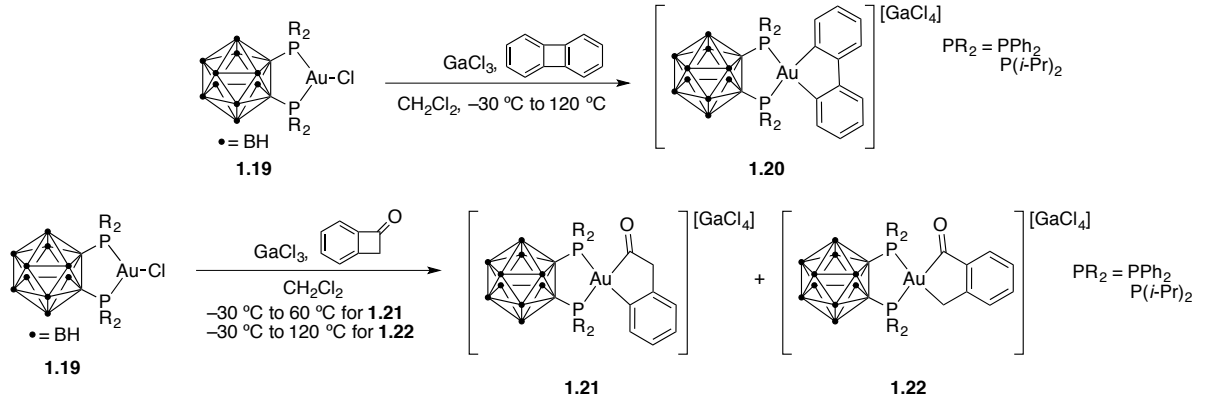

Figure 1.13. Insertion of a bent Au(I) cation into the C–C bonds of biphenylene (top) and benzocyclobutanone (bottom).

The insertion of the bent Au(I) cation into benzocyclobutanone gave **1.21** as the kinetic product, and further heating gave the isomer **1.22**. The reductive elimination of the benzocyclobutanone C–C(O) bond from **1.21** also provided the first direct evidence of this type of elimination from Au(III). Computations suggested concerted mechanisms for oxidative addition in both cases, and the Au(III) acyl complexes are members of a rare class of coordination compound.

Conclusion: Homogeneous gold catalysis has been dominated by the Lewis acidity of the metal center in its +1 oxidation state, and while numerous valuable transformations have been discovered, new reactivity that exploits the redox activity of the metal has only recently been explored. Several new synthetic methods have been reported that rely on a redox-active gold center, and studies of the fundamental reactivity of gold have also shown a variety of transformations, supporting the hypothesis that new synthetic transformations may be accessible using redox-active gold catalysis. However, a better understanding of the factors that control and affect these steps is needed to continue to improve these existing methods and to inform the design of new methods. The work summarized in this thesis presents our studies on the organometallic reactivity of Au(III) as it relates to catalysis. In particular both reductive elimination and oxidative addition have been examined.

Experimental

General Considerations

All starting materials were purchased from commercial suppliers and used as received. Glassware was dried in an oven at 150 °C overnight prior to use. Solvents were passed through a column of alumina under an argon atmosphere prior to use. All air-sensitive manipulations were carried out using a double-manifold vacuum line or under an inert nitrogen atmosphere inside a Vacuum/Atmospheres Corp. glovebox. TLC analysis was carried out on Merck silica gel 60 F254 TLC plates. Column chromatography was performed using Merck 60 silica gel (32-63 μm). NMR spectra were collected using Bruker AVQ-400, DRX-500, AV-500, or AV-600 spectrometers referenced to residual solvent peaks. Mass-spectrometry was carried out by the QB3/Chemistry Mass Spectrometry facility operated by the College of Chemistry, University of California, Berkeley. Elemental analyses were performed by the Microanalytical Facility operated by the College of Chemistry, University of California, Berkeley. X-ray crystallographic data were collected on a Bruker SMART APEX platform using MoK/α radiation. HPLC

analyses were performed on a Shimadzu VP series Chiral HPLC using a CHIRALPAK IA column.

General Procedure for kinetic experiments

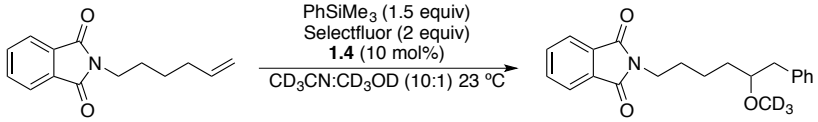

1.3 **1.6**

Kinetic experiments were performed using NMR techniques using a Bruker AV-600 spectrometer and a reported rate constant represents an individual experiment. In the glovebox, alkene **1.3** (8 mg, 0.036 mmol), Selectfluor® (26 mg, 0.072 mmol), phenyltrimethylsilane (9 mg, 0.056 mmol), 1,3-dinitrobenzene (internal standard) (7 mg, 0.043 mmol), and 10 mol% catalyst (**1.4**) were weighed into a 1 dram vial. To this mixture was added CD_3OD (16 μL, 0.36 mmol) and CD_3CN (0.7 mL). The resulting solution was transferred to a J. Young tube equipped with a sealed glass capillary containing a 0.1 M $OPPh_3$ solution in CD_3CN and sealed with a Teflon stopcock and monitored at ambient temperature (23 °C) for 20 h.

Synthesis of bis(arylphosphino)amine complexes

The ligand *i*-PrN(PPh_2)$_2$ was prepared according to literature procedures.[58] (2*S*,5*S*)-1-chloro-2,5-dimethylphospholane **1.9** was prepared using the methods reported by Burk[59] and Börner[60,61] and (2*S*,5*S*)-1-chloro-2,5-diphenylphospholane was prepared using the methods of Toffano[62] and Fox.[63]

Synthesis of bis(alkylphosphino)amine ligands and bimetallic gold complexes

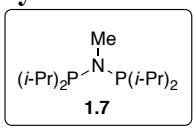

1.7

A 10-mL Schlenk bomb equipped with a magnetic stirring bar was charged with P(*i*Pr)$_2$Cl (0.2 mL, 1.25 mmol), Et_3N (0.18 mL, 2.5 mmol) and DCM (3 mL) in the glovebox. To this solution was added $MeNH_2$ in THF (2.0 M, 0.6 mL, 1.2 mmol) dropwise to afford a cloudy, colorless solution. The reaction mixture was then stirred for 20 h at ambient temperature, then concentrated and extracted with Et_2O (7 mL). The ether solution was passed through three sequential basic alumina plugs and then concentrated to afford **1.7** as a clear, colorless oil (70 mg, 22%). ^{1}H and ^{31}P NMR data match those reported in the literature.[64] ^{1}H NMR (400 MHz, CD_2Cl_2): δ 2.66 (m, 3H), 1.96 (sept, *J* = 7.2 Hz, 4H), 1.15 – 1.04 (m, 24H) ^{31}P NMR (162 MHz, CD_2Cl_2): δ 92.02.

In the glovebox, a 20-mL scintillation vial equipped with a magnetic stirring bar was charged with $MeNH_2$•HCl (35.2 mg, 0.521 mmol) and Et_3N (0.23 mL, 1.68 mmol) in DCM (3 mL). To this solution was added neat P(*i*Pr)$_2$Cl (0.17 mL, 1.1 mmol). The reaction mixture was stirred for 20 h at ambient temperature, then concentrated and extracted with Et_2O (7 mL). The ether solution was passed through three sequential basic alumina plugs and then concentrated to afford **1.7** as a clear, colorless oil (88mg, 64%).

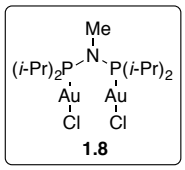

1.8

In the glovebox, **1.7** (30.3 mg, 0.115 mmol) and (DMS)AuCl (64.0 mg, 0.217 mmol) were placed in a 20-mL scintillation vial equipped with a magnetic stirring bar. DCM (7 mL) was added and the reaction was stirred for 30 min and then filtered through a plug of basic alumina and concentrated *in vacuo* to afford complex **1.8** as a white powder (78 mg, 93%). Crystals suitable for X-ray diffraction were grown by the diffusion of Et_2O vapors into a concentrated THF solution. ^{1}H

NMR (400 MHz, CD_2Cl_2): δ 2.91 (t, J = 6.4, 3H), 2.58 – 2.49 (m, 4H), 1.42 – 1.32 (m, 24H). ^{13}C NMR (125 MHz, CD_2Cl_2): δ 28.616 (t, J = 16.25 Hz), 19.246, 18.916 (t, J = 3.25 Hz). ^{31}P NMR (162 MHz, CD_2Cl_2): δ 117.56. Anal. Calcd for $C_{13}H_{31}NP_2Au_2Cl_2$: C, 21.44; H, 4.29; N, 1.92. Found: C, 21.42; H, 4.30; N, 1.83.

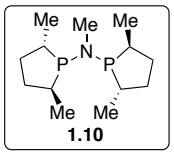

1.10

In the glovebox, chlorophospholane **1.9** (162 mg, 1.08 mmol) was weighed into a 20-mL scintillation vial, dissolved in CH_2Cl_2 (1 mL), and added to a second 20-mL scintillation vial containing a suspension of $MeNH_2$•HCl (36 mg, 0.54 mmol) and Et_3N (0.22 mL, 1.68 mmol) in CH_2Cl_2 (5 mL). The resulting mixture was magnetically stirred at ambient temperature for 20 h. The solvent was removed *in vacuo*, and the remaining white solid was extracted with Et_2O (2 x 5 mL). The ether solution was passed through three sequential basic alumina plugs and concentrated to afford **1.10** as a clear, colorless oil (93.4 mg, 67 %). The absolute configuration of the ligand was confirmed using X-ray diffraction of the corresponding gold complex **1.11**. ^1H NMR (400 MHz, CD_2Cl_2): δ 2.71 (m, 3H), 2.44 – 2.42 (m, 2H), 2.14 – 2.09 (m, 2H), 2.04 – 1.94 (m, 2H), 1.79 – 1.66 (m, 2H), 1.55 – 1.44 (m, 2H), 1.27 (q, J = 12 Hz, 6H), 1.18 (q, J = 8.4 Hz, 6H), 1.11 – 0.99 (m, 2H) ppm. ^{13}C NMR (150 MHz, CD_2Cl_2): δ 38.68 (t, J = 4.5 Hz), 37.93, 37.75 (t, J = 4.5 Hz), 35.55, 35.41, 18.60 (t, J = 18 Hz), 13.67 ppm. ^{31}P NMR (243 MHz, CD_2Cl_2): δ 97.51 ppm. HRMS (ESI) *m/z* calcd for $C_{13}H_{28}N_1P_2$ $[M + H]^+$ 260.1692; found 260.1687.

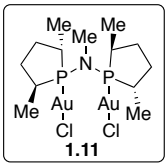

1.11

In the glovebox, a 20-mL scintillation vial equipped with a magnetic stirring bar was charged with ligand **1.10** (30.2 mg, 0.12 mmol) and (DMS)AuCl (68.4 mg, 0.23 mmol). Dichloromethane (2 mL) was added and the resulting solution was stirred for 1 h at ambient temperature. The reaction mixture was then filtered through a glass fiber filter and concentrated to give **1.11** as a white powder in quantitative yield (84 mg). Crystals suitable for X-ray diffraction were grown by the diffusion of Et_2O vapors into a saturated solution of **1.11** in THF at ambient temperature. The absolute configuration of the ligand was determined by anomalous X-ray scattering. ^1H NMR (600 MHz, CD_2Cl_2) δ 3.04 – 2.85 (m, 3H), 2.89 – 2.79 (m, 2H), 2.61 (m, 2H), 2.36 – 2.16 (m, 4H), 1.53 – 1.41 (m, 3H), 1.39 – 1.33 (m, 6H). ^{13}C NMR (150 MHz, CD_2Cl_2): δ 15.45, 18.87, 32.13. 34.20 (t, J = 18.6 Hz), 35.35, 37.14, 39.48 (t, J = 16.5 Hz). ^{31}P NMR (243 MHz, CD_2Cl_2): δ 119.72. Anal Calcd for for $C_{13}H_{27}NP_2Au_2Cl_2$: C, 21.56; H, 3.76; N, 1.93. Found: C, 22.94; H, 3.80; N, 1.85.

References

(1) Miyaura, N.; Suzuki, A. *Chem. Rev.* **1995**, *95* (7), 2457–2483.
(2) Suzuki, A. *Angew. Chem. Int. Ed.* **2011**, *50* (30), 6722–6737.
(3) Trnka, T. M.; Grubbs, R. H. *Acc. Chem. Res.* **2001**, *34* (1), 18–29.
(4) Schrock, R. R.; Hoveyda, A. H. *Angew. Chem. Int. Ed.* **2003**, *42* (38), 4592–4633.
(5) Noyori, R.; Ohkuma, T. *Angew. Chem. Int. Ed.* **2001**, *40* (1), 40–73.
(6) Noyori, R. *Angew. Chem. Int. Ed.* **2013**, *52* (1), 79–92.
(7) Kolb, H. C.; VanNieuwenhze, M. S.; Sharpless, K. B. *Chem. Rev.* **1994**, *94* (8), 2483–2547.
(8) Hartwig, J. F. *Acc. Chem. Res.* **2008**, *41* (11), 1534–1544.
(9) Wolfe, J. P.; Wagaw, S.; Marcoux, J.-F.; Buchwald, S. L. *Acc. Chem. Res.* **1998**, *31* (12), 805–818.

(10) Surry, D. S.; Buchwald, S. L. *Angew. Chem. Int. Ed.* **2008**, *47* (34), 6338–6361.
(11) Komiya, S.; Kochi, J. K. *J. Am. Chem. Soc.* **1976**, *98* (24), 7599–7607.
(12) Komiya, S.; Albright, T. A.; Hoffmann, R.; Kochi, J. K. *J. Am. Chem. Soc.* **1976**, *98* (23), 7255–7265.
(13) Tamaki, A.; Kochi, J. K. *J. Organomet. Chem.* **1974**, *64* (3), 411–425.
(14) Tamaki, A.; Magennis, S. A.; Kochi, J. K. *J. Am. Chem. Soc.* **1974**, *96* (19), 6140–6148.
(15) Tamaki, A.; Magennis, S. A.; Kochi, J. K. *J. Am. Chem. Soc.* **1973**, *95* (19), 6487–6488.
(16) Lawrence Kuch, P.; Stuart Tobias, R. *J. Organomet. Chem.* **1976**, *122* (3), 429–446.
(17) Shiotani, A.; Schmidbaur, H. *J. Organomet. Chem.* **1972**, *37* (1), C24–C26.
(18) Tamaki, A.; Kochi, J. K. *J. Organomet. Chem.* **1972**, *40* (2), C81–C84.
(19) Tai, H.-C.; Krossing, I.; Seth, M.; Deubel, D. V. *Organometallics* **2004**, *23* (10), 2343–2349.
(20) Cui, L.; Zhang, G.; Zhang, L. *Bioorg. Med. Chem. Lett.* **2009**, *19* (14), 3884–3887.
(21) Peng, Y.; Cui, L.; Zhang, G.; Zhang, L. *J. Am. Chem. Soc.* **2009**, *131* (14), 5062–5063.
(22) Zhang, G.; Cui, L.; Wang, Y.; Zhang, L. *J. Am. Chem. Soc.* **2010**, *132* (5), 1474–1475.
(23) Melhado, A. D.; Brenzovich, W. E.; Lackner, A. D.; Toste, F. D. *J. Am. Chem. Soc.* **2010**, *132* (26), 8885–8887.
(24) Brenzovich, W. E.; Benitez, D.; Lackner, A. D.; Shunatona, H. P.; Tkatchouk, E.; Goddard, W. A.; Toste, F. D. *Angew. Chem. Int. Ed.* **2010**, *49* (32), 5519–5522.
(25) Tkatchouk, E.; Mankad, N. P.; Benitez, D.; Goddard, W. A.; Toste, F. D. *J. Am. Chem. Soc.* **2011**, *133* (36), 14293–14300.
(26) Brenzovich, W. E.; Brazeau, J.-F.; Toste, F. D. *Org. Lett.* **2010**, *12* (21), 4728–4731.
(27) Ball, L. T.; Green, M.; Lloyd-Jones, G. C.; Russell, C. A. *Org. Lett.* **2010**, *12* (21), 4724–4727.
(28) Laguna, A.; Laguna, M. *Coord. Chem. Rev.* **1999**, *193–195*, 837–856.
(29) Ball, L. T.; Lloyd-Jones, G. C.; Russell, C. A. *Science* **2012**, *337* (6102), 1644–1648.
(30) Ball, L. T.; Lloyd-Jones, G. C.; Russell, C. A. *J. Am. Chem. Soc.* **2014**, *136* (1), 254–264.
(31) Cambeiro, X. C.; Boorman, T. C.; Lu, P.; Larrosa, I. *Angew. Chem. Int. Ed.* **2013**, *52* (6), 1781–1784.
(32) Cambeiro, X. C.; Ahlsten, N.; Larrosa, I. *J. Am. Chem. Soc.* **2015**, *137* (50), 15636–15639.
(33) Levin, M. D.; Toste, F. D. *Angew. Chem. Int. Ed.* **2014**, *53* (24), 6211–6215.
(34) Sahoo, B.; Hopkinson, M. N.; Glorius, F. *J. Am. Chem. Soc.* **2013**, *135* (15), 5505–5508.
(35) Hopkinson, M. N.; Sahoo, B.; Glorius, F. *Adv. Synth. Catal.* **2014**, *356* (13), 2794–2800.
(36) Kim, S.; Rojas-Martin, J.; Toste, F. D. *Chem. Sci.* **2015**, *7* (1), 85–88.
(37) Tlahuext-Aca, A.; Hopkinson, M. N.; Sahoo, B.; Glorius, F. *Chem. Sci.* **2015**, *7* (1), 89–93.
(38) Shu, X.; Zhang, M.; He, Y.; Frei, H.; Toste, F. D. *J. Am. Chem. Soc.* **2014**, *136* (16), 5844–5847.
(39) Serra, J.; Whiteoak, C. J.; Acuña-Parés, F.; Font, M.; Luis, J. M.; Lloret-Fillol, J.; Ribas, X. *J. Am. Chem. Soc.* **2015**, *137* (41), 13389–13397.
(40) Hartwig, J. F. *Organotransition Metal Chemistry: From Bonding to Catalysis*; University Science Books, Sausalito, 2010.
(41) Johnson, M. T.; Rensburg, J. M. J. van; Axelsson, M.; Ahlquist, M. S. G.; Wendt, O. F. *Chem. Sci.* **2011**, *2* (12), 2373–2377.
(42) Livendahl, M.; Goehry, C.; Maseras, F.; Echavarren, A. M. *Chem. Commun.* **2014**, *50* (13), 1533–1536.

(43) Guenther, J.; Mallet-Ladeira, S.; Estevez, L.; Miqueu, K.; Amgoune, A.; Bourissou, D. *J. Am. Chem. Soc.* **2014**, *136* (5), 1778–1781.
(44) Joost, M.; Zeineddine, A.; Estévez, L.; Mallet−Ladeira, S.; Miqueu, K.; Amgoune, A.; Bourissou, D. *J. Am. Chem. Soc.* **2014**, *136* (42), 14654–14657.
(45) Gimeno, M. C.; Laguna, A. *Chem. Rev.* **1997**, *97* (3), 511–522.
(46) Hofmann, P.; Heiß, H.; Müller, G. *Z. Für Naturforschung B* **2014**, *42* (4), 395–409.
(47) Alcazar-Roman, L. M.; Hartwig, J. F.; Rheingold, A. L.; Liable-Sands, L. M.; Guzei, I. A. *J. Am. Chem. Soc.* **2000**, *122* (19), 4618–4630.
(48) Amatore, C.; Broeker, G.; Jutand, A.; Khalil, F. *J. Am. Chem. Soc.* **1997**, *119* (22), 5176–5185.
(49) van Leeuwen, P. W. N. M.; Kamer, P. C. J.; Reek, J. N. H.; Dierkes, P. *Chem. Rev.* **2000**, *100* (8), 2741–2770.
(50) Gimeno, M. C.; Laguna, A.; Sarroca, C.; Jones, P. G. *Inorg. Chem.* **1993**, *32* (26), 5926–5932.
(51) Viotte, M.; Gautheron, B.; Kubicki, M. M.; Mugnier, Y.; Parish, R. V. *Inorg. Chem.* **1995**, *34* (13), 3465–3473.
(52) Gimeno, M. C.; Laguna, A. *Chem. Rev.* **1997**, *97* (3), 511–522.
(53) Schmidbaur, H. *Gold Bull.* **2000**, *33* (1), 3–10.
(54) Perthuisot, C.; Edelbach, B. L.; Zubris, D. L.; Simhai, N.; Iverson, C. N.; Müller, C.; Satoh, T.; Jones, W. D. *J. Mol. Catal. Chem.* **2002**, *189* (1), 157–168.
(55) Rybtchinski, B.; Milstein, D. *Angew. Chem. Int. Ed.* **1999**, *38* (7), 870–883.
(56) Wu, C.-Y.; Horibe, T.; Jacobsen, C. B.; Toste, F. D. *Nature* **2015**, *517* (7535), 449–454.
(57) Joost, M.; Estévez, L.; Miqueu, K.; Amgoune, A.; Bourissou, D. *Angew. Chem. Int. Ed.* **2015**, *54* (17), 5236–5240.
(58) Elowe, P. R.; McCann, C.; Pringle, P. G.; Spitzmesser, S. K.; Bercaw, J. E. *Organometallics* **2006**, *25* (22), 5255–5260.
(59) Burk, M. J.; Feaster, J. E.; Nugent, W. A.; Harlow, R. L. *J. Am. Chem. Soc.* **1993**, *115* (22), 10125–10138.
(60) Holz, J.; Monsees, A.; Jiao, H.; You, J.; Komarov, I. V.; Fischer, C.; Drauz, K.; Börner, A. *J. Org. Chem.* **2003**, *68* (5), 1701–1707.
(61) Holz, J.; Monsees, A.; Kadyrov, R.; Börner, A. *Synlett* **2007**, *2007* (4), 0599–0602.
(62) Galland, A.; Paris, J. M.; Schlama, T.; Guillot, R.; Fiaud, J.-C.; Toffano, M. *Eur. J. Org. Chem.* **2007**, *2007* (5), 863–873.
(63) Fox, M. E.; Jackson, M.; Lennon, I. C.; Klosin, J.; Abboud, K. A. *J. Org. Chem.* **2008**, *73* (3), 775–784.
(64) Maumela, M.; Blann, K.; de Bod, H.; Dixon, J.; Gabrielli, W.; Williams, D. B. *Synthesis* **2007**, *2007* (24), 3863–3867.

Chapter 2: Mechanistic Studies on Biaryl Reductive Elimination from Au(III).

This work was conducted in collaboration with Dr. Matthew S. Winston and portions of it have been used with permission from "Exceptionally Fast Carbon-Carbon Bond Reductive Elimination from Gold(III)" *Nat. Chem.* **2014**, *6*, 159–166. Copyright (2015) Nature Publishing Group. Portions have also been conducted with Dr. Hiroyuki Kawai and Dr. Antonio DiPasquale and used with permission from "Phosphonium Formation by Facile Carbon-Phosphorus Reductive Elimination from Gold(III). *J. Am Chem. Soc.* **2016**, *138*, 587–593. Copyright (2016) American Chemical Society.

Abstract: Oxidation of mono- and bimetallic arylgold(I) complexes at low temperature lead to observable Au(III) or Au(II)-containing intermediates, from which reductive elimination of biaryls was studied. Depending on the ligand, Au(II)-Au(II) bond-containing intermediates were formed as kinetic products of oxidation, which underwent facile isomerization to mixed-valent Au(I)/Au(III) species. C(sp^2)–C(sp^2) reductive elimination from Au(III), long considered a high-barrier process, was observed from these oxidized Au species at temperatures as low as –52 °C. We show that aryl-aryl bond reductive elimination from Au(III) was not only among the fastest observed for transition metal complexes (in one case, the rate-constant was calculated to be greater than 0.22 s^{-1} at –52 °C), but also mechanistically distinct from previously studied C(sp^3)–C(sp^3) reductive eliminations from Au(III). These studies also informed preliminary efforts towards a gold-catalyzed cross-coupling.

Introduction: Reductive elimination of C-H, C-C, and C-X bonds is a key step in many metal-catalyzed reactions.[1] These processes have been extensively studied from Ni[2–6], Pd[7–15], and Pt[16–22], yet relatively little is known about the reductive elimination from Au, which is markedly more stable toward air and water. In fact, since Kochi[23–25] and Tobias's[26] investigations of high-temperature dialkylgold(III) reductive eliminations, fundamental studies of C-C bond reductive coupling from oxidized Au centers remain rare. Previous studies have shown that *cis*-$EtMe_2Au(PPh_3)$[24] and [*cis*-$(CH_3)_2Au(PPh_3)_2](PF_6)$[26] were stable at room temperature, undergoing alkyl-alkyl bond reductive elimination at 70 °C (k_{obs} ~ 10^{-5}-10^{-3} s^{-1}), while *cis*-$(CH_3)_2AuCl(PPh_3)$[25] reductively eliminated ethane slowly at 40 °C (k_{obs} ~ 10^{-7}) as shown in Figure 2.1. Kinetic analysis suggested these processes were inverse first-order in PPh_3 and that reductive elimination does not occur directly from the 4-coordinate complex, but rather from a high-energy T-shaped intermediate, formed by slow, reversible phosphine dissociation.[23]

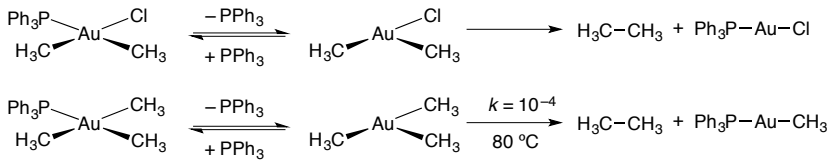

Figure 2.1. A) Alkyl-alkyl reductive elimination from Au(III) at elevated temperatures.

In contrast to the well-studied C(sp^3)–C(sp^3) reductive elimination from Au(III) centers, the analogous C(sp^2)–C(sp^2) coupling has not been extensively explored. Several examples of diaryl Au(III) complexes containing very electron poor aryl groups have been reported, as shown in Figure 2.2. The perfluorinated diaryl complex *cis*-$(Ph_3P)AuCl(C_6F_5)_2$ was stable up to 150

°C[27–29] and the subsequent reductive elimination of decafluorobiphenyl occurred at this temperature. Vicente has reported examples of cyclometallated Au(III) aryl complexes that underwent reductive elimination at room temperature.[30,31] In contrast to the Au(III) alkyl compounds in Kochi's system, Vicente observed that these eliminations proceed in the presence of exogenous Ph_3P; the ligand was proposed to coordinate to the Au(III) center prior to elimination.

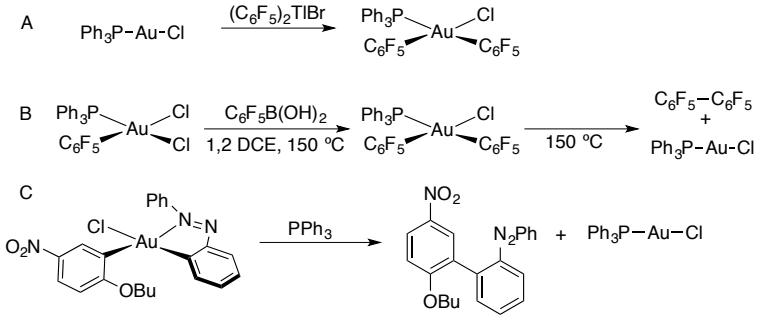

Figure 2.2. A) Synthesis of *cis*-$(Ph_3P)AuCl(C_6F_5)_2$ by oxidation with $(C_6F_5)_2TlBr$; B) Synthesis of *cis*-$(Ph_3P)AuCl(C_6F_5)_2$ by transmetalation from $C_6F_5B(OH)_2$ and subsequent biaryl elimination; C) biaryl reductive elimination from a cyclometalated Au(III) biaryl compound in the presence of Ph_3P.

Aside from these reports, very little is known about the nature of diaryl Au(III) compounds. Meanwhile, the field has not only witnessed the advent and maturation of palladium-catalyzed cross-coupling methods (driven in part by detailed mechanistic analysis of these processes) but the development of homogeneous redox-neutral gold catalysis as well. The shortage of mechanistic insight of processes at Au(III) may be due in part to synthetic challenges in accessing appropriate Au(III) models, and to the high oxidation potential of Au(I) that traditionally precludes Au(I)/Au(III) redox cycling.[32]

Electronic cooperation between metal centers is well established in redox processes. Hence, bimetallic Au complexes may be useful systems for studying the fundamental chemistry of oxidized organogold species. In the bimetallic core, each Au(I) can formally undergo a one electron oxidation, resulting in two d^9 metal centers with unpaired electrons capable of making a Au(II)-Au(II) σ-bond. Fackler[33–39] and Laguna[40–43] have shown that dihalides and alkyl halides oxidize A-frame bimetallic Au(I) complexes to access Au(II) species, yet reductive elimination processes from Au(II) have not been rigorously investigated. In fact, well-behaved reductive eliminations of carbon-carbon bonds from bimetallic Au(II) species are incredibly rare.[44] Due to the preference for linearity by Au(I), A-frame bimetallic Au(I) complexes lack available coordination sites and may only coordinate nucleophiles upon oxidation. Therefore, while non-A-frame systems may be more appropriate for mechanistic studies that ultimately inform catalysis, only one non-A-frame bis(aryl) bimetallic Au(II) complex has been prepared;[43] due to the strongly electron-withdrawing perfluorinated aryl ligands, biaryl reductive elimination does not occur at room temperature, and reductive elimination at elevated temperatures was not investigated.

Current studies of the fundamental chemistry at oxidized gold centers are essential to establishing new modes of gold reactivity – particularly those involving redox cycling.[45–47] Herein we report our preparation of several monometallic and non-A-frame bimetallic bis(aryl) gold(I) complexes that allow kinetic analysis of C-C bond-forming reductive eliminations from oxidized species. In contrast to Kochi's report, we show that C-C bond reductive elimination at Au(III) is not necessarily a disfavored process[48,49] but can instead be rapid at temperatures between –50 and –10 °C. We show that biaryl reductive elimination at monometallic Au(III)

proceeds *via* an unexpected mechanism, and report the mechanism of biaryl reductive elimination from non-A-frame bimetallic gold complexes.

Results and discussion

Biaryl reductive elimination from a mononuclear gold complex: In attempt to synthesize *cis*(Ph_3P)$AuCl_2$(4-F-C_6H_4) (**2.2**, Figure 2.3) we were surprised to find that oxidation of **2.1** with $PhICl_2$ at room temperature (20 ºC) immediately and quantitatively generated 4,4'-difluorobiphenyl and (Ph_3P)AuCl. If either (Ph_3P)Au(Ph) or (Ph_3P)Au(4-Me-C_6H_4) was treated with $PhICl_2$, the analogous biaryl was also observed; **2.1** was used because of its convenient ^{19}F NMR handle. In methylene chloride solution at –52 °C, a new species could be observed along with (Ph_3P)AuCl when **2.1** was oxidized with $PhICl_2$, whose structure was assigned as **2.3** based on ^{19}F (two 1:1 singlets at –118.4, –119.5 ppm supporting the *cis* relationship between the aryl groups) and ^{31}P NMR (one singlet at 27.9 ppm). The reaction was unaffected by equimolar or excess amounts of oxidant, indicating that transmetalation from **2.1** to **2.2** was faster than oxidation of **2.1**.

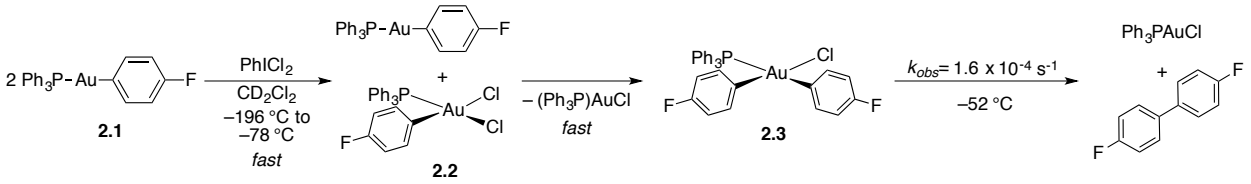

Figure 2.3. Fast *in situ* oxidation of Ph_3PAu(4-F-C_6H_4) and reduction elimination of **2.3** or **2.4** affords 4,4'-difluorobiphenyl.

Aryl-aryl reductive elimination from **2.3** could then be monitored by ^{19}F NMR (k_{obs} = (1.5 ± 0.1) x 10^{-4} s^{-1}). The rate of reductive elimination was 100 times faster (k_{obs} = 0.015 ± 0.001 s^{-1}) at –23 ºC. The observed rate constant for biaryl elimination from **2.3** at –52 ºC remained unchanged over a range of concentrations, as well as in the presence of 10 equivalents of either Bu_4NCl or Ph_3PAuCl, indicating a unimolecular process that was first-order in **2.3** as shown in Figure 2.4. In THF solution, no signals corresponding to **2.3** were observed upon low-temperature (–78 ºC) oxidation of **2.1** and no biaryl formation occurred, even after warming to 27 ºC. Attempts to monitor the reaction in toluene were unsuccessful due to the poor solubility of **2.1** at low-temperature.

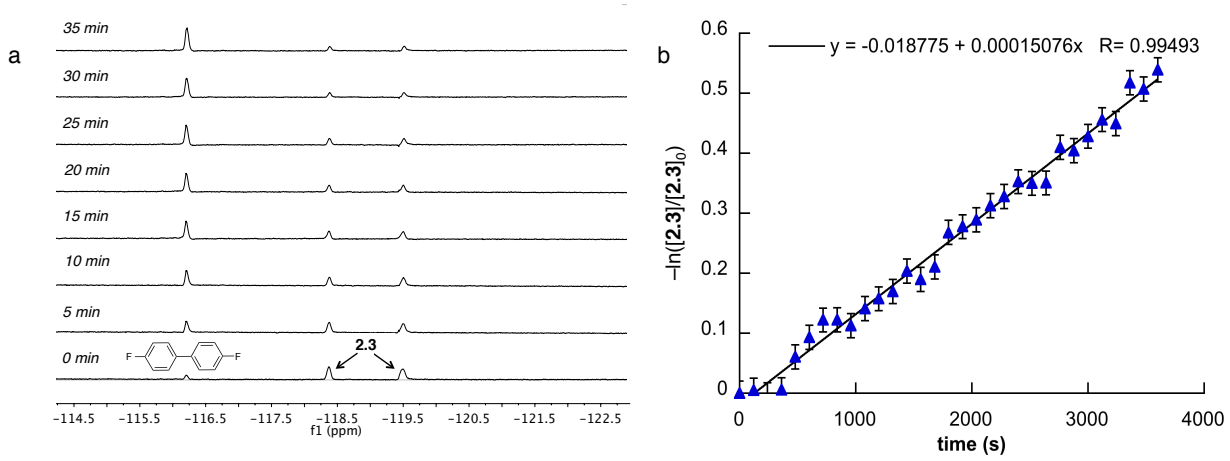

Figure 2.4. (a): First-order decay of Au(III) species **2.3** as monitored by ^{19}F NMR (470 MHz, CD_2Cl_2) at –32 °C over 35 minutes. (b): Natural log plot of [**2.3**]/[**2.3**]$_0$ at –52 ºC versus time indicative of a first order process.

The lower barrier to C(sp^2)–C(sp^2) reductive elimination from **2.3** relative to the barrier for C(sp^3)– C(sp^3) elimination from alkylgold(III) complexes may not simply be attributed to faster coupling of aryl-aryl relative to alkyl-alkyl bonds[9] but also suggests fundamentally different rate-determining steps and mechanisms. For example, in contrast to what is established for alkyl-alkyl reductive elimination of Au(III), excess PPh_3 increased the observed rate of aryl-aryl reductive elimination from **2.3** (Figure 2.5).

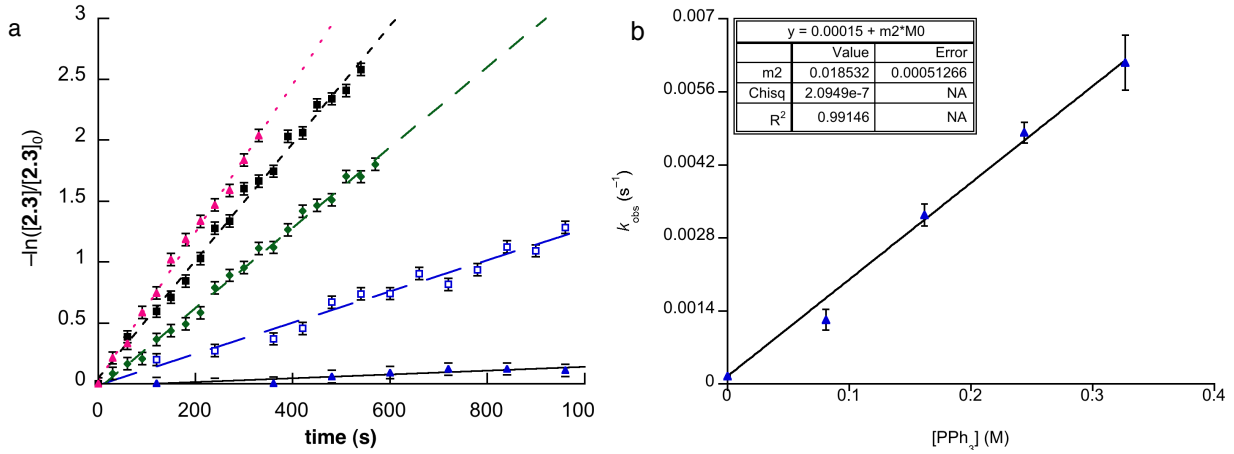

Figure 2.5. A) Acceleration of the rate of consumption of **2.3** with increasing [PPh_3] at –52 °C: ▲ (0 equiv PPh_3); □ (10 equiv PPh_3); ◆ (20 equiv PPh_3); ■ (30 equiv PPh_3); ▲ (40 equiv PPh_3). B) k_{obs} for the reductive elimination from **2.3** in the presence of PPh_3 plotted as a function of [PPh_3], indicating that ligand association to **2.3** is first-order in PPh_3 (right).

In the presence of 10 equivalents of PPh_3 at –52 °C, the rate of reductive elimination from **2.3** increased by an order of magnitude (k_{obs} = (1.2 ± 0.2) x 10^{-3} s^{-1}); with 40 equivalents, the observed pseudo-first order rate constant is (6.2 ± 0.5) x 10^{-3} s^{-1}. No new ^{19}F and ^{31}P NMR signals can be observed under these conditions. Neither Bu_4NCl (up to 40 equivalents) nor the radical trap 9,10-dihydroanthracene affect reductive elimination from **2.3**. Furthermore, the observed rate remains unchanged in the presence of excess oxidant; $PhICl_2$ acts as a phosphine scavenger, precluding the scenario in which small amounts of PPh_3 liberated from **2.3** induce reductive elimination. These observations are consistent with two operative pathways to biaryl: one independent of added PPh_3 and another involving phosphine coordination.

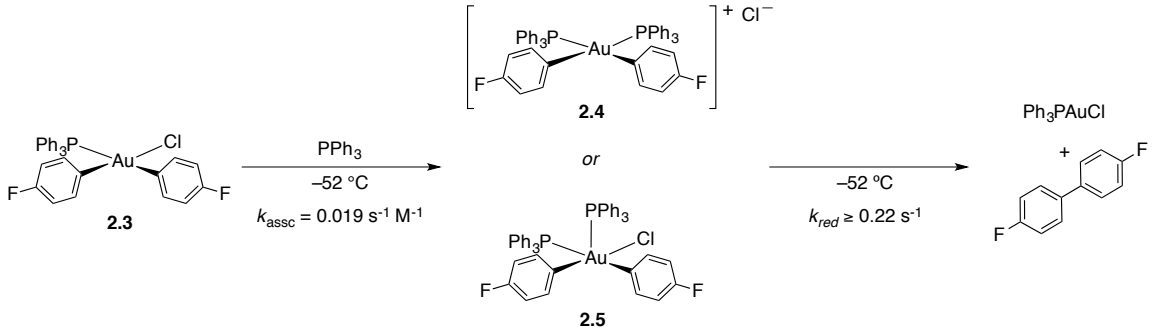

Figure 2.6. Coordination of Ph_3P to **2.3** results in an acceleration of the observed biaryl reductive elimination *via* either a four-coordinate cation or a five-coordinate intermediate.

In the absence of added phosphine, reductive elimination occurs directly from the square-planar complex **2.3**. In the presence of excess PPh_3, **2.3** can undergo associative ligand exchange to generate cation **2.4**, which rapidly reductively eliminates biaryl; or biaryl elimination can

occur from a five-coordinate complex **2.5** as shown in Figure 2.6. Both processes are first-order in PPh_3 (Figure 2.5, right.) Since neither **2.4** nor **2.5** was observable by NMR, reductive elimination from these complexes must be substantially faster than from **2.3**, given its bulkier steric environment and cationic charge.

When 10 equivalents of PPh_3 *and* 40 equivalents of Bu_4NCl were added, the rate remained unchanged from that of the phosphine-accelerated reaction, indicating a rate-limiting phosphine association step. At –52 °C, association of PPh_3 (k = 0.019 ± 0.001 s^{-1} M^{-1}) and reductive elimination from **2.4** or **2.5** ($k \geq 0.22$ s^{-1}) are remarkably facile processes. The possibility of reductive elimination from **2.5** following coordination of PPh_3 cannot be definitively discounted, as a similar effect has been observed in the study of biaryl reductive elimination from Pt(II) compounds.[50–52]

The observed reductive elimination from diarylgold(III) complexes **2.3** occurred at rapid rate at temperatures below –20 °C. The analogous Pt(II) complex, *cis*$(Ph_3P)_2Pt(Ph)_2$, reductively eliminates biphenyl at 50 ºC in toluene solution with an observed first-order rate constant of (4.95 ± 0.25) x 10^{-6} s^{-1}.[52] Rate constants for reductive elimination from other isolobal diarylplatinum(II)[19] and palladium(II)[12] complexes have been reported between 10^{-5} and 10^{-3} s^{-1} at 95 and 50 °C, respectively, although Pd-catalyzed Kumada-Corriu couplings can be achieved at temperatures as low as –65 °C.[53] Reductive elimination rate constants of ~0.1 s^{-1} have also been reported for Ni-catalyzed oxidative homocouplings at –35 °C,[6] although the presumed diarylnickel(II) intermediate is never observed. Indeed, for a 3rd row metal, the rates of aryl-aryl reductive elimination from Au(III) are particularly impressive, outcompeting even C-C bond coupling in alkynylarylpalladium(IV) complexes ($k \sim 10^{-3}$ s^{-1} at –35 °C). A direct comparison may not be useful when examining the rates of elimination due to differences in mechanism; however, it is worth noting where the rates of elimination from **2.3** lie relative to other metals and oxidation states.

The effects that govern elimination from **2.3** are not immediately obvious, and several factors affect the rates of elimination. Reductive elimination from four-coordinate square planar d^8 metal centers is a symmetry allowed process.[54–56] While **2.3** does not possess C_{2v} symmetry, the factors that affect reductive elimination from a C_{2v} system are important to consider, regardless of the symmetry of the system, and they have been conveniently elucidated by Hoffmann.[54,55] An orbital diagram for the elimination of R_2 from a C_{2v} ML_2R_2 (M = metal, L = spectator ligand) complex is shown in Figure 2.7. The activation barrier for reductive elimination is related to the energy of both $1b_2$ and $2b_2$ and their avoided crossing as shown in Figure 2.7.[56]

As the elimination proceeds (the L–M–L angle θ is held to 90º) there is a correlation between $1b_2$ and the C–C σ* orbital and between $2b_2$ and the filled metal *d*-orbital (which is M–L antibonding, if θ = 90º, as illustrated in Figure 2.7) from an empty M–R antibonding orbital to the R–R σ* orbital, while the $1b_2$ orbital correlates the M–L σ orbital to the resulting M–L σ* orbital. The energy barrier, shown as ΔE in Figure 2.7, is a result of the avoided crossing of these two orbitals.[56] It is worth noting that for four-coordinate complexes, the $2b_2$ orbital of the starting complex is antibonding in nature and is occupied. The destabilization of this orbital raises the overall energy of the elimination from four-coordinate complexes, as illustrated by the block arrows in Figure 2.7B. It should be noted than linearization of the ML_2 fragment does not significantly lower the computed barrier for elimination.[55]

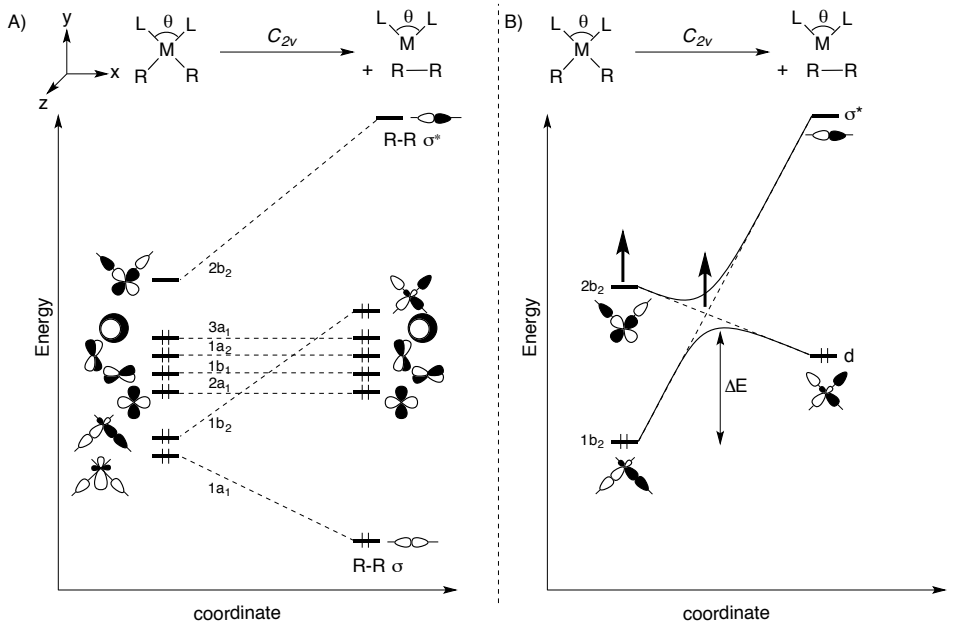

Figure 2.7. A) Schematic correlation diagram for elimination of R–R from C_{2v} *cis*-ML_2R_2 and B) the correlation between the isolated $1b_2$ and $2b_2$ orbitals. Energy levels are not shown to scale.

Hoffmann has outlined several factors that can affect the relative energy levels of the participating orbitals and the effects that control the activation barrier for elimination.[54] Generally, stronger σ-donors are eliminated more rapidly and stronger donors *trans* to the leaving groups raises the barrier to elimination. Most importantly, in four-coordinate complexes, the barrier is primarily controlled by the energy of the antisymmetric b_2 orbitals as described above, which are themselves controlled by the energy of the constituent metal orbitals.[54] As a result, lower energy atomic orbitals are directly correlated to lower barriers for elimination i.e. the computed barriers to elimination from Ni(II) complexes are lower than those computed for Pd(II) complexes due to the lower energy of the Ni 3*d* orbitals compared to the Pd 4*d* orbitals. When considering elimination from **2.3** the Au valence orbitals are sufficiently low in energy so as to create a low barrier for elimination. The Coloumb integrals (H_{11}) used by Hoffmann show that the atomic energy levels for gold[24] (5*d*: –15.07 eV, 6*s*: –10.92 eV 6*p*: –5.55 eV) are significantly lower than those of platinum[54] (5*d*: –12.59 eV, 6*s*: –9.077 eV 6*p*: –5.475 eV) and even nickel[54] (3*d*: –13.49 eV, 4*s*: –9.17 eV 6*p*: —5.15 eV). Thus, the rapid rates of elimination from **2.3** are a result of the low-lying atomic orbital energy levels of gold.

The barrier to C(sp^2)–C(sp^2) reductive elimination is generally lower than that for C(sp^3)–C(sp^3) reductive elimination[8,9,57] because of two main factors. First, steric crowding at the transition state is less pronounced in the case of C(sp^2)–C(sp^2) coupling compared to C(sp^3)–C(sp^3) coupling. Second, the C(sp^2) hybridized orbitals of the organic ligands are less directional due to a decrease in *p*-character compared to sp^3 hybrid orbitals. As a result, the participating C(sp^2) orbitals are better able to overlap and participate in three-centered bonding in the transition state. This effect undoubtedly makes a significant contribution to the difference in rate between the C(sp^3)–C(sp^3) coupling studied by Kochi and Tobias and the C(sp^2)–C(sp^2) coupling from **2.3**. Indeed, Eyring analysis revealed a low barrier to elimination ($\Delta H^{\ddagger}$ = 17.2 ± 0.2 kcal/mol; $\Delta S^{\ddagger}$ = 2.0 ± 0.8 e.u.) as shown in Figure 2.8.

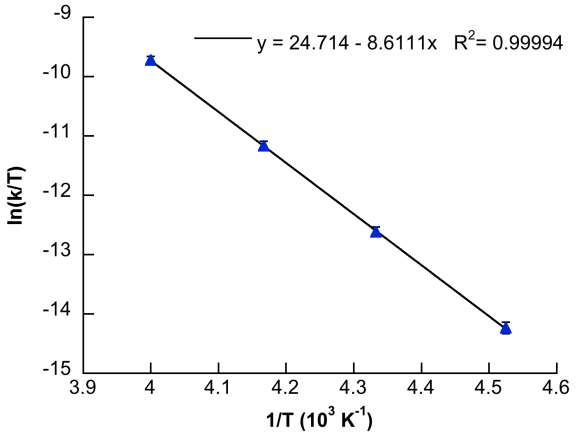

Figure 2.8. Eyring plot for reductive elimination from **2.3** over the temperature range –52 ºC to –23 ºC ($\Delta H^{\ddagger}$ = 17.2 ± 0.2 kcal/mol; $\Delta S^{\ddagger}$ = 2.0 ± 0.8 e.u.).

Biaryl reductive elimination from bimetallic gold complexes: The unexpected redox behavior of mononuclear Au(III) species led us to investigate analogous reactivity of bimetallic gold complexes. Others have reported that bimetallic complexes with three-atom linkers do not undergo two-electron oxidation at a single Au(I), but instead undergo formal one-electron oxidation at two Au(I) centers to generate a species stabilized by a Au(II)–Au(II) bond.[33–43] Electronic cooperation between metal centers in bimetallic complexes offers a lower barrier oxidation pathway relative to a two-electron oxidation at a single metal center[45], allowing, for example, oxidation of dicationic A-frame Au(I) complexes by oxidants typically unreactive toward monocationic Au(I), such as benzoyl peroxide.[39] Furthermore, electrochemical studies and DFT calculations suggest that aurophilic interactions reduce the oxidation potential of bimetallic Au(I) species relative to mononuclear complexes.[32]

To assess the role of metal-metal bonding in the C-C bond reductive elimination of oxidized gold, we prepared a bimetallic Au(I) complex stabilized by a bis(diphenylphosphinoamine) ligand Ph_2P-NR-PPh_2 (PNP).[58,59] X-ray diffraction analysis of PNP[Au(4-F-C_6H_4)]$_2$ (**2.6**, X = NMe) indicated an aurophilic interaction (Au(I)-Au(I) distance = 3.0357(2) Å) that is likely conserved in solution. Laguna has shown that direct oxidation of HN(PPh_2)[Au(C_6F_5)]$_2$ with Cl_2 generated symmetric bimetallic Au(II) complex HN(PPh_2)[Au(C_6F_5)Cl]$_2$, which was stable at room temperature; crystallographic analysis established a Au(II)-Au(II) bond (2.576(2) Å) and a *trans* relationship between chloride ligands.[43]

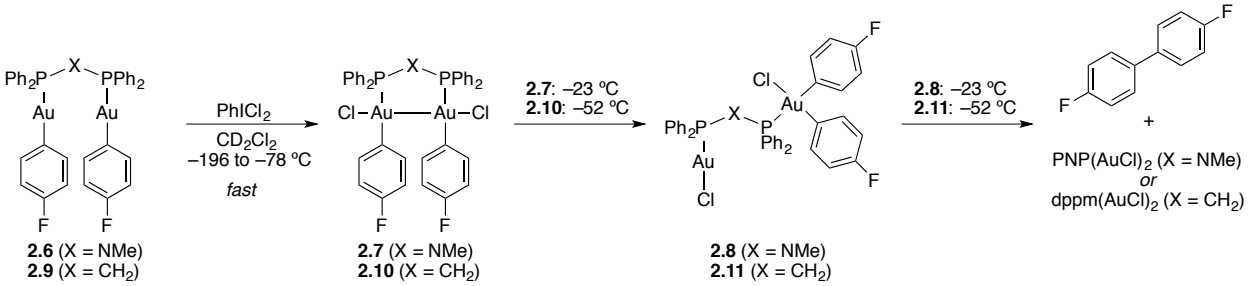

Figure 2.9. Fast *in situ* oxidation of PNP[Au(4-F-C_6H_4)]$_2$ (**2.5**) and dppm[Au(4-F-C_6H_4)]$_2$ (**2.8**) and biaryl reductive elimination via Au(II) intermediates.

The analogous low-temperature oxidation of **2.6** with $PhICl_2$ generated symmetric bimetallic Au(II) complex **2.7** (Figure 2.9; ^{19}F NMR and ^{31}P NMR singlets at –120.4 ppm and 83.5 ppm, respectively), which underwent slow reductive elimination at temperatures below –30 °C (Figure

2.9). At –23 °C, **2.7** exhibited first-order decay (k_{obs} = (1.6 ± 0.3) x 10^{-4} s^{-1}) with concomitant formation of 4,4'-difluorobiphenyl (Figure 2.10).

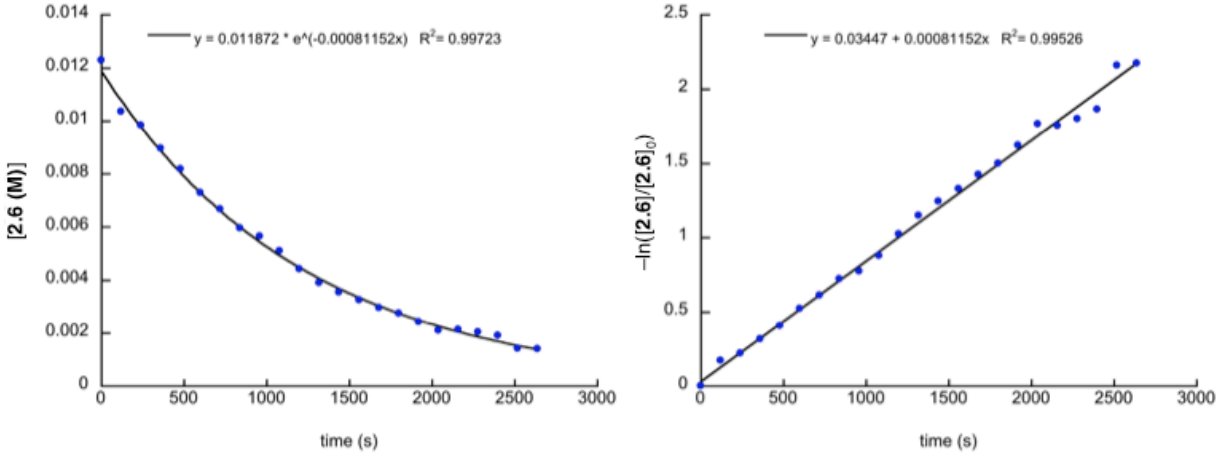

Figure 2.10. Plots of [**2.6**] against time (left) and –ln([**2.6**]/[**2.6**]$_0$) against time at –23 ºC showing the first-order behavior of the process (right).

Without observing a mixed-valent intermediate, we cannot kinetically distinguish between a pathway involving rearrangement and reductive elimination, and one involving bimetallic reductive elimination *via* a 4-centered transition state.[60] However, Laguna has reported that similar PNP-supported binuclear perfluoroarylgold(II) complexes rearranged over several hours to mixed-valent Au(I)/Au(III) species.[44] Given fast aryl transmetallation and reductive elimination of mononuclear Au(III), as well as the scarcity of reported binuclear reductive elimination, we therefore favor a mechanism involving isomerization of **2.7** to mixed-valent species **2.8**, which then undergoes fast, unobservable reductive elimination. The kinetic parameters for the rate-limiting isomerization of **2.7** to **2.8** ($\Delta H^{\ddagger}$ = 16.9 ± 0.4 kcal/mol; $\Delta S^{\ddagger}$ = –7.8 ± 1.6 e.u.) are reflective of a low-barrier process with a small entropic penalty (Figure 2.11).

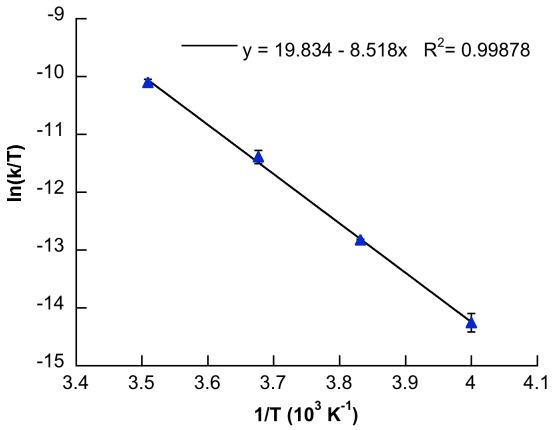

Figure 2.11. Eyring plot for isomerization of **2.6** to **2.7** over a temperature range from –23 ºC to 12 ºC ($\Delta H^{\ddagger}$ = 16.9 ± 0.4 kcal/mol; $\Delta S^{\ddagger}$ = –7.8 ± 1.6 e.u.).

This step is first-order in **2.6**, and unaffected by excess Bu_4NCl. Complex **2.6** also oxidizes excess phosphine, presumably *via* chloronium transfer; therefore, phosphine dissociation is likely not a prerequisite for either isomerization or reductive elimination, since $PNP(AuCl)_2$ was formed quantitatively when no excess ligand is added, and no decomposition of liberated ligand (PNP + **2.6**) was observed. These results are consistent with a mechanism

involving intramolecular aryl transfer from **2.7** to generate **2.8**, which then directly reductively eliminated to PNP(AuCl)$_2$ and 4,4'-difluorobiphenyl.

We reasoned that N→P π-donation in PNP-type ligands results in a barrier to N-P bond rotation that becomes significant at low temperature.[61] A more flexible ligand, such as 1,2-bis(diphenylphosphino)methane (dppm), could presumably facilitate intramolecular aryl transfer from a bimetallic Au(II) intermediate, resulting in a lower barrier to isomerization. Oxidation of dppm[Au(4-F-C$_6$H$_4$)$_2$]$_2$ (**2.9**, X = CH$_2$) at –78 °C by PhICl$_2$ afforded symmetric bimetallic Au(II) species **2.10** (^{19}F NMR and ^{31}P NMR singlets at –120.0 ppm and –18.2 ppm, respectively), which isomerized faster than analogous PNP complex **2.7** (Figure 2.9). Indeed, at –52 °C, **2.10** underwent first-order decay, with fast appearance and slow consumption of mixed-valent Au(I)/Au(III) complex **2.11**, and appearance of 4,4'-difluorobiphenyl at approximately the same rate as the disappearance of **2.10** (Figure 2.12). The kinetic profile of these species is consistent with two consecutive first-order reactions,[62] precluding a scenario in which a bimetallic reductive elimination occurs directly from **2.10**. Instead, **2.10** likely undergoes irreversible isomerization to **2.10** (k = (4.6 ± 0.1) x 10^{-4} s^{-1}), which then reductively eliminates 4,4'-difluorobiphenyl at a comparable rate (k = 3.9 x 10^{-4} s^{-1}). At –30 °C, both reactions were immeasurably fast using ^{19}F NMR techniques. While PNP-supported Au(I)/Au(III) species **2.8** could not be observed, these findings support a similar reductive elimination mechanism of PNP-supported complexes, and of other bimetallic Au(II) complexes[44] involving the intermediacy of such mixed-valent species as proposed above.

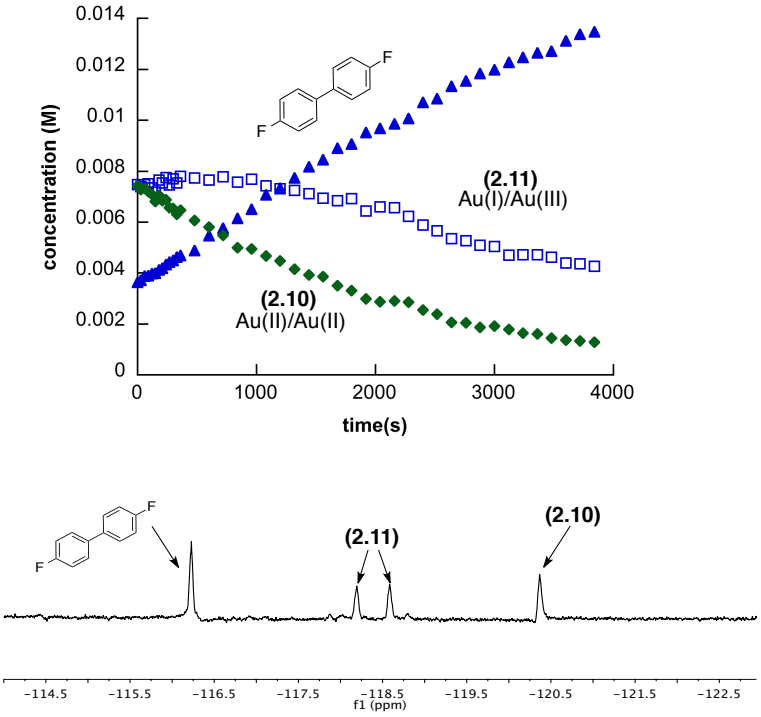

Figure 2.12. Top: Reaction profile for the isomerization of **2.10** to **2.11** and reductive elimination of biaryl from **2.11** at –52 °C. Bottom: Selected region of ^{19}F NMR spectrum (470 MHz, CD_2Cl_2) of oxidation of **2.9** at –52 °C.

Using the dppm-supported system discussed above as a benchmark, we probed the behavior of a bimetallic system with a five-atom linker that could perturb intramolecular metal-metal interactions. We hypothesized that a longer linker (such as 1,3-

(diphenylphosphino)propane (dppp)) between Au atoms might preclude formation of a 7-membered metallacyclic Au(II)-Au(II) intermediate upon oxidation. Indeed, the only product of low-temperature oxidation of dppp[Au(4-F-C_6H_4)]$_2$ (**2.12**) by $PhICl_2$ was mixed-valent species **2.14** (two 1:1 ^{19}F NMR singlets at –118.3 and –118.6 ppm and two 1:1 ^{31}P NMR singlets at 27.3 and 21.7 ppm), presumably formed via fast isomerization of **2.12** (Figure 2.13). Even at –80 °C, no NMR signals consistent with a symmetric bimetallic Au(II) species were observed, suggestive that a mixed-valent species was formed directly upon oxidation. Upon warming to –52 °C, **2.14** underwent first-order reductive elimination to dppp$(AuCl)_2$ and 4,4'-difluorobiphenyl (k_{obs} = (3.0 ± 0.1) x 10^{-5} s^{-1}). Hence, the kinetic profiles of oxidation and reductive elimination of bimetallic complexes bearing linkers that restrict metal-metal interactions resemble those of mononuclear species.

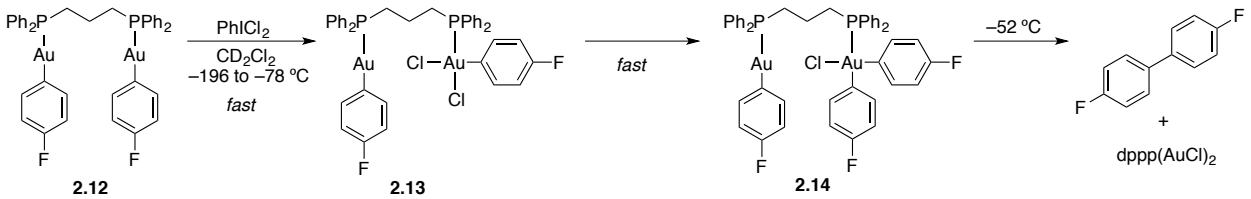

Figure 2.13. Fast *in situ* oxidation of dppp[Au(4-F-C_6H_4)]$_2$ and reductive elimination of **2.13** affords 4,4'-difluorobiphenyl.

Importantly, these studies reveal that access to a kinetic bimetallic Au(II) product of oxidation does not necessarily compromise the rate of reductive elimination from Au(III); in fact, the rate of reductive elimination from dppm-supported **2.11** is about an order of magnitude faster than that of **2.14**, perhaps due to increased steric crowding as a result of a shorter linker, aurophilic interactions between the Au centers in **2.11**, or a combination thereof. Even Au(II)/Au(II) → Au(I)/Au(III) isomerization for PNP and dppm-supported complexes is a facile process at temperatures below 0 °C.

Efforts towards gold-catalyzed cross-coupling

To investigate the effects of phosphine structure on the reductive elimination from diaryl Au(III) species, we prepared (Cy_3P)Au(4-F-C_6H_4) (**2.15**) and attempted to monitor its reaction with $PhICl_2$ in CH_2Cl_2 solution. Upon low temperature (–78 ºC) oxidation, we did not observe any biaryl reductive elimination. Instead, the complete oxidation to the complex *cis*-(Cy_3P)Au(4-F-C_6H_4)Cl_2 (**2.16**) had occurred (Figure 2.14) rather than aryl transfer to give the diaryl complex **2.17** in analogy to **2.3**. The isolated complex **2.16** did not undergo aryl transfer with **2.15** even at 20 ºC.

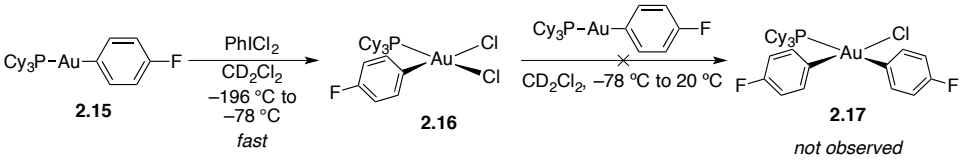

Figure 2.14. Low temperature oxidation of Cy_3P analogue of **2.3** to give a dichloro Au(III) complex **2.16**.

Both **2.15** and **2.16** would provide model platforms to study transmetallation to Au(III)[29,63] towards the development of a gold-catalyzed cross-coupling because the bulkier ligand could prevent aryl group transfer between gold species and because the isolated complex would enable direct study of transmetallation step to Au(III).[29] In CH_2Cl_2 solution **2.16** did not react with $PhSnMe_3$ at 20 ºC in either the presence or absence of KF. In attempt to open a coordination site on the gold center, **2.16** was treated with $AgSbF_6$ in CH_2Cl_2 solution at 20 ºC.

At this temperature, rapid formation of Au nanoparticles (deep purple precipitate) was accompanied by the formation the phosphonium salt $[(Cy_3P)(4\text{-}F\text{-}C_6H_4)][SbF_6]$ (**2.18**); the single crystal X-ray structure confirmed this assignment, as shown in Figure 2.15.

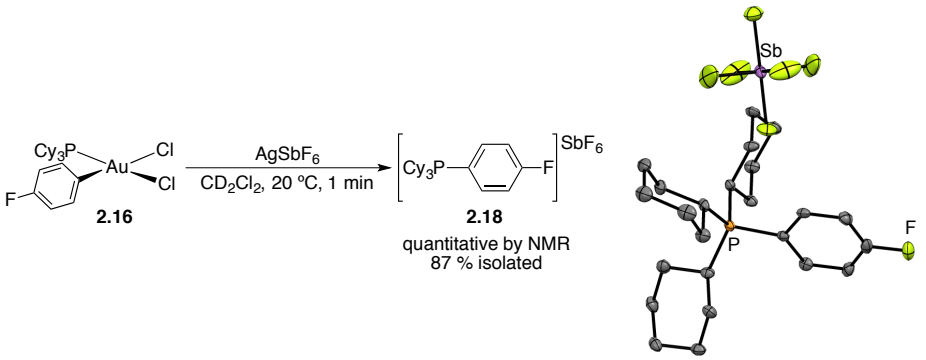

Figure 2.15. Reductive elimination of phosphonium **2.18** from Au(III) and its single crystal X-ray structure; ellipsoids are set at the 50% probability level and hydrogen atoms are omitted for clarity.

At –52 ºC a new intermediate species was observed by ^{19}F and ^{31}P NMR. The gradual warming of the sample to –20 ºC resulted in the clean formation of **2.18**, and a cross-over experiment suggested the presence of a dimeric species, **2.19**. If the chloride abstraction was conducted in the presence of pyridine, the three-coordinate cation could be trapped and isolated as shown in Figure 2.16. Abstraction of the pyridine ligand with $B(C_6F_5)_3$ at 0 ºC also gave clean elimination of **2.18**. After low-temperature generation of **2.19**, the addition of $PhSnMe_3$ resulted in the formation of 4-fluorobiphenyl presumably as a result of transmetallation and reductive elimination (Figure 2.16).

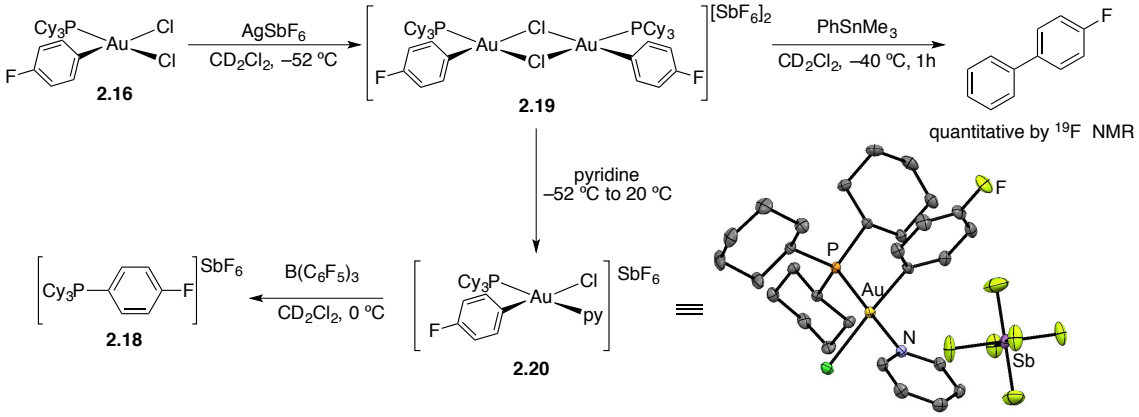

Figure 2.16. Low temperature generation of **2.19** and trapping with $PhSnMe_3$ or pyridine. The single crystal X-ray structure of **2.20** is shown with ellipsoids set at the 50 % probability level and hydrogen atoms omitted for clarity.

Given that the cross-product 4-fluorobiphenyl could be obtained in high yield from transmetallation to a Au(III) cation, we hypothesized that an aryl diazonium salt[64] might be a suitable oxidant that could generate a similar cation as shown in Figure 2.17.

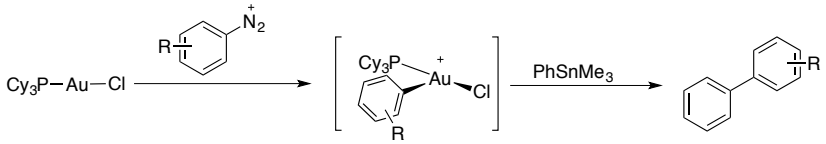

Figure 2.17. Hypothetical cross-coupling of aryldiazonium salts and aryl stannanes.

The reaction of **2.16** with $[PhN_2][BF_4]$ in CD_2Cl_2 solution gave a mixture of arene products, including fluorobenzene, 4,4'-difluorobiphenyl the cross-product 4-fluorobiphenyl in low yield, shown in Figure 2.18.

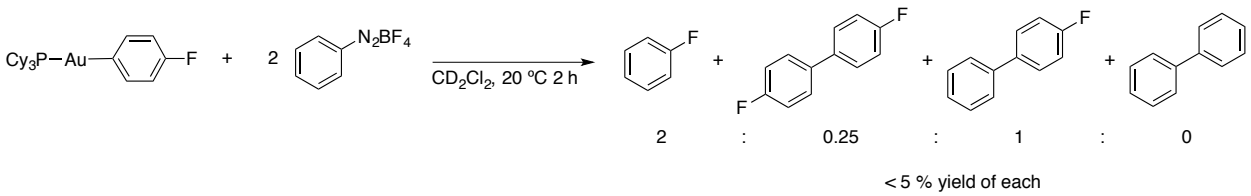

Figure 2.18. Reaction of phenyldiazonium with **2.15** to give biaryl products in low yield.

Despite the poor yield of a mixture of biaryls, we continued our pursuit of a catalytic transformation. The use of $PhSnMe_3$ and 4-fluorophenyldiazonium tetrafluoroborate as coupling partners was examined using different PCy_3 ligated gold complexes.

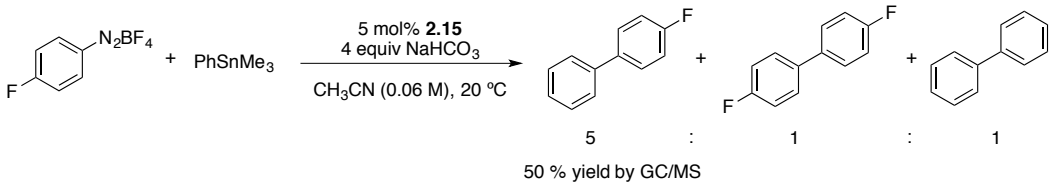

Figure 2.19. Catalytic cross-coupling of 4-fluorophenyldiazonium tetrafluoroborate with trimethylphenylstannane in the presence of **2.15**.

In CH_2Cl_2 solution, no cross-coupling was observed; however, in acetonitrile in the presence of $NaHCO_3$, 50% conversion to a mixture of biaryls was observed by GC/MS, with a 5:1:1 distribution of cross-product to the homo-coupled biaryls (Figure 2.19). Importantly, no coupling was observed in the absence of **2.15**. Neither $(Cy_3P)AuCl$ nor $[(Cy_3P)Au][BF_4]$ were competent catalysts when compared to **2.15**, suggesting a mechanism with transmetallation preceding oxidative addition. In the presence of 9,10-dihydroanthracene, conversion stopped at 10 % and a significant amount of anthracene was produced, consistent with a free-radical process. Similar gold-catalyzed cross-coupling of aryl diazoniums and alkynes has been developed, in either the presence[65,66] or absence[67] of a photoredox catalyst to assist in the oxidation of the gold catalyst. These methods are reflective of an increasing interest in redox active gold catalysis and provide continued evidence for the potential breadth of reactivity of gold that may be discovered.

Conclusions: We have studied several properties of oxidized gold that may be relevant to the development of redox active gold catalysis. First, C-C bond reductive elimination from Au(III) does not necessarily require phosphine dissociation. By avoiding this rate-limiting process, biaryl reductive eliminations from Au(III) are remarkably fast, and occur as low as –52 °C. Furthermore, by judicious choice of ligand, the barrier to oxidation of bimetallic Au(I) complexes may be reduced, allowing access to symmetric intermediates with Au(II)-Au(II) bonds. When stabilized by dppm, these complexes undergo fast isomerization and reductive elimination at very low temperature; when stabilized by more rigid PNP-type ligands, they may be arrested, although at slightly higher temperatures, isomerization and reductive elimination become facile.

The stoichiometric behavior of the complexes reported in this study inform the development of catalysis involving Au(I)/Au(III) redox cycling. For instance, that phosphine dissociation is not required for C-C bond formation may slow or entirely preclude deleterious ligand oxidation by excess oxidant under conditions relevant to catalysis. Given that transmetalation to Au(I) can be achieved at temperatures as low as –78 °C[50], and that Au(I) oxidation, isomerization and reductive elimination are facile processes below 0 °C, catalysis may be achieved at temperatures low enough to avoid unwanted side reactions between oxidant and substrate.

Experimental Information

General Considerations: Unless otherwise stated, all manipulations were carried out under an atmosphere of purified nitrogen in a Vacuum Atmospheres Corp. glovebox or with a double manifold vacuum line using standard Schlenk techniques. All glassware was dried at 150 ºC for 12 h prior to use. Solvents were dried by passage through a column of activated alumina under nitrogen pressure and degassed by sparging with dry nitrogen. CD_2Cl_2 was distilled from CaH_2 under nitrogen and stored over 4 Å molecular sieves prior to use. NMR spectra were recorded with Bruker AVB-400, DRX-500, AV-500 or AV-600 spectrometers, and chemical shifts are referenced to residual NMR solvent peaks (^{1}H and ^{13}C), $PhCF_3$ (^{19}F), or H_3PO_4 (^{31}P). Elemental analyses were performed at the College of Chemistry Microanalytical Laboratory, University of California, Berkeley. X-ray structural determinations were performed at CHEXRAY, University of California, Berkeley on Bruker SMART 1000 or SMART APEX diffractometers. Melting points were obtained using a Thomas-Hoover Unimelt Capillary Melting Point Apparatus and are uncorrected. UV-Vis data were recorded using a Varian Cary 50 Bio UV-Vis Spectrometer using a Quartz cuvette with a 1 mm path-length. GC/MS analysis was conducted using an Agilent 6890N GC system equipped with an Agilent DB-5MS column (30 m x 0.25 mm, 0.50 μm film).

The reagents $(Me_2S)AuCl$ and $PhICl_2$[68] were prepared according to literature procedures and stored in the dark at –20 ºC when not in use. The gold phosphine complexes $dppm(AuCl)_2$[69,70] $dppp(AuCl)_2$**Error! Bookmark not defined.** and Ph_3PAuCl[71] were prepared by reacting stoichiometric amounts of the appropriate phosphine at room temperature (20 ºC) with $(Me_2S)AuCl$ in CH_2Cl_2 followed by filtration, concentration *in vacuo*, washing with diethyl ether and drying *in vacuo*. The complex $Ph_3PAu(4\text{-}F\text{-}C_6H_4)$ was prepared according to the published procedure.[72] Other reagents were purchased from commercial suppliers and used as received.

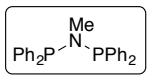

***N,N*-Bis(diphenylphosphino)methylamine**: To a suspension of methylaminehydrochloride (150 mg, 2.2 mmol, 1.0 equiv) and *N,N*-diisopropylethylamine (1.2 mL, 6.6 mmol, 3.0 equiv) in CH_2Cl_2 (10 mL) was added diphenylchlorophosphine (1.1 g, 0.9 mL, 5.0 mmol, 2.3 equiv) dropwise at 20 ºC. The resulting reaction mixture was stirred for 14 h, after which time the solvent was removed *in vacuo*. Diethyl ether (3 x 5 mL) was added to extract the ligand from the insoluble ammonium salt. The ether washes were combined by passage through a short plug of basic alumina. The combined washes were then passed through two more sequential basic alumina plugs and then

concentrated to dryness to yield the desired compound as a white powder (650 mg, 74 %). Spectroscopic data are in agreement with those values previously published.[73,74]

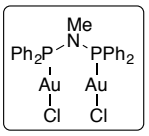

(*N*,*N*-Bis(diphenylphosphino)methylamine) bis(chlorogold): A solution of $(Me_2S)AuCl$ (738 mg, 2.51 mmol, 2.00 equiv) in CH_2Cl_2 (10 mL) was added to a solution of *N*,*N*-bis(diphenylphosphine)methylamine (500 mg, 1.25 mmol, 1.00 equiv). The resulting solution was magnetically stirred for 0.5 h at 20 ºC and then filtered through a glass fiber filter. The filtrate was concentrated to dryness *in vacuo* to give a white solid which was washed with diethyl ether and dried to yield the desired compound (1.03 g, 95 %). **^{1}H NMR** (CD_2Cl_2, 600 MHz, δ): 7.68 – 7.57 (m, 20H), 2.48 (t, *J* = 7.2 Hz, 3H). **^{13}C{^{1}H} NMR** (CD_2Cl_2, 101 MHz, δ): 133.2 (t, *J* = 7.8 Hz), 133.0 , 129.6 (t, *J* = 6.2 Hz), 128.6 (t, *J* = 34 Hz), 34.5 (t, *J* = 2.1 Hz). **^{31}P{^{1}H} NMR** (CD_2Cl_2, 242 MHz, δ): 84.5 (s). **Anal. Calcd.** for $C_{25}H_{23}Au_2Cl_2NP_2$: C, 34.74; H, 2.68; N, 1.62. Found: C, 34.37; H, 2.66; N, 1.54. **Melting Point:** 127 ºC (decomposition).

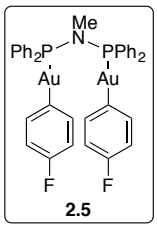

(*N*,*N*-Bis(diphenylphosphino)methylamine) bis(4-fluorophenylgold) (2.5): To a cold (–78 ºC) suspension of (*N*,*N*-Bis(diphenylphosphino)methylamine) bis(chlorogold) (100 mg, 0.12 mmol, 1.0 equiv) in THF (2 mL) was added 4-F-C_6H_4MgBr (0.66 M in THF, 1.1 mL, 0.72 mmol, 6.0 equiv) dropwise with stirring over 10 min. The reaction mixture was stirred at –78 ºC for 30 min, then warmed to 0 ºC and stirred for 1 h. The reaction was quenched at 0 ºC with sat. aq. NH_4Cl and benzene (5 mL) was added. The layers were quickly separated and the aqueous layer was washed with additional benzene (2 x 5 mL). The combined organics were dried over $MgSO_4$, filtered, and concentrated to dryness *in vacuo*. The residue was recrystallized from CH_2Cl_2/Et_2O to yield **2.5** as a white powder (110 mg, 93 %). Crystals suitable for X-ray diffraction were grown by vapor diffusion of hexane vapors into a saturated 1,2-dichloroethane solution. **^{1}H NMR** (CD_2Cl_2, 500 MHz, δ): 7.78 – 7.75 (m, 8H), 7.67 – 7.60 (m, 12H), 7.19 (d, *J* = 7.5 Hz, 4H), 6.78 (d, *J* = 9 Hz, 4H), 2.48 (t, *J* = 7.0 Hz, 3H). **^{13}C{^{1}H} NMR** (CD_2Cl_2, 125 MHz, δ): 165.4 (d, *J* = 125 Hz), 161.2 (d, *J* = 241.5 Hz), 140.7 (d, *J* = 5.3 Hz), 133.3 (t, *J* = 7.7 Hz), 132.0, 131.5 (t, *J* = 26.7 Hz), 129.2 (t, *J* = 5.4 Hz), 113.2 (d, *J* = 17.4 Hz), 35.2 (t, *J* = 3.5 Hz). **^{31}P{^{1}H} NMR** (CD_2Cl_2, 202 MHz, δ): 97.3 (s). **^{19}F NMR** (CD_2Cl_2, 470 MHz, δ): –118.0 (s). **Anal. Calcd.** for $C_{37}H_{31}F_2Au_2NP_2$: C, 45.18; H, 3.18; N, 1.42. Found: C, 44.79; H, 3.03; N, 1.37. **Melting Point:** 135 ºC (decomposition).

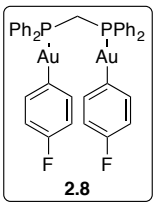

1,1-Bis(diphenylphosphino)methane) bis(4-fluorophenylgold) (2.8): To a cold (–78 ºC) suspension of $dppm(AuCl)_2$ (220 mg, 0.26 mmol, 1.0 equiv) in THF (6 mL) was added 4-F-C_6H_4MgBr (1.0 M in THF, 1.6 mL, 1.6 mmol, 6.2 equiv) dropwise with stirring. The resulting homogeneous solution was stirred at –78 ºC for 30 min, then warmed to 0 ºC and stirred for 1 h. The reaction was quenched at 0 ºC with sat. aq. NH_4Cl and benzene (5 mL) was added. The layers were quickly separated and the aqueous layer was extracted with additional benzene (2 x 5 mL). The combined organic layers were dried over $MgSO_4$, filtered and concentrated to dryness *in vacuo*. The residue was washed with diethyl ether (5 mL) and dried to afford **2.8** as a white solid (190 mg, 75 %). Crystals suitable for X-ray diffraction were grown by layering a saturated CH_2Cl_2 solution with hexanes. **^{1}H NMR** (CD_2Cl_2, 500 MHz, δ): 7.80 – 7.72 (m, 6H), 7.52 – 7.45 (m, 4H), 7.44 – 7.38 (m, 10H), 7.36 –7.30 (m, 4H), 6.84 (t, *J* = 5Hz, 4H), 3.70 (t, *J* = 10 Hz, 2H).

$^{13}C\{^1H\}$ NMR (CD_2Cl_2, 125 MHz, δ): 167.6 (d, J = 118.8 Hz), 161.3 (d, J = 241.7 Hz), 140.6 (d, J = 5.4 Hz), 133.5 (t, J = 7.0 Hz), 131.6, 131.2 (d, J = 26.5 Hz), 129.2 (t, J = 5.5 Hz), 113.4 (d, J = 17.6 Hz), 29.8 (t, J = 23.0 Hz). **$^{31}P\{^1H\}$ NMR** (CD_2Cl_2, 202 MHz, δ): 31.8 (s). **^{19}F NMR** (CD_2Cl_2, 470 MHz, δ): –117.8 (s). **Anal. Calcd.** for $C_{37}H_{30}P_2F_2Au_2$: C, 45.88; H, 3.12. Found: C, 45.93; H, 3.13. **Melting point:** 150 ºC (decomposition).

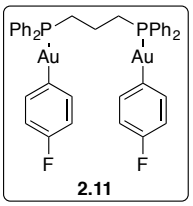

2.11

1,3-Bis(diphenylphosphino)propane) bis(4-fluorophenylgold) (2.11): To a cold (–78 ºC) suspension of dppp$(AuCl)_2$ (66.7 mg, 0.076 mmol, 1.00 equiv) in THF (5 mL) was added 4-F-C_6H_4MgBr (0.37 M in THF, 2.2 mL, 0.80 mmol, 5.7 equiv) dropwise with stirring. The reaction mixture was stirred at –78 ºC for 30 min, then warmed to 0 ºC and stirred for 1 h. The reaction was quenched at 0 ºC with sat. aq. NH_4Cl and benzene (5 mL) was added. The layers were quickly separated and the aqueous layer was washed with additional benzene (2 x 5 mL). The combined organics were dried over $MgSO_4$, filtered, and concentrated to dryness *in vacuo* to yield **2.11** (55 mg, 72 %). Crystals suitable for X-ray diffraction were grown by layering hexanes onto a saturated solution in CH_2Cl_2. **^1H NMR** (CD_2Cl_2, 500 MHz, δ): 7.76 – 7.72 (m, 8H), 7.49 – 7.43 (m, 12H), 7.41 – 7.39 (m, 4H), 6.88 (t, J = 9.5 Hz, 4H), 3.06 – 3.01 (m, 4H), 2.00 – 1.91 (m, 2H). **$^{13}C\{^1H\}$ NMR** (CD_2Cl_2, 125 MHz, δ): 168.4 (d, $J_{C\text{-}P}$ = 125.0 Hz), 162.0 (d, $J_{C\text{-}F}$ = 237.5 Hz), 141.0 (d, J = 5.4 Hz), 134.1 (d, J = 13.8 Hz), 131.8, 131.4, 129.6 (d, J = 10.0 Hz), 114.1 (dd, J = 17.5 Hz, 6.3 Hz), 28.8 (dd, J = 28.8 Hz, 8.8 Hz), 19.9. **$^{31}P\{^1H\}$ NMR** (CD_2Cl_2, 202 MHz, δ): 34.0 (s). **^{19}F NMR** (CD_2Cl_2, 470 MHz, δ): –117.3 (s). **Anal. Calcd.** for $C_{39}H_{34}P_2F_2Au_2$: C, 47.00; H, 3.44. Found: C, 47.19; H, 3.72. **Melting point:** 105 ºC (decomposition).

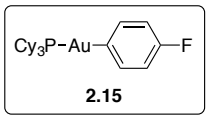

2.15

To a cold (–78 ºC) suspension of $(Cy_3P)AuCl$ (250 mg, 0.49 mmol, 1.00 equiv) in THF was added 4-F-C_6H_4MgBr (1.0 M in THF, 2 equiv) dropwise via syringe. The resulting solution was stirred at –78 ºC for 1 h then warmed to 0 ºC and stirred for 1 h. The reaction was quenched with water at 0 ºC and extracted into CH_2Cl_2 (5 mL). The layers were separated and the aqueous phase was washed with additional CH_2Cl_2 (5 mL). The combined organic layers were washed with water (5 mL) and dried over Na_2SO_4, filtered and concentrated to dryness *in vacuo*. Recrystallization from CH_2Cl_2/hexanes yielded the desired compound as colorless needles (220 mg, 79 %). **^1H NMR** (CD_2Cl_2, 400 MHz, δ): 7.39 (td, J = 7.6, 4.7 Hz, 2H), 6.98 – 6.84 (m, 2H), 2.05 (tq, J = 9.4, 3.0 Hz, 9H), 1.86 (dt, J = 10.2, 3.4 Hz, 6H), 1.79 – 1.64 (m, 3H), 1.53 (dtd, J = 16.1, 12.2, 10.3, 5.4 Hz, 6H), 1.42 – 1.23 (m, 9H). **$^{13}C\{^1H\}$ NMR** (CD_2Cl_2,126 MHz, δ): 172.6 (d, J = 109 Hz), 161.2 (d, J = 238 Hz), 139.70, (d, J = 5 Hz), 113.5 (dd, J = 17.5, 6.25 Hz), 33.2 (d, J = 23.8 Hz), 30.73, 27.2 (d, J = 11.3 Hz), 26.10. **$^{31}P\{^1H\}$ NMR** (CD_2Cl_2, 162 MHz, δ): 57.2 ppm (s). **^{19}F NMR** (CD_2Cl_2, 376 MHz, δ): –117.0 ppm (s). **Anal. Calcd.** for $C_{24}H_{37}AuPF$: C, 50.35; H, 6.51. Found: C, 50.41; H, 6.29.

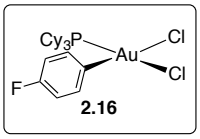

2.16

To a solution of **2.15** (105 mg, 0.183 mmol, 1.00 equiv) in CH_2Cl_2 (1 mL) was added a solution of $PhICl_2$ (50.4 mg, 0.183 mmol, 1.00 equiv) in CH_2Cl_2 (1 mL) at 20 ºC. The resulting solution was stirred for 20 min, then filtered through a glass fiber filter and concentrated to ca. 1 mL. Pentane was added to precipitate the product as colorless microcrystals (94 mg, 80 %). Complex **2** can be recrystallized as the CH_2Cl_2 solvate by layering hexanes onto a saturated solution in CH_2Cl_2: these crystals

were suitable for X-ray diffraction. **^{1}H NMR** (CD_2Cl_2, 400 MHz, δ): 7.35 – 7.27 (m, 2H), 7.03 (t, *J* = 6.8 Hz, 2H), 2.48 (q, *J* = 12 Hz, 3H), 2.01 – 1.90 (m, 6H), 1.89 – 1.78 (m, 6H), 1.77 – 1.64 (m, 9H), 1.28 (qt, *J* = 13.0, 3.6 Hz, 3H), 1.10 (qt, *J* = 12.9, 3.4 Hz, 6H). **^{13}C{^{1}H} NMR** (CD_2Cl_2, 125 MHz, δ): 161.2 (d, *J* = 245.2 Hz), 137.1, 132.8 (d, *J* = 6.5 Hz), 116.6 (d, *J* = 21.0 Hz), 35.2 (d, *J* = 27.2 Hz), 29.3 (d, *J* = 3.5 Hz), 27.1 (d, *J* = 12.0 Hz), 25.7. **^{31}P{^{1}H} NMR** (CD_2Cl_2, 162 MHz, δ): 49.3 ppm (s). **^{19}F NMR** (CD_2Cl_2, 376 MHz, δ): –117.3 ppm (s). **Anal. Calcd.** for $C_{24}H_{37}AuPFCl_2 \bullet CH_2Cl_2$: C, 41.23; H, 5.40. Found: C, 41.71; H, 5.42.

Kinetic Experiments: Kinetic experiments were performed using NMR techniques on a Bruker DRX-500 spectrometer equipped with a 5 mm Z-gradient broadband probe. A reported rate constant represents the average of two or more experiments. An NMR tube was charged with 0.3 mL of a 0.027 M stock solution of **2.3** (containing 0.016 M $PhCF_3$ NMR standard) and sealed with a rubber septum, which was secured using Teflon tape. The NMR tube was then taken out of the glovebox and immersed in liquid nitrogen to freeze the solution (Caution: the tube must be sealed well to prevent condensation of O_2 in the cooled tube). To this frozen sample was added 0.2 mL of a 0.041 M stock solution of $PhICl_2$ in CD_2Cl_2 via syringe (final sample volume: 0.5 mL). After the addition was complete, the NMR tube was immediately transferred to a dry ice/acetone bath and allowed to warm to –78 ºC. The tube was shaken to ensure mixing and then quickly transferred into the probe which was precooled to the desired temperature. The temperature of the probe was calibrated using a CH_3OH standard. The production of 4,4'-difluorobiphenyl was confirmed by GC/MS and by comparison to the ^{19}F chemical shift of an authentic sample in CD_2Cl_2.[75]
NMR spectra were phased and integrated using Bruker TopSpin software. Experimental kinetic data was analyzed and plotted using Kaleidagraph v. 4.0 and modeled using Mathematica v. 9.0.1.

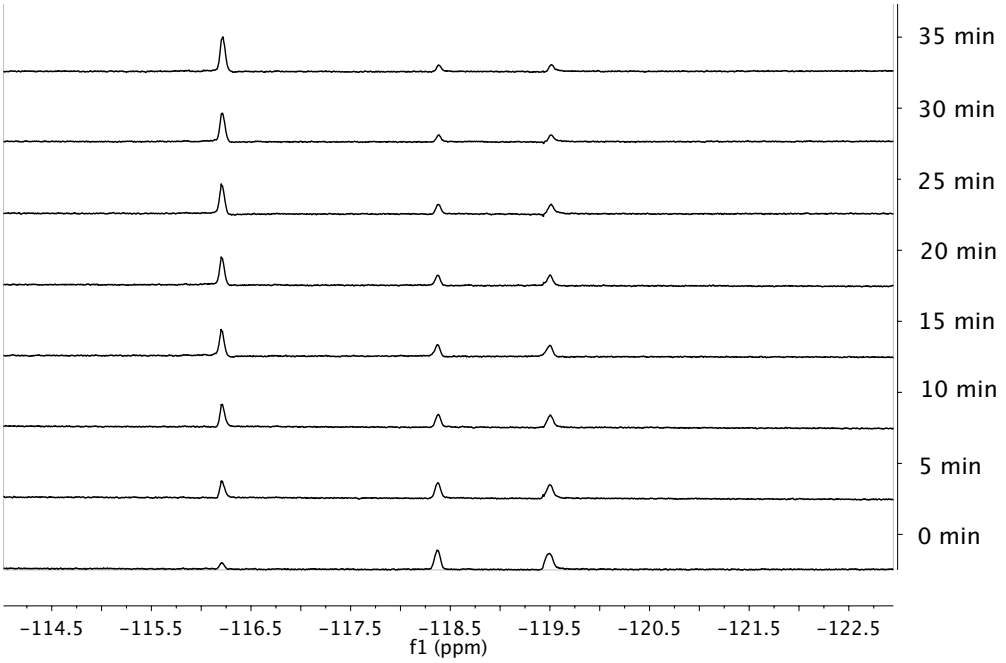

Figure 2.20. ^{19}F NMR spectra showing consumption of **2.3** (δ –118.4, –119.4 ppm) and formation of 4,4'-difluorobiphenyl (δ –116.4 ppm) at –52 ºC, referenced to $PhCF_3$ (δ –62.8 ppm).

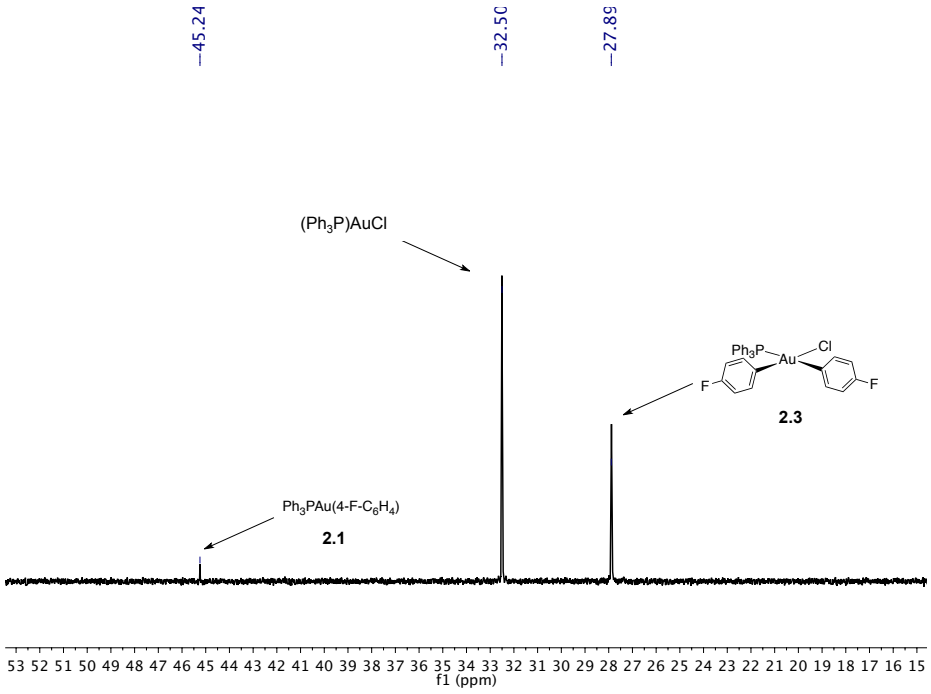

Figure 2.21. ^{31}P NMR spectrum of **2.1** upon treatment with $PhICl_2$ to generate PPh_3AuCl and **2.3** at –52 ºC (CD_2Cl_2, 202 MHz).

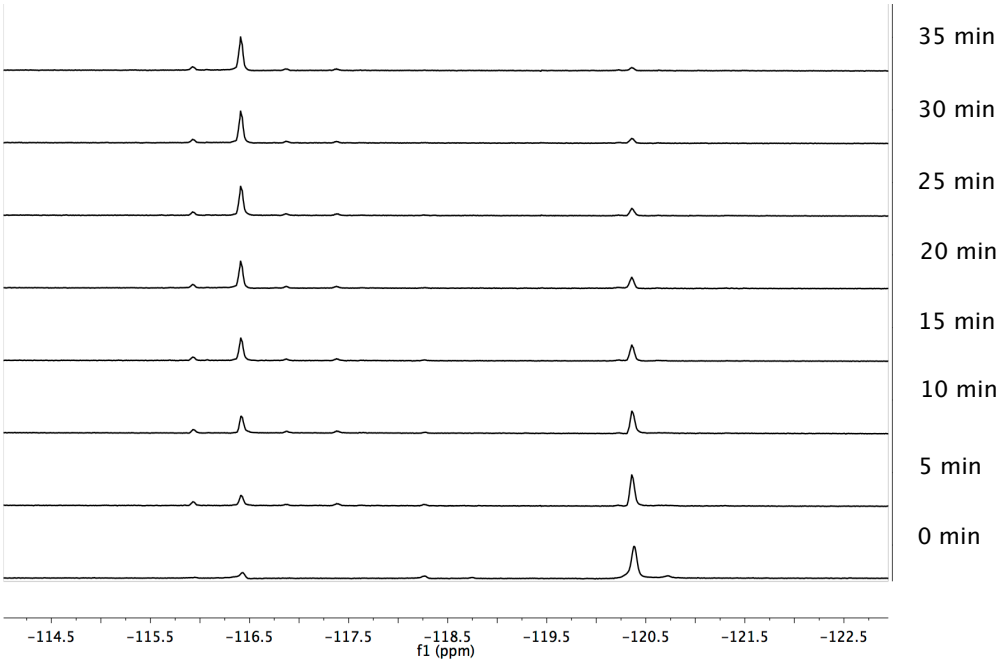

Figure 2.22. ^{19}F NMR spectra showing consumption of **2.6** (δ –120.4 ppm) and formation of 4,4'-difluorobiphenyl (δ –116.4 ppm) at –10 ºC, referenced to $PhCF_3$ (δ –62.8 ppm).

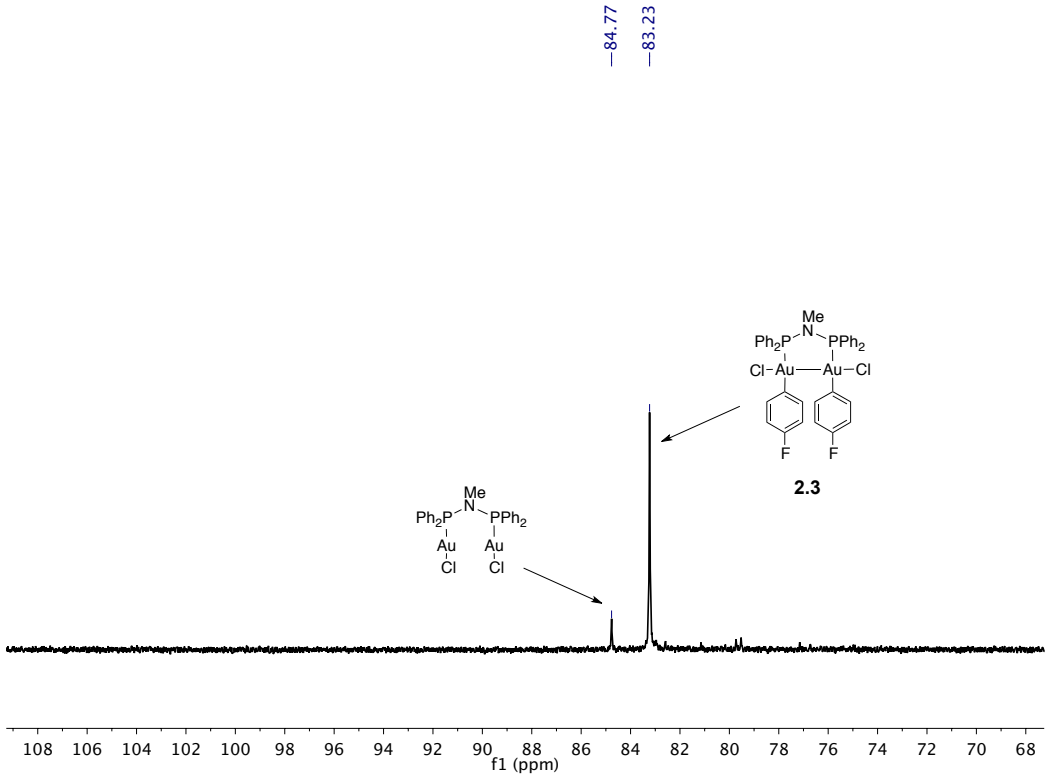

Figure 2.23. ^{31}P NMR spectrum of **5** upon treatment with $PhICl_2$ to generate **2.6** at –52 ºC (CD_2Cl_2, 202 MHz).

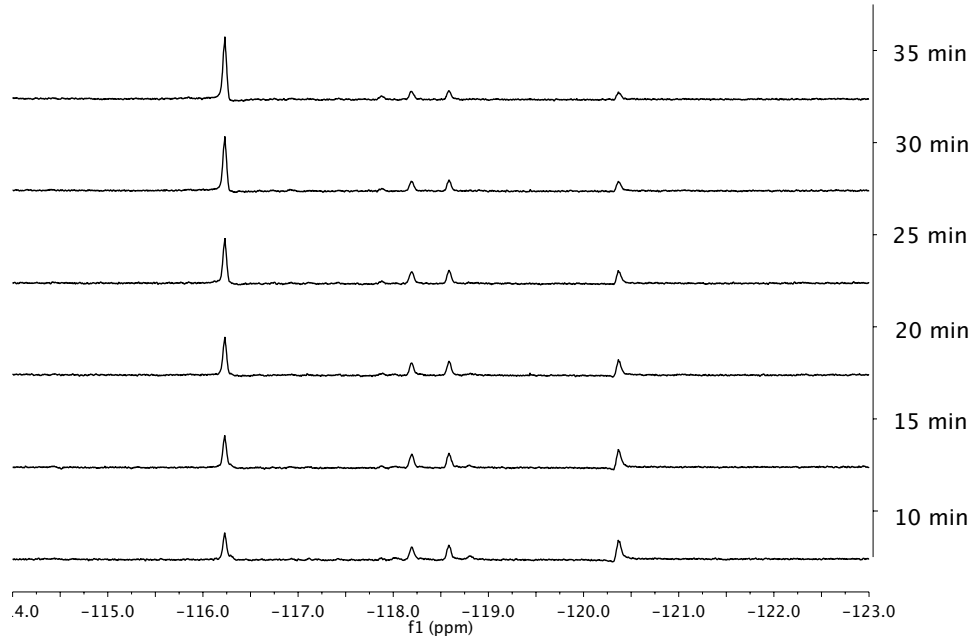

Figure 2.24. ^{19}F NMR spectra showing consumption of **2.10** (δ –120.4 ppm) and **2.11** (δ –118.2, –118.6 ppm) and formation of 4,4'-difluorobiphenyl (δ –116.4 ppm) at –52 ºC, referenced to $PhCF_3$ (δ –62.8 ppm).

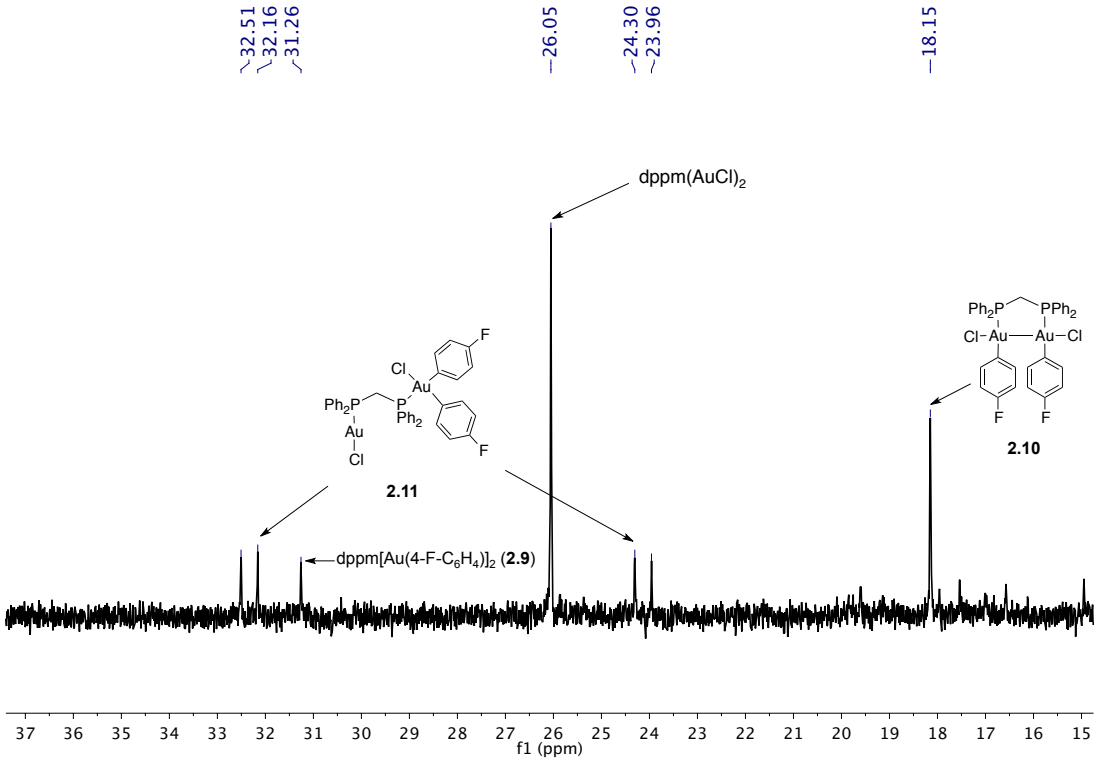

Figure 2.25. ^{31}P NMR spectrum of **2.9** upon treatment with $PhICl_2$ to generate **2.10** and **2.11** at –70 ºC (202 MHz, CD_2Cl_2).

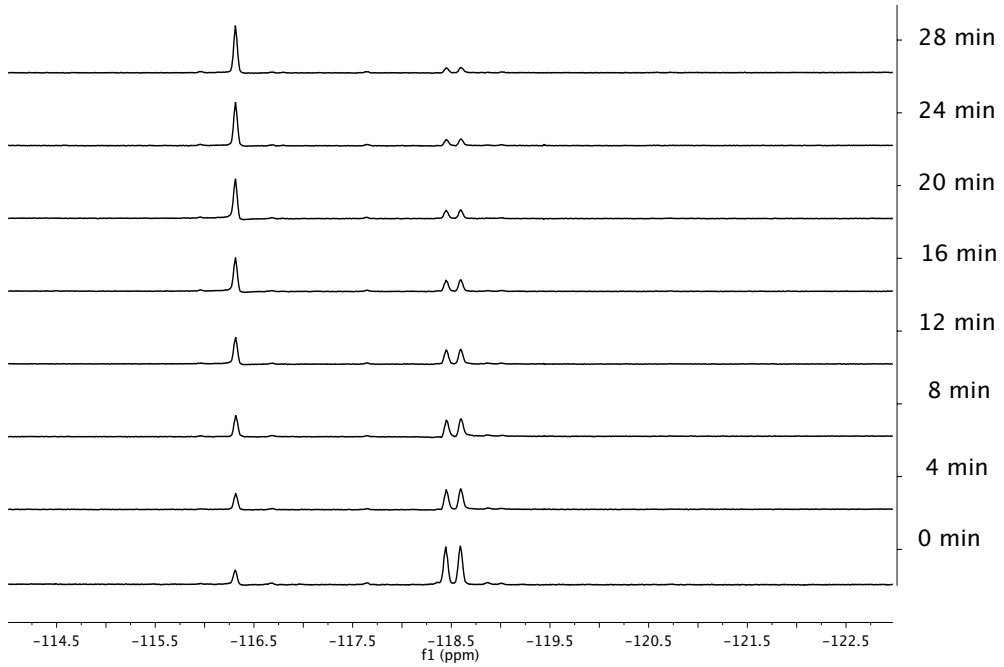

Figure 2.26. ^{19}F NMR spectra showing consumption of **2.13** (δ –118.3, –118.6 ppm) and formation of 4,4'-difluorobiphenyl (δ –116.4 ppm) at –32 ºC, referenced to $PhCF_3$ (δ –62.8 ppm).

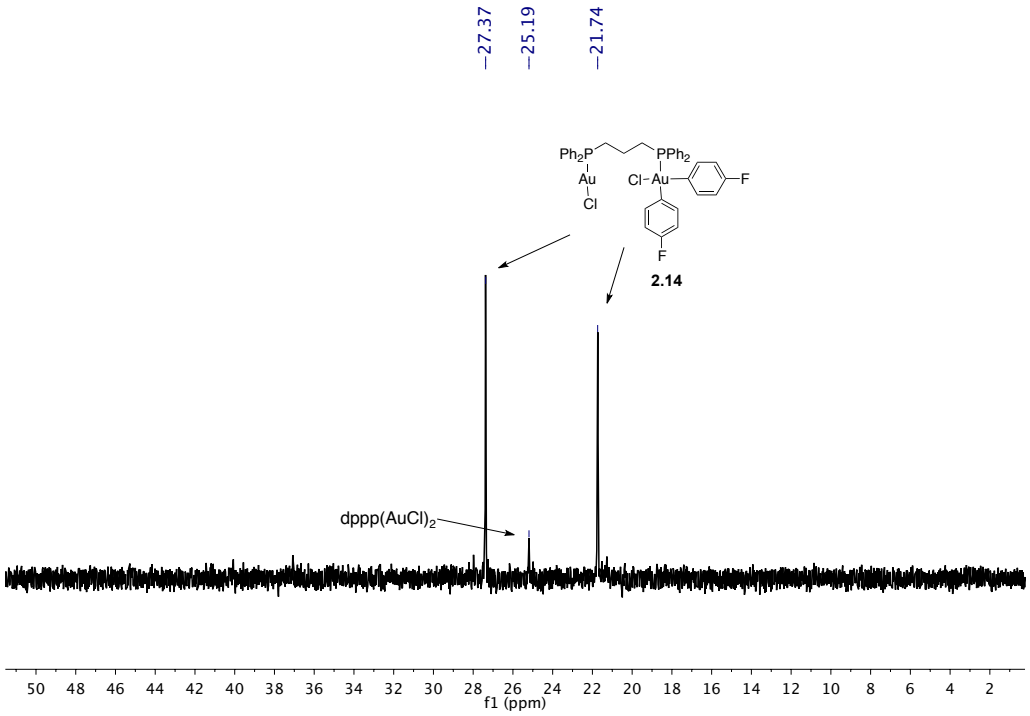

Figure 2.27. ^{31}P NMR spectrum of **2.12** upon treatment with $PhICl_2$ to generate **2.14** at –53 ºC (CD_2Cl_2, 202 MHz).

Table 2.1. ^{31}P (202 MHz) and ^{19}F NMR (470 MHz) shifts of Au(III) and Au(II) intermediates (–52 ºC, CD_2Cl_2).

Complex	^{31}P NMR (δ)	^{19}F NMR (δ)
2.3	27.9 ppm	–118.4, –119.4 ppm
2.7	83.2 ppm	–120.4 ppm
2.10	18.2 ppm	–120.4 ppm
2.11	32.3 (d, J =70.7 Hz), 24.1 (d, J = 68.7 Hz) ppm	–118.2, –118.6 ppm
2.14	27.4, 21.8 ppm	–118.3, –118.6 ppm

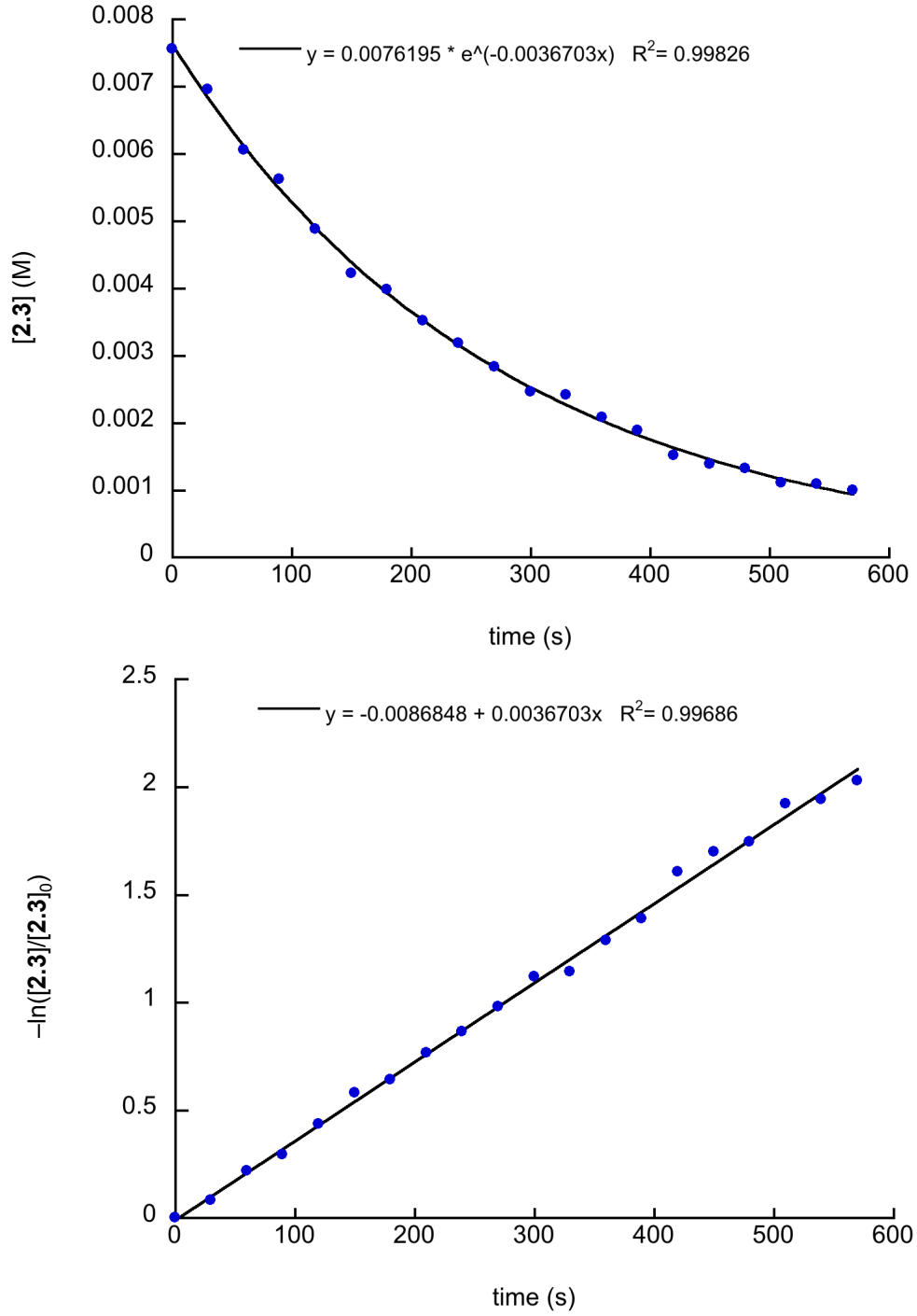

Figure 2.28. Representative plots of [**2.3**] against time (top) and of –ln([**2.3**]/[**2.3**]$_0$) against time (bottom) at –33 ºC.

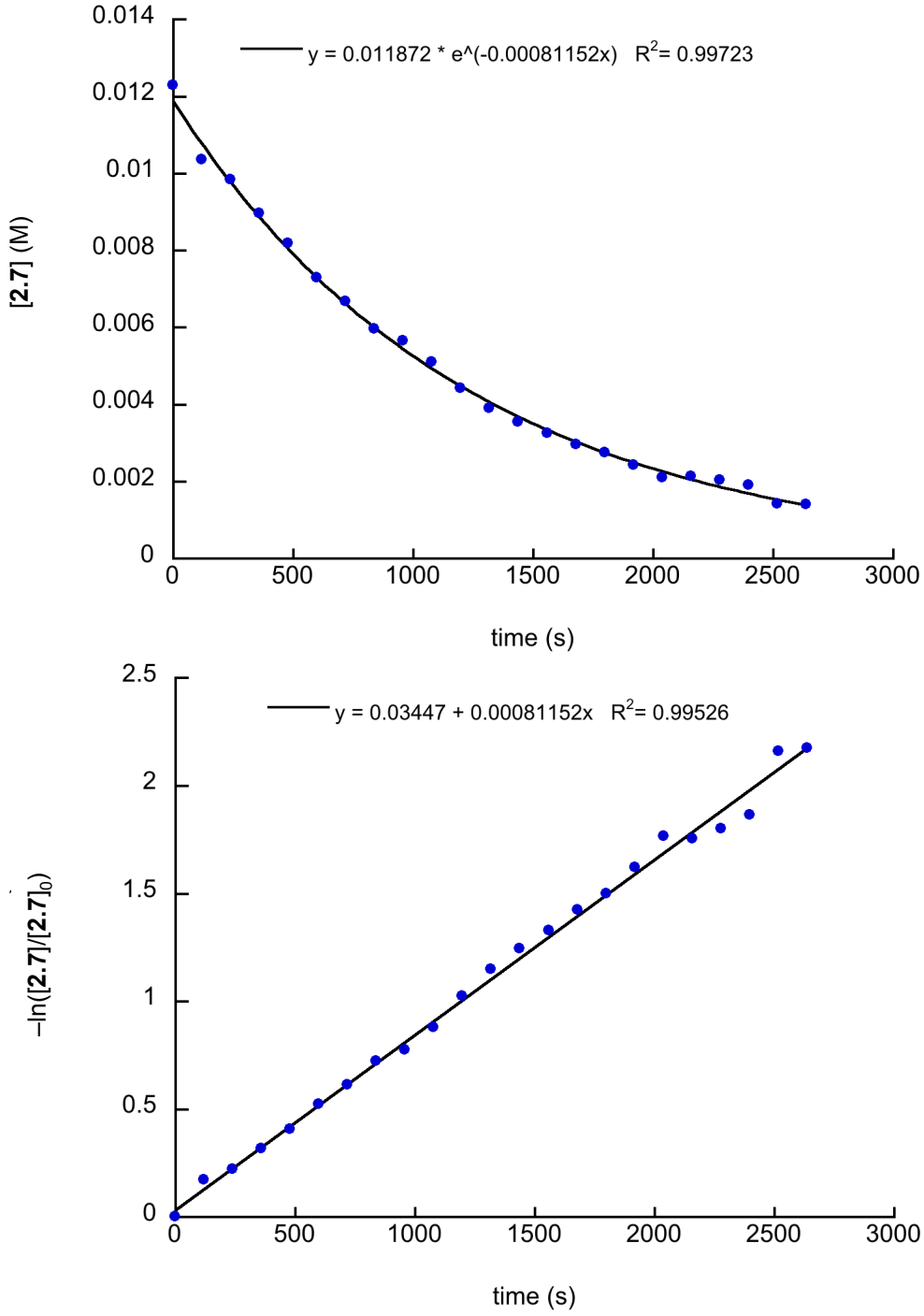

Figure 2.29. Representative plots of [**2.7**] against time (top) and of –ln([**2.7**]/[**2.7**]$_0$) against time (bottom) at –12 ºC.

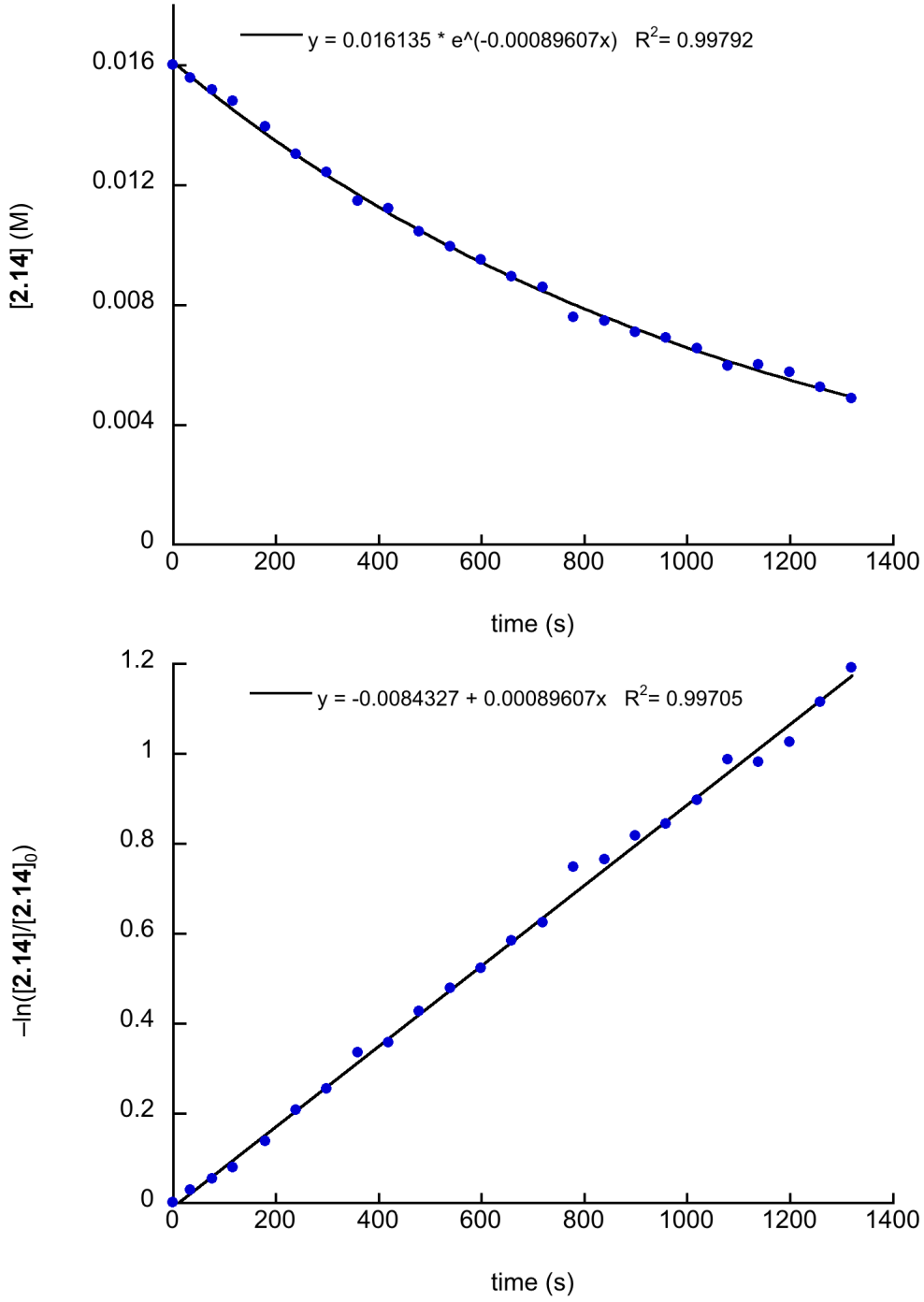

Figure 2.30. Representative plots of [**2.14**] against time (top) and of –ln([**2.14**]/[**2.14**]$_0$) against time (bottom) at –32 ºC.

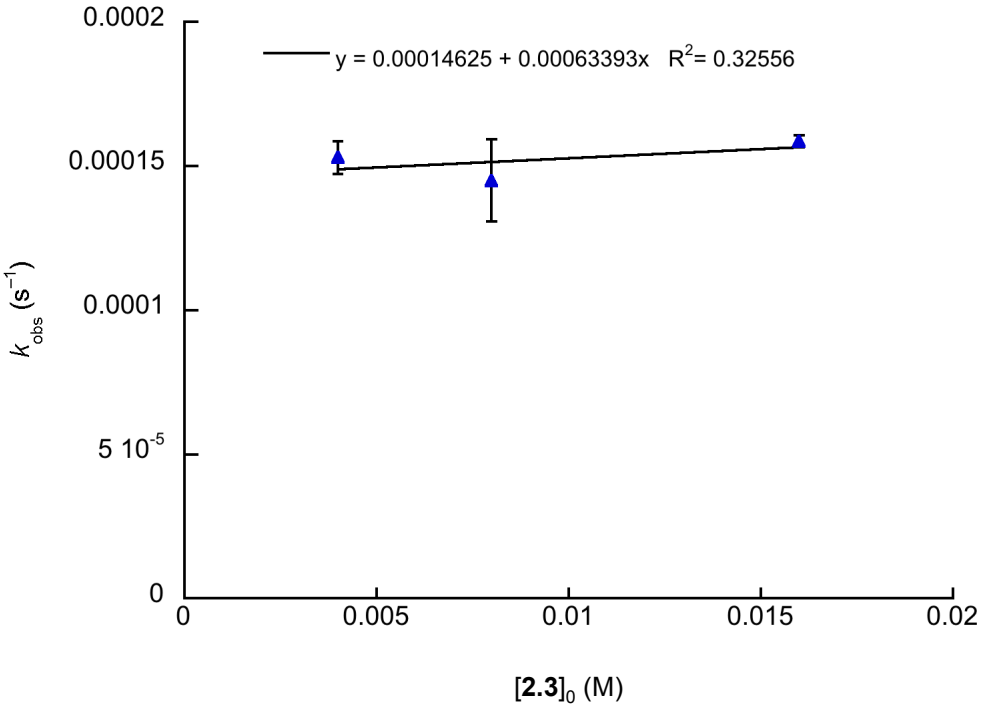

Figure 2.31. Plot of observed rate constants (k_{obs}) at –52 ºC against initial [**2.3**] showing first-order behavior for the decay of **2.3**.

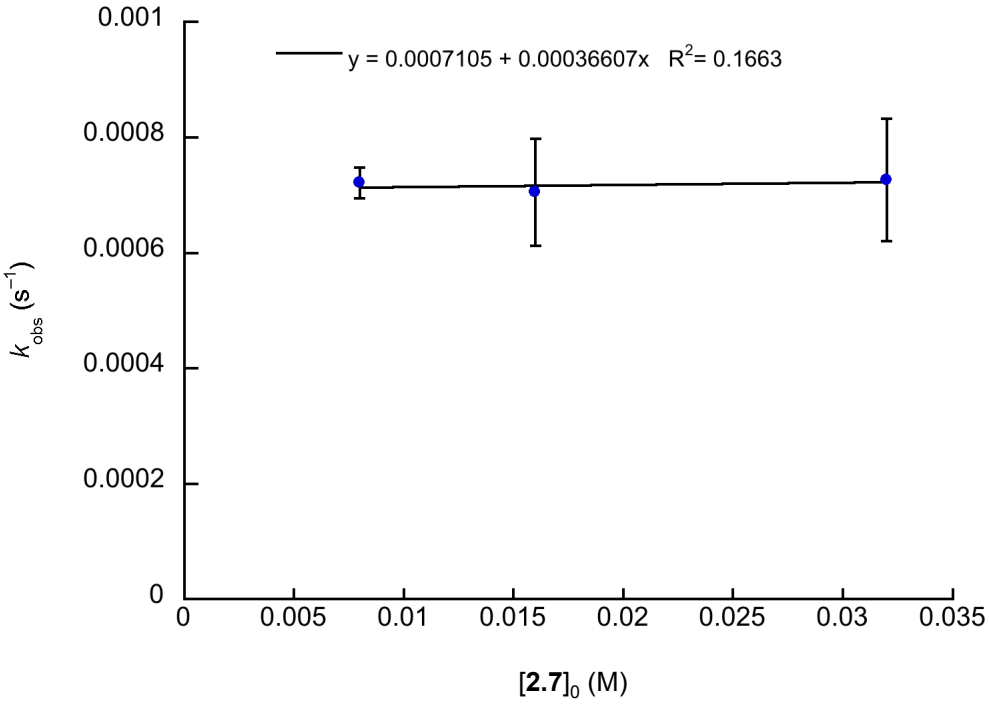

Figure 2.32. Plot of observed rate constants (k_{obs}) at –12 ºC against initial [**2.7**] showing first-order behavior for the decay of **2.7**.

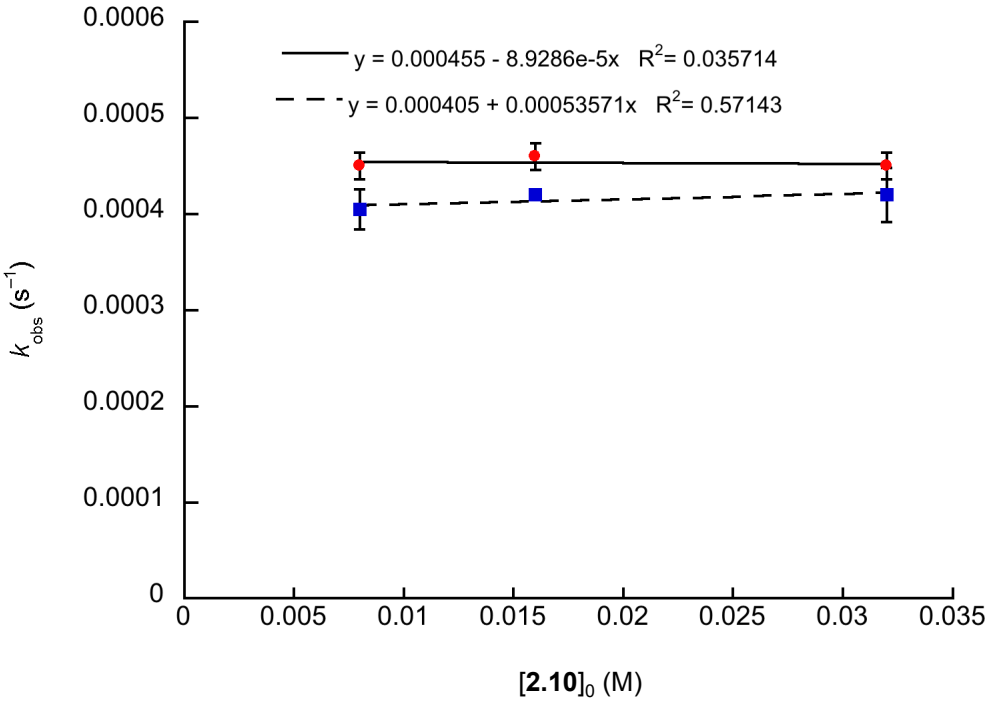

Figure 2.33. Plot of rate constants (k) at –52 ºC against initial [**2.10**] showing first-order behavior for the decay of **2.10** (•) and **2.11** (■).

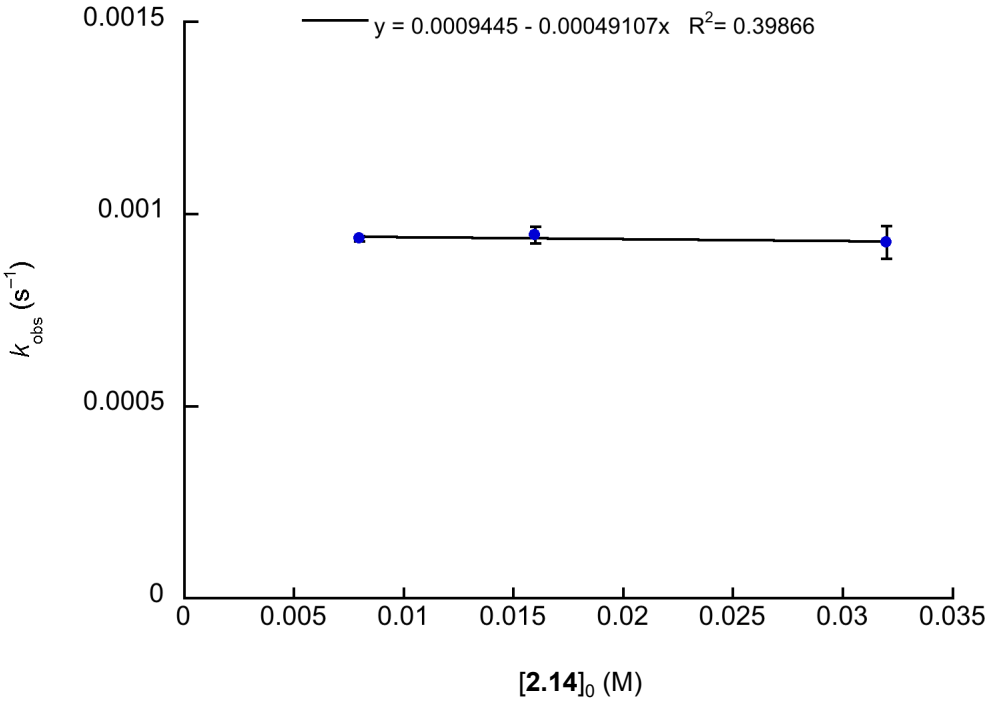

Figure 2.34. Plot of observed rate constants (k_{obs}) at –32 ºC against initial [**2.14**] showing first-order behavior for the decay of **2.14**.

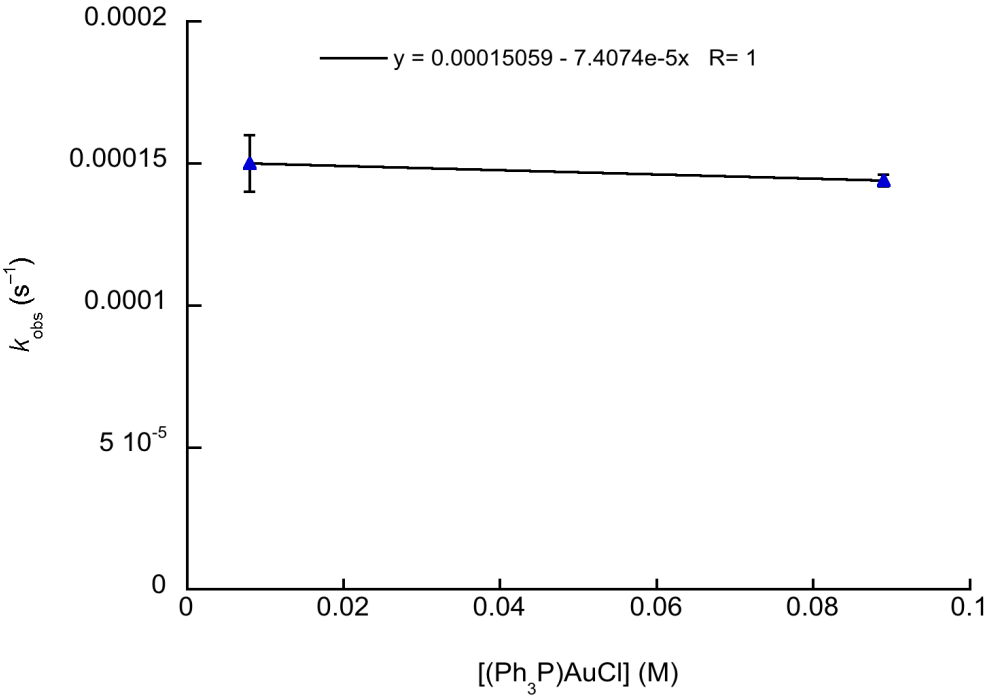

Figure 2.35. Plot of observed rate constants (k_{obs}) at –52 ºC for the reductive elimination from **2.3** against added (Ph_3P)AuCl.

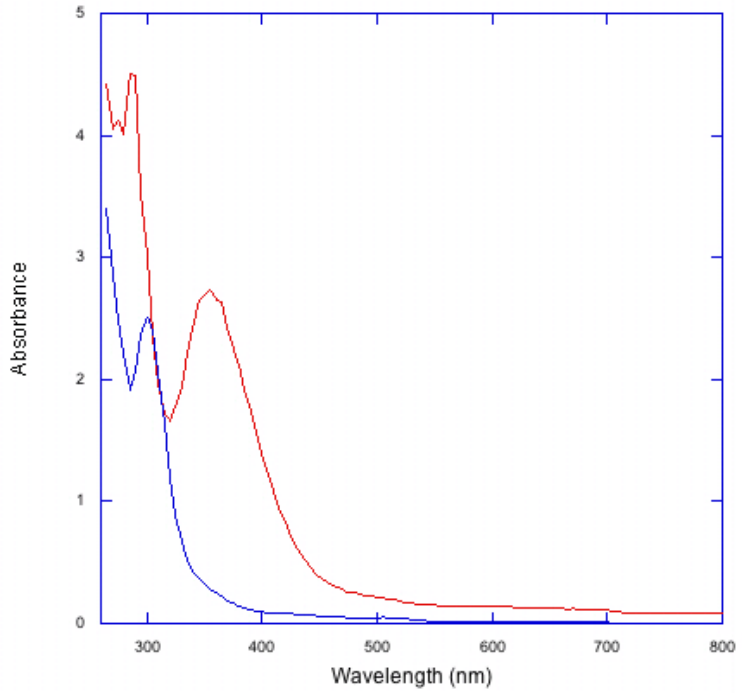

Figure 2.36. UV-Vis spectra of **2.7** (1.53 mmol/L, CH_2Cl_2, –50 ºC, red trace) showing a band at 354 nm that is absent following reductive elimination to form 4,4'-difluorobiphenyl and $(MeN(PPh_2))(AuCl)_2$ (blue trace).

Kinetic Modeling of Reductive Elimination from 2.4

For the following reaction (under pseudo-first order conditions):

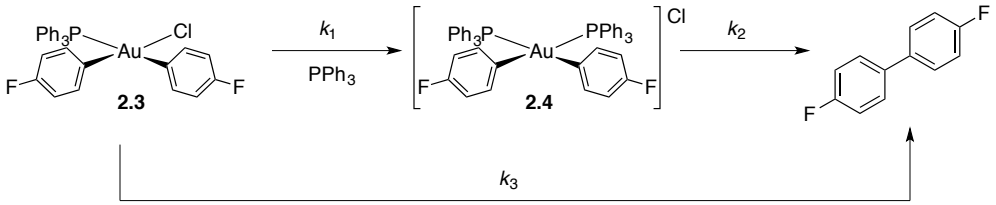

$$\frac{d[\mathbf{2.3}]}{dt} = -k_1[PPh_3][\mathbf{2.3}] - k_3[\mathbf{2.3}]$$

$$= -(k_1[PPh_3] + k_3)[\mathbf{2.3}]$$

$$= -k_{obs}[\mathbf{2.3}]$$

$$k_{obs} = k_1[PPh_3] + k_3$$

$$k_1 = \frac{k_{obs} - k_3}{[PPh_3]}$$

$$= \frac{(6.2 \times 10^{-3}\ s^{-1}) - (1.5 \times 10^{-4}\ s^{-1})}{(0.32\ M)} \quad \text{for } [\mathbf{2.3}] = 0.008\ M,\ 40 \text{ equiv } PPh_3$$

$$= 0.018\ M^{-1}s^{-1}$$

The lower limit for the rate constant (k_3) for the reductive elimination of **2.4** was calculated with the assumption that the $[\mathbf{2.4}]_{max} \leq 200$ mM (experimentally-determined lower limit of detection of Bruker DRX-500 for ^{19}F nucleus).

$$\frac{d[\mathbf{2.4}]}{dt} = k_1[PPh_3][\mathbf{2.3}] - k_2[\mathbf{2.4}]$$

$$[\mathbf{2.3}] = [\mathbf{2.3}]_0 e^{-k_{obs}t}$$

$$= k_1[PPh_3][\mathbf{2.3}]_0 e^{-k_{obs}t} - k_2[\mathbf{2.4}] = 0 \text{ using the steady state approximation}$$

$$k_2[\mathbf{2.4}] = k_1[PPh_3][\mathbf{2.3}]_0 e^{-k_{obs}t}$$

$$k_2 = \frac{k_1[PPh_3][\mathbf{2.3}]_0 e^{-k_{obs}t}}{[\mathbf{2.4}]}$$

$$\frac{d[\mathbf{2.4}]}{dt} = k_1[PPh_3][\mathbf{2.3}] - k_2[\mathbf{2.4}]$$

$$\frac{d[\mathbf{2.4}]}{dt} + k_2[\mathbf{2.4}] = k_1[PPh_3][\mathbf{2.3}]$$

$$e^{k_2 t}\frac{d[\mathbf{2.4}]}{dt} + e^{k_2 t}k_2[\mathbf{2.4}] = k_1[PPh_3][\mathbf{2.3}]_0 e^{-k_{obs}t}e^{k_2 t}$$

$$\frac{d([\mathbf{2.4}]e^{k_2 t})}{dt} = k_1[PPh_3][\mathbf{2.3}]_0 e^{(k_2 - k_{obs})t}$$

$$\int \frac{d([\mathbf{2.4}]e^{k_2 t})}{dt} = \int k_1[PPh_3][\mathbf{2.3}]_0 e^{(k_2 - k_{obs})t}$$

$$[\mathbf{2.4}]e^{k_2 t} = \frac{k_1[PPh_3][\mathbf{2.3}]_0 e^{(k_2 - k_{obs})t}}{k_2 - k_{obs}} + C$$

$$[\mathbf{2.4}] = \frac{k_1[PPh_3][\mathbf{2.3}]_0 e^{(-k_{obs})t}}{k_2 - k_{obs}} + Ce^{-k_2 t}$$

$$[\mathbf{2.4}] = [\mathbf{2.4}]_0 = 0 \text{ at } t = 0$$

$$[\mathbf{2.4}] = \frac{k_1[PPh_3][\mathbf{2.3}]_0}{k_2 - k_{obs}} + C = 0$$

$$C = -\frac{k_1[PPh_3][\mathbf{2.3}]_0}{k_2 - k_{obs}}$$

$$[\mathbf{2.4}] = \frac{k_1[PPh_3][\mathbf{2.3}]_0 e^{(-k_{obs})t}}{k_2 - k_{obs}} - \frac{k_1[PPh_3][\mathbf{2.3}]_0}{k_2 - k_{obs}} e^{-k_2 t}$$

$$[\mathbf{2.4}] = \frac{k_1[PPh_3][\mathbf{2.3}]_0}{k_2 - k_{obs}} \left(e^{-k_{obs}t} - e^{-k_2 t}\right)$$

$$\frac{d[\mathbf{2.4}]}{dt} = \frac{k_1[PPh_3][\mathbf{2.3}]_0}{k_2 - k_{obs}} \left(-k_{obs}e^{-k_{obs}t} + k_2 e^{-k_2 t}\right) = 0$$

$$-k_{obs}e^{-k_{obs}t} + k_2 e^{-k_2 t} = 0$$

$$k_2 e^{-k_2 t} = k_{obs}e^{-k_{obs}t}$$

$$\frac{k_{obs}}{k_2} = e^{(k_{obs} - k_2)t}$$

$$\ln \frac{k_{obs}}{k_2} = (k_{obs} - k_2)t$$

$$\frac{\ln \frac{k_{obs}}{k_2}}{(k_{obs} - k_2)} = t = t_{max} \text{ when } [\mathbf{2.4}] \text{ is } [\mathbf{2.4}]_{max}$$

$$[\mathbf{2.4}]_{max} = \frac{k_1[PPh_3][\mathbf{2.3}]_0}{k_2 - k_{obs}} \left(e^{-k_{obs}\left(\frac{\ln \frac{k_{obs}}{k_2}}{(k_{obs} - k_2)}\right)} - e^{-k_2\left(\frac{\ln \frac{k_{obs}}{k_2}}{(k_{obs} - k_2)}\right)}\right)$$

$$[\mathbf{2.4}]_{max} = \frac{k_1[PPh_3][\mathbf{2.3}]_0}{k_2 - k_{obs}} \left(e^{\ln \frac{k_{obs}}{k_2}\left(\frac{-k_{obs}}{(k_{obs} - k_2)}\right)} - e^{\ln \frac{k_{obs}}{k_2}\left(\frac{-k_2}{(k_{obs} - k_2)}\right)}\right)$$

$$[\mathbf{2.4}]_{max} = \frac{k_1[PPh_3][\mathbf{2.3}]_0}{k_2 - k_{obs}} \left(\frac{k_{obs}}{k_2}^{\left(\frac{-k_{obs}}{(k_{obs} - k_2)}\right)} - \frac{k_{obs}}{k_2}^{\left(\frac{-k_2}{(k_{obs} - k_2)}\right)}\right)$$

Here, k_1 = 0.018 $M^{-1}s^{-1}$, k_{obs} = 0.0061 s^{-1}, [PPh_3] = 0.342 M, [**2.3**]$_0$ = 0.0081 M. Wolfram Mathematica 9 was used to solve for k_2 under the condition that [**2.4**]$_{max}$ ≤ 200 μM: $k_2 \geq 0.22\ s^{-1}$

Alternatively, we can assume that [**2.4**] satisfies steady-state conditions:

$$\frac{d[\mathbf{2.4}]}{dt} = k_1[PPh_3][\mathbf{2.3}] - k_2[\mathbf{2.4}] = 0$$

$$k_1[PPh_3][\mathbf{2.3}] = k_2[\mathbf{2.4}]$$

$$k_1[PPh_3][\mathbf{2.3}]_0 e^{-k_{obs}t} = k_2[\mathbf{2.4}]$$

The steady-state approximation therefore assumes that [4]=[4]$_{max}$ when t=0. We set the same condition as above ([4]$_{max}$ ≤ 200 μM) at t=0 to solve for the lower limit of k_3.

$$k_2 \geq \frac{k_1[PPh_3][\mathbf{2.3}]_0}{[\mathbf{2.4}]_{max}}$$

As above, k_1 = 0.018 $M^{-1}s^{-1}$, [PPh_3] = 0.342 M, [**2.3**]$_0$ = 0.0081 M.

$k_2 \geq 0.25\ s^{-1}$

Kinetic Modeling of Reductive Elimination from 2.9.

All predicted expressions were modeled to data using Wolfram Mathematica 9, using the following scenario (two irreversible steps):

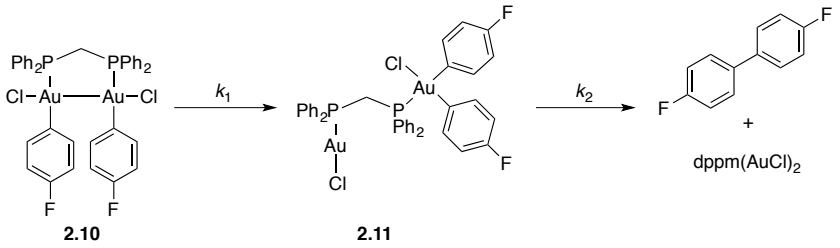

2.10 **2.11**

Derivation of [9](t) from rate law:

$$\frac{d[\mathbf{2.10}]}{dt} = -k_1[\mathbf{2.10}] \Rightarrow \int \frac{d[\mathbf{2.10}]}{[\mathbf{2.10}]} = -\int k_1 \, dt$$

$$\ln[\mathbf{2.10}] = -k_1 t + C$$

$$[\mathbf{2.10}] = Ce^{-k_1 t}$$

$[\mathbf{2.10}] = [\mathbf{2.10}]_0$ when t = 0

$[\mathbf{2.10}] = C$

$$[\mathbf{2.10}] = [\mathbf{2.10}]_0 e^{-k_1 t}$$

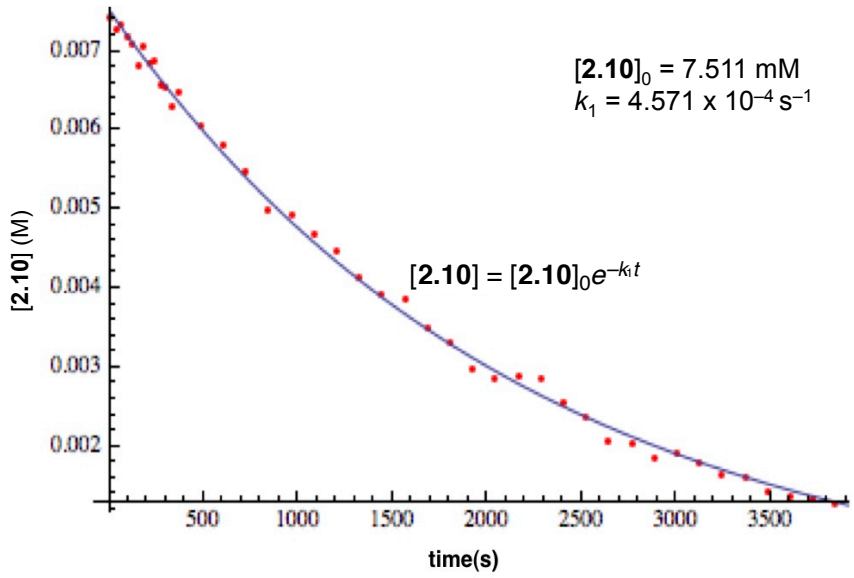

Figure 2.37. [**2.10**] versus time, with fitted model (blue line).

Derivation of [2.11](t) from rate law:

$$\frac{d[\mathbf{2.11}]}{dt} = k_1[\mathbf{2.10}] - k_2[\mathbf{2.11}]$$

$$[\mathbf{2.10}] = [\mathbf{2.10}]_0 e^{-k_1 t}$$

$$\frac{d[\mathbf{2.11}]}{dt} = k_1[\mathbf{2.10}]_0 e^{-k_1 t} - k_2[\mathbf{2.11}]$$

$$e^{k_2 t}\frac{d[\mathbf{2.11}]}{dt} + e^{k_2 t}k_2[\mathbf{2.11}] = e^{k_2 t}k_1[\mathbf{2.10}]_0 e^{-k_1 t}$$

$$= k_1[\mathbf{2.10}]_0 e^{(k_2 - k_1)t}$$

$$\frac{d([\mathbf{2.11}]e^{k_2 t})}{dt} = k_1[\mathbf{2.10}]_0 e^{(k_2 - k_1)t} \Rightarrow \int d([\mathbf{2.11}]e^{k_2 t}) = \int k_1[\mathbf{2.10}]_0 e^{(k_2 - k_1)t}$$

$$[\mathbf{2.11}]e^{k_2 t} = \frac{k_1[\mathbf{2.10}]_0 e^{(k_2 - k_1)t}}{k_2 - k_1} + C$$

$$[\mathbf{2.11}] = \frac{k_1[\mathbf{2.10}]_0 e^{(-k_1)t}}{k_2 - k_1} + Ce^{-k_2 t}$$

$[\mathbf{2.11}] = [\mathbf{2.11}]_0$ when $t = 0$

$$[\mathbf{2.11}]_0 = \frac{k_1[\mathbf{2.10}]_0}{k_2 - k_1} + C$$

$$[\mathbf{2.11}]_0 - \frac{k_1[\mathbf{2.10}]_0}{k_2 - k_1} = C$$

$$[\mathbf{2.11}] = \frac{k_1[\mathbf{2.10}]_0 e^{(-k_1)t}}{k_2 - k_1} + \left([\mathbf{2.11}]_0 - \frac{k_1[\mathbf{2.10}]_0}{k_2 - k_1}\right)e^{-k_2 t}$$

$$= \frac{k_1[\mathbf{2.10}]_0}{k_2 - k_1}\left(e^{-k_1 t} - e^{-k_2 t}\right) + [\mathbf{2.11}]_0 e^{-k_2 t}$$

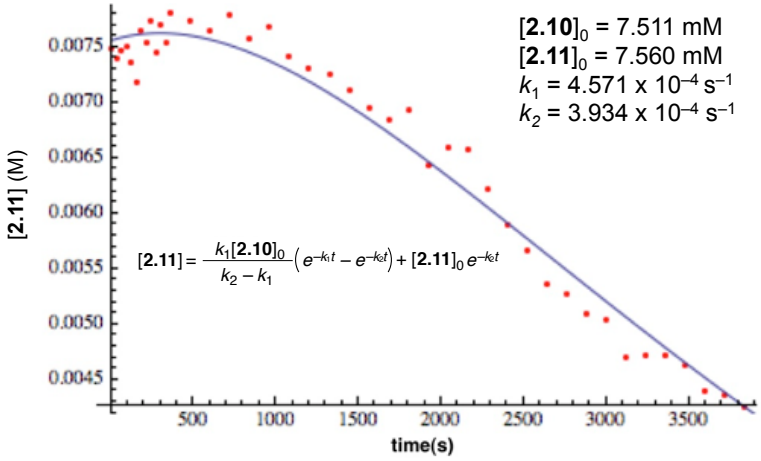

Figure 2.38. [**2.11**] versus time, with fitted model (blue line).

Derivation of [(p-F-C_6H_4)$_2$](t) from rate law:

$$\frac{d[4\text{-F-}C_6H_4)_2]}{dt} = k_2[\mathbf{2.11}] = k_2\left(\frac{k_1[\mathbf{2.10}]_0}{k_2-k_1}\left(e^{-k_1t}-e^{-k_2t}\right)+[\mathbf{2.11}]_0\,e^{-k_2t}\right)$$

$$= \frac{k_1k_2[\mathbf{2.10}]_0}{k_2-k_1}\left(e^{-k_1t}-e^{-k_2t}\right)+[\mathbf{2.11}]_0\,k_2\,e^{-k_2t}$$

$$= -\frac{k_1[\mathbf{2.10}]_0}{k_2-k_1}k_2e^{-k_2t}+\frac{k_2[\mathbf{2.10}]_0}{k_2-k_1}k_1e^{-k_1t}+[\mathbf{2.11}]_0\,k_2\,e^{-k_2t}$$

$$\int\frac{d[4\text{-F-}C_6H_4)_2]}{dt} = -\int\frac{k_1[\mathbf{2.10}]_0}{k_2-k_1}k_2e^{-k_2t}+\int\frac{k_2[\mathbf{2.10}]_0}{k_2-k_1}k_1e^{-k_1t}+\int[\mathbf{2.11}]_0\,k_2\,e^{-k_2t}$$

$$[4\text{-F-}C_6H_4)_2] = +\frac{k_1[\mathbf{2.10}]_0}{k_2-k_1}e^{-k_2t}-\frac{k_2[\mathbf{2.10}]_0}{k_2-k_1}e^{-k_1t}-[\mathbf{2.11}]_0\,e^{-k_2t}+C$$

$$[4\text{-F-}C_6H_4)_2] = [4\text{-F-}C_6H_4)_2]_0 \text{ at } t=0$$

$$[4\text{-F-}C_6H_4)_2]_0 = \frac{k_1[\mathbf{2.10}]_0}{k_2-k_1}-\frac{k_2[\mathbf{2.10}]_0}{k_2-k_1}-[\mathbf{2.11}]_0+C$$

$$= \frac{(k_1+k_2)[\mathbf{2.10}]_0}{k_2-k_1}-[\mathbf{2.11}]_0+C$$

$$= -\frac{(-k_1+k_2)[\mathbf{2.10}]_0}{k_2-k_1}-[\mathbf{2.11}]_0+C$$

$$= -[\mathbf{2.10}]_0-[\mathbf{2.11}]_0+C$$

$$C = [4\text{-F-}C_6H_4)_2]_0+[\mathbf{2.10}]_0+[\mathbf{2.11}]_0$$

$$[4\text{-F-}C_6H_4)_2] = \frac{k_1[\mathbf{2.10}]_0}{k_2-k_1}e^{-k_2t}-\frac{k_2[\mathbf{2.10}]_0}{k_2-k_1}e^{-k_1t}-[\mathbf{2.11}]_0\,e^{-k_2t}+[\mathbf{2.10}]_0+[\mathbf{2.11}]_0+[4\text{-F-}C_6H_4)_2]_0$$

$$[4\text{-F-}C_6H_4)_2] = \left(\frac{k_1[\mathbf{2.10}]_0}{k_2-k_1}-[\mathbf{2.11}]_0\right)e^{-k_2t}-\frac{k_2[\mathbf{2.10}]_0}{k_2-k_1}e^{-k_1t}+[\mathbf{2.10}]_0+[\mathbf{2.11}]_0+[4\text{-F-}C_6H_4)_2]_0$$

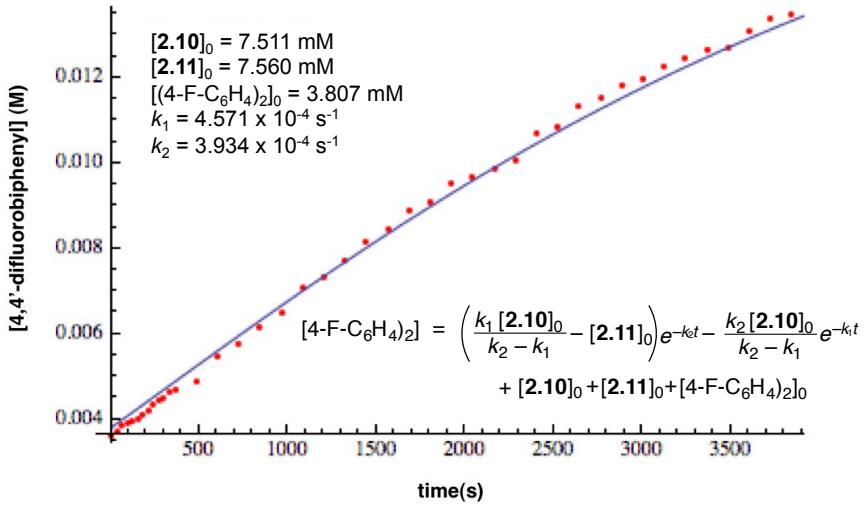

Figure 2.39. [(*p*-F-C_6H_4)$_2$] versus time, with fitted model (blue line).

References

(1) Brown, J. M.; Cooley, N. A. *Chem. Rev.* **1988**, *88* (7), 1031–1046.
(2) Tsou, T. T.; Kochi, J. K. *J. Am. Chem. Soc.* **1979**, *101* (25), 7547–7560.
(3) Komiya, S.; Abe, Y.; Yamamoto, A.; Yamamoto, T. *Organometallics* **1983**, *2* (10), 1466–1468.
(4) Komiya, S.; Akai, Y.; Tanaka, K.; Yamamoto, T.; Yamamoto, A. *Organometallics* **1985**, *4* (6), 1130–1136.
(5) Lin, B. L.; Clough, C. R.; Hillhouse, G. L. *J. Am. Chem. Soc.* **2002**, *124* (12), 2890–2891.
(6) Jin, L.; Zhang, H.; Li, P.; Sowa, J. R.; Lei, A. *J. Am. Chem. Soc.* **2009**, *131* (29), 9892–9893.
(7) Milstein, D.; Stille, J. K. *J. Am. Chem. Soc.* **1979**, *101* (17), 4981–4991.
(8) Moravskiy, A.; Stille, J. K. *J. Am. Chem. Soc.* **1981**, *103* (14), 4182–4186.
(9) Low, J. J.; Goddard, W. A. *J. Am. Chem. Soc.* **1986**, *108* (20), 6115–6128.
(10) Byers, P. K.; Canty, A. J.; Crespo, M.; Puddephatt, R. J.; Scott, J. D. *Organometallics* **1988**, *7* (6), 1363–1367.
(11) Widenhoefer, R. A.; Buchwald, S. L. *J. Am. Chem. Soc.* **1998**, *120* (26), 6504–6511.
(12) Osakada, K.; Onodera, H.; Nishihara, Y. *Organometallics* **2005**, *24* (2), 190–192.
(13) Hartwig, J. F. *Inorg. Chem.* **2007**, *46* (6), 1936–1947.
(14) Pérez-Rodríguez, M.; Braga, A. A. C.; Garcia-Melchor, M.; Pérez-Temprano, M. H.; Casares, J. A.; Ujaque, G.; de Lera, A. R.; Álvarez, R.; Maseras, F.; Espinet, P. *J. Am. Chem. Soc.* **2009**, *131* (10), 3650–3657.
(15) Racowski, J. M.; Dick, A. R.; Sanford, M. S. *J. Am. Chem. Soc.* **2009**, *131* (31), 10974–10983.
(16) Brown, M. P.; Puddephatt, R. J.; Upton, C. E. E. *J. Chem. Soc. Dalton Trans.* **1974**, No. 22, 2457–2465.
(17) Abis, L.; Sen, A.; Halpern, J. *J. Am. Chem. Soc.* **1978**, *100* (9), 2915–2916.
(18) Stahl, S. S.; Labinger, J. A.; Bercaw, J. E. *J. Am. Chem. Soc.* **1995**, *117* (36), 9371–9372.
(19) Shekhar, S.; Hartwig, J. F. *J. Am. Chem. Soc.* **2004**, *126* (40), 13016–13027.
(20) Bercaw, J. E.; Chen, G. S.; Labinger, J. A.; Lin, B.-L. *Organometallics* **2010**, *29* (19), 4354–4359.
(21) Lanci, M. P.; Remy, M. S.; Lao, D. B.; Sanford, M. S.; Mayer, J. M. *Organometallics* **2011**, *30* (14), 3704–3707.
(22) Liberman-Martin, A. L.; Bergman, R. G.; Tilley, T. D. *J. Am. Chem. Soc.* **2013**, *135* (26), 9612–9615.
(23) Tamaki, A.; Magennis, S. A.; Kochi, J. K. *J. Am. Chem. Soc.* **1974**, *96* (19), 6140–6148.
(24) Komiya, S.; Albright, T. A.; Hoffmann, R.; Kochi, J. K. *J. Am. Chem. Soc.* **1976**, *98* (23), 7255–7265.
(25) Komiya, S.; Kochi, J. K. *J. Am. Chem. Soc.* **1976**, *98* (24), 7599–7607.
(26) Lawrence Kuch, P.; Stuart Tobias, R. *J. Organomet. Chem.* **1976**, *122* (3), 429–446.
(27) Nyholm, R. S.; Royo, P. *J. Chem. Soc. Chem. Commun.* **1969**, No. 8, 421a – 421a.
(28) Baker, R. W.; Pauling, P. *J. Chem. Soc. Chem. Commun.* **1969**, No. 13, 745–745.
(29) Hofer, M.; Gomez-Bengoa, E.; Nevado, C. *Organometallics* **2014**, *33* (6), 1328–1332.
(30) Vicente, J.; Bermúdez, M.-D.; Carrión, F.-J.; Jones, P. G. *Chem. Ber.* **1996**, *129* (11), 1395–1399.

(31) Vicente, J.; Dolores Bermudez, M.; Escribano, J. *Organometallics* **1991**, *10* (9), 3380–3384.
(32) Tkatchouk, E.; Mankad, N. P.; Benitez, D.; Goddard, W. A.; Toste, F. D. *J. Am. Chem. Soc.* **2011**, *133* (36), 14293–14300.
(33) Mazany, A. M.; Fackler, J. P. *J. Am. Chem. Soc.* **1984**, *106* (3), 801–802.
(34) Fackler, J. P.; Trzcinska-Bancroft, B. *Organometallics* **1985**, *4* (10), 1891–1893.
(35) Murray, H. H.; Fackler, J. P.; Porter, L. C.; Briggs, D. A.; Guerra, M. A.; Lagow, R. J. *Inorg. Chem.* **1987**, *26* (3), 357–363.
(36) Khan, M. N. I.; Fackler, J. P.; King, C.; Wang, J. C.; Wang, S. *Inorg. Chem.* **1988**, *27* (10), 1672–1673.
(37) King, C.; Wang, J. C.; Khan, M. N. I.; Fackler, J. P. *Inorg. Chem.* **1989**, *28* (11), 2145–2149.
(38) Abdou, H. E.; Mohamed, A. A.; Fackler, J. P. *Inorg. Chem.* **2005**, *44* (2), 166–168.
(39) Abdou, H. E.; Mohamed, A. A.; Fackler, J. P. *Inorg. Chem.* **2007**, *46* (23), 9692–9699.
(40) Bardaji, M.; Gimeno, M. C.; Jones, P. G.; Laguna, A.; Laguna, M. *Organometallics* **1994**, *13* (9), 3415–3419.
(41) Bardaji, M.; Jones, P. G.; Laguna, A.; Laguna, M. *Organometallics* **1995**, *14* (3), 1310–1315.
(42) Usón, R.; Laguna, A.; Laguna, M.; Jiménez, J.; Jones, P. G. *J. Chem. Soc. Dalton Trans.* **1991**, No. 5, 1361–1365.
(43) Usón, R.; Laguna, A.; Laguna, M.; Fraile, M. N.; Jones, P. G.; Sheldrick, G. M. *J. Chem. Soc. Dalton Trans.* **1986**, No. 2, 291–296.
(44) Bennett, M. A.; Bhargava, S. K.; Hockless, D. C. R.; Welling, L. L.; Willis, A. C. *J. Am. Chem. Soc.* **1996**, *118* (43), 10469–10478.
(45) Hashmi, A. S. K.; Blanco, M. C.; Fischer, D.; Bats, J. W. *Eur. J. Org. Chem.* **2006**, *2006* (6), 1387–1389.
(46) Ball, L. T.; Lloyd-Jones, G. C.; Russell, C. A. *Science* **2012**, *337* (6102), 1644–1648.
(47) Ball, L. T.; Lloyd-Jones, G. C.; Russell, C. A. *J. Am. Chem. Soc.* **2014**, *136* (1), 254–264.
(48) *Computational Mechanisms of Au and Pt Catalyzed Reactions*; Soriano, E., Marco-Contelles, J., Eds.; Topics in Current Chemistry; Springer Berlin Heidelberg: Berlin, Heidelberg, 2011; Vol. 302.
(49) Gorin, D. J.; Toste, F. D. *Nature* **2007**, *446* (7134), 395–403.
(50) Braterman, P. S.; Cross, R. J.; Young, G. B. *J. Chem. Soc. Dalton Trans.* **1976**, No. 14, 1306–1310.
(51) Braterman, P. S.; Cross, R. J.; Young, G. B. *J. Chem. Soc. Dalton Trans.* **1976**, No. 14, 1310–1314.
(52) Braterman, P. S.; Cross, R. J.; Young, G. B. *J. Chem. Soc. Dalton Trans.* **1977**, No. 19, 1892–1897.
(53) Martin, R.; Buchwald, S. L. *J. Am. Chem. Soc.* **2007**, *129* (13), 3844–3845.
(54) Tatsumi, K.; Hoffmann, R.; Yamamoto, A.; Stille, J. K. *Bull. Chem. Soc. Jpn.* **1981**, *54* (6), 1857–1867.
(55) Hoffmann, R. Laidler, K. J., Ed.; Pergamon Press: New York, 1982; pp 247–263.
(56) Albright, T. A.; Burdett, J. K.; Whangbo, M.-H. *Orbital Interactions In Chemistry*; John Wiley & Sons, Ltd, 1985.
(57) Low, J. J.; Goddard, W. A. *Organometallics* **1986**, *5* (4), 609–622.

(58) Carter, A.; Cohen, S. A.; Cooley, N. A.; Murphy, A.; Scutt, J.; Wass, D. F. *Chem. Commun.* **2002**, No. 8, 858–859.
(59) Esswein, A. J.; Veige, A. S.; Nocera, D. G. *J. Am. Chem. Soc.* **2005**, *127* (47), 16641–16651.
(60) Whitesides, G. M.; Casey, C. P.; Krieger, J. K. *J. Am. Chem. Soc.* **1971**, *93* (6), 1379–1389.
(61) Goldwhite, H.; Rowsell, D. G. *J. Chem. Soc. Chem. Commun.* **1969**, No. 13, 713–713.
(62) Espenson, J. H. *Chemical Kinetics and Reaction Mechanisms*, 2nd ed.; McGraw-Hill, 2002.
(63) Hofer, M.; Nevado, C. *Tetrahedron* **2013**, *69* (27–28), 5751–5757.
(64) Roglans, A.; Pla-Quintana, A.; Moreno-Mañas, M. *Chem. Rev.* **2006**, *106* (11), 4622–4643.
(65) Kim, S.; Rojas-Martin, J.; Toste, F. D. *Chem. Sci.* **2015**, *7* (1), 85–88.
(66) Tlahuext-Aca, A.; Hopkinson, M. N.; Sahoo, B.; Glorius, F. *Chem. Sci.* **2015**, *7* (1), 89–93.
(67) Cai, R.; Lu, M.; Aguilera, E. Y.; Xi, Y.; Akhmedov, N. G.; Petersen, J. L.; Chen, H.; Shi, X. *Angew. Chem. Int. Ed.* **2015**, *54* (30), 8772–8776.
(68) Zhao, X.-F.; Zhang, C. *Synthesis* **2007**, *2007* (04), 551–557.
(69) Schmidbaur, H.; Wohlleben, A.; Wagner, F.; Orama, O.; Huttner, G. *Chem. Ber.* **1977**, *110* (5), 1748–1754.
(70) Brandys, M.-C.; Jennings, M. C.; Puddephatt, R. J. *J. Chem. Soc. Dalton Trans.* **2000**, No. 24, 4601–4606.
(71) Sinha, P.; Wilson, A. K.; Omary, M. A. *J. Am. Chem. Soc.* **2005**, *127* (36), 12488–12489.
(72) Croix, C.; Balland-Longeau, A.; Allouchi, H.; Giorgi, M.; Duchêne, A.; Thibonnet, J. *J. Organomet. Chem.* **2005**, *690* (21–22), 4835–4843.
(73) Maumela, M.; Blann, K.; de Bod, H.; Dixon, J.; Gabrielli, W.; Williams, D. B. *Synthesis* **2007**, *2007* (24), 3863–3867.
(74) Bollmann, A.; Blann, K.; Dixon, J. T.; Hess, F. M.; Killian, E.; Maumela, H.; McGuinness, D. S.; Morgan, D. H.; Neveling, A.; Otto, S.; Overett, M.; Slawin, A. M. Z.; Wasserscheid, P.; Kuhlmann, S. *J. Am. Chem. Soc.* **2004**, *126* (45), 14712–14713.
(75) Cahiez, G.; Chaboche, C.; Mahuteau-Betzer, F.; Ahr, M. *Org. Lett.* **2005**, *7* (10), 1943–1946.

Chapter 3: Mechanistic Studies on the Photochemical Oxidative Addition of CF_3I to $(R_3P)Au(aryl)$ complexes and $C(sp^2)$–CF_3 reductive elimination from Au(III).

This work was conducted in collaboration with Dr. Matthew S. Winston and portions of it have been used with permission from "Photoinitiated Oxidative Addition of CF_3I to Gold(I) and Fast Aryl-CF_3 Reductive Elimination from Gold(III) at Low Temperature." *J. Am. Chem. Soc.* **2014**, *136*, 7777–7782. Copyright (2014) American Chemical Society 2014.

Abstract: Studies on the mechanism of oxidative addition of CF_3I to Au(I), and remarkably fast $C(sp^2)$–CF_3 bond reductive elimination from Au(III) cations are presented. CF_3I undergoes a fast, formal oxidative addition to R_3PAuR' (R = Cy, R' = 3,5-F_2-C_6H_4, 4-F-C_6H_4, C_6H_5, 4-Me-C_6H_4, 4-MeO-C_6H_4, Me; R = Ph, R' = 4-F-C_6H_4, 4-Me-C_6H_4). When R' = aryl, complexes of the type *cis*-$R_3PAu(aryl)(CF_3)I$ can be isolated and characterized. Mechanistic studies suggest that near-ultraviolet light (λ_{max} =313 nm) photoinitiates a radical chain reaction by exciting CF_3I. Complexes supported by PPh_3 undergo reversible phosphine dissociation at 110 °C to generate a 3-coordinate intermediate that undergoes slow reductive elimination. These processes are quantitative, and heavily favor $C(sp^2)$–I reductive elimination over $C(sp^2)$–CF_3 reductive elimination. Silver-mediated halide abstraction from all complexes of the type *cis*-$R_3PAu(aryl)(CF_3)I$ results in quantitative formation of Ar-CF_3 in less than one minute at temperatures as low as –10 ºC.

Introduction: Reports of organogold complexes undergoing redox processes are typically limited to slow oxidative additions[1–6] and reductive eliminations.[2,7–10] These recent findings from our group, as well as those established by Vicente,[11–13] Hashmi,[14] and Lloyd-Jones,[15,16] suggest that the barrier for challenging reductive eliminations might be substantially diminished at Au(III) centers. C_{aryl}-CF_3 bond reductive elimination is typically a slow process requiring elevated temperatures and long reaction times, due to ground state stabilization afforded by exceptionally strong bonding between transition metals and CF_3 ligands.[17,18] For instance, (dppbz)Pd(2-tolyl)(CF_3) (dppbz = 1,2-bis(diphenylphosphino)benzene) is stable at 130 °C for 3 days,[19] while (dppp)Pd(Ph)(CF_3) (dppp = 1,3-diphenylphosphinopropane) and (dppe)Pd(Ph)(CF_3) (dppe = 1,2-diphenylphosphinoethane) yield only 10% $PhCF_3$ after 3 days at 145 °C (Figure 3.1).[20] Reductive eliminations at temperatures between 50-80 °C can be achieved at Pd(II) by employing bulky ligands, such as Xantphos[21] and Brettphos (Figure 3.1).[22]

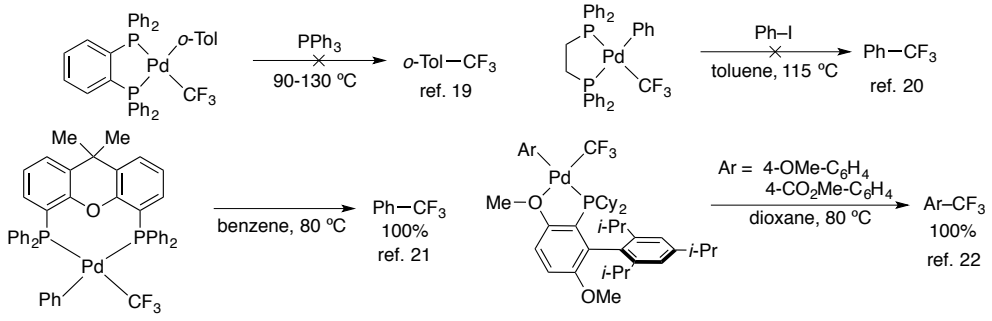

Figure 3.1. Examples of $C(sp^2)$–CF_3 reductive elimination from isolable Pd(II) complexes.

Notably, while aryl-CF_3 reductive eliminations from Pd(IV) often require similarly high temperatures,[23] Sanford has shown that they can occur at temperatures as low as 23 °C over 1 hour.[24] Despite advances in catalytic trifluoromethylation, C_{aryl}-CF_3 reductive elimination still remains a challenging step. Given the importance of trifluoromethylated arenes in pharmaceuticals and agrochemicals,[25] we were prompted to investigate potentially low-barrier C_{aryl}-CF_3 bond reductive elimination at Au(III).

To access complexes of the type $R_3PAu(aryl)(CF_3)I$, we were drawn to Puddephatt's report of the oxidative addition of CF_3I to Me_3PAuMe to afford *cis*/*trans* mixtures of $Me_3PAuMe_2(CF_3)$ and Me_3PAuI.[26] In one case, $Me_3PAu(Me)(CF_3)I$ was obtained exclusively, but its preparation was suffered from irreducibility problems. Because reaction times varied from 5 minutes to 1 day, and rates dramatically slowed in the presence of galvinoxyl, the authors concluded that a free-radical chain mechanism was operative, with $^{\bullet}CF_3$ as the propagating species.

Results and Discussion: To investigate the effects of phosphine structure on the reductive elimination from diaryl Au(III) species, we prepared $(Cy_3P)Au(4\text{-}F\text{-}C_6H_4)$ (**3.1a**) and attempted to monitor its reaction with $PhICl_2$ in CH_2Cl_2 solution. Upon low temperature (–78 ºC) oxidation, we did not observe any biaryl reductive elimination. Instead, we found *cis*-$(Cy_3P)Au(4\text{-}F\text{-}C_6H_4)Cl_2$ complex **3.2a** (Figure 3.2) rather than an unsymmetric Au(III) biaryl complex analogous to **2.3**. The bulkier PCy_3 likely acts to prevent transfer of the arene ligand, instead resulting in clean, rapid oxidation of $Cy_3PAu(4\text{-}F\text{-}C_6H_4)$.[15]

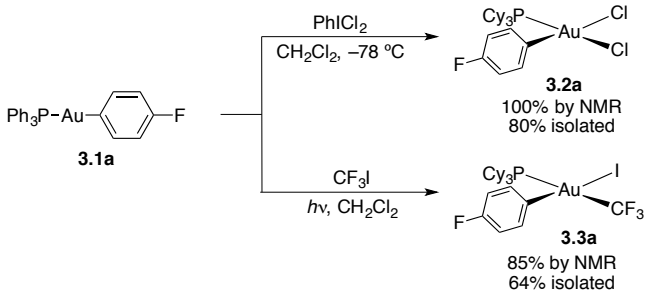

Figure 3.2. Oxidation of **3.1** with $PhICl_2$ or CF_3I to give isolable Au(III) complexes.

We thus began our investigations of Au(I) oxidation by CF_3I using **3.1a**, with the fluorinated arene ligand also providing a convenient ^{19}F NMR handle. Treatment of **3.1a** in CD_2Cl_2 with CF_3I (25 equiv) afforded the product of formal CF_3I oxidative addition **3.3a** in 1 hour in good yield (Figure 3.2). Both the CF_3 and PCy_3 ligands (doublet at δ –24.5 ppm and quartet at δ 25.6 ppm in the ^{19}F and ^{31}P NMR spectra, respectively) provide diagnostic NMR signals (Table 3.1). The substantial coupling ($^3J_{P–F}$ = 63 Hz) between fluorine and phosphorus are characteristic of a *trans* relationship between the CF_3 and phosphine ligands.[14] X-ray analysis of crystals of **3.3a** confirmed this stereochemical relationship around the square planar Au(III) (Figure 3.3A). Complex **3.3a** is not only stable to air and water, but can be purified by column chromatography as well. The photoinitiated oxidative addition of CF_3I is general for electronically diverse complexes of the type $(Cy_3P)Au(aryl)$ (Table 3.1).

Table 3.1. Synthetic scope of CF_3I oxidative addition to $(R_3P)Au(aryl)$ complexes, including tabulated diagnostic $^{31}P\{^1H\}$ and ^{19}F NMR signals.

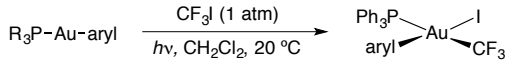

$(R_3P)Au(aryl)$	R	aryl	$(R_3P)Au(CF_3)(aryl)(I)$	yield	$\delta\ ^{31}P\{^1H\}$ (ppm)	$\delta\ ^{19}F$ (ppm)
3.1a	Cy	4-F-C_6H_4	**3.3a**	64%	25.6 (q, $^3J_{P-F}$ = 63 Hz)	-24.5 (d, $^3J_{P-F}$ = 63 Hz)
3.1b	Cy	3,5-F_2-C_6H_3	**3.3b**	44%	26.1 (q, $^3J_{P-F}$ = 63 Hz)	-22.0 (d, $^3J_{P-F}$ = 64 Hz)
3.1c	Cy	Ph	**3.3c**	59%	25.5 (q, $^3J_{P-F}$ = 62 Hz)	-22.7 (d, $^3J_{P-F}$ = 62 Hz)
3.1d	Cy	4-Me-C_6H_4	**3.3d**	38%	25.5 (q, $^3J_{P-F}$ = 62 Hz)	-23.6 (d, $^3J_{P-F}$ = 62 Hz)
3.1e	Cy	4-MeO-C_6H_4	**3.3e**	44%	23.3 (q, $^3J_{P-F}$ = 63 Hz)	-20.6 (d, $^3J_{P-F}$ = 64 Hz)
3.1f	Cy	2-Me-C_6H_4	NR	–	–	–
3.4a	Ph	4-F-C_6H_4	**3.5a**	71%	20.0 (q, $^3J_{P-F}$ = 68 Hz)	-21.0 (d, $^3J_{P-F}$ = 68 Hz)
3.4b	Ph	4-Me-C_6H_4	**3.5b**	63%	20.4 (q, $^3J_{P-F}$ = 67 Hz)	-21.3 (d, $^3J_{P-F}$ = 67 Hz)

Complex **3.1b** (aryl = 3,5-F_2-C_6H_3) reacted smoothly with CF_3I to afford **3.3b**. While complexes with more electron-rich ligands such as **3.1c** (aryl = C_6H_5) and **3.1d** (aryl = 4-Me-C_6H_4) also reacted with CF_3I to afford **3.3c** and **3.3d**, respectively, the most electron-rich complex **3.1e** (aryl = 4-MeO-C_6H_4) decomposes to Au-nanoparticles in solution and solid state (no products of C(sp^2)–I or C(sp^2)–CF_3 reductive elimination can be detected). Au(III) product **3.3e** is detectable, however, and its decomposition can be slowed substantially by addition of MeCN upon concentration of the reaction, allowing its solution-state characterization.. The results of the aryl group scope are shown in Table 3.1 and the X-ray crystallographic analysis of **3.3a-d** and **3.5a** and **3.5b** are shown in Figure 3.3.

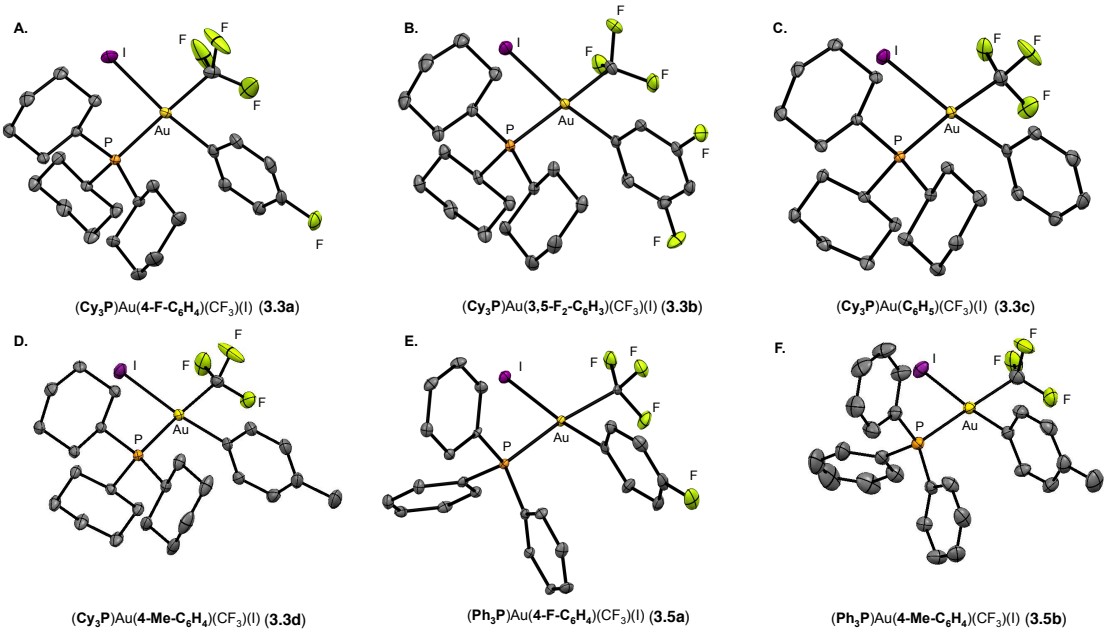

Figure 3.3. Thermal ellipsoid representations of **3.3a-d, 3.5a**, and **3.5b** at the 50% probability level. Hydrogens have been omitted for clarity. Atoms are color-coded: grey (carbon), yellow (fluorine), gold (gold), purple (iodine), orange (phosphorus). Bond lengths and angles are listed in the experimental information section.

The complex **3.1f** (aryl = 2-Me-C_6H_4) did not react with CF_3I suggesting that CF_3I oxidative addition is sensitive to the sterics of the aryl ligand, and that relaxation of $[CF_3I]^*$ is faster than oxidation of the metal center to initiate the radical chain. Fluoroform (HCF_3) was not observed when **3.1f** was irradiated in THF for 20 minutes.

The reaction of **3.1a** and CF_3I represents a rare oxidation of Au(I) to Au(III) that directly installs potentially reactive Au(III)-carbon bonds. [1–6, 27] During our attempts to monitor the oxidative addition by ^{19}F NMR, we found that no reaction occurred when the reaction mixture was placed inside the dark NMR spectrometer. However, when this same reaction mixture was exposed to ambient fluorescent light for 5 minutes, the formation of **3.3a** was detected (~20%). Given the reliance of several methods on CF_3I as a trifluoromethyl source,[28–30] we investigated its photochemical reactivity. Actinometry experiments were carried out to determine the overall quantum yield, using the Norrish II fragmentation of valerophenone as a standard.[31] The oxidative addition of CF_3I to **3.1a** was complete after 20 sec of irradiation by a Hg vapor lamp (transmittance λ_{max} = 313 nm), while the fragmentation of valerophenone (Φ = 1) took place over 24 h under identical conditions. This rate difference, in addition to the ability of ambient light to bring the reaction to full conversion over variable reaction times (between 15 minutes and 1 hour), is indicative of a radical chain reaction as the mechanism of Au(I) oxidation by CF_3I.

The reaction of excess CF_3I and **3.1a** is also fast in THF (Eq 3.2), but the conversion is never greater than 65% (52% yield of **3.3a**), even when irradiated by a Hg vapor lamp for 1 hour. An excess of HCF_3 is generated in THF, regardless of light source (only DCF_3 is formed when d_8-THF is used). GC-MS analysis of reaction mixtures reveals products of THF oxidation (3-butenol, acetaldehyde), likely formed as a consequence of $H^\bullet$ abstraction by $^\bullet CF_3$.

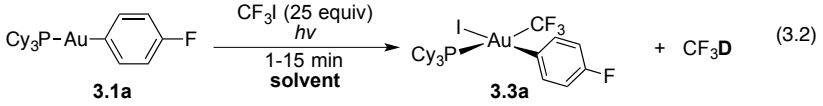

CD_2Cl_2 :	*Full conversion*	*85% NMR yield*	*not observed*
d^8-THF :	*65% conversion*	*52% NMR yield*	*900-2100% NMR yield*

hv : Hg Hanovia lamp (τ_{max} = 313 nm, 450 W) or ambient fluorescent light

Several control experiments, using HCF_3 production relative to a standard as a probe to detect $^\bullet CF_3$ generation, support the involvement of Au(I) during the initiation of the chain reaction. The UV absorption of CF_3I is centered at 270 nm, but tails beyond 350 nm.[32] When irradiated at 313 nm, CF_3I undergoes fast, reversible C–I bond homolysis. However, in the absence of **3.1a**, only negligible amounts of HCF_3 were observed when THF solutions of CF_3I are irradiated for 30 min, indicating that carbon/iodine radical recombination is substantially faster than $H^\bullet$ abstraction from THF. Similarly insignificant quantities of HCF_3 were observed when 20 equivalents (relative to CF_3I) of the $H^\bullet$ donors 1,4-cyclohexadiene, 9,10-dihydroanthracene, or triphenylmethane are added (Figure 3.4A). Additionally, $Cy_3PAu(2\text{-}(CH_2CH{=}CH_2)C_6H_4)$ (**3.1g**), containing a pendent olefin to either capture a putative Au(II) intermediate and/or $^\bullet CF_3$, was fully consumed upon irradiation in the presence of excess CF_3I (Figure 3.4B). This oxidation afforded multiple Au(III) products of indiscriminate $^\bullet CF_3$ addition to the terminal olefin and gold atom (and HCF_3 when THF is used as solvent). Because 2-allylbromobenzene (**3.6**) does not react with CF_3I when irradiated under similar conditions (no HCF_3 is observed after 5 min, and less than 2% after 30 min), we conclude that the Au(I) aryl complex is necessary for chain initiation. These results are also consistent with an initiation mechanism involving $[CF_3I]^{\bullet-}$, which generates iodide and $^\bullet CF_3$ following C–I bond homolysis.

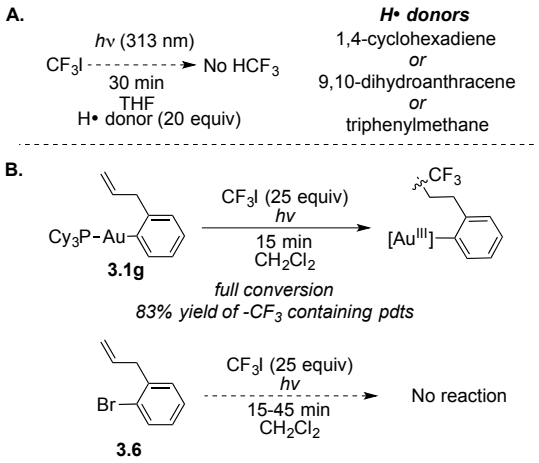

Figure 3.4. Control experiments to assess involvement of Au(I) in the initiation of the radical chain mechanism. A) Irradiation of CF_3I solutions containing $H^{\bullet}$ donors to detect CF_3H in the absence of gold. B) Radical trapping using an olefin with and without a pendant gold center.

We envisioned two possible initiation mechanisms for generating $^{\bullet}CF_3$ as a propagating species from $[CF_3I]^{\bullet-}$ in a chain reaction: (1) initial photoexcitation of **3.1** followed by electron transfer to CF_3I, or (2) initial photoexcitation of CF_3I followed by electron transfer from **3.1** (Scheme 3.1).

Scheme 3.1. Possible initiation mechanisms involving photoexcitation of either Au(I) complex **6** (mechanism 1) or CF_3I (mechanism 2).

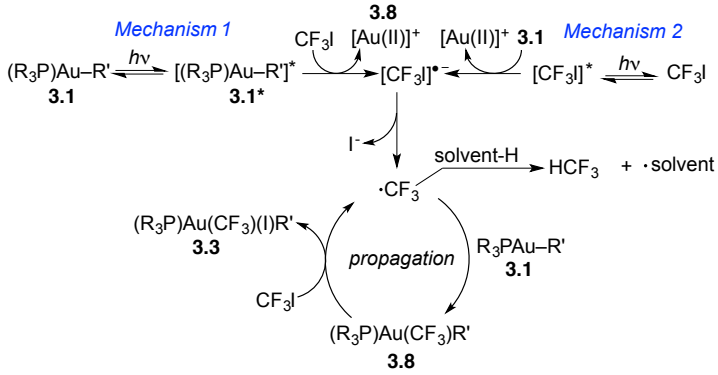

Au(I) aryl complexes are well-known chromophores and their photophysical properties have been investigated previously.[33–38] While **3.1a** absorbs weakly above 310 nm as shown in Figure 3.5A (the cut-off for many laboratory fluorescent lamps[39]), excitation at 320 nm (ε = 37 M^{-1} cm^{-1}) results in a weak, broad luminescence from 340-460 nm, classified as fluorescence based on the lifetime of excited species **3.1a*** (<10 ns, quantum yield of fluorescence = 0.03; our instrumentation was unable to detect shorter fluorescence lifetimes). Despite the short lifetime of **3.1a***, CF_3I effectively quenches its fluorescence (Stern-Volmer quenching constant K_{SV} = 30 M^{-1}, Figure 3.5B). Although this energy transfer could conceivably generate $^{\bullet}CF_3$ and initiate a chain reaction (mechanism 1, Scheme 3.1), when CF_3I is removed from fluorimetry samples under vacuum, fluorescence is restored to the same intensity prior to introduction of the gas, indicating that consumption of Au(I) has not occurred.

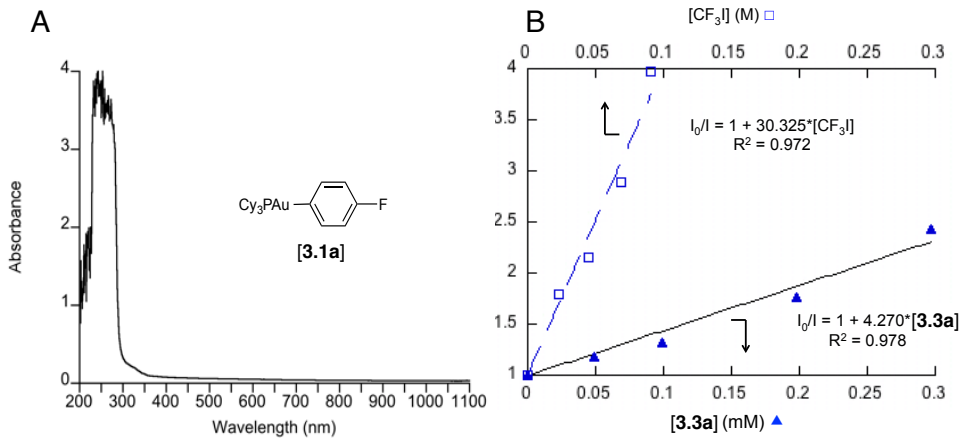

Figure 3.5. A) UV-Vis spectrum of **3.1a** in CH_2Cl_2 solution (2.0 mM). B) Stern-Volmer plots of fluorescence quenching of **3.1a** by different concentrations of CF_3I (□) and Au(III) complex **3.3a** (▲) in CH_2Cl_2. Concentrations of Au(III) are in mol/L and CF_3I concentrations are in mmol/L.

Surprisingly, fluorescence quenching by the Au(III) complex **3.3a** is more than two orders of magnitude more effective (K_{SV} = 4270 M^{-1}) than quenching by CF_3I (Figure 3.5B). If propagating species terminate frequently, a critical concentration of Au(III) product may impede productive energy transfer from an excited species, halting re-initiation of the chain reaction.

In light of Puddephatt's report, Au(I) alkyl complexes, such as $(Me_3P)AuMe$, clearly reacted with CF_3I.[26] However, there is no mention of the dependence of light on this process, although if the reaction was photoinitiated, mechanism 1 (Scheme 3.1) would seem unlikely given the absence of a chromophoric aryl ligand in Puddephatt's examples. To test this hypothesis, we irradiated Cy_3PAuMe (**3.9**) in the presence of CF_3I (Scheme 2). While **3.9** does not absorb above 300 nm (Figure 3.6) the reaction is quantitative in CD_2Cl_2 when irradiated with ambient light, and does not proceed in the dark.

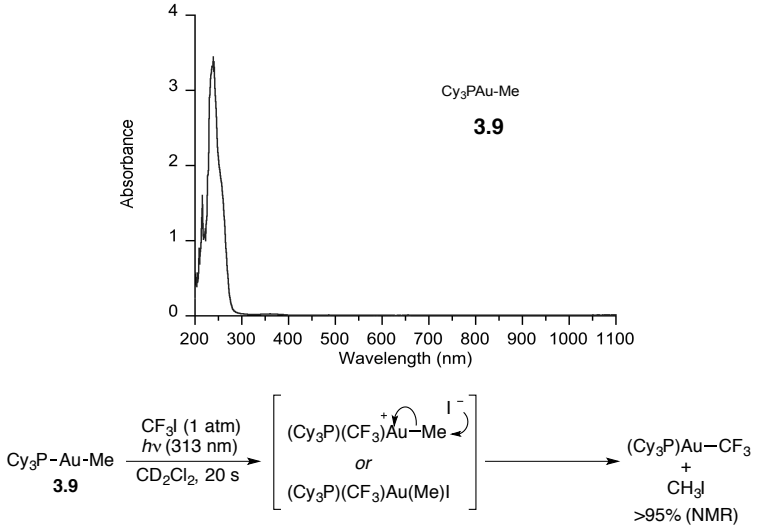

Figure 3.6. UV-Vis spectrum of **3.9** in CH_2Cl_2 solution (2.0 mM) and proposed mechanism for the photochemical oxidative addition of CF_3I to **3.9** in CD_2Cl_2 and spontaneous reductive elimination of CH_3I.

The oxidized product is unobservable, eliminating CH_3I to generate $(Cy_3P)AuCF_3$ at room temperature.[40] Johnson and Puddephatt proposed a mechanism similar to the one shown in

Figure 3.6 where outer sphere attack by iodide generates methyl iodide and $(Cy_3P)AuCF_3$. In THF**,** the reaction generates excess HCF in THF_3, presumably also from solvent H• abstraction by •CF_3. If initiation mechanism 2 is operative, then •CF_3 could be generated by irradiating CF_3I solutions containing electron donors other than Au(I), such as phosphines (Figure 3.7).[41] Indeed, irradiation of PMe_3 or PCy_3 in the presence of CF_3I resulted in formation of $[Me_3P\text{-}CF_3]I$ (**3.10a**, $^2J_{P\text{-}F}$ = 63 Hz) or $[Cy_3P\text{-}CF_3]I$ (**3.10b,** $^2J_{P\text{-}F}$ = 42 Hz) and neither reaction proceeded in the dark. Consistent with quenching of $[CF_3I]$* by Au(III), the oxidation of PCy_3 stalled at roughly 45% conversion (by ^{31}P NMR) in the presence of 25 mol% Au(III) complex **3a**.

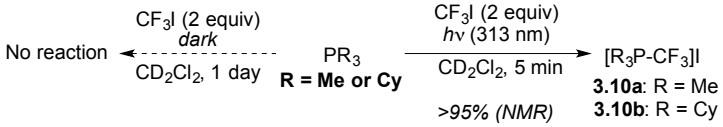

Figure 3.7. Photochemical oxidation of trialkylphosphines by CF_3I.

PPh_3 does not react with CF_3I (eq. 3), presumably due to its lower oxidation potential relative to PMe_3 and PCy_3. When PCy_3 and PPh_3 were irradiated together with CF_3I, only PCy_3 was consumed, suggesting that PPh_3 neither initiates the chain nor reacts with •CF_3 during propagation.

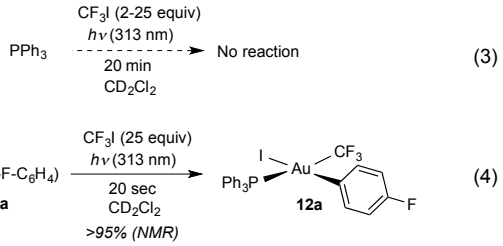

Based on these results, we propose that while photoexcited $[CF_3I]$* undergoes rapid C–I bond homolysis and recombination, it also oxidizes Au(I) aryl and alkyl complexes by accepting electrons into a low-lying SOMO to generate radical anion $[CF_3I]^{\bullet-}$ (mechanism 2, Scheme 3.1). Homolysis of the C-I bond of $[CF_3I]^{\bullet-}$ generates iodide and •CF_3, which oxidizes $(R_3P)AuR'$ (**6**) to Au(II) intermediate **3.8**. Iodine atom abstraction of CF_3I by **3.8** affords Au(III) complex **3.3** and regenerates •CF_3. In THF, oxidation of **3.1** by •CF_3 is competitive with solvent H• abstraction to make HCF_3 and terminate the radical chain. At sufficiently high concentrations, the Au(III) product (**3.3**) quenches $[CF_3I]$* before it can re-initiate the radical chain reaction.

Reductive Elimination from Au(III) Complexes. We next probed C(sp^2)–CF_3 reductive eliminations from Au(III). Under thermolytic conditions, **3.5a** underwent quantitative C(sp^2)–I reductive elimination in toluene-d_8 at 110 °C to afford 4-fluoroiodobenzene and $(Ph_3P)AuCF_3$ over 40 minutes (Figure 3.8).[40,42] No 4-fluoro(trifluoromethyl)benzene was observed by ^{19}F NMR or GC. This process is severely inhibited in the presence of PPh_3 (0.1 or 1.0 equiv) at 110 °C for 12 hours. Treatment of **3.5a** with PPh_3-d_{15} at room temperature results in immediate formation of ***d*$_{15}$-3.5a**.

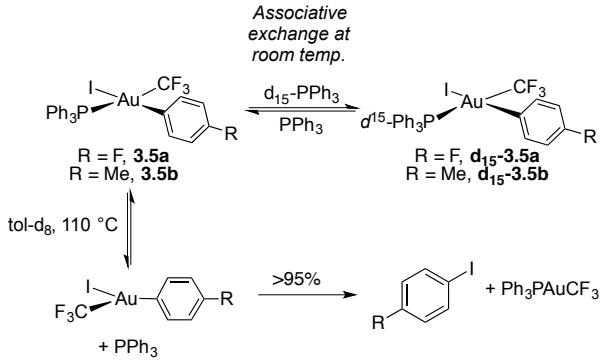

Figure 3.8. Behavior of Au(III) complex **12a** and **12b** in the presence of free PPh_3 and at elevated temperatures.

More electron-rich aryl ligands, such as 4-Me-C_6H_4 (**3.5b**), do not significantly affect the relative rates of C(sp^2)–I and C(sp^2)–CF_3 reductive elimination (Scheme 4). At 110°C, complex **3.5b** underwent mostly C(sp^2)–I reductive elimination within 10 minutes to afford 4-methyliodobenzene.[26] Both C(sp^2)–I and C(sp^2)–CF_3 reductive eliminations were also inhibited in the presence PPh_3 (0.1 or 1.0 equiv), while PPh_3-d_{15} reacted immediately at room temperature to afford **3.5b-*d*$_{15}$**, also via associative ligand exchange. These observations are consistent with a mechanism involving highly reversible PPh_3 dissociation from **3.5a** and **3.5b**, followed by slow C(sp^2)–I reductive elimination from **13a** or **13b**, respectively.

The thermolytic behavior of **3.5a** and **3.5b** is similar to Au(III)alkyl complexes studied by Kochi, which not only reductively eliminate C(sp^3)–C(sp^3) bonds between 70 and 100 °C *via* a dissociative mechanism, but also undergo associative ligand exchange at ambient temperature with excess phosphine.[2,7–10] In contrast, the analogous PCy_3-ligated complexes **3.3a** and **3.3d** are stable at 110 °C for at least 12 hours, presumably due to the greater σ-donating ability of PCy_3 relative to PPh_3 that slows ligand dissociation. Phosphine exchange with excess P(n-Bu)$_3$, PBn_3, or PCy_3 does not occur even at these temperatures, precluding not only the lower-barrier associative exchange mechanism observed with the PPh_3-supported systems (attributed to the larger cone angle of PCy_3 relative to PPh_3), but also PCy_3 dissociation to form a three-coordinate complex.

Because C(sp^2)–I reductive elimination is significantly faster than C(sp^2)–CF_3 reductive elimination, a cycle for gold-catalyzed trifluoromethylation must necessarily involve iodide abstraction from the Au(III) product of CF_3I oxidative addition. Despite the apparent kinetic stabilities of the Au(III) complexes **3.3a**-**e**, **3.5a** and **3.5b**, they all undergo quantitative C(sp^2)–CF_3 reductive elimination in less than 1 minute upon treatment with $AgSbF_6$ at room temperature.

To consider the effects of the phosphine ligand on the silver-mediated C(sp^2)–CF_3 reductive elimination of Au(III), we used variable-temperature NMR to follow the reductive elimination from **3.3a** and **3.5a** in the presence of $AgSbF_6$**.** PCy_3-substituted complex **3.3a** underwent very fast (quantitative conversion in less than 1 minute) C(sp^2)–CF_3 reductive elimination at –10 °C, while the analogous PPh_3-stabilized **3.5a** reacted similarly fast at room temperature (eq 3.5). At lower temperatures, a large number of signals was observed by ^{19}F NMR, and no definitive evidence for a reductive elimination from a single Au(III) species was determined.

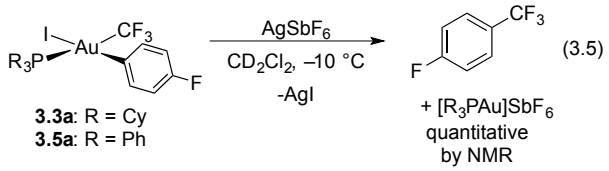

When this reactivity is viewed in the context of a hypothetical catalytic cycle in analogy to cross-coupling, the three fundamental steps required to close such a cycle: oxidative addition, reductive elimination, and transmetallation, have all been demonstrated as shown in Figure 3.9.

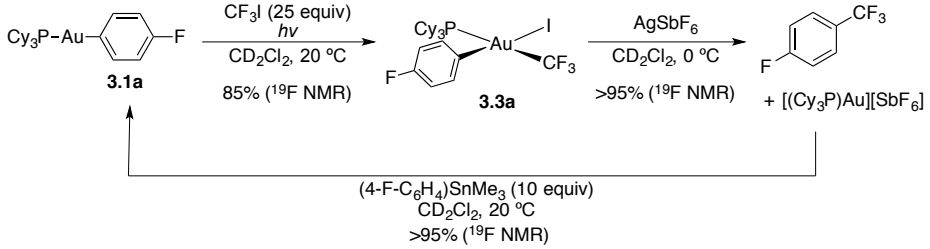

Figure 3.9. Oxidation of CF_3I to **3.1a**, Aryl-CF_3 reductive elimination, and regeneration of**3.1a** *via* transmetallation supporting the feasibility of a mild, catalytic trifluoromethylation

Preliminary attempts at combining both the photochemical CF_3I oxidative addition and the facile C(sp^2)–CF_3 reductive elimination to realize this catalysis were unsuccessful, and are summarized in Table 3.2A. Various stoichiometric silver(I) salts were incompatible with the propagating $^{\bullet}CF_3$ species, and several other Lewis acids were unable to abstract the iodide ligand (Table 3.2); these factors are believed to be responsible for this lack of reactivity.

Table 3.2. A) Brief summary of aryl nucleophiles tested in attempts at a gold-catalyzed aryl trifluoromethylation. B) Summary of Lewis Acids used in attempt to induce C(sp^2)–CF_3 reductive elimination from **3.2a**.

A

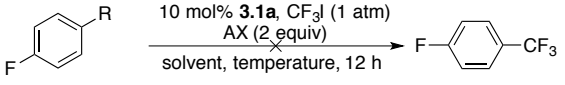

R	AX	solvent	temperature
–$B(OH)_2$	Cs_2CO_3	CH_2Cl_2:H_2O (1:1 v:v)	20 °C or 45 °C
–$B(OH)_2$	AgOAc	THF	20 °C or 65 °C
–$B(OH)_2$	Ag_2CO_3	THF	20 °C or 65 °C
–$SnMe_3$	$Ba(OH)_2$	THF	20 °C or 45 °C

B

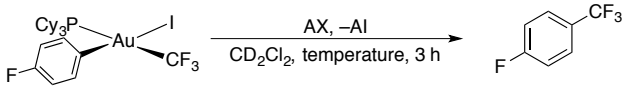

AX	temperature	yield of Ar–CF_3 (^{19}F NMR)
$AgSbF_6$	–78 °C to 0 °C	100 %
AgOTf	20 °C	100 %
$Mg(OTf)_2$	20 °C	0 %
$Ba(OH)_2$	20 or 45 °C	0 %
Cs_2CO_3	20 °C	0 %
$NaSbF_6$	20 °C or 45 °C	0 %
$NaBArF_{24}$	20 °C or 45 °C	0 %
$AlCl_3$	20 °C	15 %
$Ba(OTf)_2$	20 °C	0 %
CsOH[a]	60 °C	0 %

[a]Reaction conducted in THF:toluene:H_2O (1:1:1 v:v:v)

Conclusion: These results reported describe the oxidative addition of CF_3I to Au(I) *via* a photoinitiated chain reaction. The reactions are fast at room temperature for both Au(I) aryl and alkyl complexes and generate a single product of oxidative addition. C(sp^2)–CF_3 reductive elimination is typically a high-barrier process, but occurs in seconds at room temperature from a Au(III) cation. The Au(I)aryl species may be regenerated via one of the numerous transmetallation strategies available involving carbon nucleophiles. While we initially set out to probe C(sp^2)–CF_3 reductive elimination at Au(III), we also explored the oxidative addition of

CF_3I to Au(I). The possibility of photoinitiated oxidation of transition metals or main group elements by CF_3I should not be discounted in methods employing this reagent as a trifluoromethyl source, particularly since ambient fluorescent laboratory lighting is sufficient to initiate a chain in the presence of a suitable reductant. The results presented also suggest that substrate photoexcitation may provide a low-barrier avenue to kinetically challenging oxidative additions by Au(I), providing access to potentially reactive Au(III) complexes.

Experimental

General Considerations: Unless otherwise stated, all manipulations were carried out at ambient temperature (20 ºC) under an atmosphere of purified nitrogen in a Vacuum Atmospheres Corp. glovebox or with a double manifold vacuum line using standard Schlenk techniques. All glassware was borosilicate and dried at 150 ºC for 12 h prior to use. Solvents were dried by passage through a column of activated alumina under nitrogen pressure and degassed by sparging with dry nitrogen. CD_2Cl_2 was distilled from CaH_2 under nitrogen and stored over 4 Å molecular sieves prior to use. THF-d_8 was distilled from Na/Ph_2CO under nitrogen. CF_3I was purchased from Sigma or from Oakwood and connected to a double-manifold vacuum line fitted with Hg manometers to regulate pressure. $Ph_3PAu(4\text{-}F\text{-}C_6H_4)$,[43] 2-allyl-1-bromobenzene (**3.6**)[44] were prepared according to literature procedure. Complexes **3.1b-f, 3.4a** and **3.4b** were synthesized by the methods of Gray,[33,45] Hashmi[46] and Gagné,[47] respectively.

NMR spectra were recorded using Bruker AVQ-400, DRX-500, AV-500 or AV-600 spectrometers, and chemical shifts are referenced to residual NMR solvent peaks (^1H and ^{13}C), $PhCF_3$ (^{19}F), or H_3PO_4 (^{31}P). Elemental analyses were performed at the College of Chemistry Microanalytical Laboratory, University of California, Berkeley. X-ray structural determinations were performed at CHEXRAY, University of California, Berkeley on Bruker SMART 1000 or SMART APEX diffractometers. UV-Vis spectra were recorded using a Hewlett-Packard 8453 Spectrophotometer; Fluorometry and fluorescence lifetime measurements were performed on Varian Cary Eclipse Fluorescence Spectrophotometer. All spectrophotometry was performed using 10 mm quartz cuvettes. Melting points were obtained using a Thomas-Hoover Unimelt Capillary Melting Point Apparatus and are uncorrected.

Quantum yields were determined using a merry-go-round apparatus constructed from a test-tube rack and a turntable.

Synthetic procedures

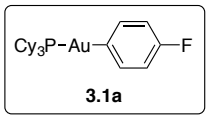

3.1a

To a cold (–78 ºC) suspension of $(Cy_3P)AuCl$ (250 mg, 0.49 mmol, 1.00 equiv) in THF was added 4-F-C_6H_4MgBr (1.0 M in THF, 2 equiv) dropwise via syringe. The resulting solution was stirred at –78 ºC for 1 h then warmed to 0 ºC and stirred for 1 h. The reaction was quenched with water at 0 ºC and extracted into CH_2Cl_2 (5 mL). The layers were separated and the aqueous phase was washed with additional CH_2Cl_2 (5 mL). The combined organic layers were washed with water (5 mL) and dried over Na_2SO_4, filtered and concentrated to dryness *in vacuo*. Recrystallization from CH_2Cl_2/hexanes yielded the desired compound as colorless needles (220 mg, 79 %). **^{1}H NMR**

(CD_2Cl_2, 400 MHz, δ): 7.39 (td, *J* = 7.6, 4.7 Hz, 2H), 6.98 – 6.84 (m, 2H), 2.05 (tq, *J* = 9.4, 3.0 Hz, 9H), 1.86 (dt, *J* = 10.2, 3.4 Hz, 6H), 1.79 – 1.64 (m, 3H), 1.53 (dtd, *J* = 16.1, 12.2, 10.3, 5.4 Hz, 6H), 1.42 – 1.23 (m, 9H). **^{13}C{^{1}H} NMR** (CD_2Cl_2,126 MHz, δ): 172.6 (d, *J* = 109 Hz), 161.2 (d, *J* = 238 Hz), 139.70, (d, *J* = 5 Hz), 113.5 (dd, *J* = 17.5, 6.25 Hz), 33.2 (d, *J* = 23.8 Hz), 30.73, 27.2 (d, *J* = 11.3 Hz), 26.10. **^{31}P{^{1}H} NMR** (CD_2Cl_2, 162 MHz, δ): 57.2 ppm (s). **^{19}F NMR** (CD_2Cl_2, 376 MHz, δ): –117.0 ppm (s). **Anal. Calcd.** for $C_{24}H_{37}AuPF$: C, 50.35; H, 6.51. Found: C, 50.41; H, 6.29.

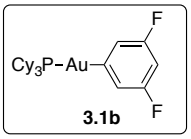

3.1b

A mixture of Cs_2CO_3 (109 mg, 0.33 mmol, 1.9 equiv), 3,5-difluorophenylboronic acid (56 mg, 0.34 mmol, 1.9 equiv), and (Cy_3P)AuBr (100 mg, 0.18 mmol, 1.0 equiv) was suspended in acetonitrile (8 mL) and heated to 65 ºC for 3 h. The reaction mixture was cooled to 20 ºC and the acetonitrile was removed *in vacuo*. The product was extracted into benzene (10 mL) and filtered through a pad of Celite. The filtrate was concentrated and the product was precipitated with hexanes. The supernatant was removed and the remaining solid was washed with hexanes (5 mL) and methanol (5 mL) and dried *in vacuo*. Recrystallization from benzene/hexanes yielded the desired product as colorless plates (70 mg, 70%). **^{1}H NMR** (CD_2Cl_2, 500 MHz, δ): 7.04 – 6.94 (m, 2H), 6.45 (tt, *J* = 9.8, 2.6 Hz, 1H), 2.06 (ddd, *J* = 20.1, 12.4, 5.2 Hz, 9H), 1.93 – 1.82 (m, 6H), 1.79 – 1.69 (m, 3H), 1.60 – 1.44 (m, 6H), 1.41 – 1.22 (m, 9H). **^{13}C{^{1}H} NMR** (CD_2Cl_2, 126 MHz, δ): 182.19 (d, *J* = 111.0 Hz), 162.70 (dt, *J* = 250.4, 10.0 Hz), 128.29 , 120.69 – 119.49 (m), 33.09 (d, *J* = 25.1 Hz), 30.76 , 27.19 (d, *J* = 11.3 Hz), 26.07 . **^{31}P{^{1}H} NMR** (CD_2Cl_2, 162 MHz, δ): 56.65 (t, *J* = 6.5 Hz). **^{19}F NMR** (CD_2Cl_2, 376 MHz, δ): -114.21 – -114.50 (m). **Anal. Calcd.** for $C_{24}H_{36}F_2PAu$: C, 48.82; H, 6.15. Found: C, 48.81; H, 6.16.

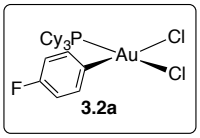

3.2a

To a solution of (Cy_3P)Au(4-F-C_6H_4) (105 mg, 0.183 mmol, 1.00 equiv) in CH_2Cl_2 (1 mL) was added a solution of $PhICl_2$ (50.4 mg, 0.183 mmol, 1.00 equiv) in CH_2Cl_2 (1 mL) at 20 ºC. The resulting solution was stirred for 20 min, then filtered through a glass fiber filter and concentrated to ca. 1 mL. Pentane was added to precipitate the product as colorless microcrystals (94 mg, 80 %). Complex **2** can be recrystallized as the CH_2Cl_2 solvate by layering hexanes onto a saturated solution in CH_2Cl_2: these crystals were suitable for X-ray diffraction. **^{1}H NMR** (CD_2Cl_2, 400 MHz, δ): 7.35 – 7.27 (m, 2H), 7.03 (t, *J* = 6.8 Hz, 2H), 2.48 (q, *J* = 12 Hz, 3H), 2.01 – 1.90 (m, 6H), 1.89 – 1.78 (m, 6H), 1.77 – 1.64 (m, 9H), 1.28 (qt, *J* = 13.0, 3.6 Hz, 3H), 1.10 (qt, *J* = 12.9, 3.4 Hz, 6H). **^{13}C{^{1}H} NMR** (CD_2Cl_2, 125 MHz, δ): 161.2 (d, *J* = 245.2 Hz), 137.1, 132.8 (d, *J* = 6.5 Hz), 116.6 (d, *J* = 21.0 Hz), 35.2 (d, *J* = 27.2 Hz), 29.3 (d, *J* = 3.5 Hz), 27.1 (d, *J* = 12.0 Hz), 25.7. **^{31}P{^{1}H} NMR** (CD_2Cl_2, 162 MHz, δ): 49.3 ppm (s). **^{19}F NMR** (CD_2Cl_2, 376 MHz, δ): –117.3 ppm (s). **Anal. Calcd.** for $C_{24}H_{37}AuPFCl_2$•CH_2Cl_2: C, 41.23; H, 5.40. Found: C, 41.71; H, 5.42.

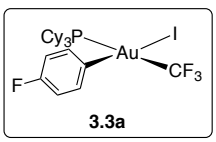

3.3a

A solution of $Cy_3PAu(4\text{-}F\text{-}C_6H_4)$ (150 mg, 0.26 mmol) in CH_2Cl_2 (16 mL) was placed in a 20 mL glass bomb and cooled to –78 ºC. The reaction was degassed under vacuum, warmed to room temperature, and backfilled with CF_3I (1 atm, 0.16 mmol in headspace, 6.4 mmol in solution). The vessel was

sealed and irradiated in the photoreactor for 20 s, then taken into the glovebox. The reaction was filtered through a pad of Celite and concentrated to *ca.* 1 mL. Pentane was added to precipitate the desired product as slightly yellow microcrystals (130 mg, 64%). Crystals suitable for X-ray diffraction were grown by layering pentane onto a saturated CH_2Cl_2 solution. **^{1}H NMR** (CD_2Cl_2, 500 MHz, δ): 8.55 (s, 2H), 8.05 (s, 1H), 7.65 (s, 2H), 7.46 (dd, J = 8.5, 5.3 Hz, 2H), 7.08 (t, J = 8.6 Hz, 2H), 2.56 (q, J = 12.1 Hz, 3H), 2.04 (dd, J = 12.3, 6.4 Hz, 6H), 1.99 – 1.86 (m, 9H), 1.79 (dtt, J = 16.3, 11.9, 4.0 Hz, 10H), 1.34 (tdd, J = 16.1, 12.8, 6.3 Hz, 4H), 1.17 (dddd, J = 16.7, 13.0, 8.0, 3.6 Hz, 6H). **^{13}C{^{1}H} NMR** (CD_2Cl_2, 126 MHz, δ): 161.2 (d, J = 242 Hz), 141.9, 132.3 (d, J = 6 Hz), 115.6 (d, J = 21 Hz), 34.7, (d, J = 25 Hz), 29.7, 27.2 (d, J = 11 Hz), 25.8; due to direct bonding to Au, as well as coupling to ^{31}P and ^{19}F, the Au-CF_3 carbon was not found. **^{31}P{^{1}H} NMR** (CD_2Cl_2, 162 MHz, δ) 25.6 (q, $^3J_{P\text{-}F}$ = 63 Hz). **^{19}F NMR** (CD_2Cl_2, 376 MHz, δ): –24.5 (d, $^3J_{P\text{-}F}$ = 63 Hz), –117.0 (s). **Anal. Calcd.** for $C_{25}H_{37}AuF_4IP$: C, 39.08; H, 4.85. Found C, 38.74; H, 4.70. **Melting point** 170 ºC (decomposition).

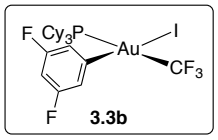

3.3b

A solution of $Cy_3PAu(3,5\text{-}F_2\text{-}C_6H_3)$ (45 mg, 0.076 mmol) in CH_2Cl_2 (2.5 mL) was placed in a 25 mL glass bomb and cooled to –78 ºC. The reaction was degassed under vacuum, warmed to room temperature, and backfilled with CF_3I (1 atm, 0.92 mmol in headspace, 1.0 mmol in solution). The vessel was sealed and irradiated in the photoreactor for 5 min. The crude reaction mixture was concentrated and purified by flash chromatography (SiO_2, 1:3 benzene:hexanes, R_f = 0.2) to afford the desired product as a white solid (26 mg, 44%). Crystals suitable for X-ray diffraction were grown by layering a saturated CH_2Cl_2 solution with hexane. **^{1}H NMR** (500 MHz, CD_2Cl_2, δ): 6.83 (d, J = 6.4, 2H), 6.76 (t, J = 9.3 Hz, 1H), 2.44 (q, J = 12.1 Hz, 3H), 2.03 – 1.81 (m, 12H), 1.79 – 1.60 (m, 9H), 1.31 (m, 3H), 1.15 (m, 6H). **^{13}C{^{1}H} NMR** (126 MHz, CD_2Cl_2, δ): 162.0 (dd, J = 253, 11 Hz), 148.9 (d, J = 6.8 Hz), 114.8 (dd, J = 20, 5 Hz), 101.4 (t, J = 25 Hz), 34.9 (d, J = 25 Hz), 29.8 (d, J = 3 Hz), 27.2 (d, J = 11 Hz), 25.8 (CF_3 carbon not observed due to complex coupling). **^{31}P{^{1}H} NMR** (202 MHz, CD_2Cl_2, δ): 26.1 (q, $^3J_{P\text{-}F}$ = 63 Hz). **^{19}F NMR** (CD_2Cl_2, 376 MHz, δ): -22.0 (q, $^3J_{P\text{-}F}$ = 64 Hz), -109.8 – -110.0 (m). **Anal. Calcd.** for $C_{25}H_{36}AuF_5IP$: C, 38.18; H, 4.61. Found C, 38.01; H, 4.93.

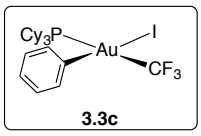

3.3c

A solution of $Cy_3PAu(C_6H_5)$ (50 mg, 0.090 mmol) in CH_2Cl_2 (4.5 mL) was placed in a 10 mL bomb and cooled to –78 ºC. The reaction was degassed under vacuum, warmed to room temperature, and backfilled with CF_3I (1 atm, 0.22 mmol in headspace, 1.8 mmol in solution). The vessel was sealed and irradiated in the photoreactor for 5 min. The crude reaction mixture was concentrated and purified by flash chromatography (SiO_2, 2:1 benzene:hexanes R_f = 0.2) to afford the desired product as a white solid (40 mg, 59%). Crystals suitable for X-ray diffraction were grown by layering a saturated CH_2Cl_2 solution with hexane. **^{1}H NMR** (CD_2Cl_2, 400 MHz, δ): 7.23 – 7.11 (m, 5H), 2.39 (q, J = 12.2 Hz, 3H), 1.93 – 1.83 (m, 6H), 1.83 – 1.74 (m, 6H), 1.72 – 1.55 (m, 9H), 1.33 – 1.18 (m, 3H), 1.15 – 1.00 (m, 6H). **^{13}C{^{1}H} NMR** (CD_2Cl_2, 126 MHz, δ): 148.4 (d, J = 9 Hz), 131.6, 129.2, 126.2, 34.7 (d, J = 25 Hz), 29.7 (d, J = 3 Hz), 27.2 (d, J = 11 Hz), 25.9. **^{31}P{^{1}H} NMR** (CD_2Cl_2, 202 MHz, δ): 25.5 (q, $^3J_{P\text{-}F}$ = 62 Hz). **^{19}F NMR** (CD_2Cl_2, 376 MHz, δ): -22.7 (d, $^3J_{P\text{-}F}$ = 62 Hz). **Anal. Calcd.** for $C_{25}H_{38}AuF_3IP$: C, 40.01; H, 5.10. Found C, 40.30; H, 4.76.

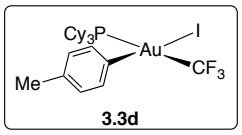

3.3d

A solution of $Cy_3PAu(4\text{-}Me\text{-}C_6H_4)$ (45 mg, 0.079 mmol) in CH_2Cl_2 (2.5 mL) was placed in a 25 mL glass bomb and cooled to –78 ºC. The reaction was degassed under vacuum, warmed to room temperature, and backfilled with CF_3I (1 atm, 0.92 mmol in headspace, 1.0 mmol in solution). The vessel was sealed and irradiated in the photoreactor for 5 min. The crude reaction mixture was concentrated and purified by flash chromatography (SiO_2, 1:4 → 1:1 benzene:hexanes, R_f = 0.3) to afford the desired product as a white solid (23 mg, 38 %). Crystals suitable for X-ray diffraction were grown by layering a saturated CH_2Cl_2 solution with hexane. **^{1}H NMR** (CD_2Cl_2, 500 MHz, δ): 7.06 (d, *J* = 8.3 Hz, 2H), 7.02 (d, *J* = 8.2 Hz, 2H), 2.40 (m, 3H), 1.91 – 1.85 (m, 6H), 1.84 – 1.74 (m, 6H), 1.72 – 1.55 (m, 9H), 1.32 – 1.19 (m, 3H), 1.15 – 1.00 (m, 6H). **^{13}C{^{1}H} NMR** (CD_2Cl_2, 126 MHz, δ): 145.3-145.0 (m), 136.3, 131.7, 130.3, 35.2 (d, *J* = 25 Hz), 30.3 (d, *J* = 3 Hz), 27.8 (d, *J* = 11 Hz), 26.5, 21.0. **^{31}P{^{1}H} NMR** (CD_2Cl_2, 202 MHz, δ): 25.5 (q, $^3J_{P\text{-}F}$ = 62 Hz). **^{19}F NMR** (CD_2Cl_2, 376 MHz, δ): -20.6 (d, $^3J_{P\text{-}F}$ = 62 Hz). **Anal. Calcd.** for $C_{26}H_{40}AuF_3IP$: C, 40.85; H, 5.27. Found C, 40.94; H, 4.98.

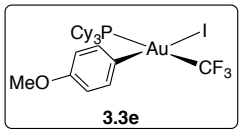

3.3e

A solution of $Cy_3PAu(4\text{-}OMe\text{-}C_6H_4)$ (150 mg, 0.26 mmol) in CH_2Cl_2 (16 mL) was placed in a 20 mL glass bomb and cooled to –78 ºC. The reaction was degassed under vacuum, warmed to room temperature, and backfilled with CF_3I (1 atm, 0.16 mmol in headspace, 6.4 mmol in solution). The vessel was sealed and irradiated in the photoreactor for 5 min, then cooled to 0 °C. To the cold reaction was added MeCN (1 mL), after which it was concentrated *in vacuo* while cooling. After ~0.5 mL of solvent remained, the reaction was warmed to room temperature and dried completely over 5 minutes to afford a yellow solid, which was dissolved in a minimal amount of benzene. Pentane was added dropwise to induce crystallization. The white crystals (89 mg, 44%) were collected after 5 minutes, washed with pentane, then dried *in vacuo* for 1 minute. The material was immediately characterized by NMR. **^{1}H NMR** (C_6D_6, 500 MHz, δ): 7.07 (d, *J* = 8.6 Hz, 2H), 6.69 (d, *J* = 8.7 Hz, 2H), 3.31 (s, 3H), 2.43 – 2.30 (m, 3H), 1.78 – 1.68 (m, 6H), 1.58 – 1.48 (m, 8H), 1.48 – 1.34 (m, 10H), 1.32 – 1.21 (m, 6H). **^{13}C{^{1}H} NMR** (C_6D_6, 126 MHz, δ): 158.4, 155.4-155.2 (m), 132.3, 114.8, 54.8, 34.8 (d, *J* = 35 Hz), 30.0 (d, *J* = 3 Hz), 27.4 (d, *J* = 11 Hz), 26.1. **^{31}P{^{1}H} NMR** (C_6D_6, 202 MHz, δ): 23.3 (q, $^3J_{P\text{-}F}$ = 63 Hz). **^{19}F NMR** (C_6D_6, 376 MHz, δ): –20.6 (d, $^3J_{P\text{-}F}$ = 64 Hz). Multiple attempts were made to subject **3e** to elemental analysis. Even at -20 °C, compound **3e** decomposes to Au nanoparticles and several Au-CF_3 containing species in solution and in the solid state. No products of Ar-X reductive elimination can be detected.

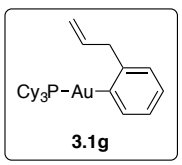

3.1g

To a cold (–78 ºC) suspension of $(Cy_3P)AuCl$ (250 mg, 0.49 mmol, 1.00 equiv) in THF was added (*o*-allyl)C_6H_4MgBr (1.0 M in THF, 2 equiv) dropwise via syringe. The resulting solution was stirred at –78 ºC for 1 h then warmed to 0 ºC and stirred for 1 h. The reaction was quenched with water at 0 ºC and extracted into CH_2Cl_2 (5 mL). The layers were separated and the aqueous phase was washed with additional CH_2Cl_2 (5 mL). The combined organic layers were washed with water (5 mL) and dried over Na_2SO_4, filtered and concentrated to dryness *in vacuo*. Recrystallization

from CH_2Cl_2/hexanes yielded the desired compound as colorless needles (220 mg, 79 %). **^{1}H NMR** (CD_2Cl_2, 500 MHz, δ): 7.36 (t, *J* = 5.9 Hz, 1H), 7.11 (d, *J* = 7.4 Hz, 1H), 7.05 (t, *J* = 7.4, 1H), 6.96 (t, *J* = 7.3 Hz, 1H), 6.11 (m, 1H), 5.03 (d, *J* = 17.2 Hz, 1H), 4.93 (d, *J* = 10.3 Hz, 1H), 3.58 (d, *J* = 6.8 Hz, 2H), 2.14 – 2.01 (m, 10H), 1.87 (d, *J* = 11.7 Hz, 6H), 1.74 (d, *J* = 10.3 Hz, 3H), 1.61 – 1.49 (m, 4H), 1.40 – 1.24 (m, 10H). **^{13}C{^{1}H} NMR** (CD_2Cl_2,126 MHz, δ): 178.3 (d, *J* = 108 Hz), 148.9, 141.2, 139.3, 128.0 (d, *J* = 6 Hz), 125.1, 124.9 (d, *J* = 5 Hz), 113.7, 46.0, 33.6 (d, *J* = 24 Hz), 31.1, 27.6 (d, *J* = 11 Hz), 26.5. **^{31}P{^{1}H} NMR** (CD_2Cl_2, 162 MHz, δ): 57.6 (s). **Anal. Calcd.** for $C_{27}H_{42}AuP$: C, 54.54; H, 7.12. Found: C, 54.25; H, 7.10.

(Cy_3P)AuMe (9). To a cold (–78 ºC) suspension of (Cy_3P)AuCl (250 mg, 0.49 mmol, 1.00 equiv) in THF was added MeMgBr (3.0 M in THF, 0.5 mL, 2.0 equiv) dropwise via syringe. The resulting solution was stirred at –78 ºC for 1 h then warmed to 0 ºC and stirred for 1 h. The reaction was quenched with water at 0 ºC and extracted into Et_2O (5 mL). The layers were separated and the aqueous phase was washed with additional Et_2O (5 mL). The combined organic layers were washed with water (5 mL) and dried over Na_2SO_4, filtered and concentrated to dryness *in vacuo* to give (Cy_3P)AuMe as a white powder (220 mg, 79 %). **^{1}H NMR** (CD_2Cl_2, 400 MHz, δ): 2.00 – 1.90 (m, 9H), 1.85 – 1.75 (m, 6H), 1.72 – 1.60 (m, 3H), 1.55 – 1.35 (m, 6H), 1.30 – 1.15 (m, 9H), 0.11 (d, $^3J_{H\text{-}P}$ = 7.2 Hz) **^{13}C{^{1}H} NMR** (CD_2Cl_2, 100 MHz, δ): 33.2 (d, *J* = 23 Hz), 30.5, 27.2 (d, *J* = 11 Hz), 26.0, 10.0 (d, *J* = 92 Hz). **^{31}P{^{1}H} NMR** (CD_2Cl_2, 162 MHz, δ): 60.1 (s). **Anal. Calcd.** for $C_{19}H_{36}AuP$: C, 46.34; H, 7.37. Found: C, 46.12; H, 6.98.

[Me_3P-CF_3]I (10a). A solution of PMe_3 (8 mg, 0.11 mmol) in CD_2Cl_2 (1 mL) was degassed under vacuum in a 2 mL J. Young NMR tube. The tube was backfilled with CF_3I (1 atm, 41 mmol in headspace, 0.44 mmol in solution) and sealed and placed in the photoreactor. Following irradiation for 5 minutes, white crystals formed in the reaction vessel. The reaction was cooled to 0 °C and placed under vacuum for 1 minute to remove excess CF_3I (but not CD_2Cl_2). If dried, the white powdery product cannot be re-dissolved in either CD_2Cl_2 or $CDCl_3$, and reacts with d_6-DMSO to generate Me_3PO. Because the reaction is quantitative and affords a single product, **10a** was characterized directly from the reaction mixture. **^{1}H NMR** (CD_2Cl_2, 500 MHz, δ): 1.25 (d, $^2J_{H\text{-}P}$ = 2.8 Hz, 9H). **^{13}C{^{1}H} NMR** (CD_2Cl_2, 126 MHz, δ): 8.4 (dq, $^1J_{C\text{-}P}$ = 14 Hz, $^3J_{C\text{-}F}$ = 4 Hz); CF_3 carbon not observed. **^{31}P{^{1}H} NMR** (CD_2Cl_2, 162 MHz, δ): -25.5 (q, $^2J_{P\text{-}F}$ = 65 Hz). **^{19}F NMR** (CD_2Cl_2, 376 MHz, δ): –64.3 (d, $^2J_{P\text{-}F}$ = 64 Hz). **MS** (ESI) $[Me_3P\text{-}CF_3]^+$: calcd mass 145.0, measured mass 145.2. The iodide was also found.

[Cy_3P-CF_3]I (10b). A solution of PCy_3 (31 mg, 0.11 mmol) in CD_2Cl_2 (1 mL) was degassed under vacuum in a 2 mL J. Young NMR tube. The tube was backfilled with CF_3I (1 atm, 41 mmol in headspace, 0.44 mmol in solution) and sealed and placed in the photoreactor. The reaction was irradiated for 10 minutes, then cooled to 0 °C and placed under vacuum for 1 minute to remove excess CF_3I (but not CD_2Cl_2). The product decomposes upon concentration. Attempts to isolate or crystallize the product by anion metathesis with $NaB(Ar_F)_4$ (Ar_F = 3,5-$(CF_3)_2C_6H_3$) were unsuccessful as well. Because the reaction is quantitative and affords a single product, **10b** was spectroscopically characterized directly from the reaction mixture. **^{1}H NMR** (CD_2Cl_2, 500 MHz, δ): 4.48 – 4.03 (m, 1H), 2.29 – 2.15 (m, 2H), 2.11 – 1.63 (m, 18H), 1.57 – 1.22 (m, 6H). **^{13}C{^{1}H} NMR** (CD_2Cl_2, 126 MHz, δ): 39.7, 31.1 (d, *J* = 15 Hz), 29.5 (d, *J* = 8 Hz), 29.4 (s), 27.2 (d, *J* = 9 Hz), 27.0 (d, *J* = 6 Hz), 26.02 (s), 25.1 (s); CF_3 carbon not observed. **^{31}P{^{1}H} NMR** (CD_2Cl_2, 162 MHz, δ): 18.2 (q, $^2J_{P\text{-}F}$ = 53 Hz). **^{19}F NMR** (CD_2Cl_2, 376 MHz, δ):

–49.0 (d, $^{2}J_{P\text{-}F}$ = 53 Hz). **MS** (ESI) $[Cy_3P\text{-}CF_3]^+$: calcd mass 349.2, measured mass 349.2. A peak corresponding to Cy_3PO (m/z = 297.3) was also found

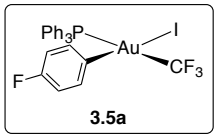

3.5a

A solution of $(Ph_3P)Au(4\text{-}F\text{-}C_6H_4)$ (28 mg, 0.050 mmol) in CH_2Cl_2 (2.8 mL) was placed in a 10 mL glass bomb and cooled to –78 ºC. The reaction was degassed under vacuum, warmed to room temperature, and backfilled with CF_3I (1 atm, 0.29 mmol in headspace, 1.1 mmol in solution). The crude reaction mixture was concentrated and purified by flash chromatography (SiO_2, 1:3 benzene:hexanes, R_f = 0.2) to afford the desired product as a white solid (27 mg, 71%). Crystals suitable for X-ray diffraction were grown by layering pentane onto a saturated CH_2Cl_2 solution. **^{1}H NMR** (CD_2Cl_2, 500 MHz, δ): 7.60 – 7.37 (m, 15H), 6.79 (dd, J = 8.1, 5.3 Hz, 2H), 6.58 (t, J = 8.9 Hz, 2H). **^{13}C{^{1}H} NMR** (CD_2Cl_2, 125 MHz, δ): 161.5 (d, *J* = 244 Hz), 135.1 (d, *J* = 10 Hz), 132.3 (d, *J* = 3 Hz), 131.6 (d, J = 7 Hz), 131.5 (d, J = 7 Hz), 129.1 (d, J = 11 Hz), 126.6 (d, J = 59 Hz), 116.1 (d, J = 21 Hz); due to direct bonding to Au, as well as coupling to ^{31}P and ^{19}F, the Au-CF_3 carbon was not found. **^{31}P{^{1}H} NMR** (CD_2Cl_2, 162 MHz, δ) 20.0 (q, $^{3}J_{P\text{-}F}$ = 68 Hz). **^{19}F NMR** (CD_2Cl_2, 376 MHz, δ): –21.0 (d, $^{3}J_{P\text{-}F}$ = 68 Hz), –117.7 (s). **Melting point** 162 ºC (decomposition). **Anal. Calcd.** for $C_{26}H_{22}AuF_3IP$: C, 40.02; H, 2.55. Found C, 39.78; H, 2.51.

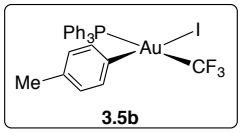

3.5b

A solution of $(Ph_3P)Au(4\text{-}Me\text{-}C_6H_4)$ (29 mg, 0.054 mmol) in CH_2Cl_2 (2.8 mL) was placed in a 10 mL glass bomb and cooled to –78 ºC. The reaction was degassed under vacuum, warmed to room temperature, and backfilled with CF_3I (1 atm, 0.29 mmol in headspace, 1.1 mmol in solution). The vessel was sealed and irradiated in the photoreactor for 5 min, then taken into the glovebox. The crude reaction mixture was concentrated and purified by flash chromatography (SiO_2, 1:3 → 1:1 benzene:hexanes, R_f = 0.2) to afford the desired product as a white solid (25 mg, 63%). Crystals suitable for X-ray diffraction were grown by layering pentane onto a saturated CH_2Cl_2 solution. **^{1}H NMR** (CD_2Cl_2, 500 MHz, δ): 7.54 – 7.47 (m, 3H), 7.47 – 7.32 (m, 12H), 6.66 (d, *J* = 8.2 Hz, 2H), 6.62 (d, *J* = 8.1 Hz, 2H), 2.14 (s, 3H). **^{13}C{^{1}H} NMR** (CD_2Cl_2, 125 MHz, δ): 147.5 – 147.0 (m), 136.1, 135.3 (d, *J* = 10 Hz), 132.3 (d, *J* = 3 Hz), 130.6 (d, *J* = 10 Hz), 129.1 (d, *J* = 10 Hz), 127.2, 126.7, 20.7. **^{31}P{^{1}H} NMR** (CD_2Cl_2, 162 MHz, δ) 20.4 (q, $^{3}J_{P\text{-}F}$ = 67 Hz). **^{19}F NMR** (CD_2Cl_2, 376 MHz, δ): –21.3 (d, $^{3}J_{P\text{-}F}$ = 67 Hz). **Anal. Calcd.** for $C_{26}H_{22}AuF_3IP$: C, 41.84; H, 2.97. Found C, 42.03; H, 2.83.

Typical Procedure for Photochemical Reactions

Most reactions were conducted in borosilicate J. Young NMR tubes. Prior to irradiation, reactions were degassed under vacuum. The tube was then warmed to room temperature, and backfilled with CF_3I (1 atm). Control reactions were set up identically, except they were wrapped in foil prior to introduction of CF_3I, and kept in the dark until just before being placed in the NMR probe. For irradiated reactions, NMR tubes containing the reaction mixture were placed into borosilicate test tubes containing an optical filter solution (2 mM aq. K_2CrO_4,, 1% w/v K_2CO_3) and irradiated using a 450 W Hanovia Hg-Vapor lamp for the indicated time period. After irradiation, the samples were then analyzed by ^{19}F NMR. For reactions run in glass bombs: the reaction vessel was placed in a Pyrex beaker containing the optical filter solution.

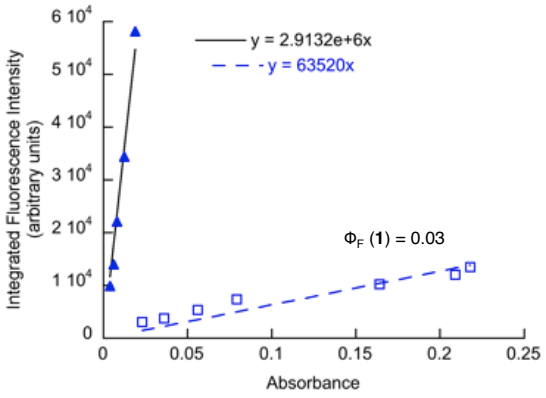

Figure 3.10. Fluorescence quantum yield measurements for $Cy_3PAu(4\text{-}F\text{-}C_6H_4)$ (**1a**) in CH_2Cl_2 (□) verses quinine sulfate in 0.1 M aq. H_2SO_4 (**Δ**). Excitation at 320 nm.

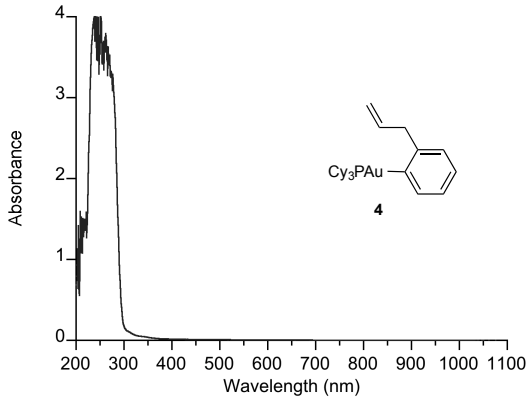

Figure 3.11. UV/Vis absorption spectrum of $Cy_3PAu(2\text{-}(CH_2CH{=}CH_2)C_6H_4)$ (**4**) in CH_2Cl_2 (2.0 mM).

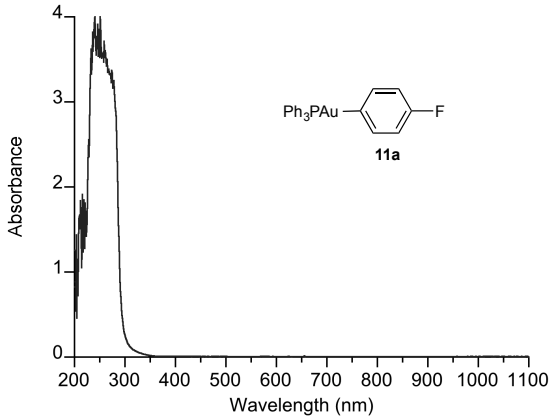

Figure 3.12. UV/Vis absorption spectrum of $Ph_3PAu(4\text{-}F\text{-}C_6H_4)$ (**11a**) in CH_2Cl_2 (2.0 mM).

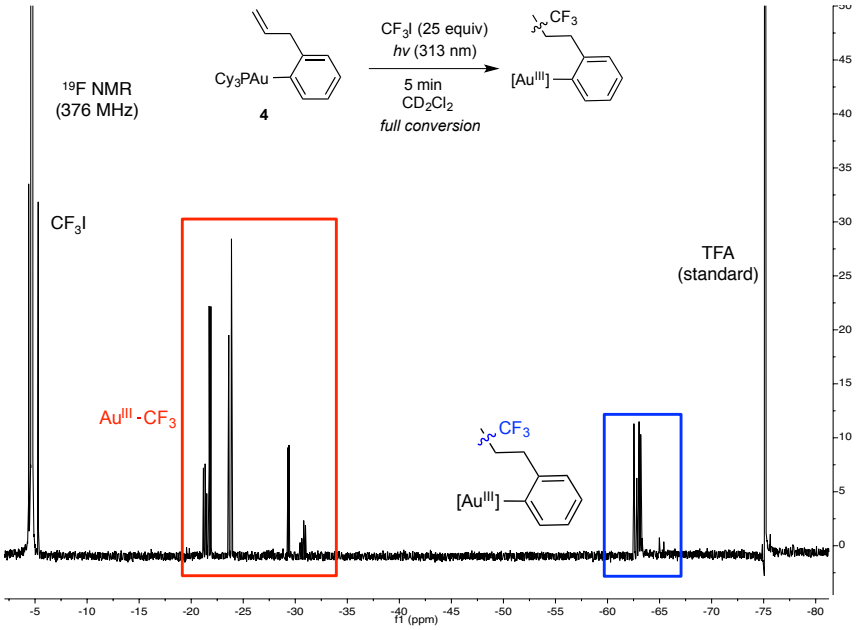

Figure 3.13. ^{19}F NMR spectrum (376 MHz, CD_2Cl_2) of irradiation of **4** (313 nm) in the presence of CF_3I for 5 minutes (trifluoroacetic acid as a standard).

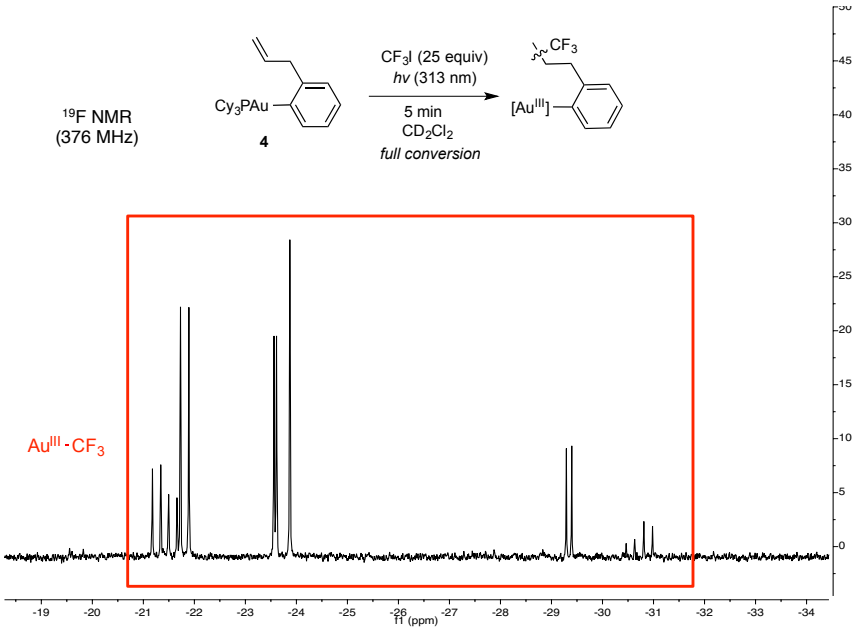

Figure 3.14. Selected regions of ^{19}F NMR spectrum (376 MHz, CD_2Cl_2) of irradiation of **4** (313 nm) in the presence of CF_3I for 5 minutes (trifluoroacetic acid as a standard).

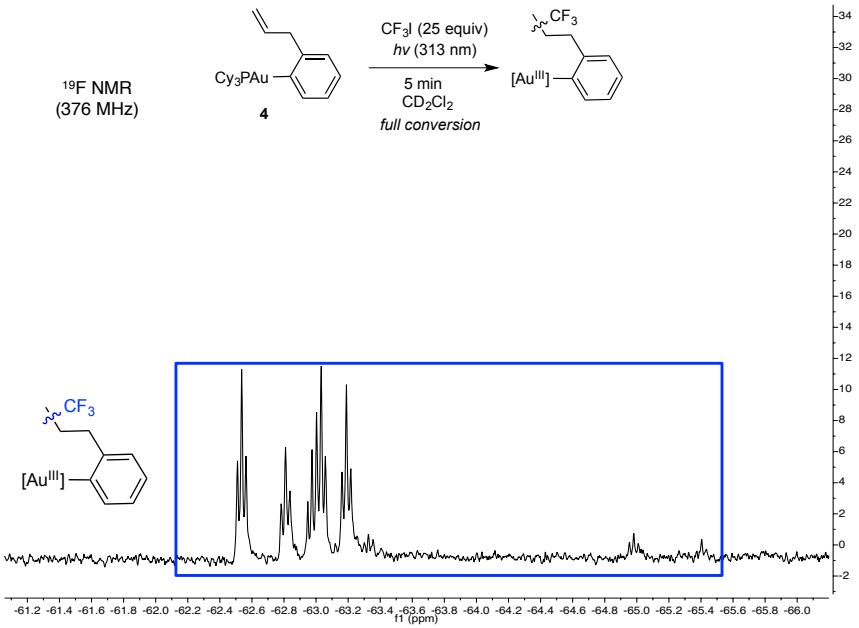

Figure 3.15. Selected regions of ^{19}F NMR spectrum (376 MHz, CD_2Cl_2) of irradiation of **4** (313 nm) in the presence of CF_3I for 5 minutes (trifluoroacetic acid as a standard).

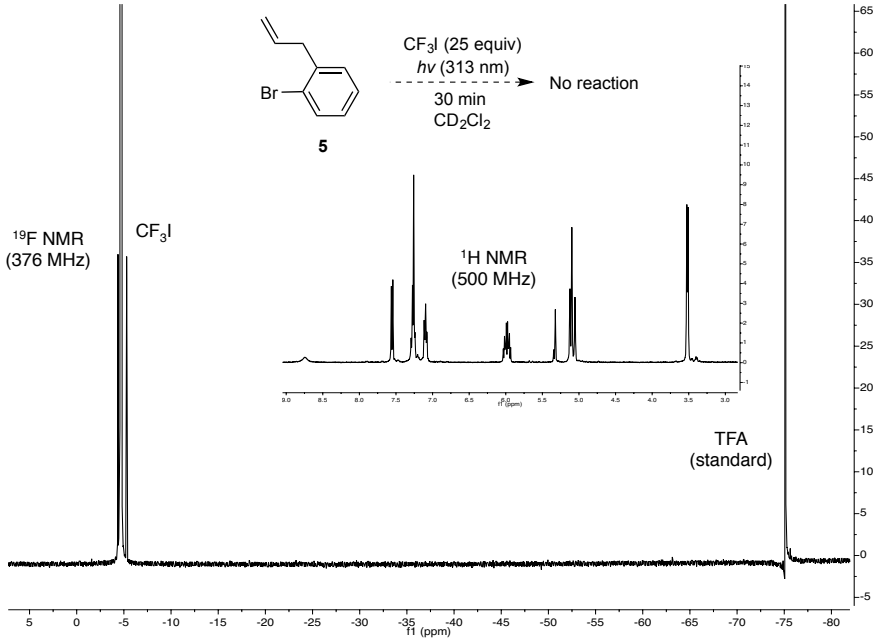

Figure 3.16. ^{19}F NMR spectrum (376 MHz, CD_2Cl_2) of irradiation of 2-allyl-1-bromobenzene (**5**) (313 nm) in the presence of CF_3I for 30 minutes (trifluoroacetic acid as a standard.) Inset: ^1H NMR spectrum (500 MHz, CD_2Cl_2) of the same reaction (signals at d 8.76, 5.32 and 5.30 are TFA, $CDHCl_2$ and CH_2Cl_2, respectively).

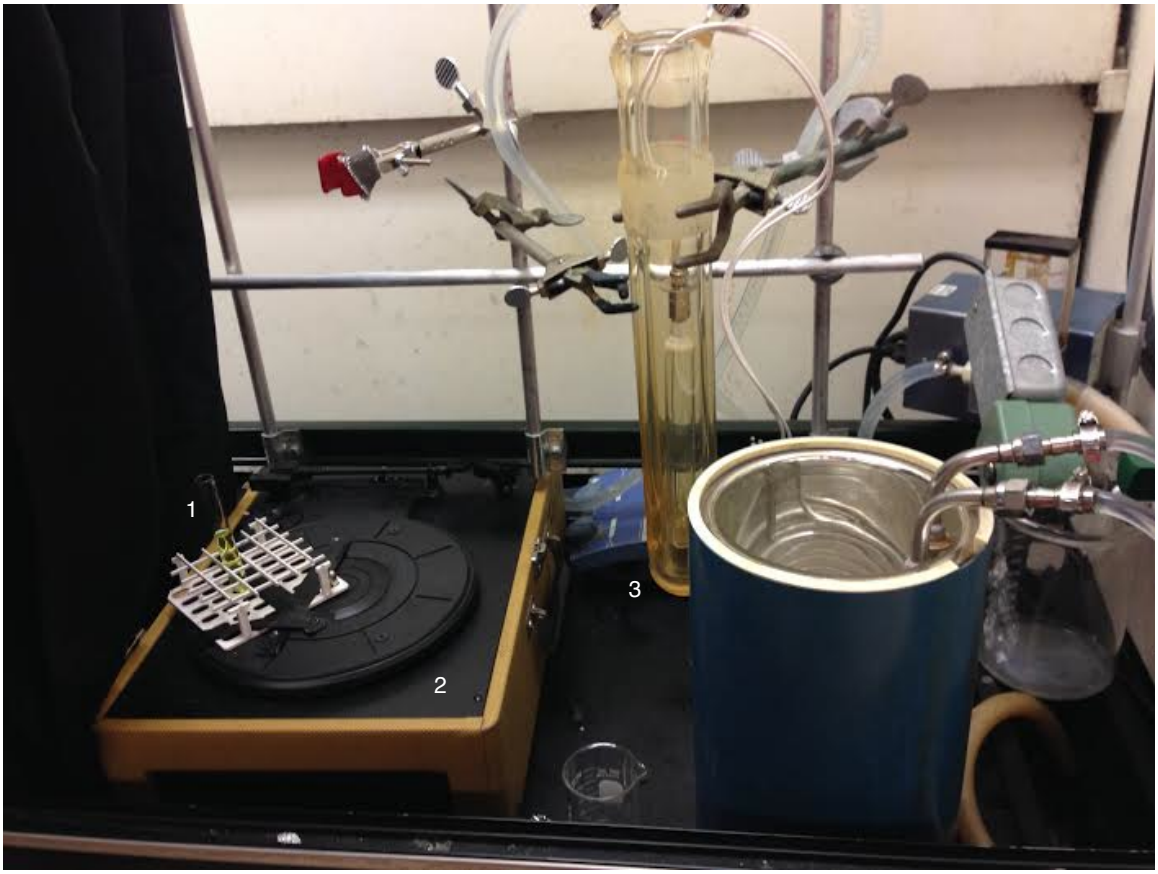

Figure 3.17. Photochemical experimental setup for irradiation of NMR reactions (1: borosilicate test tube with 2 mM aq. K_2CrO_4,, 1% w/v K_2CO_3 optical solution; 2: turntable; 3: 450 W Hanovia Hg vapor lamp).

References:

(1) Johnson, A.; Puddephatt, R. J. *Inorg. Nucl. Chem. Lett.* **1973**, *9* (11), 1175–1177.
(2) Tamaki, A.; Kochi, J. K. *J. Organomet. Chem.* **1974**, *64* (3), 411–425.
(3) Johnson, A.; Puddephatt, R. J. *J. Organomet. Chem.* **1975**, *85* (1), 115–121.
(4) Shiotani, A.; Schmidbaur, H. *J. Organomet. Chem.* **1972**, *37* (1), C24–C26.
(5) Tamaki, A.; Magennis, S. A.; Kochi, J. K. *J. Am. Chem. Soc.* **1973**, *95* (19), 6487–6488.
(6) Fackler Jr, J. P. *Polyhedron* **1997**, *16* (1), 1–17.
(7) Tamaki, A.; Magennis, S. A.; Kochi, J. K. *J. Am. Chem. Soc.* **1974**, *96* (19), 6140–6148.
(8) Komiya, S.; Albright, T. A.; Hoffmann, R.; Kochi, J. K. *J. Am. Chem. Soc.* **1976**, *98* (23), 7255–7265.
(9) Komiya, S.; Kochi, J. K. *J. Am. Chem. Soc.* **1976**, *98* (24), 7599–7607.
(10) Lawrence Kuch, P.; Stuart Tobias, R. *J. Organomet. Chem.* **1976**, *122* (3), 429–446.
(11) Vicente, J.; Dolores Bermudez, M.; Escribano, J. *Organometallics* **1991**, *10* (9), 3380–3384.
(12) Vicente, J.; Bermúdez, M. D.; Carrión, F. J. *Inorganica Chim. Acta* **1994**, *220* (1), 1–3.
(13) Vicente, J.; Bermúdez, M.-D.; Carrión, F.-J.; Jones, P. G. *Chem. Ber.* **1996**, *129* (11), 1395–1399.
(14) Hashmi, A. S. K.; Blanco, M. C.; Fischer, D.; Bats, J. W. *Eur. J. Org. Chem.* **2006**, *2006* (6), 1387–1389.

(15) Ball, L. T.; Lloyd-Jones, G. C.; Russell, C. A. *Science* **2012**, *337* (6102), 1644–1648.
(16) Ball, L. T.; Lloyd-Jones, G. C.; Russell, C. A. *J. Am. Chem. Soc.* **2014**, *136* (1), 254–264.
(17) Hughes, R. P. In *Advances in Organometallic Chemistry*; West, F. G. A. S. and R., Ed.; Academic Press, 1990; Vol. 31, pp 183–267.
(18) Morrison, J. A. In *Advances in Organometallic Chemistry*; West, F. G. A. S. and R., Ed.; Academic Press, 1993; Vol. 35, pp 211–239.
(19) Culkin, D. A.; Hartwig, J. F. *Organometallics* **2004**, *23* (14), 3398–3416.
(20) Grushin, V. V.; Marshall, W. J. *J. Am. Chem. Soc.* **2006**, *128* (14), 4632–4641.
(21) Grushin, V. V.; Marshall, W. J. *J. Am. Chem. Soc.* **2006**, *128* (39), 12644–12645.
(22) Cho, E. J.; Senecal, T. D.; Kinzel, T.; Zhang, Y.; Watson, D. A.; Buchwald, S. L. *Science* **2010**, *328* (5986), 1679–1681.
(23) Ball, N. D.; Kampf, J. W.; Sanford, M. S. *J. Am. Chem. Soc.* **2010**, *132* (9), 2878–2879.
(24) Ball, N. D.; Gary, J. B.; Ye, Y.; Sanford, M. S. *J. Am. Chem. Soc.* **2011**, *133* (19), 7577–7584.
(25) Tomashenko, O. A.; Grushin, V. V. *Chem. Rev.* **2011**, *111* (8), 4475–4521.
(26) Johnson, A.; Puddephatt, R. J. *J. Chem. Soc. Dalton Trans.* **1976**, No. 14, 1360–1363.
(27) Joost, M.; Zeineddine, A.; Estévez, L.; Mallet−Ladeira, S.; Miqueu, K.; Amgoune, A.; Bourissou, D. *J. Am. Chem. Soc.* **2014**, *136* (42), 14654–14657.
(28) Nagib, D. A.; Scott, M. E.; MacMillan, D. W. C. *J. Am. Chem. Soc.* **2009**, *131* (31), 10875–10877.
(29) Kino, T.; Nagase, Y.; Ohtsuka, Y.; Yamamoto, K.; Uraguchi, D.; Tokuhisa, K.; Yamakawa, T. *J. Fluor. Chem.* **2010**, *131* (1), 98–105.
(30) Ye, Y.; Sanford, M. S. *J. Am. Chem. Soc.* **2012**, *134* (22), 9034–9037.
(31) Wagner, P. J.; Kemppainen, A. E. *J. Am. Chem. Soc.* **1972**, *94* (21), 7495–7499.
(32) US Department of Commerce, N. NIST Manuscript Publication Search http://www.nist.gov/manuscript-publication-search.cfm?pub_id=913405 (accessed Feb 25, 2016).
(33) Partyka, D. V.; Zeller, M.; Hunter, A. D.; Gray, T. G. *Angew. Chem. Int. Ed.* **2006**, *45* (48), 8188–8191.
(34) Partyka, D. V.; Esswein, A. J.; Zeller, M.; Hunter, A. D.; Gray, T. G. *Organometallics* **2007**, *26* (14), 3279–3282.
(35) Vogt, R. A.; Gray, T. G.; Crespo-Hernández, C. E. *J. Am. Chem. Soc.* **2012**, *134* (36), 14808–14817.
(36) Visbal, R.; Ospino, I.; López-de-Luzuriaga, J. M.; Laguna, A.; Gimeno, M. C. *J. Am. Chem. Soc.* **2013**, *135* (12), 4712–4715.
(37) Crespo, O.; Díez-Gil, C.; Gimeno, M. C.; Jones, P. G.; Laguna, A.; Ospino, I.; Tapias, J.; Villacampa, M. D.; Visbal, R. *Dalton Trans.* **2013**, *42* (23), 8298–8306.
(38) Monzittu, F. M.; Fernández-Moreira, V.; Lippolis, V.; Arca, M.; Laguna, A.; Gimeno, M. C. *Dalton Trans.* **2014**, *43* (16), 6212–6220.
(39) Nyden, M. R. In *Fire Suppression System Performance of Alternative Agents in Aircraft Engine and Dry Bay Laboratory Simulations*; Gann, R. G., Ed.; National Institutes of Standards and Technology: Washington D.C.; pp 77–95.
(40) Usui, Y.; Noma, J.; Hirano, M.; Komiya, S. *Inorganica Chim. Acta* **2000**, *309* (1–2), 151–154.
(41) Buckler, S. A.; Doll, L.; Lind, F. K.; Epstein, M. *J. Org. Chem.* **1962**, *27* (3), 794–798.

(42) Blaya, M.; Bautista, D.; Gil-Rubio, J.; Vicente, J. *Organometallics* **2014**, *33* (22), 6358–6368.
(43) Croix, C.; Balland-Longeau, A.; Allouchi, H.; Giorgi, M.; Duchêne, A.; Thibonnet, J. *J. Organomet. Chem.* **2005**, *690* (21–22), 4835–4843.
(44) Watson, I. D. G.; Ritter, S.; Toste, F. D. *J. Am. Chem. Soc.* **2009**, *131* (6), 2056–2057.
(45) Partyka, D. V.; Zeller, M.; Hunter, A. D.; Gray, T. G. *Inorg. Chem.* **2012**, *51* (15), 8394–8401.
(46) Hashmi, A. S. K.; Ramamurthi, T. D.; Rominger, F. *J. Organomet. Chem.* **2009**, *694* (4), 592–597.
(47) Weber, D.; Jones, T. D.; Adduci, L. L.; Gagné, M. R. *Angew. Chem. Int. Ed.* **2012**, *51* (10), 2452–2456.

Chapter 4: Halide dependent mechanisms of C(sp^2)–X reductive elimination from Au(III) and synthesis of a nucleophilic Au(III) fluoride.

Portions of work were conducted in collaboration with Dr. Matthew S. Winston and have been used with permission from "Halide Dependent Mechanisms of C-X and C-C reductive elimination from Gold(III)." *J. Am Chem. Soc.* **2015**, *137*, 7921–7928. Copyright (2015) American Chemical Society. Another portion was used with permission from "The Chemistry of Gold Fluorides" from *PATAI'S Chemistry of Functional Groups*; Rappoport, Z., Ed.; John Wiley & Sons, Ltd: Chichester, UK, 2014; pp 391–408. Copyright (2014) John Wiley and Sons, Ltd.

Abstract: Two organometallic halide series (Ph_3P)Au(4-Me-C_6H_4)(CF_3)(X) and (Cy_3P)Au(4-F-C_6H_4)(CF_3)(X) (X = I, Br, Cl, F) have been synthesized and mechanistic studies of thermolysis at 122 °C reveal a dramatic reactivity dependence on the identity of the halide ligand. For X = I or F, zero-order kinetic behavior is observed, while for X = Cl or Br, kinetic studies implicate product catalysis. Furthermore, the kinetic selectivity for C(sp^2)–X or C(sp^2)–CF_3 reductive elimination is affected by nature of the halide. The selectivity for C(sp^2)–CF_3 bond formation increases in the order X = I < Br < Cl < F, with exclusively C(sp^2)–I bond formation when X = I, and exclusively C(sp^2)–CF_3 bond formation when X = F. Thermodynamic measurements show that Au(III)–X bond dissociation energies increase in the order X = I < Br < Cl, and that ground state Au(III)–X bond strength ultimately dictates selectivities for C(sp^2)–X and C(sp^2)–CF_3 reductive elimination.

Introduction: Transition metal catalyzed transformations proceed through a series of fundamental steps i.e. oxidative addition, migratory insertion, and reductive elimination. To minimize deleterious side reactions and maximize overall catalyst efficiency, the metal must undergo the proper series of reactions with excellent selectivity. A fundamental understanding of the factors that affect these steps is critical in designing and improving new metal catalyzed transformations.

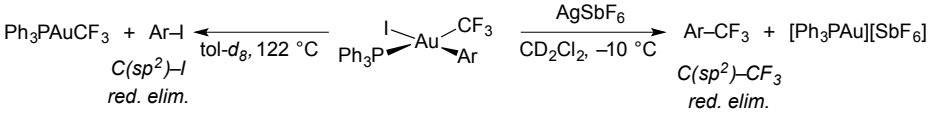

Figure 4.1. Divergent reductive elimination behavior of Au(III) complexes

The photochemical oxidative addition to CF_3I to Au(I) aryl complexes gives the Au(III) complexes (Ph_3P)Au(CF_3)(aryl)(I). These complexes undergo rapid C(sp^2)–CF_3 reductive elimination when treated with $AgSbF_6$ (Figure 4.1). This transformation presumably proceeds *via* the cation [(Ph_3P)Au(aryl)(CF_3)]$^+$. Although this step demonstrates the oxidizing ability of Au(III) cations, a reliance on stoichiometric Ag(I) salts to generate the reactive cation is ultimately impractical if a catalytic process involving such Au(III) intermediates is to be realized. Since efforts to photochemically or catalytically induce iodide dissociation with Lewis acids failed, we also investigated thermolytic routes and found that neutral **4.1-I** undergoes solely C(sp^2)–I reductive elimination at high temperatures (122 °C) (Figure 4.1). Although C(sp^2)–I reductive elimination from these complexes is facile, the factors controlling selectivity are unclear due to a lack of other members of the halide family that could allow a comparative study.

Hartwig has shown that the rates of reversible C(sp^2)–X reductive elimination from three-coordinate Pd(II) increase with halide polarizability (X = Cl < Br < I), while the thermodynamic driving force increases in the order X = I < Br < Cl.[1] However, because C− X (X = halide) reductive elimination is often endothermic, studies typically rely on using high-valent late metals such as Cu(III), Pd(IV) and Pt(IV) to establish a thermodynamic driving force.[2–18] In this vein, Au-catalyzed halogenations likely involve C(sp^2)−X reductive elimination from Au(III),[19–22] and C(sp^3)−F[23] and C(sp^3)−I[24] eliminations from Au(III) have also been demonstrated.

C(sp^2)−X reductive elimination is not necessarily productive, and may be a decomposition pathway for high-valent organometallic species with halide ligands. Importantly, Au(III) catalysts, which are often generated using dihalogen (or formal dihalogen) oxidants and stabilized by halide ligands,[25] could undergo deleterious, irreversible C(sp^2)−X bond formation to deplete active catalyst concentrations. With access to a full family of Au(III) halides, trends in the rates of C(sp^2)−X reductive elimination from Au(III) could be established. Perhaps slower C(sp^2)−X bond formation could also be exploited to promote selectivity for otherwise challenging reductive eliminations, such as C(sp^2)−CF_3 bond formation in complexes of the type (R_3P)Au(aryl)(CF_3)(X). Studies of competitive reductive eliminations should inform factors dictating selectivity in catalytic cycles.[9,17] The synthesis and characterization of a series of well-defined complexes of the type (R_3P)Au(aryl)-(CF_3)(X) (X = I, Br, Cl, F) that undergo both C(sp^2)−X and C(sp^2)− CF_3 reductive elimination with different, halide-dependent kinetic ratios is described. These ratios vary systematically among the halide series, showing that halide ligands can dramatically influence reaction behavior. The synthesis and solution state characterization of a novel Au(III) hydride is also discussed.

Results and Discussion: Sonication of **4.1-I** or **4.2-I** with excess AgX (X = Br, Cl, F) affords metathesis products **4.1-X** and **4.2-X** (X = Br, Cl, F) in high yield (Figure 4.2). The compounds **4.1-F** and **4.2-F** represents rare examples of an isolable organometallic Au(III) fluoride (Figure 4.3).

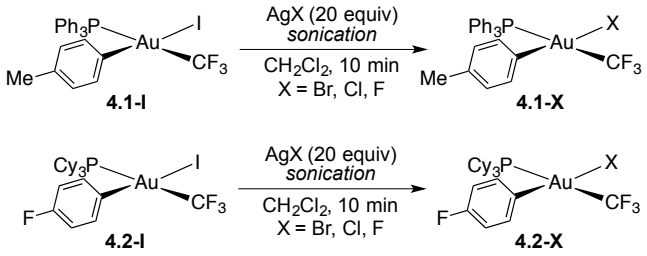

Figure 4.2. Synthesis of Au(III) halide series *via* halide metathesis.

Fluoride complexes of the coinage metals are scarce.[13–15] Gold fluorides, especially ligand-supported complexes, remain uncommon; an anomaly considering the recent interest in gold complexes and gold catalysis.[16]The first attempt to synthesize a gold fluoride was made by Moissan when he heated gold metal under an atmosphere of fluorine gas in 1889.[26,27] He obtained a hygroscopic orange powder, but was unable to identify the substance. Since then, evidence for the existence of the homoleptic gold fluorides AuF, AuF_3, and AuF_5 has been reported.

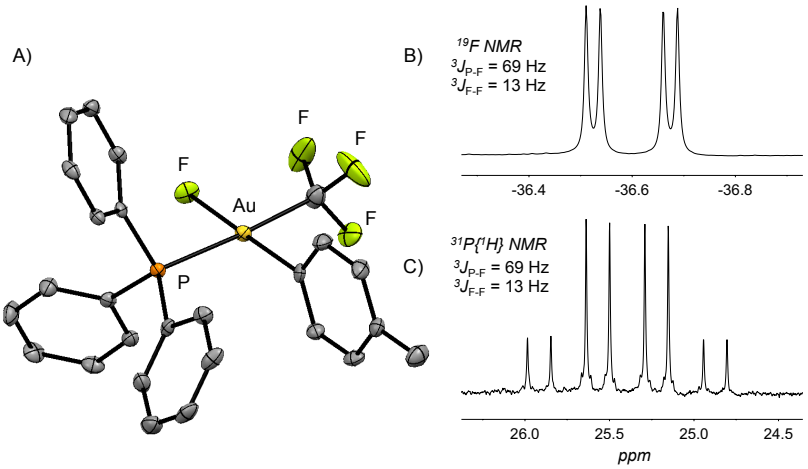

Figure 4.3. A) Thermal ellipsoid representation of **4.1-F** at the 50% probability level. B) ^{19}F NMR signal corresponding to the Au-CF_3 functionality. C) $^{31}P\{^1H\}$ NMR signal in CD_2Cl_2 corresponding to the Au-PPh$_3$ functionality

The simplest gold fluoride, AuF, has been the target of numerous theoretical and experimental investigations. Gold fluoride is potentially the most mismatched of all the transition metal halides due to the hard basicity of fluoride and the soft acidity of gold in the +1 oxidation state. Waddington performed lattice energy calculations for AuF that revealed that the solid compound was unstable relative to the elements.[28] He calculated the enthalpy of formation (ΔH_f) to be between +39 and +45 kcal mol^{-1}, depending on the ionic radius used in the calculation. Indeed, attempts to generate AuF by the reduction of AuF_3 were unsuccessful.[18] In 1992, Saenger and Sun presented spectroscopic evidence for AuF in the form of a yellow emission band observed when gold foil was etched using O_2–CF_4 or O_2–SF_6 plasmas; however, this assignment was not definitive as the observed band could also have been from AuO, AuO^+, or AuF^+.[29] However, computational work supported the spectral assignment by Saenger and Sun and predicted that AuF was accessible in the gas-phase[18,21].

In 1994, the first definitive evidence for AuF was reported[22]. Neutralization-reionization mass spectrometry (NRMS) was used to detect a recovery signal for AuF^+ ions following *in situ* neutralization and reionization (Figure 4.4). A stream of AuF^+ (generated by the ionization of AuF_3) was neutralized by collision with a stream of Xe atoms to generate a transient amount of AuF. Reionization was accomplished by colliding the stream of AuF with a stream of oxygen and the regenerated AuF^+ was then detected *via* mass spectrometry.

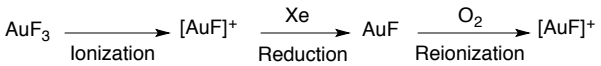

Figure 4.4. Schematic depiction of NRMS characterization of AuF.

The lifetime of AuF in the gas phase was estimated to be at least 25 μs based on the distance traveled between neutralization and reionization chambers of the NRMS instrument. Microwave spectroscopy[30] confirmed the existence of AuF in the gas phase and the Au–F bond length was found to be 1.918 Å, consistent with computational predictions[31–33]. The Au–F bond dissociation energy was also estimated to be between 68 and 85 kcal mol^{-1}. This value is remarkably similar to bond dissociation energies (as determined by microwave spectroscopy) for

Au–Cl (78 kcal mol^{-1})[34], Au–Br (68 kcal mol^{-1})[30], and Au–I (66 kcal mol^{-1})[35] and it is possible that the inaccessibility of a bulk sample of AuF is thus not due to the inherent instability of the compound, but is instead the result of facile intermolecular decomposition pathways in the condensed phase such as disproportionation to AuF_3 and Au metal.[36]

Despite the synthetic inaccessibility of AuF, other coinage metal fluorides are stable compounds, especially with the metal in lower oxidation states (+I or +II). Both silver fluoride (AgF)[37] and copper difluoride (CuF_2)[38] find use in organic synthesis as a means of introducing fluorine and AgF has also found use as a catalyst for a mild fluorination method.[39] Silver difluoride (AgF_2) is more reactive than either CuF_2 or AgF, as it is a strong oxidant,[40,41] but it has been shown to selectively fluorinate pyridines.[42] These more common coinage metal fluorides illustrate the preference of copper and silver for lower formal oxidation states; a fact that can be attributed to the large relativistic effects that are manifest in gold.

One important difference between gold, silver, and copper that contributes to the different preferences in oxidation states is the pronounced relativistic effects that alter the electronic structure of gold and its compounds (Table 4.1).[43] The large nuclear charge of Au (*Z*) causes the *s*- and *p*-orbitals to contract due to increased binding energy as a result of increased Coulombic attraction between the large *Z* and the electrons in these orbitals. As these orbitals contract, they act to shield the valence *d*-orbitals from the large *Z*, and the result is expanded *d*-shell. The valence electron configuration of both silver and gold is $(n)d^{10}(n+1)s^1$ (Ag: $n = 4$; Au: $n = 5$), but the first and second ionization potentials for the metals reveal both the significant relativistic contraction of the Au 6*s* orbital compared to the Ag 5*s* orbital and the expansion of the 5*d* orbitals of Au relative the 4*d* orbitals of Ag. The result of these effects is that, compared to silver, gold metal is more difficult oxidize to the +1 oxidation state. However, the extent of oxidation is greater for gold than for silver or even copper.[44] These effects likely contribute to the instability of AuF relative to AgF or CuF_2 as further oxidation of the gold compound is energetically favorable, particularly under the harsh conditions required to oxidize gold metal. Indeed, the simplest isolable homoleptic gold fluoride is AuF_3, which was first prepared by treating Au metal with BrF_3 to yield $AuF_3 \cdot BrF_3$. Thermolysis of this complex at 180 °C gives the pure AuF_3 as an orange powder (eq 4.1).[45]

$$Au + 2\,BrF_3 \xrightarrow[-Br]{} AuF_3{\cdot}BrF_3 \xrightarrow[-BrF_3]{180\ ^oC} AuF_3 \qquad (4.1)$$

Table 4.1. Electronic configuration and selected ionization energies of Ag and Au.

	Ag	Au
electron configuration	$4d^{10}5s^1$	$5d^{10}6s^1$
1st ionization energy	7.576 eV	9.225 eV
2nd ionization energy	21.5 eV	20.5 eV

Other syntheses involve fluoride exchange of F_2 and $AuCl_3$; but long reaction times (4 d) and elevated temperatures (300 °C) are necessary[46] (Figure 4.5). Chlorine trifluoride can be used to oxidize Au metal to AuF_3, but the product is often of lower purity.[47] A direct synthesis from the elements is also possible; ignition of Au wire at 800 °C under an atmosphere of F_2 yields high purity AuF_3.[47] This method is described as a "convenient and safe one-pot laboratory scale

reaction." Bartlett and coworkers obtained single crystals of AuF_3 by sublimation during the reaction of Au metal and F_2 at 350 °C and 10 atm.[48]

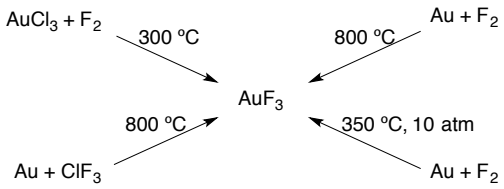

Figure 4.5. Common syntheses of AuF_3.

Powder diffraction experiments indicated that the solid-state structure of AuF_3 was different from that of $AuCl_3$ (which crystallizes as Au_2Cl_6 dimer, Figure 4.6). Single crystal X-ray diffraction revealed that AuF_3 adopts a "fluorine-bridged helical-chain polymer" structure (Figure 4.XX).[48] Each Au(III) center is approximately square-planar, with Au–F bond lengths of 2.04(3) and 1.91(4) Å for the terminal and bridging fluorides, respectively. In the gas phase, electron diffraction supports a slightly distorted T-shaped monomer.[49]

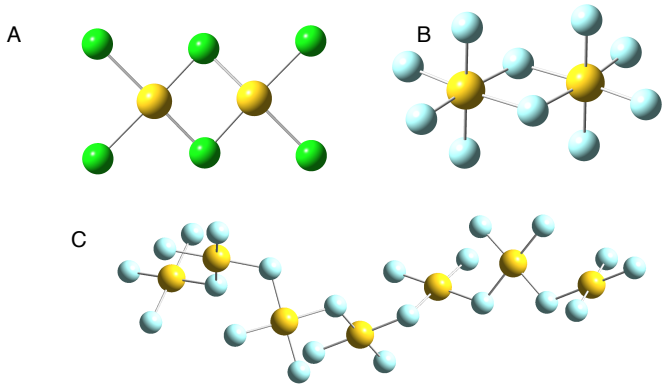

Figure 4.6. Solid state structures of $AuCl_3$ (A), AuF_5 (B), and AuF_3 (C).

Gold trifluoride is extremely electrophilic and it is a strong fluorinating reagent. The compound reacts violently with water to yield $Au(OH)_3$ and HF and it can react explosively with organic solvents.[27] However, AuF_3 does find synthetic utility in the synthesis of "naked" metal cations. The high electrophilicity of the compound results in a high fluoride affinity and AuF_3 forms a stable fluoride adduct: the $[AuF_4]^-$ anion. This anion has been used to stabilize cationic metal centers of the formula $[M(II)][AuF_4]_2$. Müller and coworkers have used the tetrafluoroaurate anion to stabilize cationic complexes of Ni, Zn, Ba,[50,51] Hg(II) and Cd(II),[52] Ni(II) and Pd(II).[53] The $[AuF_4]^-$ anion is invariably square planar, and, in these compounds, its fluoride ligands form bridges between the Au(III) and the cationic metal centers. The compound $[Cs][Au_2F_7]$ has also been characterized as a minor byproduct from the synthesis of $[Cs][AuF_4]$: the anion is an adduct of AuF_3 and $[AuF_4]^-$.

The next major development was the isolation of salts of $[AuF_6]^-$, containing Au(V), the highest known oxidation state for gold.[54] This was achieved by the oxidation of AuF_3 with XeF_2 under an atmosphere of F_2 (68 atm) at 400 °C (eq 4.2). The pale yellow solid isolated from this process was identified as $[Xe_2F_{11}][AuF_6]$ based on Xe content. The unit cell measurements were isomorphous with other octahedrally coordinated $[MF_6]^-$ salts of Xe_2F_{11}, which further supported

the $[AuF_6]^-$ structure. Treatment of $[Xe_2F_{11}][AuF_6]$ with CsF gave $CsAuF_6$ directly, with the loss of XeF_6 (eq 4.3). Bartlett and coworkers also noted $[AuF_6]^-$ could also be generated by oxidizing AuF_3 with dioxygen difluoride to give the dioxygenyl salt $[O_2][AuF_6]$ (*vide infra*). Despite the structural similarity between $[O_2][PtF_6]$ and $[O_2][AuF_6]$, the filled t_{2g} subshell of $[AuF_6]^-$ makes it poor oxidant relative to PtF_6, as the added electron must occupy a σ* orbital.[55]

$$AuF_3 + XeF_2 \xrightarrow[400\ ^oC]{F_2\ (68\ atm)} [Xe_2F_{11}][AuF_6] \qquad (4.2)$$

$$[Xe_2F_{11}][AuF_6] \xrightarrow[110\ ^oC]{CsF} CsAuF_6 + XeF_6 \qquad (4.3)$$

The solid-state structure of $[Xe_2F_{11}][AuF_6]$ was established by Mössbauer spectroscopy and single crystal X-ray diffraction, confirming the octahedral geometry of the anion as predicted from its t_{2g}^6 electronic configuration.[56,57]

The next synthetic target was the neutral AuF_5, which was first prepared by the thermal decomposition of $[AuF_6]^-$ salts. Treatment of gold metal with KrF_2 at 20 °C gives the salt $[KrF][AuF_6]$, which yields AuF_5 and liberates F_2 and Kr upon gentle heating.[58] The compound $[O_2][AuF_6]$ can also be decomposed to give AuF_5. The dioxygenyl salt is prepared by heating gold powder under *ca* 8 atm of a 4:1 F_2:O_2 mixture at 350–380 °C for periods of 48–60 h (equation).[59,60] The resulting mixture is then heated to 160–200 °C in a fused silica sublimation apparatus to decompose the dioxygenyl salt (eq 4.5). If the cold-finger of the sublimation apparatus is precisely controlled between 23 and 27 °C, AuF_5 can be isolated by sublimation as a dark red, amorphous solid.

$$Au \xrightarrow[350\ ^oC,\ 48\text{-}60\ h]{F_2O_2\ (8\ atm)} [O_2][AuF_6] \xrightarrow{160\text{-}200\ ^oC} AuF_5 \qquad (4.4)$$

$$Au \xrightarrow[20\ ^oC,\ 48\text{-}60\ h]{KrF_2} [KrF][AuF_6] \xrightarrow[8\ h]{60\text{-}65\ ^oC} AuF_5 \qquad (4.5)$$

AuF_5 is a dimeric, diamagnetic solid that is poorly soluble in anhydrous HF.[60] It is a powerful oxidant and fluorinating reagent and it reacts violently with moisture and organic compounds, similar to AuF_3. The solid-state structure is shown in Figure 4.6. This dimerization is unique to AuF_5 as it is the only dimeric pentafluoride; other pentafluorides of the main group and transition metals are either monomeric, tetrameric, or polymeric in the solid state.[60] The preference for dimerization is likely a result of the high Lewis acidity of AuF_5: in the gas phase, $(AuF_5)_2$ remains strongly associated. A mixture of the monomeric, dimeric, and trimeric forms of AuF_5 were all detected by mass spectrometry, with the dimer being the most prevalent form.[59] The calculated fluoride affinity of AuF_5 is higher than that of SbF_5.[60] However, $HAuF_6$ (which would then potentially be a stronger Brønsted acid than $HSbF_6$) cannot be prepared from HF and AuF_5 because AuF_5 decomposes in the presence of HF to give AuF_3 and F_2; the higher +5 oxidation state is unstable in the acidic medium.[61] Interestingly, AuF_5 forms an unusual adduct of F_2, with the difluorine fragment coordinated end-on to AuF_5.[62] Again, the high electrophilicity and Lewis acidity of AuF_5 is likely the reason for this complexation.

The fluoride complexes AuF_3 and AuF_5 represent the most simple homoleptic gold fluorides; however, the highly reactive nature of these compounds has limited their study and

application to synthetic chemistry. The complexes AuF_3, AuF_5, and the anion $[AuF_6]^-$ are all powerful oxidants that fluorinate both organic and inorganic substrates in an uncontrolled manner, and as a result, they are of little use to the synthetic chemist. The development of the reactivity of gold fluorides, particularly under mild conditions, requires the preparation of less reactive complexes. The use of ancillary ligands could act to stabilize similarly reactive species and provide access to more stable compounds containing the Au–F bond. This strategy has been employed successfully in the synthesis of gold fluorides containing gold in the +1, +2, and +3 oxidation states.

The first organometallic Au(I) fluoride was prepared by Sadighi and coworkers using an *N*-heterocyclic carbene (NHC) to stabilize the molecular gold fluoride.[63] The precursor (SIPr)Au(O*t*-Bu) (SIPr = 1,3-bis(2,6-diisopropylphenyl)imidazolin-2-ylidene) is protonated with $Et_3N{\cdot}3HF$ (eq 4.6) to give (SIPr)AuF. The solid-state structure shows significant hydrogen bonding between the fluoride ligand and co-crystallized CH_2Cl_2.

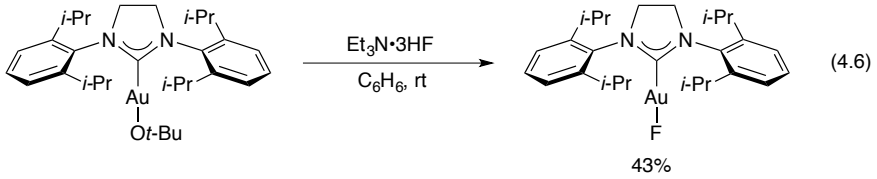

(4.6)

Computational studies showed that the Au–F bond was highly ionic. Population analysis of the complex found a large negative charge (–0.77) on the fluoride ligand. This charge distribution is believed to polarize the C–H bonds of the solvent to induce the hydrogen bonding observed in the solid state. The overall Au–F bond order was 0.933, and all Au–F π* molecular orbitals are fully occupied, indicating significant dπ–pπ repulsion between the Au center and the fluoride ligand. This polarization is expected to cause the fluoride ligand to be nucleophilic; indeed, in the presence of alkynes, (SIPr)AuF reacts to give the formal product of insertion, a β-(fluorovinyl)gold(I) complex.[64] The insertion is reversible and, when 3-hexyne is used, K_{eq} was found to be $2.7 \pm 0.2\ M^{-1}$. The insertion product can be treated with acid to achieve protodeauration and liberate *trans*-3-fluoro-3-hexene in near quantitative yield (eq 4.7).

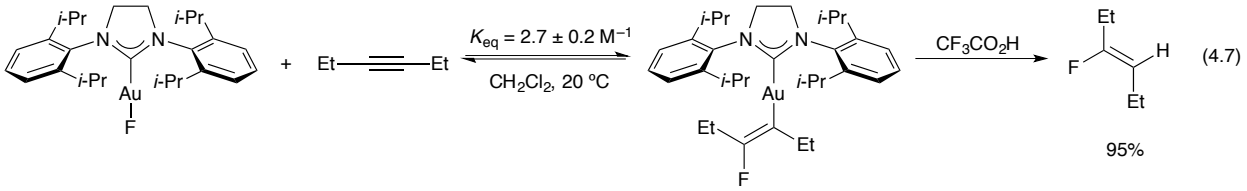

(4.7)

To date, there are no known phosphine supported Au(I) fluorides. Halide metathesis between Ph_3PAuCl and AgF in the presence of water leads to the formation of $[((Ph_3P)Au)_3O][H_2F_3]$; no reaction occurs under anhydrous conditions (eq 4.8 and 4.9).[65] While $(Ph_3P)Au(O$*t*$\text{-Bu})$ is a known compound, it is reported to be unstable, so a similar protonolysis route to $(Ph_3P)AuF$ may not be viable.[66] The larger size of SIPr compared to PPh_3 likely helps to prevent the aggregation of the gold cations during the formation of $[((Ph_3P)Au)_3O]^+$. Additionally, NHC ligands are more difficult to oxidize relative to trialkyl and –aryl phosphines, preventing ligand oxidation and reduction to Au metal.

$$Ph_3PAuCl + AgF \longrightarrow \text{no reaction} \qquad (4.8)$$

$$Ph_3PAuCl + AgF \xrightarrow{H_2O} [O(AuPPh_3)_3][H_2F_3] \qquad (4.9)$$

Fackler and coworkers prepared a Au(II) fluoride containing a bimetallic core supported by two bridging formamidinate ligands in an A-frame complex.[67] The bimetallic core stabilizes the Au(II) oxidation by allowing the formation of a Au–Au bond. A large variety of bimetallic Au(II) complexes have been prepared using this strategy.[68]

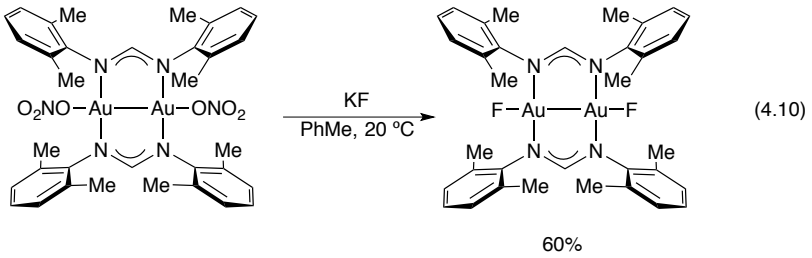

(4.10)

Anion metathesis with the Au(II) nitrate complex yield the desired Au(II) fluoride (Eq 4.10). The Au–F bond lengths (2.287 Å) are longer than that of (SIPr)AuF (2.0281 Å), reflecting the trans influence of the Au–Au bond. The metal–metal bond is slightly elongated in the fluoride complex than in the analogous chloride complex, which was attributed to a fluoride π-electron effect.

A series of Au(III) fluorides have been prepared in an effort to study C–C bond formation from oxidized gold species.[69] The oxidation of (IPr)AuMe (IPr = 1,3-bis(2,6-diisopropylphenyl)imidazol-2-ylidene) with XeF_2 gives *cis*-(IPr)AuMeF_2 which is in equilibrium with a μ-fluoro-bridged dimer. The equilibrium is nearly thermoneutral, but *cis*-(IPr)AuMeF_2 is favored in solution while the dimer crystallizes more readily. The lability of the fluoride ligand is likely induced by the $d\pi$–$p\pi$ repulsion between the fluoride and the d^8 Au(III) center (Figure 4.7).

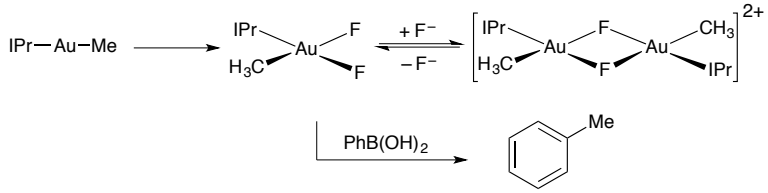

Figure 4.7. Dimerization of a difluoroalkyl Au(III) and its reaction with $PhB(OH)_2$.

The complex *cis*-(IPr)AuMeF_2 reacts with $PhB(OH)_2$ to give toluene, the product of C(sp^2)–C(sp^3) coupling. The stability of *cis*-(IPr)Au$(F)_2$(Me) is unique to the methyl substituted compound. The *t*-Bu analogue, *cis*-(IPr)Au$(F)_2$(*t*-Bu) is unstable in solution, and decomposes over the course of several hours. Oxidation of other alkylgold analogoues with XeF_2 resulted in overall C(sp^3)–F reductive elimination (eq 4.11).[23] The C–F elimination competes with a formal β-hydride elimination giving mixtures of alkyl fluorides and alkenes; though the elimination pathway can be slowed if β-substituted alkyl groups are used. In the case of (IPr)AuBn, reductive elimination gives (IPr)AuF the analogue of (SIPr)AuF.

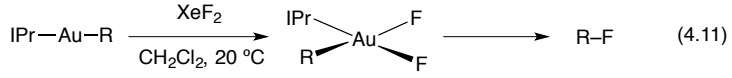

This transformation is noteworthy because C–F reductive elimination from transition metals remains a challenging process. While the strength of the C–F bond offers a thermodynamic driving force for the elimination, the metal-fluoride bond is also strong, providing a certain degree of ground-state stabilization that limits the kinetic feasibility of the transformation from the neutral Au(III) species.[70,71] The C–F bond forming event likely occurs from a three-coordinate cation formed by reversible fluoride dissociation. The unsaturated Au(III) cation imparts a significant partial positive change on the alkyl group, leading to the observed products of carbocation elimination and rearrangement.

The nature of the Au–F bond has not been extensively explored beyond the examples shown above, and **4.2-F** provides a unique platform to access other potentially interesting reactivity or coordination compounds of Au(III). Given that (IPr)AuF_2Me reacted with boronic acids in a nucleophilic manner (Figure 4.8) we hypothesized that the strong silicon-fluorine bond may also enable ligand exchange reactions between silanes and **4.2-F**. Treatment of **4.2-F** with Me_3Si-OTf at room temperature leads to the formation of Me_3Si–F and 4-F-C_6H_4-CF_3, similar to the reaction between AgOTf and **4.2-I**. Silanes may provide a convenient route to gold(III) hydrides *via* a similar exchange mechanism; the rarity of these complexes makes them an interesting synthetic target.[72] When **4.2-F** was treated with triethoxysilane or phenylsilane in CD_2Cl_2, the Au–F resonance at δ –249 ppm disappeared and the [Au]–CF_3 resonance shifted, though it retained an *dd* splitting pattern, indicative of coupling to both the phosphine and a hydride (Figures 4.9 and 4.10).

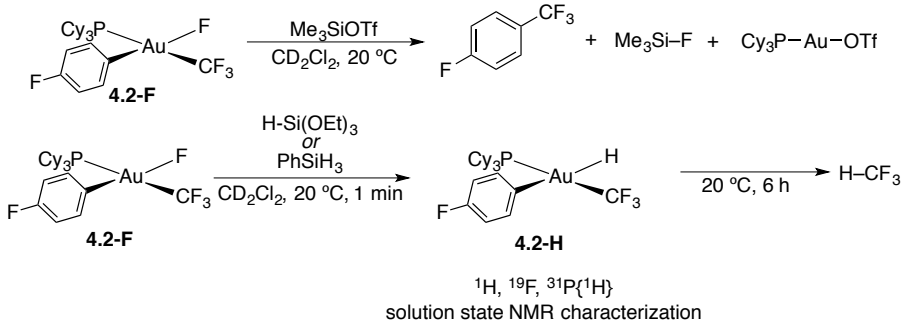

Figure 4.8. Reactivity of **4.2-F** with silanes to induce C(sp^2)–CF_3 elimination (top) or to generate a semi-stable Au(III) hydride (bottom).

Additionally, the characteristic splitting of the phosphorous resonance simplified to a quartet in the $^{31}P\{^1H\}$ NMR spectrum. A new resonance appeared at δ –0.9 ppm in the ^1H NMR spectrum, characteristic of a metal hydride. After 6 hours at room temperature, HCF_3 was observed in the ^{19}F NMR spectrum, likely as a result of elimination from **4.2-H**. Attempts to isolate the compound from solution resulted in decomposition to gold metal and attempts to crystallize the compound from solution at low temperature were unsuccessful. In order to gain additional solution state characterization, the analogous deuterated complex was synthesized using $PhSiD_3$. The ^2D NMR showed the same diagnostic shift for the Au–D at δ –0.9 ppm and the absence of D–F coupling to the [Au]–CF_3 moiety supported the formation of **4.2-D**. Over the

course of 6 hours, DCF_3 was observed by ^{19}F NMR, consistent with the formation of a Au(III) deuteride in analogy to **4.2-H**.

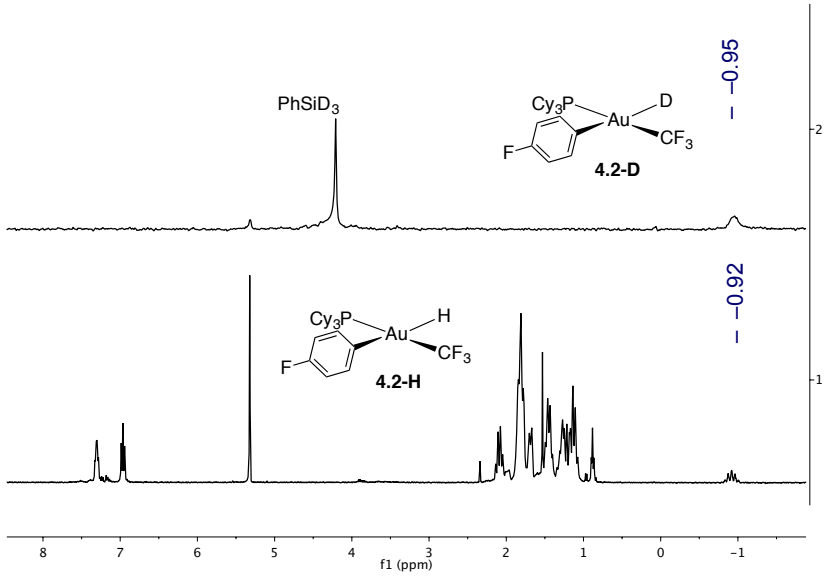

Figure 4.9. ^2D (62 MHz) and ^1H NMR (400 MHz) spectra of **4.2-D** (top) and **4.2-H** (bottom). Both spectra are referenced to the solvent; CD_2Cl_2 in the top spectrum and CH_2Cl_2 in the bottom spectrum. **4.2-D** was synthesized using an excess $PhSiD_3$, which is shown at δ 4.21 ppm in the top spectrum.

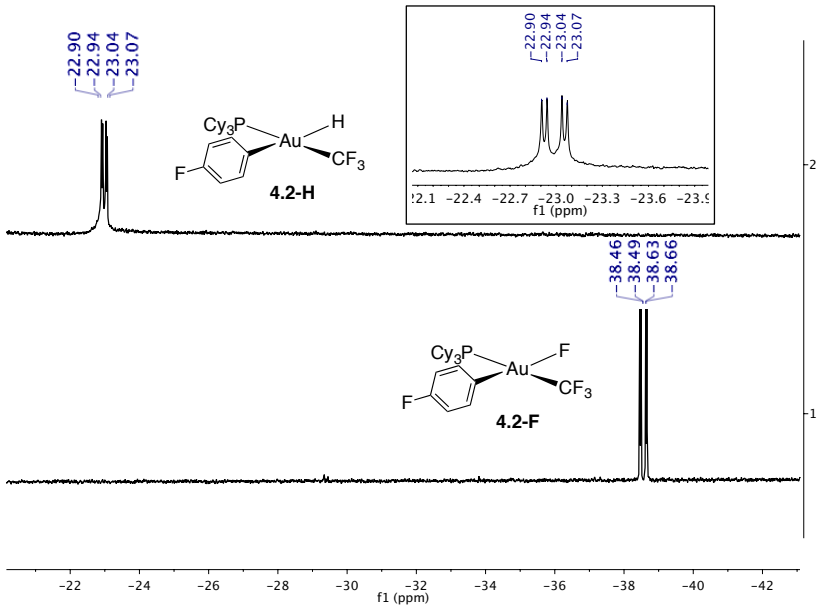

Figure 4.10. ^{19}F NMR spectra (CD_2Cl_2, 376 MHz) of **4.2-H** (top) and **4.2-F** (bottom) showing the Au–CF_3 resonances for both compounds. The signal for **4.2-H** is also magnified to show its characteristic *dd* splitting pattern (inset).

Unlike the known Au(III) hydride, **4.2-H** did not insert olefins into the Au–H bond. In the presence of norbornene, **4.2-H** only eliminated HCF_3 and no other products were observed by ^{19}F NMR (Figure 4.11). Additionally, no reaction was observed with O_2, again unlike the Bochmann's Au(III) hydride.[72]

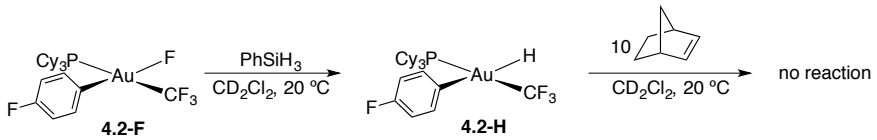

Figure 4.11. Generation of **4.2-H** and attempted reaction with norbornene.

All complexes within the **4.1-X** halide series underwent thermolysis to products of C(sp^2)–X and C(sp^2)–CF_3 reductive elimination, and (when X = F) solvent activation. All reactions were followed by ^{19}F NMR at 122 °C in toluene-d_8 ([**1-X**] = 14.0-16.0 mM). All values were quantified relative to 1-trifluoromethylnaphthalene (^{19}F δ: –59 ppm) as an internal standard. Due to irreversible formation of a new Au(III) species upon treatment with $[Bu_4N]X$ (presumably the aurates $[Bu_4N][Au(aryl)(CF_3)(X)_2]$ (^{19}F NMR singlet at δ: –21 to –25 ppm), we could not determine the kinetic order of halide anions. Reactions run in the significantly more polar[73] $PhNO_2$ were only slightly affected as shown in Figure 4.ZZ B, providing some evidence against an ionic mechanism involving tight or dissociated ion pairs.

Complex **4.1-I** underwent thermolysis at 110 °C to exclusively generate Ph_3PAuCF_3 and 4-Me-C_6H_4–I; at 122 ºC (the calibrated temperature of the NMR probe) the half life ($t_{1/2}$) for this process is 2.5 min. Consumption of **4.1-I** followed unusual zero-order kinetics over a range of concentrations (k_{obs} = 4.5 x 10^{-5} M s^{-1} from 6 to 35 mM [**4.1-I**], Figure 4.12 A).

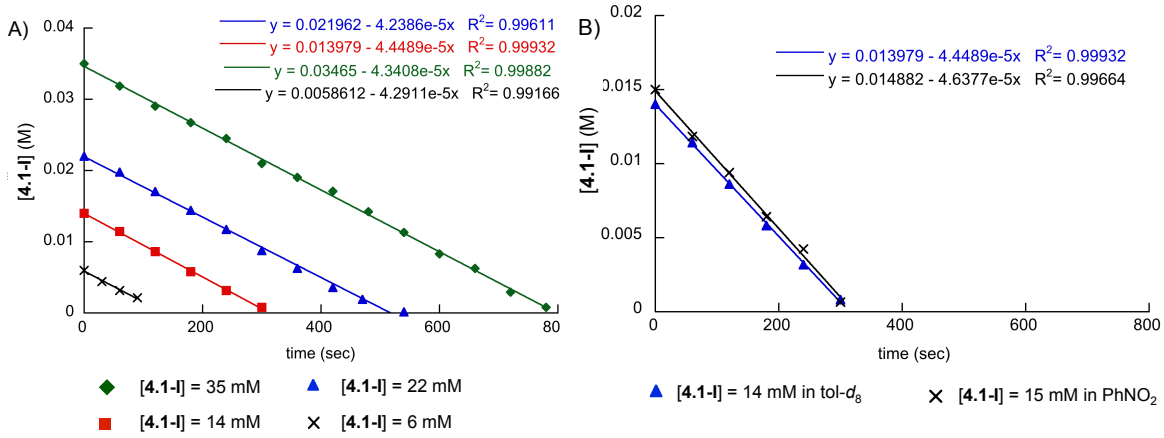

Figure 4.12. A) Plot of [**4.1-I**] against time showing zero-order behavior over a concentration range of 6-35 mM. B) Plot of [**4.1-I**] against time in toluene and nitrobenzene solution.

When 0.005 equivalents PPh_3 (70 μM) was added, the rate slows substantially ($t_{1/2}$ = 28 min), and the reaction exhibited first-order behavior in **4.1-I** with k_{obs} = 4.1 x 10^{-5} s^{-1} (Figure 4.13). The observed rate constant (k_{obs}) was inverse first-order in PPh_3, implicating PPh_3 predissociation from **4.1-I** and reductive elimination from a short-lived three-coordinate Au(III) complex **4.3-I** under these conditions (Figure 4.14). Consistent with this sequence, PCy_3-

supported **4.2-I** did not react at 122 °C over 2 days, presumably due to the increased donor strength of the trialkylphosphine.

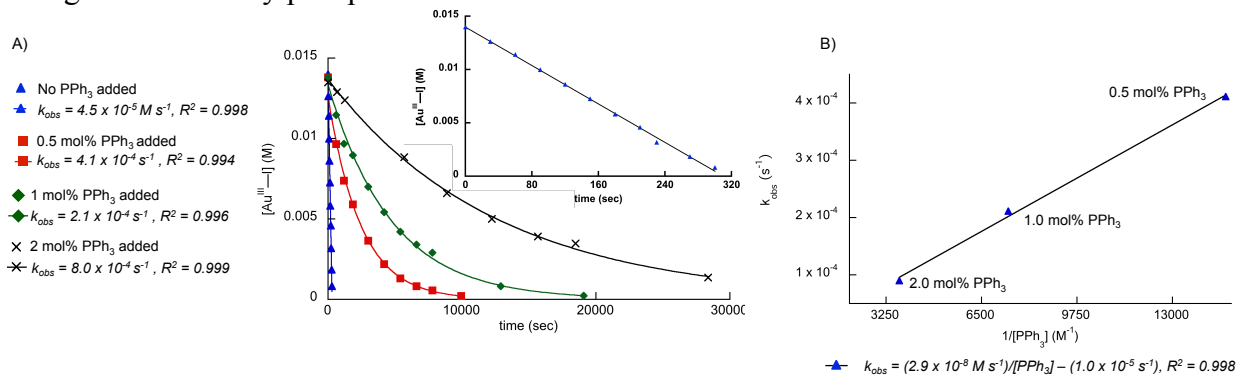

Figure 4.13. A) Time courses for thermolysis of **4.1-I** with 0, 0.005, 0.01, and 0.02 equivalents of PPh_3 added. Inset: Time course with no added PPh_3. B) Inverse relationship between k_{obs} and [PPh_3] indicating inverse first-order behavior of PPh_3 in the thermolysis of **4.1-I**.

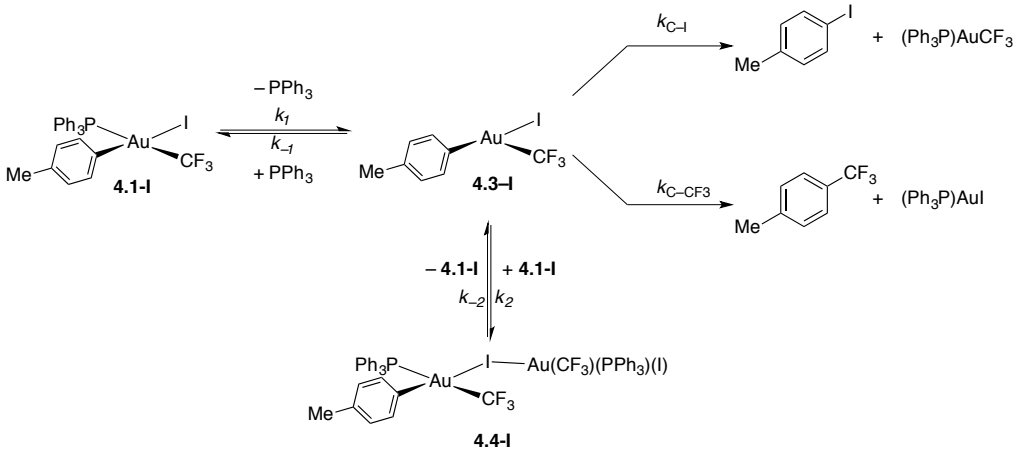

Figure 4.14. Proposed General Mechanism of C(sp^2)–X and C(sp^2)–CF_3 Reductive Eliminations from 1-X (X = I, Br, Cl, F).

The zero-order kinetic profile in the absence of PPh_3 suggest reversible reaction inhibition by starting material. If reductive elimination proceeds through the coordinatively unsaturated **4.3-I**, a possible origin of this unusual behavior is trapping by **4.1-I** to μ-iodo bimetallic adduct **4.4-I** (Figure 4.14). The formation of μ-halide bridges between Au(III) atoms to avoid coordinative unsaturation at the metal is observed in several systems: $[AuCl_3]_2$, $[Me_2AuI]_2$, $[(F_3C)AuX]_2$ (X = I, Br), and $([SIPr)Au(Me)F]_2)^{2+}$ (SIPr = 1,3,-bis(2',6'-diisopropylphenyl)imidazolin-2-ylidene).[69,74,75]

Treating **4.3-I** as a steady-state intermediate, a complex rate law consistent with experimental observations can be derived (eq. 4.12).

$$-\frac{d[\mathbf{4.1\text{-}I}]}{dt} = \frac{k_{C\text{–}I}(k_1[\mathbf{4.1\text{-}I}]+k_{-2}[\mathbf{4.4\text{-}I}])}{k_{-1}[PPh_3]+k_{C\text{–}I}+k_2[\mathbf{4.1\text{-}I}]} \qquad (4.12)$$

Since [**4.4-I**] must be less than [**4.3-I**], the assumption that [**4.4-I**] ≈ 0 is valid. If the formation of **4.4-I** is significantly faster than the recombination of PPh_3 and **4.3-I,** than k_2[**4.1-I**] >> k_{-1}[PPh_3] + $k_{C\text{-}I}$, and eq. 1 simplifies to the zero-order rate law $-d$[**4.1-I**]/dt = $k_{C\text{-}I}k_1/k_2$, which at 122 °C, is 4.5 x 10^{-5} M s^{-1}.

Under steady-state conditions, [PPh_3] must be very low. Since even small amounts of PPh_3 dramatically alter the reaction behavior, k_{-1} must be substantially larger than k_2. Therefore, when PPh_3 is added, the rate law simplifies to

$$-\frac{d[\mathbf{4.1\text{-}I}]}{dt} = \frac{k_{C-I}k_1[\mathbf{4.1\text{-}I}]}{k_{-1}[PPh_3]} \qquad (4.13)$$

where $k_{C\text{-}I}k_1/k_{-1}$ = 2.9 x 10^{-8} M s^{-1}. Thus, k_{-1} = (1600)k_2, in accordance with the previous assumption that $k_{-1} >> k_2$.

Qualitatively, the thermolyses of **4.1-Br** and **4.1-Cl** were notably slower ($t_{1/2}$ ~ 75 min and 400 min, respectively) than **4.1-I**, and products of both C(sp^2)–X and C(sp^2)–CF_3 reductive elimination are detected after full conversion ([4-Me-C_6H_4–Br]:[4-Me-C_6H_4–CF_3] = 1.5:1 for **4.1-Br,** and [4-Me-C_6H_4–Cl]:[4-Me-C_6H_4–CF_3] = 1:4.5 for **4.1-Cl**). To our surprise, reaction rates increased with time for both thermolyses (Figure 4.15A and 4.16A), suggestive of catalysis by products or nanoparticles.[11] Indeed, in the presence of excess (Ph_3P)$AuCF_3$, the rates of these thermolyses dramatically accelerated, behaving first-order in **4.1-Br** or **4.1-Cl** and Ph_3PAuCF_3 (Figures 4.15B and 4.16B).

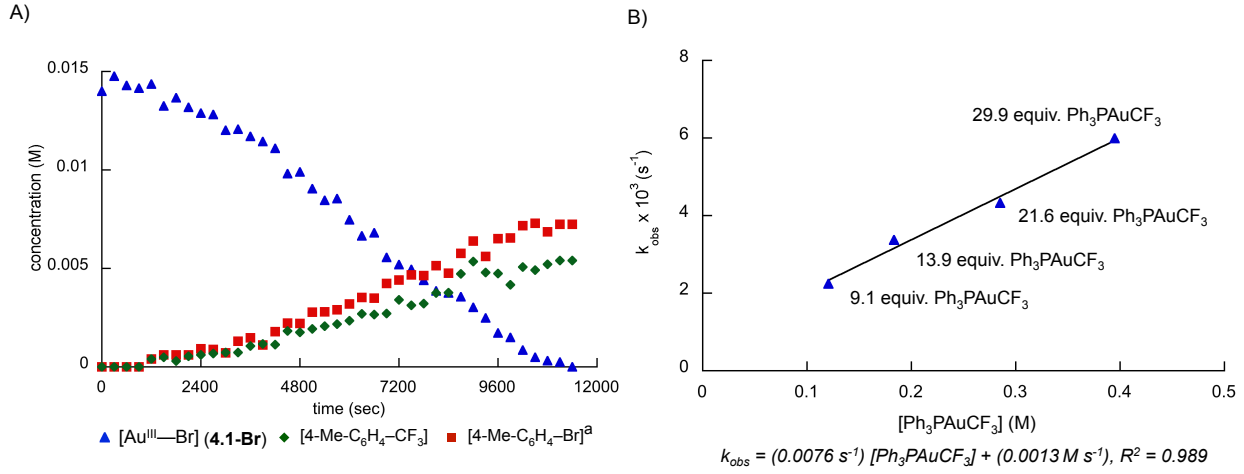

Figure 4.15. A) Time course for thermolysis of Au(III)–bromide **4.1-Br** at 122 ºC. [a]Obtained by measuring [(Ph_3P)Au(CF_3)]. B) Direct relationship between k_{obs} and [Ph_3PAuCF_3] indicating first-order behavior of Ph_3PAuCF_3 in the thermolysis of **4.1-Br**.

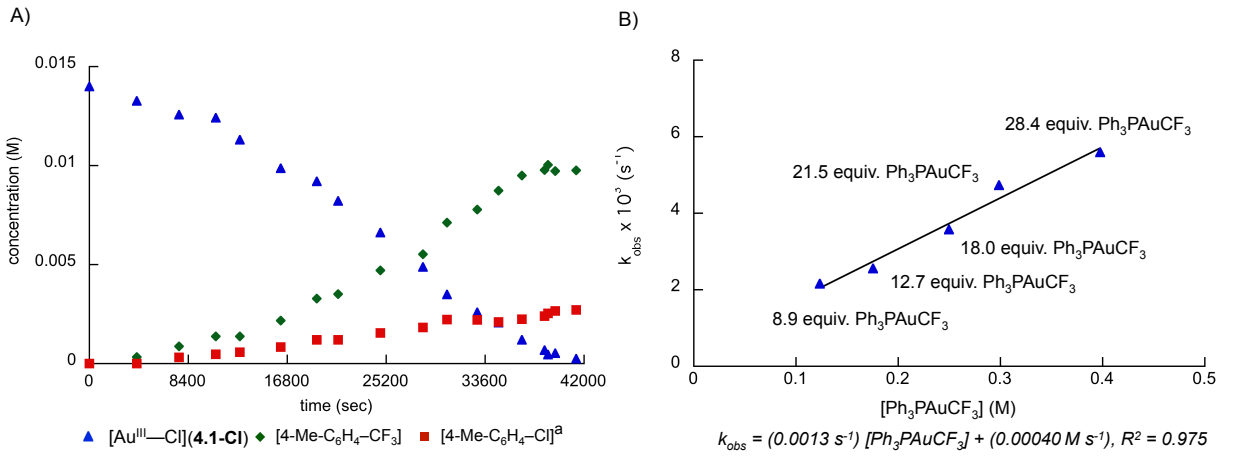

Figure 4.16. A) Time course for thermolysis of Au(III)–chloride **4.1-Cl** in the presence of 8.9-28.4 equivalents of Ph_3PAuCF_3. B) Direct relationship between k_{obs} and [Ph_3PAuCF_3] indicating first-order behavior of Ph_3PAuCF_3 in the thermolysis of **4.1-Cl**.

The addition of 0.01 equivalent (0.014 mM) PPh_3 dramatically slowed the rates of thermolysis of **4.1-Br** and **4.1-Cl** with and without excess Ph_3PAuCF_3, consistent with phosphine dissociation preceding reductive elimination in both the non-accelerated and product-accelerated pathways (Figure 4.17).

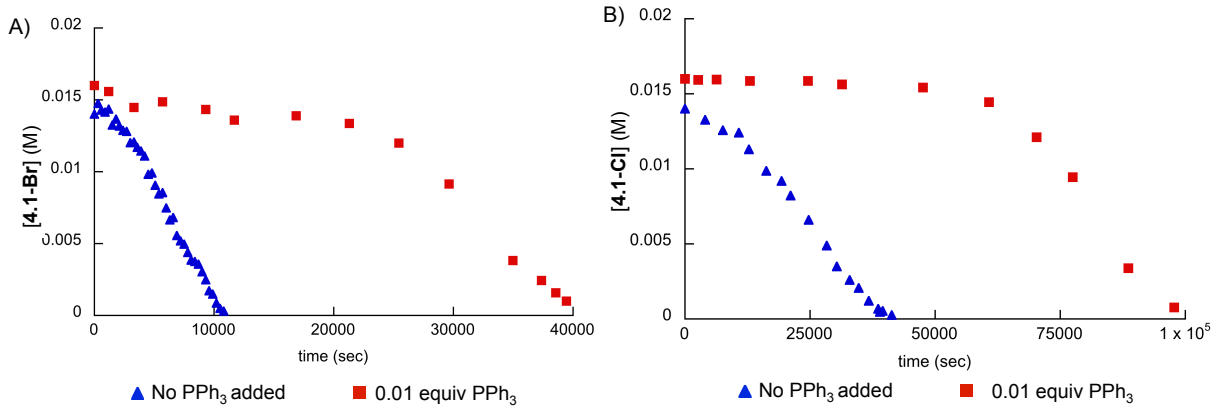

Figure 4.17. A) Plot of [**4.1-Br**] against time in the absence and presence of PPh_3 (0.01 equiv). B) Plot of [**4.1-Cl**] against time in the absence and presence of PPh_3 (0.01 equiv).

Consistent with at least two processes with different product-determining steps, the ratios [4-Me-C_6H_4–X]:[4-Me-C_6H_4–CF_3] varied over time during the thermolyses of **4.1-Br** and **4.1-Cl**. For instance, when t < 20 min, the accelerated pathway has not significantly contributed to consumption of **4.1-Br**, and there was almost no kinetic preference for C(sp^2)–Br or C(sp^2)–CF_3 bond formation ([4-Me-C_6H_4–Br]:[4-Me-C_6H_4–CF_3] is roughly 1:1)**.** However, in the presence of a large excess of (Ph_3P)$AuCF_3$ (140 mM), the accelerated pathway dominated even at early reaction times, and C(sp^2)–Br reductive elimination is slightly favored (2.3:1, presumably the intrinsic kinetic product distribution of the accelerated pathway.) For **4.1-Cl,** the product ratio [4-Me-C_6H_4–Cl]:[4-Me-C_6H_4–CF_3] for the non-accelerated pathway is 1:2.8, while the accelerated pathway heavily favors C(sp^2)–CF_3 reductive elimination (1:7.6).

We propose that the electron-withdrawing effect[76] of the CF_3 ligand renders Ph_3PAuCF_3 sufficiently Lewis acidic to coordinate the halide of **4.1-Br** or **4.1-Cl** in a μ-bridging fashion,[13] effectively withdrawing electron density from the Au(III) center and perturbing the relative kinetic preferences for C(sp^2)–X and C(sp^2)–CF_3 reductive elimination from **6-X**. Inhibition by PPh_3, the absence of saturation behavior at high [Ph_3PAuCF_3], and spectroscopically unobservable intermediates suggest a process involving fast, reversible coordination of Ph_3PAuCF_3 to **4.1-Br** or **4.1-Cl,** followed by PPh_3 dissociation and slow C(sp^2)–X and C(sp^2)–CF_3 reductive elimination (Figure 4.18).

For both **4.1-Br** and **4.1-Cl**, kinetic details of the non-accelerated pathway are masked by the accelerated reaction. However, the slower pathway is likely analogous to **4.1-I** thermolysis (Scheme 4.xx), given the reaction's sensitivity to excess phosphine and the diversity of Au(III)-supported μ-halide bridges.[11] The unambiguous first-order behavior in the presence of excess Ph_3PAuCF_3 clearly indicates that the accelerated reaction is substantially faster than the non-accelerated process.

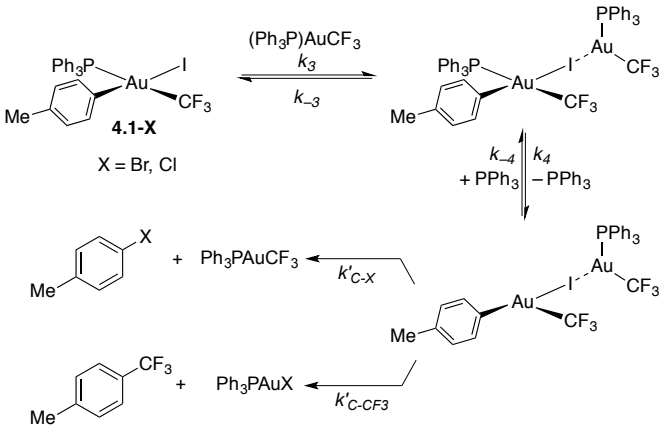

Figure 4.18. Proposed Mechanism for accelerated thermolysis of **4.1-Br** or **4.1-Cl**.

The thermolysis of **4.1-F** was slower ($t_{1/2}$ = 33 min) than **4.1-I**, but significantly faster than **4.1-Br** and **4.1-Cl** (Figure 4.19A). Consistent with the apparent trend of decreasing selectivity of C(sp^2)–X reductive elimination in the order X = I > Br > Cl,, no products of C(sp^2)–F bond formation were observed upon heating **4.1-F**. Instead, 4-Me-C_6H_4–CF_3 is the major product. The formation of significant amounts of d_7 isotopologues of 2,4'-, 3,4'-, and 4,4'-dimethylbiphenyl (biaryl-d_7) and equimolar $(Ph_3P)AuCF_3$ suggest competitive activation of toluene-d_8 solvent and C(sp^2)–C(sp^2) reductive elimination from a putative species Au(4-MeC_6H_4)(aryl-d_7)(CF_3).[14,15] Since the ratio [4-Me-C_6H_4–CF_3]:[biaryl-d_7] remains constant (3.6:1) throughout the reaction, the rate laws for both C(sp^2)–CF_3 and C(sp^2)–C(sp^2) reductive elimination must have the same molecularity to first approximation.

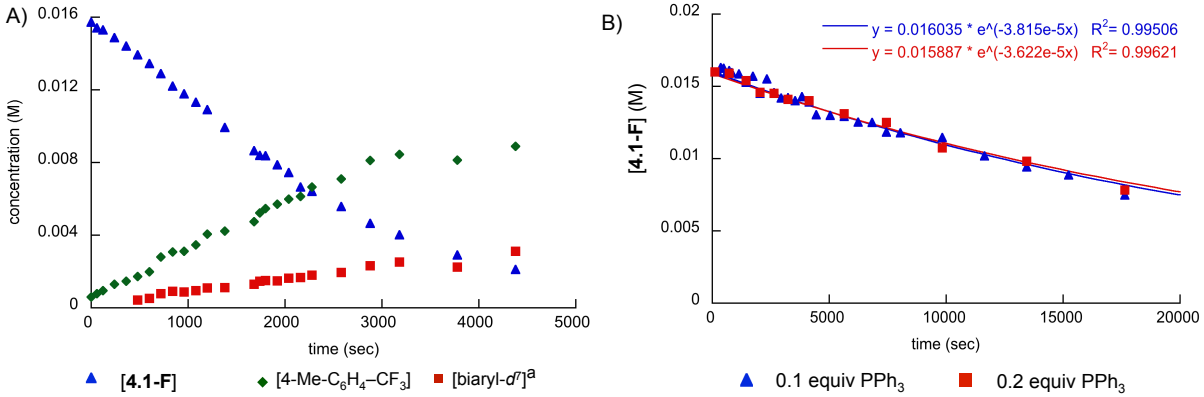

Figure 4.19. A) Time course for thermolysis of Au(III)–fluoride **4.1-F**. [a]Obtained by monitoring [Ph_3PAuCF_3]. B) Plot of [**4.1-F**] against time in the presence of 0.1 and 0.2 equiv. of PPh_3.

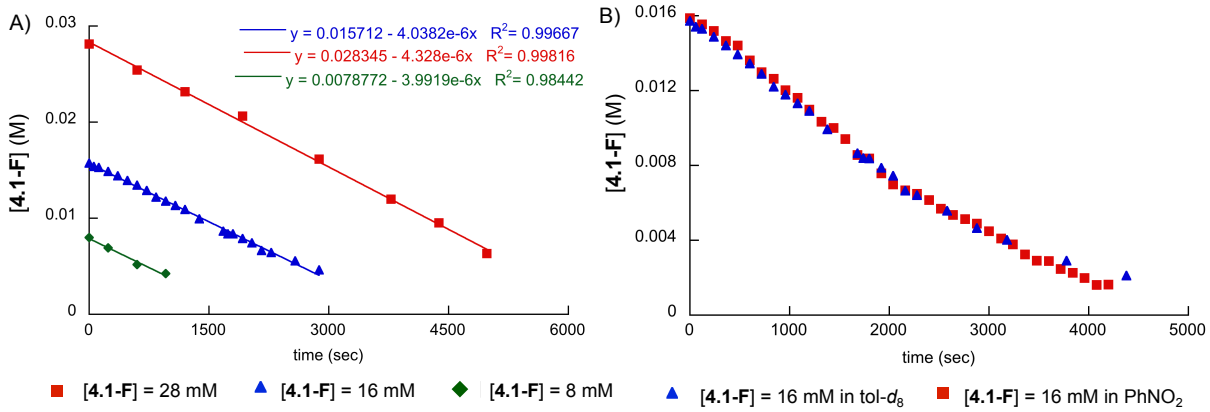

Figure 4.20. A) Time course for thermolysis of **4.1-F** at 122 ºC over a range of concentrations from 8–28 mM. B) Time course for the thermolysis of **4.1-F** at 122 ºC in toluene-d_8 and $PhNO_2$.

Although the selective C(sp^2)–I reductive elimination from **4.1-I** stands in contrast to the selective C(sp^2)–CF_3 reductive elimination from **4.1-F,** the kinetic behavior for both thermolyses are notably similar. For instance, the thermolysis of **4.1-F** exhibited zero-order behavior (up to 80% conversion) over a range of concentrations (Figures 4.19A and 4.20A) and is dramatically inhibited by PPh_3 (Figure 4.19B), consistent with slow C(sp^2)–CF_3 reductive elimination and slow solvent activation from three-coordinate intermediate **4.3-F**, which can be trapped by starting material, similar to **4.1-I**. Although solvent activation is in all likelihood a bimolecular process, [tol-d_8] is essentially constant (~8.3 M at 122 °C in a sealed tube),[16] and the ratio of products expressed as rate terms $k_{C\text{-}CF3}/(k_{Ar}$[toluene-d_8]) is also constant (3.6) (Figure 4/XX). That **4.3-F** can activate solvent implicates an ionic Au(III)–F bond that imparts sufficient Lewis acidity for formal C–H activation by electrophilic aromatic substitution, fluoride-assisted deprotonation, or σ-bond metathesis.[17]

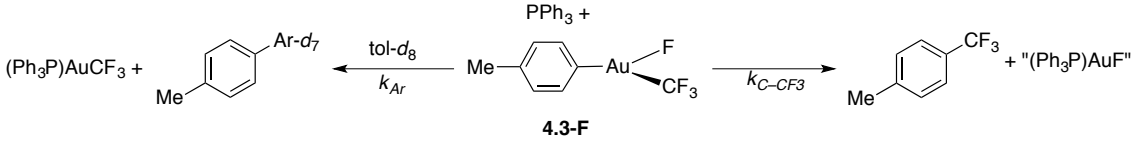

Figure 4.21. Proposed C(sp^2)–CF_3 and C(sp^2)–C(sp^2) coupling reactions of thermolysis intermediate **3-F**

Like **4.1-I**, addition of 0.1 equiv PPh_3 (1.4 mM) slows the reaction ($t_{1/2}$ = 300 min) and alters its behavior in **4.1-F** from zero-order to first-order. However, only biaryl-d_7 is formed under these conditions, suggesting an alternative, slower solvent activation pathway that does not involve **3-F**. Although the Au(III) center in **4.1-F** is less electron-deficient and more sterically shielded than in **3-F** due to coordinative saturation, it may still be sufficiently Lewis acidic to activate solvent (Scheme 6). Consistent with this proposal, the reaction rate was independent of [PPh_3] (from 1.4 mM to 14 mM), and the more electron-rich, sterically-encumbered **4.2-F** did not react with toluene-d_8.

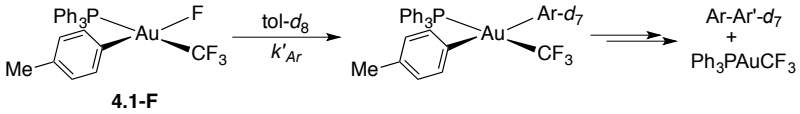

Figure 4.22. Proposed Mechanism of solvent activation and C(sp^2)–C(sp^2) Coupling by **4.1-F**.

A rate law consistent with the mechanism of **4.1-F** thermolysis is shown in eq 4.14 where the zero-order term is significantly larger than the pseudo first-order term in the absence of PPh_3, and $k_1(k_{C\text{-}CF3} + k_{Ar}[\text{tol-}d^8])/k_2 = 3.9 \times 10^{-6}$ M s^{-1}.

$$-\frac{d[\mathbf{4.1\text{-}F}]}{dt} = k'_{Ar}[\mathbf{4.1\text{-}F}][\text{tol-}d_8] + \frac{(k_{Ar}[\text{tol-}d_8] + k_{C-CF3})k_1}{k_2} \qquad (4.14)$$

These kinetic investigations reveal that selectivity for C(sp^2)–X versus C(sp^2)–CF_3 reductive elimination from Au(III) decreases in the order X = I > Br > Cl > F (Figure 4.23). While rate of C(sp^2)—X bond formation corresponds to halide polarizibility,[7] thermodynamic studies were necessary to determine the role of ground state effects in the reaction selectivities.

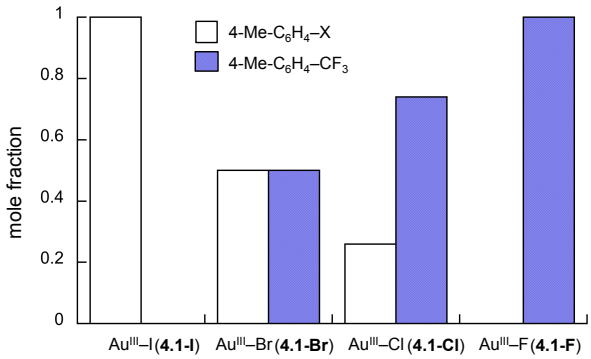

Figure 4.23. Distributions of products of reductive elimination from Au(III) halides **4.1-X**. For **4.1-Br** and **4.1-Cl**, these values represent the distributions of the non-accelerated pathway.

To gain insight into what extent thermodynamics govern reductive elimination selectivity, we carried out van't Hoff analyses between **4.2-X** and the trityl halides. The halide metathesis equilibria were monitored in toluene-d_8 by ^{19}F NMR at temperatures between 25 and 78 °C. Complexes **4.2-I** and **4.2-Br** were treated with an excess of Ph_3C–Cl (30 equiv.) to ensure fast approach to equilibrium, and to hold [Ph_3C-Cl] constant for determination of the equilibrium constant. The equilibrium between **4.2-Cl** (+ Ph_3C–I) and **4.2-I** (+ Ph_3C–Cl) is moderately exothermic (ΔH^o = –4.8 kcal/mol) with a negligible loss of entropy (ΔS^o = –2.1 e.u.) (Figure 4.24). Similarly, the equilibrium between **4.2-Cl** (+ Ph_3C–Br) and **4.2-Br** (+ Ph_3C–Cl) also lies to the right ((ΔH^o = –3.1 kcal/mol) with a negligible entropy loss (ΔS^o = –1.8 e.u.) (Figure 4.25).

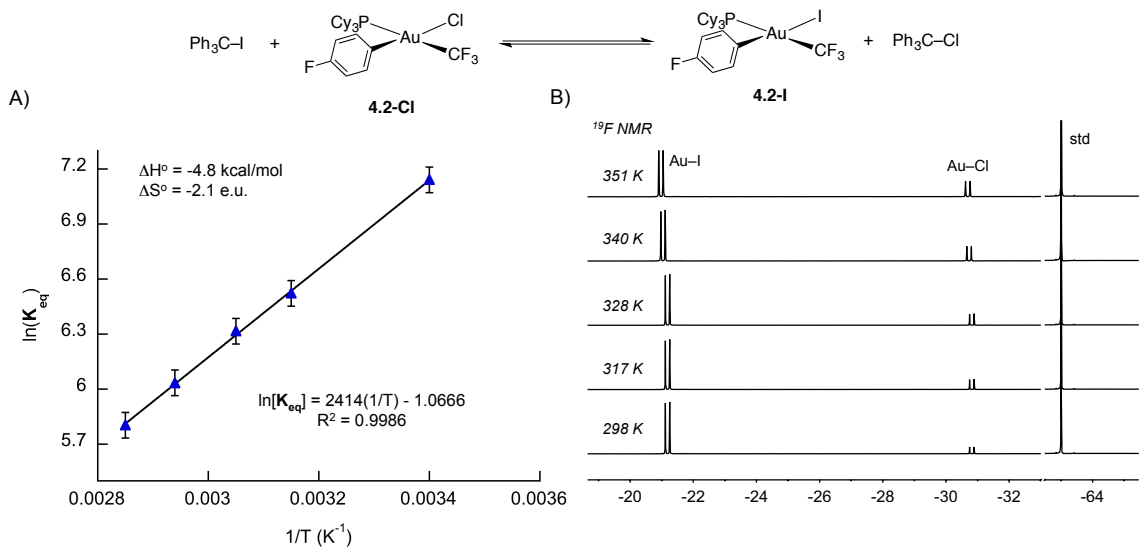

Figure 4.24. A) van't Hoff plot of the equilibrium of **4.2-Cl** (+ Ph_3C–I) and **4.2-I** (+ Ph_3C–Cl) (shown above) in toluene-d_8 between 25 and 78 °C. Initial conditions: **4.2-I** + Ph_3C–Cl (30 equiv). B) ^{19}F NMR array showing the –CF_3 resonances for each compound between 298 K and 351 K.

Using the thermodynamic parameters above, and differences in Benson group increments for tertiary alkyl halide groups[77] we obtain the differences in heats of formation ($\Delta\Delta H^o_f$) of **4.2-Cl, 4.2-Br,** and **4.2-I**: ΔH^o_f**(4.2-I)** is 13 kcal/mol greater than ΔH^o_f **(4.2-Br)**, and 21 kcal/mol greater than ΔH^o_f**(4.2-Cl)**.

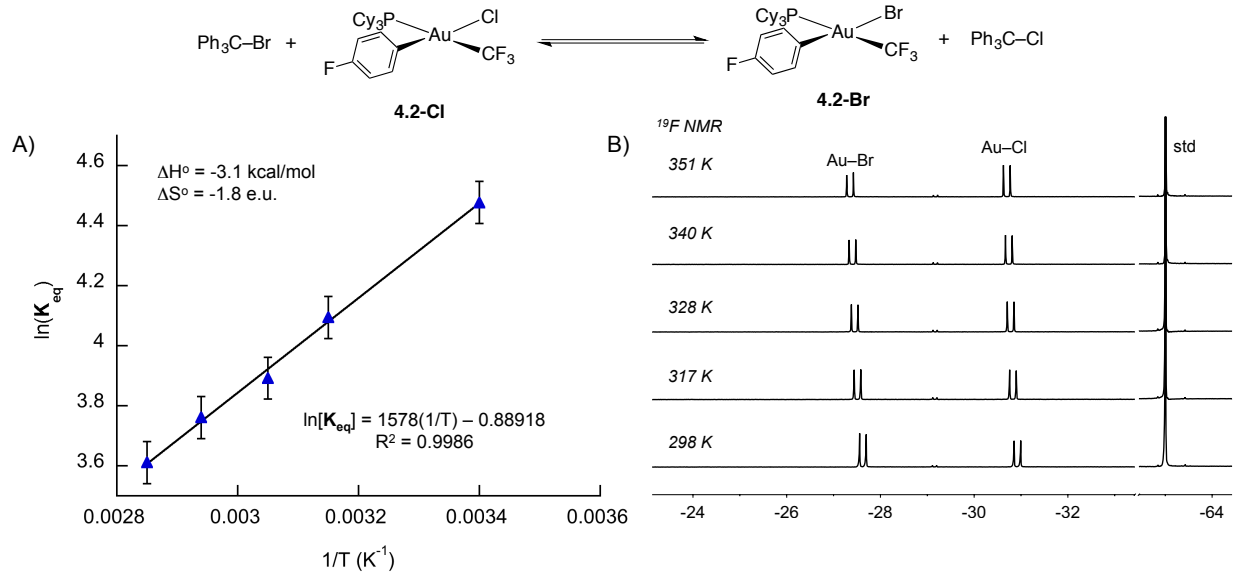

Figure 4.25. A) van't Hoff plot of the equilibrium of **4.2-Cl** (+ Ph_3C–Br) and **4.2-Br** (+ Ph_3C-Cl) (shown above) in toluene-d_8 between 25 and 78 °C. Initial conditions: **4.2-Br** + Ph_3C–Cl (30 equiv). B) ^{19}F NMR array showing both –CF_3 resonances for each compound at temperatures between 298 K and 351 K.

The differences in bond dissociation energies (ΔBDE) of each Au(III)–X bond are functions of $\Delta\Delta H^o_f$ (**4.2-X**) and BDEs of the diatomic halogens. Although rough approximations, these values suggest that the Au(III)–I bond in **4.2-I** is 18 kcal/mol weaker than the Au(III)–Br bond in **4.2-Br**, and 33 kcal/mol weaker than the Au(III)–Cl bond in **4.2-Cl**.[21] On the other hand, the trend in Au(III)–X bond strengths follows C(sp^2)–X bond strengths, with the variation in Au(III)–X BDEs only slightly greater. That the bond dissociation energies decrease in the order Au(III)–Cl > Au(III)–Br > Au(III)–I suggest that selectivities for C(sp^2)–X and C(sp^2)–CF_3 reductive elimination are ultimately guided by the strength of the Au(III)–X bond in the starting material (Figure XX), and that Au–X bonding must be substantially diminished in the transition state to C(sp^2)–X reductive elimination. Halide polarizability, or softness, is correlated with nucleophilicity, and may also play a role in dictating relative rates of C(sp^2)–X bond formation, as noted by Hartwig for Pd(II) systems.[1]

Conclusions: We have accessed full Au(III) halide families through formal oxidative addition of CF_3I to Au(I) followed by halide metathesis, and have systematically studied the thermolysis of **4.1-X** (X = F, Cl, Br, I) and the competitive C(sp^2)–X and C(sp^2)–CF_3 reductive eliminations from Au(III). The mechanisms and kinetic selectivities for these steps are highly dependent on the identity of the halide ligand. When X = I, thermolysis exclusively generates the products of C(sp^2)–I bond formation. The selectivity for C(sp^2)–CF_3 reductive elimination increases in the order X = I < Br < Cl < F, and is completely selective for C(sp^2)–CF_3 bond formation when X = F (Figure 6). Thermodynamic studies reveal that the Au(III)–X bond strength increases in the order X = I < Br < Cl, a trend that mirrors selectivity for C(sp^2)–CF_3 reductive elimination. These observations suggest that selectivity for reductive elimination is strongly dictated by the Au(III)–X bond strength in the reactant, and possibly halide polarizability. Highlighting stark reactivity differences between fluoride and higher halide ligands, we have also shown that the Au(III)–F bond is relatively ionic, and can activate C–H/D bonds in arene solvent at elevated temperatures. Surprisingly, the thermolyses of **4.1-Br** and **4.1-Cl** are accelerated by $(Ph_3P)AuCF_3$, presumably by its coordination to the Au(III)–bound halide.

In conclusion, C(sp^2)–X reductive elimination, generally an infrequently observed process, can be facile from Au(III) at elevated temperatures, and may even outcompete desirable transformations (such as C(sp^2)–CF_3 bond formation); as a result, irreversible C(sp^2)–X reductive elimination should not be discounted as a possible, deleterious thermodynamic sink in studies of Au(III) halides or Au(I) under oxidative conditions. These studies also suggest that challenging C(sp^2)–C reductive elimination from Au(III) halides are favored when X = Cl or F, due to relatively stronger Au(III)–X bonds compared to the higher halides. For the Au(III) complexes discussed above, halide ligand dramatically affects reductive elimination behavior. Reductive elimination is a fundamental step in many catalytic cycles, and judicious choice of halide, often considered a spectator ligand, may be important in developing new reactivity of Au(III).

Experimental

General Considerations: Unless otherwise stated, all manipulations were carried out at ambient temperature (20 ºC) under an atmosphere of purified nitrogen in a Vacuum Atmospheres Corp. glovebox or with a double manifold vacuum line using standard Schlenk techniques. All

glassware was dried at 150 ºC for 12 h prior to use. Solvents were dried by passage through a column of activated alumina under nitrogen pressure and degassed by sparging with dry nitrogen. Toluene-d_8 was distilled from sodium ketyl. CF_3I was purchased from Oakwood and connected to a double-manifold vacuum line fitted with Hg manometers to regulate pressure. AgI, AgBr, and AgCl were prepared by treating $AgNO_3$ with the respective NaX (X = halide) salt in water at room temperature, then filtering and drying. AgF was purchased from Strem and used without further purification. Ph_3C-Cl and Ph_3C-Br were purchased from Sigma-Aldrich and used as received. Ph_3C-F was prepared according to literature procedure. $(Ph_3P)Au(4\text{-Me-}C_6H_4)(CF_3)(I)$ (**4.1-I**), $(Cy_3P)Au(4\text{-F-}C_6H_4)(CF_3)(I)$ (**4.2-I**) and Ph_3PAuCF_3 were prepared as previously reported.
NMR spectra were recorded using Bruker AVQ-400, DRX-500, AV-500 or AV-600 spectrometers, and chemical shifts are referenced to residual NMR solvent peaks (^1H and ^{13}C), 1-CF_3-naphthalene (^{19}F), or H_3PO_4 (^{31}P). Elemental analyses were performed at the College of Chemistry Microanalytical Laboratory, University of California, Berkeley. X-ray structural determinations were performed at CheXray, University of California, Berkeley on Bruker SMART 1000 or SMART APEX diffractometers.

Improved procedure for the synthesis of 4.1-I and 4.2-I. A 25 mL Pyrex Schlenk tube was charged with $Ph_3PAu(4\text{-Me-}C_6H_4)$ or $Cy_3PAu(4\text{-F-}C_6H_4)$ (up to 3 mmol) and the solid was dissolved in CH_2Cl_2 to give a 0.2 molar solution. The tube was sealed and degassed with three freeze-pump-thaw cycles. CF_3I gas was introduced (1 atm) and the reaction vessel was sealed and placed in direct sunlight for 15 minutes. The reaction mixture turned yellow within seconds of irradiation. After irradiation, the excess CF_3I was vented and the reaction mixture was adsorbed to neutral alumina and concentrated to dryness. The alumina mixture was then loaded onto a silica column and the desired Au(III) compounds were eluted in benzene:hexanes (1:1 (v:v), R_f = 0.2 for **1-I**; R_f = 0.55 for **2-I**). Yields typically ranged between 60 and 90 %. All spectroscopic data match those previously reported.

Halide metathesis between 4.1-I or 4.2-I with AgX: 4.1-I (75 mg, 0.10 mmol) or **4.2-I** (77 mg, 0.10 mmol) was dissolved in CH_2Cl_2 (5 mL) in a vial. AgX (X = Br, Cl, F) (1.0 mmol) was added at once, and the reaction was capped and sonicated for 5 minutes in the dark, followed by a second addition of AgX (1.0 mmol) and further sonication for 5 minutes. When X = Br or Cl, the solid turns increasingly yellow with the formation of AgI. The suspension is filtered through a bed of Celite and concentrated *in vacuo* to a white powder (quantitative yield) that can be recrystallized twice in 1:3 CH_2Cl_2:pentane to afford **4.1-Br** (52 mg, 0.074 mmol), **4.2-Br** (61 mg, 0.081 mmol), **4.1-Cl** (51 mg, 0.078 mmol), **4.2-Cl** (60 mg, 0.089 mmol), **4.1-F** (45 mg, 0.071 mmol), or **4.2-F** (55 mg, 0.083 mmol) in analytical purity as white solids.

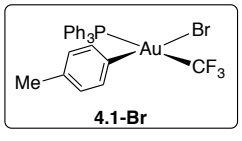

4.1-Br

^{1}H NMR (CD_2Cl_2, 500 MHz, δ): 7.54 – 7.49 (m, 3H), 7.46 – 7.35 (m, 12H), 6.77 (d, J = 8.4 Hz, 2H), 6.64 (d, J = 8.4 Hz, 2H), 2.15 (s, 3H). **^{13}C{^{1}H} NMR** (CD_2Cl_2, 125 MHz, δ): 135.9, 134.9 (d, J = 10 Hz), 132.2 (d, J = 3 Hz), 130.7 (d, J = 3 Hz), 130.6, 129.1 (d, J = 11 Hz), 126.2, 125.7, 20.6.

^{31}P{^{1}H} NMR (CD_2Cl_2, 162 MHz, δ): 24.2 (q, $^{3}J_{P\text{-}F}$ = 68 Hz). **^{19}F NMR** (CD_2Cl_2, 376 MHz, δ): -27.6 (d, $^{3}J_{P\text{-}F}$ = 68 Hz). **Anal. Calcd.** for $C_{26}H_{22}AuBrF_3P$: C, 44.66; H, 3.17. Found C, 44.94; H, 3.33.

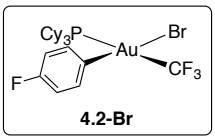

4.2-Br

^{1}H NMR (CD_2Cl_2, 500 MHz, δ): 7.31 – 7.26 (m, 2H), 7.01 – 6.96 (m, 2H), 2.38 – 2.26 (m, 3H), 1.91 – 1.76 (m, 12H), 1.73 – 1.55 (m, 9H), 1.32 – 1.20 (m, 3H), 1.14 – 1.00 (m, 6H). **^{13}C{^{1}H} NMR** (CD_2Cl_2, 125 MHz, δ): 161.7 (d, *J* = 246 Hz), 139.3 – 139.1 (m), 133.0 (dd, *J* = 6 Hz, *J* = 1 Hz), 116.3 (d, *J* = 20 Hz), 34.1 (d, *J* = 25 Hz), 29.8 (d, *J* = 3 Hz), 27.6 (d, *J* = 11 Hz), 26.3 (d, *J* = 1 Hz). **^{31}P{^{1}H} NMR** (CD_2Cl_2, 162 MHz, δ): 28.0 (q, $^{3}J_{P\text{-}F}$ = 64 Hz). **^{19}F NMR** (CD_2Cl_2, 376 MHz, δ): -29.5 (d, $^{3}J_{P\text{-}F}$ = 63 Hz, Au-C*F*$_3$), -117.3 – -117.4 (m, Ar-*F*). **Anal. Calcd.** for $C_{25}H_{37}AuBrF_4P$: C, 41.62; H, 5.17. Found C, 41.47; H, 5.33.

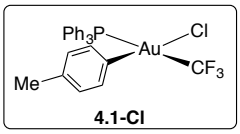

4.1-Cl

^{1}H NMR (CD_2Cl_2, 500 MHz, δ): 7.55 – 7.50 (m, 3H), 7.44 – 7.35 (m, 12H), 6.79 (d, *J* = 8.1 Hz), 6.64 (d, *J* = 8.1 Hz), 2.15 (s, 3H). **^{13}C{^{1}H} NMR** (CD_2Cl_2, 125 MHz, δ): 140.0, 134.8 (d, *J* = 11 Hz), 132.2 (d, *J* = 3 Hz), 131.0 (d, *J* = 3 Hz), 130.7, 129.2 (d, *J* = 11 Hz), 125.8, 125.3, 20.6. **^{31}P{^{1}H} NMR** (CD_2Cl_2, 162 MHz, δ): 25.6 (q, $^{3}J_{P\text{-}F}$ = 69 Hz). **^{19}F NMR** (CD_2Cl_2, 376 MHz, δ): -30.5 (d, $^{3}J_{P\text{-}F}$ = 69 Hz). **Anal. Calcd.** for $C_{26}H_{22}AuClF_3P$: C, 47.69; H, 3.39. Found C, 47.75; H, 3.51.

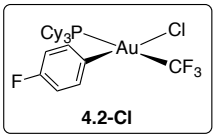

4.2-Cl

^{1}H NMR (CD_2Cl_2, 500 MHz, δ): 7.34 – 7.30 (m, 2H), 7.00 – 6.96 (m, 2H), 2.33 – 2.22 (m, 3H), 1.90 – 1.76 (m, 12H), 1.73 – 1.58 (m, 9H), 1.32 – 1.21 (m, 3H), 1.14 – 1.02 (m, 6H). **^{13}C{^{1}H} NMR** (CD_2Cl_2, 125 MHz, δ): 161.6 (d, *J* = 243 Hz), 136.6 – 136.4 (m), 133.2 (dd, *J* = 7 Hz, *J* = 1 Hz), 116.4 (d, *J* = 21 Hz), 33.5 (d, *J* = 25 Hz), 29.6 (d, *J* = 2 Hz), 27.7 (d, *J* = 11 Hz), 26.3 (d, *J* = 1 Hz). **^{31}P{^{1}H} NMR** (CD_2Cl_2, 162 MHz, δ): 28.7 (q, $^{3}J_{P\text{-}F}$ = 64 Hz). **^{19}F NMR** (CD_2Cl_2, 376 MHz, δ): -32.8 (d, $^{3}J_{P\text{-}F}$ = 64 Hz, Au-C*F*$_3$), -117.4 – -117.5 (m, Ar-*F*). **Anal. Calcd.** for $C_{25}H_{37}AuClF_4P$: C, 44.36; H, 5.51. Found C, 44.29; H, 5.40.

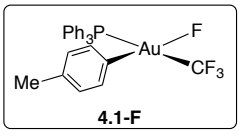

4.1-F

^{1}H NMR (CD_2Cl_2, 500 MHz, δ): 7.56 – 7.51 (m, 3H), 7.49 – 7.43 (m, 6H), 7.43 – 7.37 (m, 6H), 6.77 (dd, *J* = 8.2 Hz, *J* = 3.3 Hz), 6.60 (d, *J* = 8.0 Hz), 2.15 (s, 3H). **^{13}C{^{1}H} NMR** (CD_2Cl_2, 125 MHz, δ): 135.9, 134.6 (dd, *J* = 11 Hz, *J* = 2 Hz), 132.4 (d, *J* = 3 Hz), 131.3 (dd, *J* = 5 Hz, *J* = 2 Hz), 130.2 (d, *J* = 5 Hz), 129.4 (d, *J* = 11 Hz), 125.5, 125.0, 20.6. **^{31}P{^{1}H} NMR** (CD_2Cl_2, 162 MHz, δ): 25.4 (qd, $^{3}J_{P\text{-}F}$ = 69 Hz, $^{2}J_{P\text{-}F}$ = 28 Hz). **^{19}F NMR** (CD_2Cl_2, 376 MHz, δ): -36.6 (dd, $^{3}J_{P\text{-}F}$ = 70 Hz, $^{3}J_{F\text{-}F}$ = 13 Hz), -236.4 – -236.6 (m). **Anal. Calcd.** for $C_{26}H_{22}AuF_4P$: C, 48.92; H, 3.47. Found C, 48.64; H, 3.68.

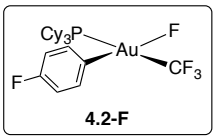

4.2-F

^{1}H NMR (CD_2Cl_2, 500 MHz, δ): 7.30 – 7.24 (m, 2H), 6.96 – 6.90 (m, 2H), 2.24 – 2.12 (m, 3H), 1.92 – 1.76 (m, 12H), 1.75 – 1.53 (m, 9H), 1.34 – 1.21 (m, 3H), 1.17 – 1.05 (m, 6H). **^{13}C{^{1}H} NMR** (CD_2Cl_2, 125 MHz, δ): 161.7 (d, *J* = 244 Hz), 133.4 – 133.2 (m), 116.1 (dd, *J* = 21 Hz, *J* = 5 Hz), 32.6 (d, *J* = 24 Hz), 29.4 (d, *J* = 2 Hz), 27.6 (d, *J* = 11 Hz), 26.2 (d, *J* = 1 Hz) (*ipso*-^{13}C signals not observed due to heteroatom coupling.) **^{31}P{^{1}H} NMR** (CD_2Cl_2, 162 MHz, δ): 33.2 (qd, $^{3}J_{P\text{-}F}$ = 65 Hz, $^{2}J_{P\text{-}F}$

= 23 Hz). **^{19}F NMR** (CD_2Cl_2, 376 MHz, δ): –39.3 (dd, $^{3}J_{P\text{-}F}$ = 64 Hz, $^{3}J_{F\text{-}F}$ = 13 Hz, Au-CF_3), -117.8 – -117.9 (m, Ar-*F*), -249.0 – -249.2 (m). **Anal. Calcd.** for $C_{25}H_{37}AuF_5P$: C, 45.46; H, 5.65. Found C, 45.21; H, 5.36.

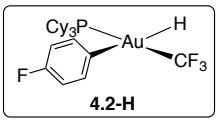

4.2-H

To a solution of **4.2-F** (7 mg, 0.01 mmol) in CD_2Cl_2 (0.5 mL) was added 10 μL of $HSi(OEt)_3$ (8.9 mg, 0.05 mmol, 5 equiv) at 20 ºC. The reaction mixture became a pale yellow color and was transferred to a J-Young tube which was then sealed with a Teflon valve. ^{19}F NMR analysis showed quantitative consumption of **4.2-F** to give **4.2-H**. ^{31}P and ^{1}H NMR spectra were also recorded showing new resonances at δ 34.5 ppm (q, J = 64 Hz) and δ –0.93 ppm (m, 1H). The same signals were also observed when $PhSiH_3$ was used instead of $HSi(OEt)_3$. The use of $PhSiD_3$ gave the analogous **4.2-D**. These complexes are unstable in solution and decompose over the course of several hours at ambient temperature.

Table 4.2 NMR data for **4.1-X** and **4.2-X**.

	X	PR_3	aryl	δ ^{31}P{^{1}H} (ppm)	δ ^{19}F Au-CF_3 (ppm)
4.1-I	I	PPh_3	4-Me-C_6H_4	20.4 (q, $^{3}J_{P\text{-}F}$ = 67 Hz)	–21.3 (d, $^{3}J_{P\text{-}F}$ = 67 Hz)
4.2-I	I	PCy_3	4-F-C_6H_4	25.6 (q, $^{3}J_{P\text{-}F}$ = 64 Hz)	–24.5 (d, $^{3}J_{P\text{-}F}$ = 63 Hz)
4.1-Br	Br	PPh_3	4-Me-C_6H_4	24.2 (q, $^{3}J_{P\text{-}F}$ = 68 Hz)	–27.6 (d, $^{3}J_{P\text{-}F}$ = 67 Hz)
4.2-Br	Br	PCy_3	4-F-C_6H_4	28.0 (q, $^{3}J_{P\text{-}F}$ = 64 Hz)	–29.5 (d, $^{3}J_{P\text{-}F}$ = 63 Hz)
4.1-Cl	Cl	PPh_3	4-Me-C_6H_4	25.6 (q, $^{3}J_{P\text{-}F}$ = 69 Hz)	–30.5 (d, $^{3}J_{P\text{-}F}$ = 69 Hz)
4.2-Cl	Cl	PCy_3	4-F-C_6H_4	28.7 (q, $^{3}J_{P\text{-}F}$ = 64 Hz)	–32.8 (d, $^{3}J_{P\text{-}F}$ = 64 Hz)
4.1-F	F	PPh_3	4-Me-C_6H_4	25.4 (qd, $^{3}J_{P\text{-}F}$ = 69 Hz, $^{2}J_{P\text{-}F}$ = 28 Hz)	–36.6 (dd, $^{3}J_{P\text{-}F}$ = 70 Hz, $^{3}J_{F\text{-}F}$ = 13 Hz)
4.2-F	F	PCy_3	4-F-C_6H_4	33.2 (qd, $^{3}J_{P\text{-}F}$ = 65 Hz, $^{2}J_{P\text{-}F}$ = 23 Hz)	–39.3 (dd, $^{3}J_{P\text{-}F}$ = 64 Hz, $^{3}J_{F\text{-}F}$ = 13 Hz)
4.2-H	F	PCy_3	4-F-C_6H_4	34.5 (q, $^{3}J_{P\text{-}F}$ = 64 Hz)	–23.0 (dd, $^{3}J_{P\text{-}F}$ = 64 Hz, $^{3}J_{H\text{-}F}$ = 19 Hz)

Kinetic Experiments: A 14-16 mM solution of **1-X** in tol-d_8 was prepared in an inert atmosphere glovebox. The internal standard (1-trifluoromethylnaphthalene) was added by microsyringe, and 500 μL aliquots of the solution were transferred to oven-dried NMR tubes. The tubes were capped with greased rubber septa and sealed with Teflon tape. When appropriate, PPh_3 or Ph_3PAuCF_3 were added directly to the NMR tube as a solid prior to injection of the tol-d_8 solution of **1-X** and standard.

The thermolyses of **1-I** and **1-F** were carried out in a Bruker DRX-500 NMR probe that was temperature calibrated using ethylene glycol and pre-heated to 122 °C for 30 minutes. The spectrometer was shimmed and tuned with a solution of standard, and then the NMR tube containing the solution of interest was lowered into the probe. All other reactions were carried out in sealed J-Young NMR tubes at 122 °C in an oil bath shielded from light. At certain intervals, the tubes were removed from the oil bath and cooled to room temperature before NMR

spectra were recorded. The tubes were then returned to the oil bath and this process was repeated until the reactions were complete.

Kinetic Derivations:

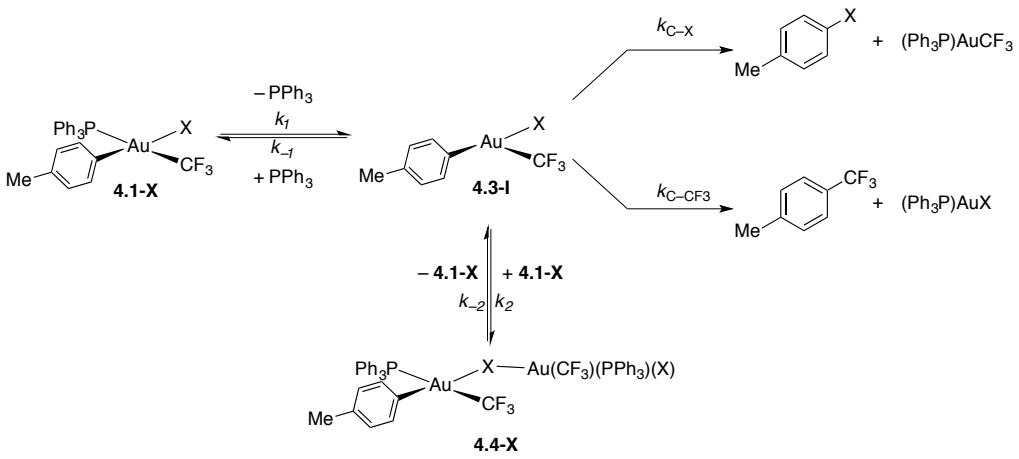

$$\frac{d\,[\mathbf{4.3\text{-}X}]}{dt} = k_1\,[\mathbf{4.1\text{-}X}] + k_{-2}[\mathbf{4.4\text{-}X}] - k_{-1}[PPh_3][\mathbf{4.3\text{-}X}] - k_2[\mathbf{4.3\text{-}X}][\mathbf{4.1\text{-}X}] - k_{C\text{-}X}[\mathbf{4.3\text{-}X}] - k_{C-CF3}[\mathbf{4.3\text{-}X}] = 0$$

$$[\mathbf{4.3\text{-}X}] = \frac{k_1\,[\mathbf{4.1\text{-}X}] - k_{-2}[\mathbf{4.4\text{-}X}]}{k_{-1}[PPh_3] + k_2[\mathbf{4.1\text{-}X}] + k_{C\text{-}X} + k_{C-CF3}}$$

$$\frac{-d[\mathbf{4.1\text{-}X}]}{dt} = (k_{C-X} + k_{C-CF3})[\mathbf{4.3\text{-}X}] = (k_{C-X} + k_{C-CF3})\frac{k_1\,[\mathbf{4.1\text{-}X}] - k_{-2}[\mathbf{4.4\text{-}X}]}{k_{-1}[PPh_3] + k_2[\mathbf{4.1\text{-}X}] + k_{C\text{-}X} + k_{C-CF3}}$$

$$[\mathbf{4.4\text{-}X}] = 0$$

$$\frac{-d[\mathbf{4.1\text{-}X}]}{dt} = \frac{(k_{C-X} + k_{C-CF3})k_1\,[\mathbf{4.1\text{-}X}]}{k_{-1}[PPh_3] + k_2[\mathbf{4.1\text{-}X}] + k_{C\text{-}X} + k_{C-CF3}}$$

$$k_{C\text{-}CF3} = 0,\ [PPh_3] = 0$$

$$\frac{-d[\mathbf{4.1\text{-}X}]}{dt} = \frac{k_{C-X}k_1\,[\mathbf{4.1\text{-}X}]}{k_2[\mathbf{4.1\text{-}X}] + k_{C\text{-}X}}$$

If $k_{C-X} < k_2[\mathbf{4.1\text{-}X}]$ (as is the case for X= I) then

$$\frac{-d[\mathbf{4.1\text{-}X}]}{dt} = \frac{k_{C-X}k_1\,[\mathbf{4.1\text{-}X}]}{k_2[\mathbf{4.1\text{-}X}]} = \frac{k_{C-X}k_1}{k_2}$$

When X = F, $k_{C\text{-}CF3} = 0$ and the general reaction scheme includes a solvent activation pathway,

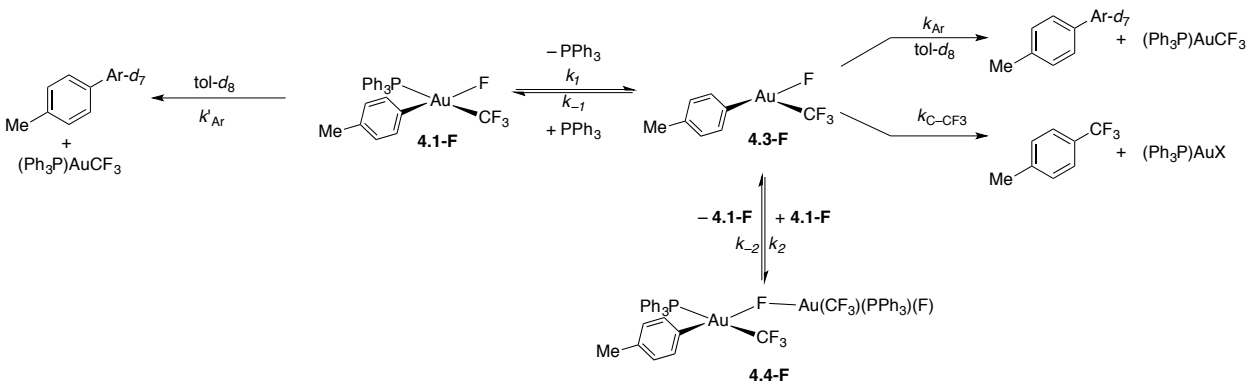

$$-\frac{d[\mathbf{4.1\text{-}F}]}{dt} = k'_{Ar}[\mathbf{4.1\text{-}F}][\text{tol-}d_8] + \frac{(k_{Ar}[\text{tol-}d_8] + k_{C–CF3})k_1[\mathbf{4.1\text{-}F}]}{k_{-1}[PPh_3] + k_2[\mathbf{4.1\text{-}F}] + k_{C–Ar}[\text{tol-}d_8] + k_{C–CF3}}$$

Because $k_{-1}[PPh_3] + k_2[\mathbf{4.1\text{-}F}] >> k_{C\text{-}CF3} + k_{Ar}[\text{tol-}d^8]$,

$$-\frac{d[\mathbf{4.1\text{-}F}]}{dt} = k'_{Ar}[\mathbf{4.1\text{-}F}][\text{tol-}d_8] + \frac{(k_{Ar}[\text{tol-}d_8] + k_{C–CF3})k_1[\mathbf{4.1\text{-}F}]}{k_{-1}[PPh_3] + k_2[\mathbf{4.1\text{-}F}]}$$

In the absence of added PPh_3, the arylation pathway is the slower path, and $k_2[\mathbf{1\text{-}F}] >> k_{-1}[PPh_3]$

$$-\frac{d[\mathbf{4.1\text{-}F}]}{dt} = \frac{(k_{Ar}[\text{tol-}d_8] + k_{C–CF3})k_1[\mathbf{4.1\text{-}F}]}{k_2[\mathbf{4.1\text{-}F}]} = \frac{(k_{Ar}[\text{tol-}d_8] + k_{C–CF3})k_1}{k_2}$$

When PPh_3 is added, $k_{-1}[PPh_3] >> k_2[\mathbf{1\text{-}F}]$, and the arylation pathway is faster

$$-\frac{d[\mathbf{4.1\text{-}F}]}{dt} = k'_{Ar}[\mathbf{4.1\text{-}F}][\text{tol-}d_8]$$

When X = Br or Cl, there is both a non-accelerated and accelerated pathway. By analogy to **4.1-I** and **4.1-F**, the non-accelerated pathway likely involves **4.3-X**

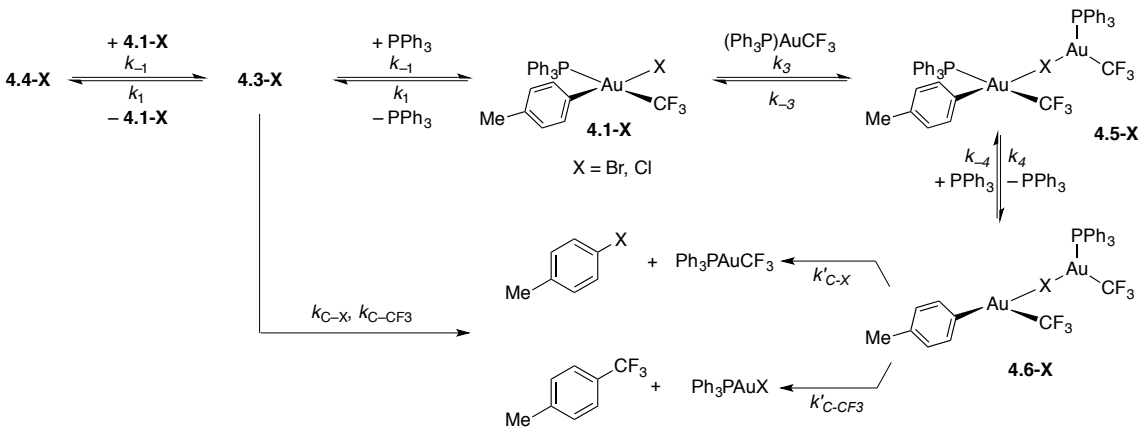

Using steady-state approximations to describe [**4.5-X**] and [**4.6-X**] (accelerated path)

$$\frac{d[\textbf{4.5-X}]}{dt} = k_3[(Ph_3P)AuCF_3][\textbf{4.1-X}] - k_{-3}[\textbf{4.5-X}] - k_4[\textbf{4.5-X}] + k_{-4}[PPh_3][\textbf{4.6-X}] = 0$$

$$[\textbf{4.5-X}] = \frac{k_3[(Ph_3P)AuCF_3][\textbf{4.1-X}] + k_{-4}[PPh_3][\textbf{4.6-X}]}{k_{-3} + k_4}$$

$$\frac{d[\textbf{4.6-X}]}{dt} = k_4[\textbf{4.5-X}] - k_{-4}[PPh_3][\textbf{4.6-X}] - k'_{C\text{-}X}[\textbf{4.6-X}] - k'_{C-CF3}[\textbf{4.6-X}] = 0$$

$$[\textbf{4.6-X}] = \frac{k_4[\textbf{4.5-X}]}{k_{-4}[PPh3] + k'_{C\text{-}X} + k'_{C-CF3}}$$

$$[\textbf{4.6-X}] = \frac{k_3k_4[(Ph_3P)AuCF_3][\textbf{4.1-X}]}{k_{-3}k_{-4}[PPh_3] + (k'_{C\text{-}X} + k'_{C-CF3})(k_{-3} + k_4)}$$

The accelerated pathway is then:

$$\frac{-d[\textbf{4.1-X}]}{dt} = (k'_{C-X} + k'_{C-CF3})[\textbf{4.6-X}] = (k'_{C-X} + k'_{C-CF3})\frac{k_3k_4[(Ph_3P)AuCF_3][\textbf{4.1-X}]}{k_{-3}k_{-4}[PPh_3] + (k'_{C\text{-}X} + k'_{C-CF3})(k_{-3} + k_4)}$$

The overall rate is the sum of the rates for the non-accelerated and accelerated reactions

$$\frac{-d[\textbf{4.1-X}]}{dt} = (k'_{C-X} + k'_{C-CF3})[\textbf{4.6-X}] = (k'_{C-X} + k'_{C-CF3})\frac{k_3k_4[(Ph_3P)AuCF_3][\textbf{4.1-X}]}{k_{-3}k_{-4}[PPh_3] + (k'_{C\text{-}X} + k'_{C-CF3})(k_{-3} + k_4)}$$
$$+ \frac{(k_{C-X} + k_{C-CF3})k_1[\textbf{4.1-X}]}{k_{-1}[PPh_3] + k_2[\textbf{4.1-X}] + k_{C\text{-}X} + k_{C-CF3}}$$

Thermodynamic Experiments: A 14-16 mM solution **2-X** in tol-d_8 was prepared in an inert atmosphere glovebox. Standard (1,3-bis(trifluoromethyl)-5-bromobenzene) was added by

microsyringe, and 500 μL aliquots of the solution were transferred to oven-dried NMR tubes charged with Ph_3C–Cl (63 mg, 0.23 mmol). The tubes were capped with greased rubber septa and sealed with Teflon tape. All experiments were heated in an NMR probe that was calibrated as described above. The equilibria were first monitored at 25 °C after 10 minutes at room temperature. After each increase in temperature, the probe was re-calibrated, and the solution of interest was heated in the probe for 10 minutes. After equilibrium at maximum temperature (78 °C) was reached, the reaction was cooled to 25 °C and the equilibrium measured.

Derivations for Thermodynamic Analysis

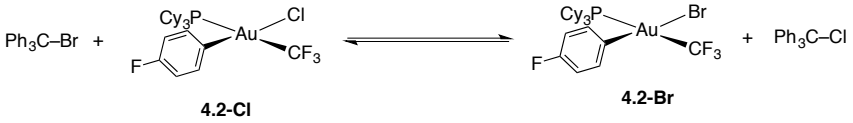

$$\Delta H^{o} = [\Delta H_f^{o}(Au^{III}\text{-}X) + \Delta H_f^{o}(Ph_3C\text{-}Cl)] - [\Delta H_f^{o}(Au^{III}\text{-}Cl) + \Delta H_f^{o}(Ph_3C\text{-}X)]$$

$$\Delta\Delta H_f^{o}(Au^{III}_{Cl\rightarrow X}) = \Delta H^{o} + [\Delta H_f^{o}(Ph_3C\text{-}X) - \Delta H_f^{o}(Ph_3C\text{-}Cl)]$$

Using Benson equivalents to estimate the heats of formation of the trityl halides

$$\Delta\Delta H_f^{o}(Au^{III}_{Cl\rightarrow X}) = \Delta H^{o} + [\Delta H_f^{o}(C\text{-}(C)_3X) - \Delta H_f^{o}(C\text{-}(C)Cl)]$$

The bond dissociation enthalpy (BDE) of [**4.2-X**] is defined as ΔH^{o} for the following reaction

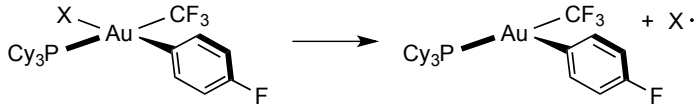

$$\Delta H^{o} = \Delta H_f^{o}(X\bullet) + \Delta H_f^{o}(Au^{II}) - \Delta H_f^{o}(Au^{III}\text{-}X)$$

Although $\Delta H^{o}{}_f(Au^{II})$ is unknown, it is independent of X and will cancel out in calculations of Δ(BDE). Since

$$BDE(X_2) = 2\Delta H_f^{o}(X\bullet) - \Delta H_f^{o}(X_2) = 2\Delta H_f^{o}(X\bullet)$$

$$\frac{1}{2}BDE(X_2) = \Delta H_f^{o}(X\bullet)$$

then the differences in bond dissociation energies between [**4.2-Cl**] and other halide [**4.2-X**] (Δ(BDE)) is

$$\Delta\Delta H^{o} = \Delta BDE^{o}(Au^{III}_{Cl\rightarrow X}) = \frac{1}{2}(BDE^{o}(Cl_2) - BDE^{o}(X_2)) + \Delta H_f^{o}(Au^{III}\text{-}X) - \Delta H_f^{o}(Au^{III}\text{-}Cl)$$

$$\Delta BDE^{o}(Au^{III}_{Cl\rightarrow X}) = \frac{1}{2}(BDE^{o}(Cl_2) - BDE^{o}(X_2)) + \Delta\Delta H_f^{o}(Au^{III}_{Cl\rightarrow X})$$

For the reaction

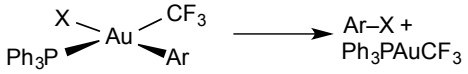

$$\Delta H^{o} = \Delta H^{o}_{f}(\text{Ar-X}) + \Delta H^{o}_{f}(\text{Ph}_3\text{PAuCF}_3) - \Delta H^{o}_{f}(\text{Au}^{III}\text{–X})$$

As above, the unknown $\Delta H^{o}_{f}(Ph_3PAuCF_3)$ cancels out for $\Delta\Delta H^{o}$ between reactions

$$\Delta\Delta H^{o} = [\Delta H^{o}_{f}(\text{Ar-Cl}) - \Delta H^{o}_{f}(\text{Au}^{III}\text{-Cl}] - [\Delta H^{o}_{f}(\text{Ar-X}) - \Delta H^{o}_{f}(\text{Au}^{III}\text{-X})]$$

$$\Delta\Delta H^{o} = \Delta H^{o}_{f}(\text{Ar-Cl}) - \Delta H^{o}_{f}(\text{Ar-X}) + \Delta\Delta H^{o}_{f}(\text{Au}^{III}_{\text{Cl}\rightarrow\text{X}})$$

References:

(1) Roy, A. H.; Hartwig, J. F. *J. Am. Chem. Soc.* **2003**, *125* (46), 13944–13945.
(2) Klapars, A.; Buchwald, S. L. *J. Am. Chem. Soc.* **2002**, *124* (50), 14844–14845.
(3) Zanon, J.; Klapars, A.; Buchwald, S. L. *J. Am. Chem. Soc.* **2003**, *125* (10), 2890–2891.
(4) Casitas, A.; Poater, A.; Solà, M.; Stahl, S. S.; Costas, M.; Ribas, X. *Dalton Trans.* **2010**, *39* (43), 10458–10463.
(5) Lin, B.-L.; Kang, P.; Stack, T. D. P. *Organometallics* **2010**, *29* (17), 3683–3685.
(6) Sheppard, T. D. *Org. Biomol. Chem.* **2009**, *7* (6), 1043.
(7) Dekleva, T. W.; Forster, D. In *Advances in Catalysis*; D.D. Eley, H. P. and P. B. W., Ed.; Academic Press, 1986; Vol. 34, pp 81–130.
(8) Goldberg, K. I.; Yan, J. Y.; Winter, E. L. *J. Am. Chem. Soc.* **1994**, *116* (4), 1573–1574.
(9) Goldberg, K. I.; Yan, J.; Breitung, E. M. *J. Am. Chem. Soc.* **1995**, *117* (26), 6889–6896.
(10) Maitlis, P. M.; Haynes, A.; Sunley, G. J.; Howard, M. J. *J. Chem. Soc. Dalton Trans.* **1996**, No. 11, 2187–2196.
(11) Frech, C. M.; Milstein, D. *J. Am. Chem. Soc.* **2006**, *128* (38), 12434–12435.
(12) Whitfield, S. R.; Sanford, M. S. *J. Am. Chem. Soc.* **2007**, *129* (49), 15142–15143.
(13) Furuya, T.; Ritter, T. *J. Am. Chem. Soc.* **2008**, *130* (31), 10060–10061.
(14) Racowski, J. M.; Gary, J. B.; Sanford, M. S. *Angew. Chem. Int. Ed.* **2012**, *51* (14), 3414–3417.
(15) O'Reilly, M. E.; Pahls, D. R.; Cundari, T. R.; Gunnoe, T. B. *Organometallics* **2014**, *33* (22), 6504–6510.
(16) Rivada-Wheelaghan, O.; Roselló-Merino, M.; Díez, J.; Maya, C.; López-Serrano, J.; Conejero, S. *Organometallics* **2014**, *33* (21), 5944–5947.
(17) Pérez-Temprano, M. H.; Racowski, J. M.; Kampf, J. W.; Sanford, M. S. *J. Am. Chem. Soc.* **2014**, *136* (11), 4097–4100.
(18) Camasso, N. M.; Sanford, M. S. *Science* **2015**, *347* (6227), 1218–1220.
(19) Mo, F.; Yan, J. M.; Qiu, D.; Li, F.; Zhang, Y.; Wang, J. *Angew. Chem. Int. Ed.* **2010**, *49* (11), 2028–2032.

(20) Qiu, D.; Mo, F.; Zheng, Z.; Zhang, Y.; Wang, J. *Org. Lett.* **2010**, *12* (23), 5474–5477.
(21) Nguyen, K. H.; Tomasi, S.; Le Roch, M.; Toupet, L.; Renault, J.; Uriac, P.; Gouault, N. *J. Org. Chem.* **2013**, *78* (16), 7809–7815.
(22) Serra, J.; Whiteoak, C. J.; Acuña-Parés, F.; Font, M.; Luis, J. M.; Lloret-Fillol, J.; Ribas, X. *J. Am. Chem. Soc.* **2015**, *137* (41), 13389–13397.
(23) Mankad, N. P.; Toste, F. D. *Chem. Sci.* **2011**, *3* (1), 72–76.
(24) Scott, V. J.; Labinger, J. A.; Bercaw, J. E. *Organometallics* **2010**, *29* (18), 4090–4096.
(25) Toste, F. D.; Michelet, V. *Gold Catalysis: An Homogeneous Approach*; Imperial College Press: London, U. K., 2014.
(26) Moissan, H. *Compt. Rend. 109*, 807.
(27) Mohr, F. *Gold Bull.* **2004**, *37* (3-4), 164–169.
(28) Waddington, T. C. *Trans. Faraday Soc.* **1959**, *55* (0), 1531–1535.
(29) Saenger, K. L.; Sun, C. P. *Phys. Rev. A* **1992**, *46* (1), 670–673.
(30) Evans, C. J.; Gerry, M. C. L. *J. Am. Chem. Soc.* **2000**, *122* (7), 1560–1561.
(31) Schwerdtfeger, P.; McFeaters, J. S.; Liddell, M. J.; Hrušák, J.; Schwarz, H. *J. Chem. Phys.* **1995**, *103* (1), 245–252.
(32) Iliaš, M.; Furdík, P.; Urban, M. *J. Phys. Chem. A* **1998**, *102* (27), 5263–5268.
(33) Laerdahl, J. K.; Saue, T.; Jr, K. F. *Theor. Chem. Acc.* **1997**, *97* (1-4), 177–184.
(34) Evans, C. J.; Gerry, M. C. L. *J. Mol. Spectrosc.* **2000**, *203* (1), 105–117.
(35) Reynard, L. M.; Evans, C. J.; Gerry, M. C. L. *J. Mol. Spectrosc.* **2001**, *205* (2), 344–346.
(36) Schröder, D.; Hrušák, J.; Tornieporth-Oetting, I. C.; Klapötke, T. M.; Schwarz, H. *Angew. Chem. Int. Ed. Engl.* **1994**, *33* (2), 212–214.
(37) Busse, J. K.; Stoner, E. J.; Ladd, C. L. In *e-EROS Encyclopedia of Reagents for Organic Synthesis*; John Wiley & Sons, Ltd: Chichester, UK.
(38) Subramanian, M. A.; Manzer, L. E. *Science* **2002**, *297* (5587), 1665–1665.
(39) Tang, P.; Furuya, T.; Ritter, T. *J. Am. Chem. Soc.* **2010**, *132* (34), 12150–12154.
(40) Zweig, A.; Fischer, R. G.; Lancaster, J. E. *J. Org. Chem.* **1980**, *45* (18), 3597–3603.
(41) Schroeder, H.; Kober, E.; Ulrich, H.; Rätz, R.; Agahigian, H.; Grundmann, C. *J. Org. Chem.* **1962**, *27* (7), 2580–2584.
(42) Fier, P. S.; Hartwig, J. F. *Science* **2013**, *342* (6161), 956–960.
(43) Gorin, D. J.; Toste, F. D. *Nature* **2007**, *446* (7134), 395–403.
(44) Bartlett, N. *Gold Bull.* **1998**, *31* (1), 22–25.
(45) Sharpe, A. G. *J. Chem. Soc. Resumed* **1949**, No. 0, 2901–2902.
(46) Engelmann, U.; Müller, B. G. *Z. Für Anorg. Allg. Chem.* **1992**, *618* (12), 43–52.
(47) Tornieporth-Oetting, I. C.; Klapötke, T. M. *Chem. Ber.* **1995**, *128* (9), 957–958.
(48) Einstein, F. W. B.; Rao, P. R.; Trotter, J.; Bartlett, N. *J. Chem. Soc. Inorg. Phys. Theor.* **1967**, No. 0, 478–482.
(49) Wang, X.; Andrews, L.; Willmann, K.; Brosi, F.; Riedel, S. *Angew. Chem. Int. Ed.* **2012**, *51* (42), 10628–10632.
(50) Müller, B. G. *Z. Für Anorg. Allg. Chem.* **1987**, *555* (12), 57–63.
(51) Fischer, R.; Müller, B. G. *Z. Für Anorg. Allg. Chem.* **1997**, *623* (11), 1729–1733.
(52) Bialowons, H.; Müller, B. G. *Z. Für Anorg. Allg. Chem.* **1997**, *623* (11), 1719–1722.
(53) Bialowons, H.; Müller, B. G. *Z. Für Anorg. Allg. Chem.* **1997**, *623* (1-6), 434–438.
(54) Leary, K.; Bartlett, N. *J. Chem. Soc. Chem. Commun.* **1972**, No. 15, 903–904.

(55) Graudejus, O.; Elder, S. H.; Lucier, G. M.; Shen, C.; Bartlett, N. *Inorg. Chem.* **1999**, *38* (10), 2503–2509.
(56) Kaindl, G.; Leary, K.; Bartlett, N. *J. Chem. Phys.* **1973**, *59* (9), 5050–5054.
(57) Leary, K.; Zalkin, A.; Bartlett, N. *J. Chem. Soc. Chem. Commun.* **1973**, No. 4, 131–132.
(58) Holloway, J. H.; Schrobilgen, G. J. *J. Chem. Soc. Chem. Commun.* **1975**, No. 15, 623–624.
(59) Vasile, M. J.; Richardson, T. J.; Stevie, F. A.; Falconer, W. E. *J. Chem. Soc. Dalton Trans.* **1976**, No. 4, 351–353.
(60) Hwang, I.-C.; Seppelt, K. *Angew. Chem. Int. Ed.* **2001**, *40* (19), 3690–3693.
(61) Elder, S. H.; Lucier, G. M.; Hollander, F. J.; Bartlett, N. *J. Am. Chem. Soc.* **1997**, *119* (5), 1020–1026.
(62) Himmel, D.; Riedel, S. *Inorg. Chem.* **2007**, *46* (13), 5338–5342.
(63) Laitar, D. S.; Müller, P.; Gray, T. G.; Sadighi, J. P. *Organometallics* **2005**, *24* (19), 4503–4505.
(64) Akana, J. A.; Bhattacharyya, K. X.; Müller, P.; Sadighi, J. P. *J. Am. Chem. Soc.* **2007**, *129* (25), 7736–7737.
(65) Nugent, W. A. *Angew. Chem. Int. Ed.* **2012**, *51* (36), 8936–8949.
(66) Sutherland, B. R.; Folting, K.; Streib, W. E.; Ho, D. M.; Huffman, J. C.; Caulton, K. G. *J. Am. Chem. Soc.* **1987**, *109* (11), 3489–3490.
(67) Melgarejo, D. Y.; Chiarella, G. M.; Fackler, J. P.; Perez, L. M.; Rodrigue-Witchel, A.; Reber, C. *Inorg. Chem.* **2011**, *50* (10), 4238–4240.
(68) Laguna, A.; Laguna, M. *Coord. Chem. Rev.* **1999**, *193–195*, 837–856.
(69) Mankad, N. P.; Toste, F. D. *J. Am. Chem. Soc.* **2010**, *132* (37), 12859–12861.
(70) Tomashenko, O. A.; Grushin, V. V. *Chem. Rev.* **2011**, *111* (8), 4475–4521.
(71) Furuya, T.; Kamlet, A. S.; Ritter, T. *Nature* **2011**, *473* (7348), 470–477.
(72) Roşca, D.-A.; Smith, D. A.; Hughes, D. L.; Bochmann, M. *Angew. Chem. Int. Ed.* **2012**, *51* (42), 10643–10646.
(73) Reichardt, C. *Chem. Rev.* **1994**, *94* (8), 2319–2358.
(74) Margrave, J. L.; Whitmire, K. H.; Hauge, R. H.; Norem, N. T. *Inorg. Chem.* **1990**, *29* (17), 3252–3253.
(75) Zharkova, G. I.; Baidina, I. A.; Igumenov, I. K. *J. Struct. Chem.* **2007**, *48* (1), 108–113.
(76) Kieltsch, I.; Dubinina, G. G.; Hamacher, C.; Kaiser, A.; Torres-Nieto, J.; Hutchison, J. M.; Klein, A.; Budnikova, Y.; Vicic, D. A. *Organometallics* **2010**, *29* (6), 1451–1456.
(77) Domalski, E. S.; Hearing, E. D. *J. Phys. Chem. Ref. Data* **1993**, *22* (4), 805–1159.

Appendix: Crystallographic Data

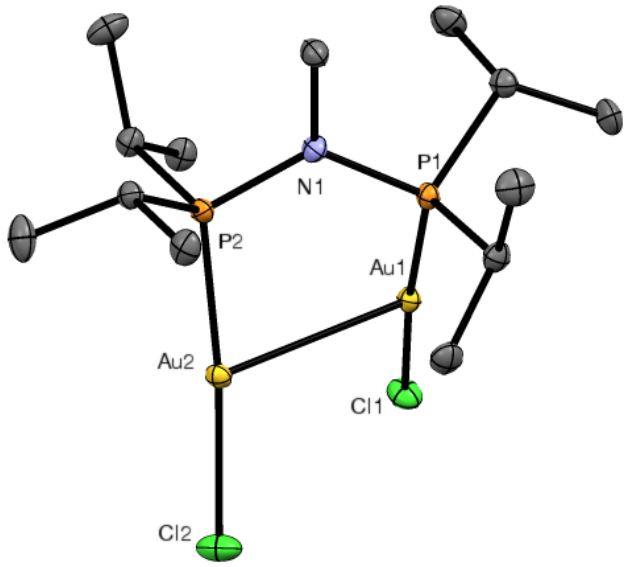

Figure A1. ORTEP plot of 1.4 with thermal ellipsoids set at the 50% probability level and hydrogen atoms omitted for clarity.

Table A1. Crystal data and structure refinement for 1.4.

Identification code	npm043	
Empirical formula	$C_{13}\,H_{31}\,Au_2\,Cl_2\,N\,P_2$	
Formula weight	728.16	
Temperature	100(2) K	
Wavelength	0.71073 Å	
Crystal system	Triclinic	
Space group	P-1	
Unit cell dimensions	a = 8.9869(6) Å	α= 89.4460(10)°.
	b = 10.2140(6) Å	β= 88.4150(10)°.
	c = 11.0205(7) Å	γ = 83.6880(10)°.
Volume	1005.06(11) $Å^3$	
Z	2	
Density (calculated)	2.406 Mg/m^3	
Absorption coefficient	14.997 mm^{-1}	
F(000)	676	
Crystal size	0.50 x 0.20 x 0.10 mm^3	
Theta range for data collection	1.85 to 26.37°.	
Index ranges	-11<=h<=11, -12<=k<=12, -13<=l<=13	
Reflections collected	37121	
Independent reflections	4087 [R(int) = 0.0386]	
Completeness to theta = 26.37°	99.8 %	
Absorption correction	Semi-empirical from equivalents	
Max. and min. transmission	0.3155 and 0.0498	
Refinement method	Full-matrix least-squares on F^2	
Data / restraints / parameters	4087 / 0 / 190	
Goodness-of-fit on F^2	1.061	
Final R indices [I>2sigma(I)]	R1 = 0.0174, wR2 = 0.0419	
R indices (all data)	R1 = 0.0183, wR2 = 0.0425	
Largest diff. peak and hole	1.106 and -1.334 $e.Å^{-3}$	

Table A2. Atomic coordinates (x 10^4) and equivalent isotropic displacement parameters ($Å^2$x 10^3) for npm043. U(eq) is defined as one third of the trace of the orthogonalized U^{ij} tensor.

	x	y	z	U(eq)
Au(1)	4637(1)	2764(1)	4003(1)	11(1)
Au(2)	4576(1)	2487(1)	1225(1)	12(1)
Cl(1)	2250(1)	2406(1)	4609(1)	18(1)
Cl(2)	2249(1)	3482(1)	779(1)	23(1)
P(1)	7029(1)	3087(1)	3657(1)	11(1)
P(2)	6871(1)	1448(1)	1456(1)	11(1)
N(1)	7870(3)	2090(3)	2547(2)	13(1)
C(1)	8120(4)	2681(3)	5021(3)	14(1)
C(2)	8101(4)	1226(4)	5353(3)	21(1)
C(3)	7485(4)	3557(4)	6068(3)	22(1)
C(4)	7270(4)	4805(3)	3289(3)	15(1)
C(5)	6298(4)	5314(4)	2229(3)	19(1)
C(6)	8903(4)	5086(4)	3089(4)	22(1)
C(7)	6783(4)	-307(3)	1777(3)	14(1)
C(8)	5776(4)	-497(3)	2898(3)	16(1)
C(9)	8294(4)	-1145(4)	1874(4)	22(1)
C(10)	8019(4)	1528(3)	66(3)	13(1)
C(11)	7318(4)	849(4)	-975(3)	24(1)
C(12)	8205(4)	2959(4)	-269(3)	18(1)
C(13)	9531(4)	1818(4)	2509(3)	16(1)

Table A3. Bond lengths [Å] and angles [°] for npm043.

Au(1)-P(1)	2.2323(8)		
Au(1)-Cl(1)	2.2958(8)	C(5)-H(5C)	0.9800
Au(1)-Au(2)	3.0800(3)	C(6)-H(6A)	0.9800
Au(2)-P(2)	2.2325(8)	C(6)-H(6B)	0.9800
Au(2)-Cl(2)	2.2870(8)	C(6)-H(6C)	0.9800
P(1)-N(1)	1.705(3)	C(7)-C(9)	1.529(5)
P(1)-C(4)	1.831(3)	C(7)-C(8)	1.534(4)
P(1)-C(1)	1.837(3)	C(7)-H(7)	1.0000
P(2)-N(1)	1.698(3)	C(8)-H(8A)	0.9800
P(2)-C(10)	1.830(3)	C(8)-H(8B)	0.9800
P(2)-C(7)	1.834(3)	C(8)-H(8C)	0.9800
N(1)-C(13)	1.488(4)	C(9)-H(9A)	0.9800
C(1)-C(3)	1.526(5)	C(9)-H(9B)	0.9800
C(1)-C(2)	1.529(5)	C(9)-H(9C)	0.9800
C(1)-H(1)	1.0000	C(10)-C(11)	1.531(5)
C(2)-H(2A)	0.9800	C(10)-C(12)	1.530(5)
C(2)-H(2B)	0.9800	C(10)-H(10)	1.0000
C(2)-H(2C)	0.9800	C(11)-H(11A)	0.9800
C(3)-H(3A)	0.9800	C(11)-H(11B)	0.9800
C(3)-H(3B)	0.9800	C(11)-H(11C)	0.9800
C(3)-H(3C)	0.9800	C(12)-H(12A)	0.9800
C(4)-C(5)	1.530(5)	C(12)-H(12B)	0.9800
C(4)-C(6)	1.536(5)	C(12)-H(12C)	0.9800
C(4)-H(4)	1.0000	C(13)-H(13A)	0.9800
C(5)-H(5A)	0.9800	C(13)-H(13B)	0.9800
C(5)-H(5B)	0.9800	C(13)-H(13C)	0.9800

P(1)-Au(1)-Cl(1)	172.90(3)
P(1)-Au(1)-Au(2)	84.17(2)
Cl(1)-Au(1)-Au(2)	102.78(2)
P(2)-Au(2)-Cl(2)	173.98(3)
P(2)-Au(2)-Au(1)	83.35(2)
Cl(2)-Au(2)-Au(1)	102.62(2)
N(1)-P(1)-C(4)	109.41(15)
N(1)-P(1)-C(1)	105.39(15)
C(4)-P(1)-C(1)	105.86(15)
N(1)-P(1)-Au(1)	112.56(10)
C(4)-P(1)-Au(1)	112.88(11)
C(1)-P(1)-Au(1)	110.26(11)
N(1)-P(2)-C(10)	104.76(14)
N(1)-P(2)-C(7)	109.08(15)
C(10)-P(2)-C(7)	106.13(15)
N(1)-P(2)-Au(2)	114.47(10)
C(10)-P(2)-Au(2)	111.31(11)
C(7)-P(2)-Au(2)	110.64(11)
C(13)-N(1)-P(2)	119.2(2)
C(13)-N(1)-P(1)	118.8(2)
P(2)-N(1)-P(1)	121.89(16)
C(3)-C(1)-C(2)	110.7(3)
C(3)-C(1)-P(1)	109.6(2)
C(2)-C(1)-P(1)	110.3(2)
C(3)-C(1)-H(1)	108.7
C(2)-C(1)-H(1)	108.7
P(1)-C(1)-H(1)	108.7
C(1)-C(2)-H(2A)	109.5
C(1)-C(2)-H(2B)	109.5
H(2A)-C(2)-H(2B)	109.5
C(1)-C(2)-H(2C)	109.5
H(2A)-C(2)-H(2C)	109.5
H(2B)-C(2)-H(2C)	109.5
C(1)-C(3)-H(3A)	109.5
C(1)-C(3)-H(3B)	109.5
H(3A)-C(3)-H(3B)	109.5
C(1)-C(3)-H(3C)	109.5
H(3A)-C(3)-H(3C)	109.5
H(3B)-C(3)-H(3C)	109.5
C(5)-C(4)-C(6)	111.6(3)
C(5)-C(4)-P(1)	111.3(2)
C(6)-C(4)-P(1)	114.8(2)
C(5)-C(4)-H(4)	106.1
C(6)-C(4)-H(4)	106.1
P(1)-C(4)-H(4)	106.1
C(4)-C(5)-H(5A)	109.5
C(4)-C(5)-H(5B)	109.5
H(5A)-C(5)-H(5B)	109.5
C(4)-C(5)-H(5C)	109.5
H(5A)-C(5)-H(5C)	109.5
H(5B)-C(5)-H(5C)	109.5
C(4)-C(6)-H(6A)	109.5
C(4)-C(6)-H(6B)	109.5
H(6A)-C(6)-H(6B)	109.5
C(4)-C(6)-H(6C)	109.5
H(6A)-C(6)-H(6C)	109.5
H(6B)-C(6)-H(6C)	109.5
C(9)-C(7)-C(8)	111.0(3)
C(9)-C(7)-P(2)	115.6(2)
C(8)-C(7)-P(2)	110.8(2)
C(9)-C(7)-H(7)	106.2
C(8)-C(7)-H(7)	106.2
P(2)-C(7)-H(7)	106.2
C(7)-C(8)-H(8A)	109.5
C(7)-C(8)-H(8B)	109.5
H(8A)-C(8)-H(8B)	109.5
C(7)-C(8)-H(8C)	109.5
H(8A)-C(8)-H(8C)	109.5
H(8B)-C(8)-H(8C)	109.5
C(7)-C(9)-H(9A)	109.5
C(7)-C(9)-H(9B)	109.5
H(9A)-C(9)-H(9B)	109.5
C(7)-C(9)-H(9C)	109.5
H(9A)-C(9)-H(9C)	109.5
H(9B)-C(9)-H(9C)	109.5
C(11)-C(10)-C(12)	110.5(3)
C(11)-C(10)-P(2)	110.3(2)
C(12)-C(10)-P(2)	110.6(2)
C(11)-C(10)-H(10)	108.5
C(12)-C(10)-H(10)	108.5
P(2)-C(10)-H(10)	108.5
C(10)-C(11)-H(11A)	109.5
C(10)-C(11)-H(11B)	109.5
H(11A)-C(11)-H(11B)	109.5
C(10)-C(11)-H(11C)	109.5
H(11A)-C(11)-H(11C)	109.5
H(11B)-C(11)-H(11C)	109.5
C(10)-C(12)-H(12A)	109.5
C(10)-C(12)-H(12B)	109.5
H(12A)-C(12)-H(12B)	109.5
C(10)-C(12)-H(12C)	109.5
H(12A)-C(12)-H(12C)	109.5
H(12B)-C(12)-H(12C)	109.5
N(1)-C(13)-H(13A)	109.5
N(1)-C(13)-H(13B)	109.5
H(13A)-C(13)-H(13B)	109.5
N(1)-C(13)-H(13C)	109.5
H(13A)-C(13)-H(13C)	109.5
H(13B)-C(13)-H(13C)	109.5

Symmetry transformations used to generate equivalent atoms:

Table A4. Anisotropic displacement parameters ($Å^2 x\ 10^3$)for npm043. The anisotropic displacement factor exponent takes the form: $-2\pi^2[\ h^2 a^{*2} U^{11} + ... + 2\ h\ k\ a^*\ b^*\ U^{12}\ ]$

	U^{11}	U^{22}	U^{33}	U^{23}	U^{13}	U^{12}
Au(1)	11(1)	12(1)	9(1)	0(1)	1(1)	-1(1)
Au(2)	12(1)	13(1)	9(1)	1(1)	-1(1)	-1(1)
Cl(1)	12(1)	25(1)	18(1)	1(1)	0(1)	-4(1)
Cl(2)	14(1)	28(1)	24(1)	10(1)	0(1)	3(1)
P(1)	12(1)	12(1)	9(1)	0(1)	1(1)	-1(1)
P(2)	12(1)	12(1)	9(1)	0(1)	0(1)	-1(1)
N(1)	12(1)	15(2)	11(1)	-2(1)	2(1)	0(1)
C(1)	15(2)	16(2)	12(2)	1(1)	0(1)	-1(1)
C(2)	25(2)	23(2)	15(2)	5(1)	-3(1)	0(2)
C(3)	28(2)	26(2)	13(2)	-5(2)	-5(1)	0(2)
C(4)	17(2)	12(2)	15(2)	0(1)	1(1)	-2(1)
C(5)	24(2)	13(2)	18(2)	3(1)	-1(1)	0(1)
C(6)	21(2)	19(2)	28(2)	4(2)	1(2)	-7(2)
C(7)	18(2)	12(2)	13(2)	1(1)	1(1)	-2(1)
C(8)	21(2)	14(2)	15(2)	3(1)	2(1)	-4(1)
C(9)	20(2)	15(2)	31(2)	4(2)	5(2)	3(1)
C(10)	14(2)	15(2)	11(2)	0(1)	1(1)	0(1)
C(11)	31(2)	27(2)	15(2)	-6(2)	6(2)	-11(2)
C(12)	23(2)	18(2)	13(2)	2(1)	4(1)	-3(1)
C(13)	14(2)	21(2)	14(2)	-2(1)	-1(1)	-1(1)

Table A5. Hydrogen coordinates ($x\ 10^4$) and isotropic displacement parameters ($Å^2 x\ 10^3$) for npm043.

	x	y	z	U(eq)
H(1)	9180	2854	4849	17
H(2A)	8737	1010	6051	32
H(2B)	8482	681	4660	32
H(2C)	7073	1053	5559	32
H(3A)	6436	3417	6229	33
H(3B)	7546	4483	5851	33
H(3C)	8064	3335	6796	33
H(4)	6879	5331	4012	18
H(5A)	6306	6269	2150	28
H(5B)	5269	5109	2382	28
H(5C)	6697	4888	1477	28
H(6A)	9279	4743	2298	34
H(6B)	9517	4657	3731	34
H(6C)	8956	6039	3109	34
H(7)	6276	-661	1073	17
H(8A)	5636	-1431	2988	25
H(8B)	4801	20	2799	25
H(8C)	6247	-200	3622	25
H(9A)	8756	-949	2636	34
H(9B)	8951	-942	1189	34

H(9C)	8143	-2080	1858	34
H(10)	9032	1052	212	16
H(11A)	6302	1275	-1101	36
H(11B)	7276	-82	-771	36
H(11C)	7927	921	-1719	36
H(12A)	8858	2981	-994	27
H(12B)	8652	3378	406	27
H(12C)	7223	3433	-434	27
H(13A)	9816	870	2605	24
H(13B)	9944	2289	3169	24
H(13C)	9925	2116	1728	24

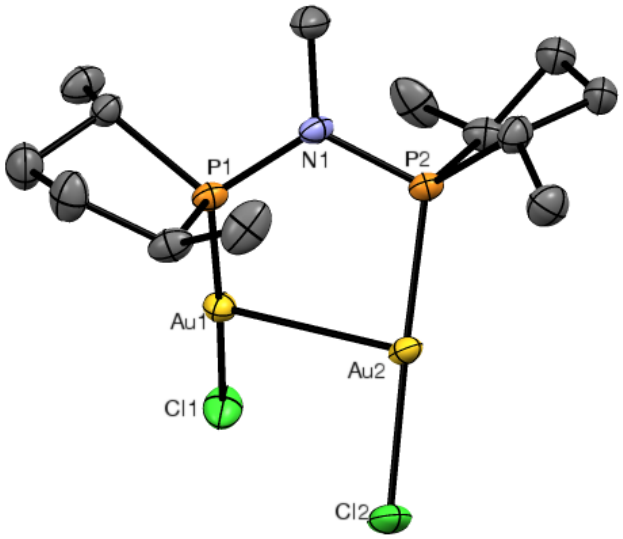

Figure A2 ORTEP plot of **1.11** with thermal ellipsoids set at the 50% probability level and hydrogen atoms omitted for clarity.

Table A6. Crystal data and structure refinement for wjw188.

Identification code	shelxl	
Empirical formula	$C_{30}\ H_{62}\ Au_4\ Cl_4\ N_2\ O\ P_4$	
Formula weight	1520.36	
Temperature	100(2) K	
Wavelength	0.71069 Å	
Crystal system	Monoclinic	
Space group	P2(1)	
Unit cell dimensions	a = 9.854(5) Å	α= 90.000(5)°.
	b = 13.591(5) Å	β= 90.442(5)°.
	c = 16.484(5) Å	γ = 90.000(5)°.
Volume	2207.6(15) $Å^3$	
Z	2	
Density (calculated)	2.287 Mg/m^3	
Absorption coefficient	13.663 mm^{-1}	
F(000)	1416	
Crystal size	0.50 x 0.10 x 0.08 mm^3	
Theta range for data collection	1.94 to 25.39°.	

Index ranges	-11<=h<=11, -16<=k<=15, -19<=l<=19
Reflections collected	56234
Independent reflections	7739 [R(int) = 0.0367]
Completeness to theta = 25.00°	100.0 %
Absorption correction	Semi-empirical from equivalents
Max. and min. transmission	0.4078 and 0.0557
Refinement method	Full-matrix least-squares on F^2
Data / restraints / parameters	7739 / 1 / 416
Goodness-of-fit on F^2	1.073
Final R indices [I>2sigma(I)]	R1 = 0.0226, wR2 = 0.0542
R indices (all data)	R1 = 0.0232, wR2 = 0.0545
Absolute structure parameter	-0.015(5)
Largest diff. peak and hole	1.505 and -0.925 e.Å^{-3}

Table A7. Atomic coordinates (x 10^4) and equivalent isotropic displacement parameters (Å^{2}x 10^3) for wjw188. U(eq) is defined as one third of the trace of the orthogonalized U^{ij} tensor.

	x	y	z	U(eq)
C(1)	1408(7)	2322(6)	6021(5)	28(2)
C(2)	2481(9)	3125(6)	5858(5)	38(2)
C(3)	3213(8)	2885(7)	5077(5)	38(2)
C(4)	3635(6)	1791(5)	5133(4)	22(2)
C(5)	1169(9)	2120(7)	6922(5)	40(2)
C(6)	4222(7)	1349(7)	4374(4)	32(2)
C(7)	1708(7)	-1762(6)	5861(5)	30(2)
C(8)	2335(7)	-2292(6)	6589(5)	33(2)
C(9)	1476(7)	-2038(6)	7331(5)	32(2)
C(10)	1283(7)	-922(6)	7345(4)	27(2)
C(11)	2565(10)	-1702(7)	5105(5)	42(2)
C(12)	108(8)	-574(7)	7875(5)	35(2)
C(13)	3741(7)	207(6)	6461(5)	32(2)
C(14)	6826(7)	248(5)	1907(4)	20(1)
C(15)	7348(7)	-807(6)	1837(4)	27(2)
C(16)	8054(7)	-868(6)	1013(4)	25(2)
C(17)	7048(7)	-492(5)	362(4)	22(2)
C(18)	5775(7)	421(6)	2564(4)	28(2)
C(19)	7708(7)	-270(6)	-456(4)	27(2)
C(20)	2333(7)	1652(6)	86(4)	28(2)
C(21)	1108(7)	1058(7)	369(5)	35(2)
C(22)	935(8)	1278(8)	1264(5)	44(2)
C(23)	2325(7)	1260(6)	1701(4)	27(2)
C(24)	2849(10)	1463(8)	-762(5)	46(2)
C(25)	2379(8)	1998(7)	2402(5)	37(2)
C(26)	3962(7)	-463(6)	744(5)	26(2)
C(27)	3793(9)	6923(8)	1865(6)	47(2)
C(28)	2388(10)	6954(10)	2200(6)	57(3)
C(29)	2406(10)	7810(11)	2762(6)	63(3)
C(30)	3854(9)	7843(9)	3035(5)	45(2)
N(1)	2372(5)	286(5)	6087(3)	20(1)
N(2)	4593(5)	518(4)	778(3)	19(1)
P(1)	2024(2)	1236(1)	5450(1)	20(1)
P(2)	1158(2)	-563(1)	6273(1)	19(1)
P(3)	6313(2)	599(1)	869(1)	16(1)
P(4)	3593(2)	1525(1)	906(1)	20(1)
Cl(1)	-361(2)	221(2)	3259(1)	35(1)

Cl(2)	-2941(2)	558(2)	5459(1)	34(1)
Cl(3)	8745(2)	3203(1)	12(1)	30(1)
Cl(4)	5648(2)	4360(1)	1543(1)	33(1)
Au(1)	747(1)	748(1)	4401(1)	21(1)
Au(2)	-847(1)	-9(1)	5838(1)	20(1)
Au(3)	7321(1)	1982(1)	460(1)	17(1)
Au(4)	4765(1)	2877(1)	1173(1)	20(1)
O(1)	4611(7)	7559(6)	2354(4)	60(2)

Table A8. Bond lengths [Å] and angles [°] for wjw188.

C(1)-C(5)	1.530(11)	C(14)-H(14)	1.0000
C(1)-C(2)	1.544(11)	C(15)-C(16)	1.533(10)
C(1)-P(1)	1.855(8)	C(15)-H(15A)	0.9900
C(1)-H(1)	1.0000	C(15)-H(15B)	0.9900
C(2)-C(3)	1.516(11)	C(16)-C(17)	1.543(10)
C(2)-H(2A)	0.9900	C(16)-H(16A)	0.9900
C(2)-H(2B)	0.9900	C(16)-H(16B)	0.9900
C(3)-C(4)	1.546(12)	C(17)-C(19)	1.532(9)
C(3)-H(3A)	0.9900	C(17)-P(3)	1.851(7)
C(3)-H(3B)	0.9900	C(17)-H(17)	1.0000
C(4)-C(6)	1.507(10)	C(18)-H(18A)	0.9800
C(4)-P(1)	1.836(7)	C(18)-H(18B)	0.9800
C(4)-H(4)	1.0000	C(18)-H(18C)	0.9800
C(5)-H(5A)	0.9800	C(19)-H(19A)	0.9800
C(5)-H(5B)	0.9800	C(19)-H(19B)	0.9800
C(5)-H(5C)	0.9800	C(19)-H(19C)	0.9800
C(6)-H(6A)	0.9800	C(20)-C(24)	1.512(11)
C(6)-H(6B)	0.9800	C(20)-C(21)	1.528(11)
C(6)-H(6C)	0.9800	C(20)-P(4)	1.837(7)
C(7)-C(11)	1.513(11)	C(20)-H(20)	1.0000
C(7)-C(8)	1.526(10)	C(21)-C(22)	1.516(12)
C(7)-P(2)	1.848(8)	C(21)-H(21A)	0.9900
C(7)-H(7)	1.0000	C(21)-H(21B)	0.9900
C(8)-C(9)	1.532(11)	C(22)-C(23)	1.543(10)
C(8)-H(8A)	0.9900	C(22)-H(22A)	0.9900
C(8)-H(8B)	0.9900	C(22)-H(22B)	0.9900
C(9)-C(10)	1.529(12)	C(23)-C(25)	1.530(12)
C(9)-H(9A)	0.9900	C(23)-P(4)	1.853(7)
C(9)-H(9B)	0.9900	C(23)-H(23)	1.0000
C(10)-C(12)	1.529(10)	C(24)-H(24A)	0.9800
C(10)-P(2)	1.837(7)	C(24)-H(24B)	0.9800
C(10)-H(10)	1.0000	C(24)-H(24C)	0.9800
C(11)-H(11A)	0.9800	C(25)-H(25A)	0.9800
C(11)-H(11B)	0.9800	C(25)-H(25B)	0.9800
C(11)-H(11C)	0.9800	C(25)-H(25C)	0.9800
C(12)-H(12A)	0.9800	C(26)-N(2)	1.472(9)
C(12)-H(12B)	0.9800	C(26)-H(26A)	0.9800
C(12)-H(12C)	0.9800	C(26)-H(26B)	0.9800
C(13)-N(1)	1.483(8)	C(26)-H(26C)	0.9800
C(13)-H(13A)	0.9800	C(27)-O(1)	1.427(11)
C(13)-H(13B)	0.9800	C(27)-C(28)	1.495(13)
C(13)-H(13C)	0.9800	C(27)-H(27A)	0.9900
C(14)-C(18)	1.523(9)	C(27)-H(27B)	0.9900
C(14)-C(15)	1.528(10)	C(28)-C(29)	1.486(16)
C(14)-P(3)	1.843(7)	C(28)-H(28A)	0.9900

C(28)-H(28B)	0.9900
C(29)-C(30)	1.493(12)
C(29)-H(29A)	0.9900
C(29)-H(29B)	0.9900
C(30)-O(1)	1.406(11)
C(30)-H(30A)	0.9900
C(30)-H(30B)	0.9900
N(1)-P(2)	1.691(6)
N(1)-P(1)	1.699(6)
N(2)-P(4)	1.701(6)
N(2)-P(3)	1.705(5)
P(1)-Au(1)	2.2320(18)
P(2)-Au(2)	2.2271(19)
P(3)-Au(3)	2.2327(18)
P(4)-Au(4)	2.212(2)
Cl(1)-Au(1)	2.2840(18)
Cl(2)-Au(2)	2.2851(19)
Cl(3)-Au(3)	2.2980(18)
Cl(4)-Au(4)	2.277(2)
Au(1)-Au(2)	3.0311(8)
Au(3)-Au(4)	3.0406(11)

C(5)-C(1)-C(2)	114.0(7)
C(5)-C(1)-P(1)	113.8(6)
C(2)-C(1)-P(1)	104.3(5)
C(5)-C(1)-H(1)	108.2
C(2)-C(1)-H(1)	108.2
P(1)-C(1)-H(1)	108.2
C(3)-C(2)-C(1)	109.0(7)
C(3)-C(2)-H(2A)	109.9
C(1)-C(2)-H(2A)	109.9
C(3)-C(2)-H(2B)	109.9
C(1)-C(2)-H(2B)	109.9
H(2A)-C(2)-H(2B)	108.3
C(2)-C(3)-C(4)	106.7(7)
C(2)-C(3)-H(3A)	110.4
C(4)-C(3)-H(3A)	110.4
C(2)-C(3)-H(3B)	110.4
C(4)-C(3)-H(3B)	110.4
H(3A)-C(3)-H(3B)	108.6
C(6)-C(4)-C(3)	116.0(6)
C(6)-C(4)-P(1)	114.2(5)
C(3)-C(4)-P(1)	100.3(5)
C(6)-C(4)-H(4)	108.6
C(3)-C(4)-H(4)	108.6
P(1)-C(4)-H(4)	108.6
C(1)-C(5)-H(5A)	109.5
C(1)-C(5)-H(5B)	109.5
H(5A)-C(5)-H(5B)	109.5
C(1)-C(5)-H(5C)	109.5
H(5A)-C(5)-H(5C)	109.5
H(5B)-C(5)-H(5C)	109.5
C(4)-C(6)-H(6A)	109.5
C(4)-C(6)-H(6B)	109.5
H(6A)-C(6)-H(6B)	109.5
C(4)-C(6)-H(6C)	109.5
H(6A)-C(6)-H(6C)	109.5
H(6B)-C(6)-H(6C)	109.5
C(11)-C(7)-C(8)	116.6(6)
C(11)-C(7)-P(2)	115.0(6)
C(8)-C(7)-P(2)	104.2(5)
C(11)-C(7)-H(7)	106.8
C(8)-C(7)-H(7)	106.8
P(2)-C(7)-H(7)	106.8
C(7)-C(8)-C(9)	107.3(6)
C(7)-C(8)-H(8A)	110.2
C(9)-C(8)-H(8A)	110.2
C(7)-C(8)-H(8B)	110.2
C(9)-C(8)-H(8B)	110.2
H(8A)-C(8)-H(8B)	108.5
C(10)-C(9)-C(8)	107.8(6)
C(10)-C(9)-H(9A)	110.1
C(8)-C(9)-H(9A)	110.1
C(10)-C(9)-H(9B)	110.1
C(8)-C(9)-H(9B)	110.1
H(9A)-C(9)-H(9B)	108.5
C(9)-C(10)-C(12)	114.2(6)
C(9)-C(10)-P(2)	104.8(5)
C(12)-C(10)-P(2)	114.9(5)
C(9)-C(10)-H(10)	107.5
C(12)-C(10)-H(10)	107.5
P(2)-C(10)-H(10)	107.5
C(7)-C(11)-H(11A)	109.5
C(7)-C(11)-H(11B)	109.5
H(11A)-C(11)-H(11B)	109.5
C(7)-C(11)-H(11C)	109.5
H(11A)-C(11)-H(11C)	109.5
H(11B)-C(11)-H(11C)	109.5
C(10)-C(12)-H(12A)	109.5
C(10)-C(12)-H(12B)	109.5
H(12A)-C(12)-H(12B)	109.5
C(10)-C(12)-H(12C)	109.5
H(12A)-C(12)-H(12C)	109.5
H(12B)-C(12)-H(12C)	109.5
N(1)-C(13)-H(13A)	109.5
N(1)-C(13)-H(13B)	109.5
H(13A)-C(13)-H(13B)	109.5
N(1)-C(13)-H(13C)	109.5
H(13A)-C(13)-H(13C)	109.5
H(13B)-C(13)-H(13C)	109.5
C(18)-C(14)-C(15)	115.4(6)
C(18)-C(14)-P(3)	115.9(5)
C(15)-C(14)-P(3)	105.3(4)
C(18)-C(14)-H(14)	106.5
C(15)-C(14)-H(14)	106.5
P(3)-C(14)-H(14)	106.5
C(14)-C(15)-C(16)	105.8(6)
C(14)-C(15)-H(15A)	110.6
C(16)-C(15)-H(15A)	110.6
C(14)-C(15)-H(15B)	110.6
C(16)-C(15)-H(15B)	110.6
H(15A)-C(15)-H(15B)	108.7

C(15)-C(16)-C(17)	107.8(6)	H(25A)-C(25)-H(25B)	109.5
C(15)-C(16)-H(16A)	110.2	C(23)-C(25)-H(25C)	109.5
C(17)-C(16)-H(16A)	110.2	H(25A)-C(25)-H(25C)	109.5
C(15)-C(16)-H(16B)	110.2	H(25B)-C(25)-H(25C)	109.5
C(17)-C(16)-H(16B)	110.2	N(2)-C(26)-H(26A)	109.5
H(16A)-C(16)-H(16B)	108.5	N(2)-C(26)-H(26B)	109.5
C(19)-C(17)-C(16)	113.8(6)	H(26A)-C(26)-H(26B)	109.5
C(19)-C(17)-P(3)	114.2(5)	N(2)-C(26)-H(26C)	109.5
C(16)-C(17)-P(3)	101.7(5)	H(26A)-C(26)-H(26C)	109.5
C(19)-C(17)-H(17)	108.9	H(26B)-C(26)-H(26C)	109.5
C(16)-C(17)-H(17)	108.9	O(1)-C(27)-C(28)	107.1(8)
P(3)-C(17)-H(17)	108.9	O(1)-C(27)-H(27A)	110.3
C(14)-C(18)-H(18A)	109.5	C(28)-C(27)-H(27A)	110.3
C(14)-C(18)-H(18B)	109.5	O(1)-C(27)-H(27B)	110.3
H(18A)-C(18)-H(18B)	109.5	C(28)-C(27)-H(27B)	110.3
C(14)-C(18)-H(18C)	109.5	H(27A)-C(27)-H(27B)	108.5
H(18A)-C(18)-H(18C)	109.5	C(29)-C(28)-C(27)	104.2(8)
H(18B)-C(18)-H(18C)	109.5	C(29)-C(28)-H(28A)	110.9
C(17)-C(19)-H(19A)	109.5	C(27)-C(28)-H(28A)	110.9
C(17)-C(19)-H(19B)	109.5	C(29)-C(28)-H(28B)	110.9
H(19A)-C(19)-H(19B)	109.5	C(27)-C(28)-H(28B)	110.9
C(17)-C(19)-H(19C)	109.5	H(28A)-C(28)-H(28B)	108.9
H(19A)-C(19)-H(19C)	109.5	C(28)-C(29)-C(30)	102.6(9)
H(19B)-C(19)-H(19C)	109.5	C(28)-C(29)-H(29A)	111.3
C(24)-C(20)-C(21)	117.7(7)	C(30)-C(29)-H(29A)	111.3
C(24)-C(20)-P(4)	115.7(6)	C(28)-C(29)-H(29B)	111.3
C(21)-C(20)-P(4)	104.8(5)	C(30)-C(29)-H(29B)	111.3
C(24)-C(20)-H(20)	105.9	H(29A)-C(29)-H(29B)	109.2
C(21)-C(20)-H(20)	105.9	O(1)-C(30)-C(29)	105.2(7)
P(4)-C(20)-H(20)	105.9	O(1)-C(30)-H(30A)	110.7
C(22)-C(21)-C(20)	106.8(6)	C(29)-C(30)-H(30A)	110.7
C(22)-C(21)-H(21A)	110.4	O(1)-C(30)-H(30B)	110.7
C(20)-C(21)-H(21A)	110.4	C(29)-C(30)-H(30B)	110.7
C(22)-C(21)-H(21B)	110.4	H(30A)-C(30)-H(30B)	108.8
C(20)-C(21)-H(21B)	110.4	C(13)-N(1)-P(2)	121.2(5)
H(21A)-C(21)-H(21B)	108.6	C(13)-N(1)-P(1)	119.4(5)
C(21)-C(22)-C(23)	110.2(7)	P(2)-N(1)-P(1)	119.4(3)
C(21)-C(22)-H(22A)	109.6	C(26)-N(2)-P(4)	119.3(4)
C(23)-C(22)-H(22A)	109.6	C(26)-N(2)-P(3)	118.8(5)
C(21)-C(22)-H(22B)	109.6	P(4)-N(2)-P(3)	120.9(3)
C(23)-C(22)-H(22B)	109.6	N(1)-P(1)-C(4)	108.5(3)
H(22A)-C(22)-H(22B)	108.1	N(1)-P(1)-C(1)	110.9(3)
C(25)-C(23)-C(22)	111.6(7)	C(4)-P(1)-C(1)	96.0(3)
C(25)-C(23)-P(4)	112.8(5)	N(1)-P(1)-Au(1)	111.3(2)
C(22)-C(23)-P(4)	105.5(5)	C(4)-P(1)-Au(1)	112.7(2)
C(25)-C(23)-H(23)	108.9	C(1)-P(1)-Au(1)	116.4(2)
C(22)-C(23)-H(23)	108.9	N(1)-P(2)-C(10)	108.2(3)
P(4)-C(23)-H(23)	108.9	N(1)-P(2)-C(7)	109.0(3)
C(20)-C(24)-H(24A)	109.5	C(10)-P(2)-C(7)	95.8(3)
C(20)-C(24)-H(24B)	109.5	N(1)-P(2)-Au(2)	109.8(2)
H(24A)-C(24)-H(24B)	109.5	C(10)-P(2)-Au(2)	116.9(2)
C(20)-C(24)-H(24C)	109.5	C(7)-P(2)-Au(2)	116.2(2)
H(24A)-C(24)-H(24C)	109.5	N(2)-P(3)-C(14)	109.3(3)
H(24B)-C(24)-H(24C)	109.5	N(2)-P(3)-C(17)	107.5(3)
C(23)-C(25)-H(25A)	109.5	C(14)-P(3)-C(17)	96.1(3)
C(23)-C(25)-H(25B)	109.5	N(2)-P(3)-Au(3)	118.2(2)

C(14)-P(3)-Au(3)	112.3(2)	P(2)-Au(2)-Cl(2)	177.07(7)
C(17)-P(3)-Au(3)	111.2(2)	P(2)-Au(2)-Au(1)	84.42(5)
N(2)-P(4)-C(20)	111.9(3)	Cl(2)-Au(2)-Au(1)	98.28(6)
N(2)-P(4)-C(23)	109.0(3)	P(3)-Au(3)-Cl(3)	168.16(6)
C(20)-P(4)-C(23)	94.8(3)	P(3)-Au(3)-Au(4)	81.30(5)
N(2)-P(4)-Au(4)	113.0(2)	Cl(3)-Au(3)-Au(4)	110.19(6)
C(20)-P(4)-Au(4)	114.7(3)	P(4)-Au(4)-Cl(4)	170.46(7)
C(23)-P(4)-Au(4)	112.0(3)	P(4)-Au(4)-Au(3)	91.36(5)
P(1)-Au(1)-Cl(1)	174.19(7)	Cl(4)-Au(4)-Au(3)	98.16(6)
P(1)-Au(1)-Au(2)	77.77(5)	C(30)-O(1)-C(27)	108.4(7)
Cl(1)-Au(1)-Au(2)	106.92(6)		

Symmetry transformations used to generate equivalent atoms:

Table A9. Anisotropic displacement parameters ($Å^2$x 10^3)for wjw188. The anisotropic displacement factor exponent takes the form: $-2\pi^2[h^2a^{*2}U^{11} + ... + 2 h k a^* b^* U^{12}]$

	U^{11}	U^{22}	U^{33}	U^{23}	U^{13}	U^{12}
C(1)	21(3)	32(5)	31(4)	-10(3)	2(3)	2(3)
C(2)	44(5)	25(5)	44(5)	-4(4)	12(4)	-1(4)
C(3)	40(4)	30(5)	43(5)	6(4)	8(3)	-1(4)
C(4)	18(3)	23(4)	25(3)	0(3)	3(3)	-2(3)
C(5)	42(4)	45(6)	33(4)	-20(4)	14(3)	-10(4)
C(6)	24(4)	44(5)	27(4)	-2(3)	6(3)	-1(3)
C(7)	26(4)	33(5)	30(4)	-4(3)	-2(3)	6(3)
C(8)	27(4)	31(5)	42(4)	6(4)	1(3)	2(3)
C(9)	25(3)	26(5)	43(4)	9(4)	3(3)	-1(3)
C(10)	24(3)	32(4)	24(3)	3(3)	5(3)	-3(3)
C(11)	58(5)	33(5)	34(4)	-2(4)	9(4)	21(4)
C(12)	30(4)	42(5)	33(4)	2(4)	8(3)	2(4)
C(13)	21(3)	43(5)	32(4)	10(4)	-4(3)	-2(3)
C(14)	23(3)	19(4)	19(3)	-2(3)	1(3)	-5(3)
C(15)	33(4)	18(4)	31(4)	-3(3)	-14(3)	1(3)
C(16)	29(4)	16(4)	30(4)	-8(3)	-6(3)	1(3)
C(17)	22(3)	17(4)	27(4)	-8(3)	5(3)	-7(3)
C(18)	31(4)	29(4)	22(3)	-4(3)	4(3)	-2(3)
C(19)	25(4)	26(4)	30(4)	-11(3)	6(3)	-5(3)
C(20)	27(4)	31(5)	26(4)	5(3)	-8(3)	5(3)
C(21)	23(4)	35(5)	47(5)	-3(4)	-11(3)	-5(3)
C(22)	22(4)	65(7)	46(5)	6(5)	-7(3)	-9(4)
C(23)	17(3)	38(5)	27(4)	13(3)	4(3)	1(3)
C(24)	51(5)	61(7)	26(4)	-4(4)	-3(4)	26(5)
C(25)	35(4)	41(5)	34(4)	4(4)	15(3)	0(4)
C(26)	21(3)	19(4)	36(4)	-1(3)	0(3)	-6(3)
C(27)	50(5)	44(6)	46(5)	-4(5)	1(4)	-4(5)
C(28)	49(5)	78(8)	44(5)	-14(5)	7(4)	-23(6)
C(29)	46(5)	89(9)	53(6)	-21(6)	-2(4)	17(6)
C(30)	46(5)	52(6)	37(4)	0(4)	3(4)	-6(5)
N(1)	13(3)	32(4)	15(3)	2(2)	1(2)	-1(2)
N(2)	16(3)	17(3)	24(3)	-1(2)	-1(2)	-7(2)
P(1)	15(1)	25(1)	19(1)	-2(1)	1(1)	1(1)
P(2)	15(1)	22(1)	20(1)	-2(1)	1(1)	1(1)
P(3)	15(1)	15(1)	17(1)	-1(1)	1(1)	-3(1)
P(4)	16(1)	24(1)	19(1)	5(1)	0(1)	-1(1)

Cl(1)	38(1)	42(1)	24(1)	6(1)	-12(1)	-15(1)
Cl(2)	16(1)	34(1)	51(1)	2(1)	-3(1)	5(1)
Cl(3)	21(1)	23(1)	46(1)	13(1)	3(1)	-4(1)
Cl(4)	36(1)	24(1)	39(1)	-4(1)	-11(1)	-1(1)
Au(1)	19(1)	24(1)	19(1)	2(1)	-3(1)	-1(1)
Au(2)	13(1)	22(1)	26(1)	-2(1)	0(1)	0(1)
Au(3)	14(1)	17(1)	21(1)	2(1)	1(1)	-1(1)
Au(4)	17(1)	22(1)	21(1)	1(1)	0(1)	2(1)
O(1)	48(4)	75(6)	58(4)	-18(4)	19(3)	-29(4)

Table A10. Hydrogen coordinates (x 10^4) and isotropic displacement parameters ($Å^2$x 10^3) for wjw188.

	x	y	z	U(eq)
H(1)	530	2539	5772	34
H(2A)	2034	3776	5810	45
H(2B)	3139	3154	6314	45
H(3A)	4024	3308	5018	45
H(3B)	2606	2992	4604	45
H(4)	4311	1716	5584	26
H(5A)	2031	1946	7185	60
H(5B)	526	1575	6979	60
H(5C)	796	2711	7179	60
H(6A)	3554	1393	3932	48
H(6B)	4448	657	4473	48
H(6C)	5044	1709	4224	48
H(7)	866	-2131	5710	36
H(8A)	3284	-2073	6674	40
H(8B)	2336	-3011	6496	40
H(9A)	585	-2371	7295	38
H(9B)	1942	-2259	7833	38
H(10)	2135	-626	7571	32
H(11A)	3416	-1359	5231	63
H(11B)	2068	-1340	4683	63
H(11C)	2765	-2368	4912	63
H(12A)	-743	-861	7673	53
H(12B)	49	145	7853	53
H(12C)	266	-784	8436	53
H(13A)	3904	776	6814	48
H(13B)	4427	191	6033	48
H(13C)	3798	-399	6782	48
H(14)	7629	665	2051	24
H(15A)	6586	-1281	1863	33
H(15B)	7996	-956	2283	33
H(16A)	8315	-1557	896	30
H(16B)	8884	-458	1017	30
H(17)	6319	-994	280	26
H(18A)	5011	-31	2484	41
H(18B)	5449	1102	2532	41
H(18C)	6189	305	3098	41
H(19A)	8423	223	-382	40
H(19B)	7019	-17	-835	40

H(19C)	8102	-875	-676	40
H(20)	2041	2357	93	34
H(21A)	284	1254	61	42
H(21B)	1265	347	285	42
H(22A)	328	782	1509	53
H(22B)	512	1933	1331	53
H(23)	2491	584	1920	33
H(24A)	3105	770	-814	69
H(24B)	3642	1879	-863	69
H(24C)	2133	1619	-1158	69
H(25A)	2160	2657	2198	55
H(25B)	3292	2001	2642	55
H(25C)	1718	1808	2815	55
H(26A)	3000	-410	883	38
H(26B)	4419	-901	1132	38
H(26C)	4048	-732	195	38
H(27A)	4152	6244	1884	56
H(27B)	3790	7150	1294	56
H(28A)	1708	7049	1762	68
H(28B)	2177	6339	2495	68
H(29A)	1790	7705	3225	75
H(29B)	2145	8424	2477	75
H(30A)	4106	8515	3211	54
H(30B)	4010	7383	3492	54

X-ray Diffraction Details

A colorless block 0.10 x 0.05 x 0.05 mm in size was mounted on a Cryoloop with Paratone oil. Data were collected in a nitrogen gas stream at 100(2) K using phi and omega scans. Crystal-to-detector distance was 40 mm and exposure time was 10 seconds per frame using a scan width of 0.5°. Data collection was 100.0% complete to 25.00° in θ. A total of 107338 reflections were collected covering the indices, -21<=h<=21, -13<=k<=13, -19<=l<=19. 31203 reflections were found to be symmetry independent, with an R_{int} of 0.0554. Indexing and unit cell refinement indicated a C-centered, monoclinic lattice. The space group was found to be C2/c (No. 15). The data were integrated using the Bruker SAINT software program and scaled using the SADABS software program. Solution by direct methods (SIR-2011) produced a complete heavy-atom phasing model consistent with the proposed structure. All non-hydrogen atoms were refined anisotropically by full-matrix least-squares (SHELXL-97). The Crystallographic Information File (.cif) has been deposited in the Cambridge Structural Database; Reference Number CCDC 955222.

CheckCIF alerts: The crystal was twinned, resulting in a low ratio of unique:observed reflections. The alerts related to the Hirshfeld tests are a result of thermal movement of the phenyl rings.

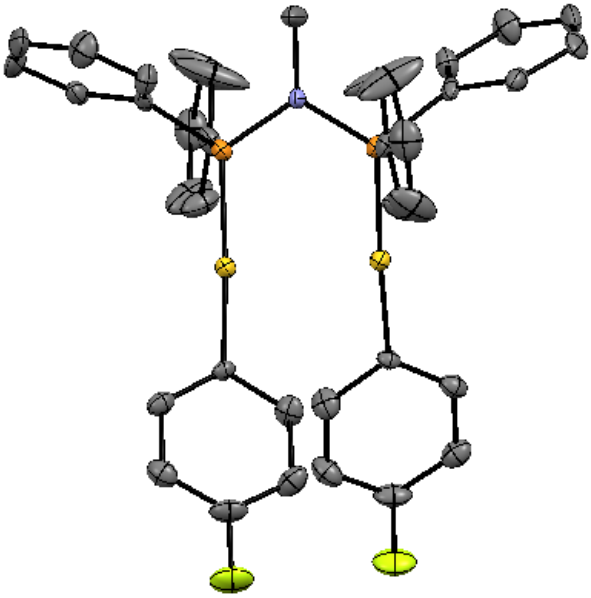

Figure A3. ORTEP representation of **2.6**. Thermal ellipsoids are set at 50% probability and hydrogen atoms are removed for clarity. Atoms are color-coded: carbon (grey), fluorine (yellow), gold (gold), phosphorus (orange), nitrogen (blue).

Table A11. Crystal data and structure refinement for wjw485.

Identification code	WJW485	
Empirical formula	$C_{37}\ H_{31}\ Au_2\ F_2\ N\ P_2$	
Formula weight	983.50	
Temperature	100(2) K	
Wavelength	0.71073 Å	
Crystal system	Monoclinic	
Space group	C2/c	
Unit cell dimensions	a = 18.1260(14) Å	α= 90º.
	b = 11.4795(9) Å	β= 106.7430(10)º.
	c = 16.1829(13) Å	γ = 90º.
Volume	3224.5(4) $Å^3$	
Z	4	
Density (calculated)	2.026 Mg/m^3	
Absorption coefficient	9.228 mm^{-1}	
F(000)	1864	
Crystal size	0.10 x 0.05 x 0.05 mm^3	
Theta range for data collection	2.13 to 25.36º.	
Index ranges	-21<=h<=21, -13<=k<=13, -19<=l<=19	
Reflections collected	107338	
Independent reflections	31203 [R(int) = 0.0554]	
Completeness to theta = 25.00º	100.0 %	
Absorption correction	Multi_scan	
Max. and min. transmission	0.6555 and 0.4589	
Refinement method	Full-matrix least-squares on F^2	
Data / restraints / parameters	31203 / 0 / 201	
Goodness-of-fit on F^2	1.058	

Final R indices [I>2sigma(I)]	R1 = 0.0286, wR2 = 0.0806
R indices (all data)	R1 = 0.0312, wR2 = 0.0826
Largest diff. peak and hole	1.240 and -0.678 e.Å^{-3}

Table A12. Atomic coordinates (x 10^4) and equivalent isotropic displacement parameters (Å^{2}x 10^3) for wjw485. U(eq) is defined as one third of the trace of the orthogonalized U^{ij} tensor.

	x	y	z	U(eq)
C(1)	5000	4533(3)	7500	43(1)
C(2)	3759(1)	-939(2)	7226(1)	16(1)
C(3)	4224(1)	-1605(2)	7894(1)	26(1)
C(4)	3997(1)	-2692(2)	8116(1)	30(1)
C(5)	3292(1)	-3108(2)	7660(1)	30(1)
C(6)	2814(1)	-2487(2)	6993(1)	27(1)
C(7)	3053(1)	-1408(2)	6787(1)	22(1)
C(8)	3682(1)	3301(2)	6095(1)	17(1)
C(9)	3207(1)	3668(2)	6576(1)	25(1)
C(10)	2499(1)	4188(2)	6178(2)	36(1)
C(11)	2272(1)	4302(2)	5294(2)	35(1)
C(12)	2726(1)	3930(2)	4802(1)	31(1)
C(13)	3432(1)	3434(2)	5196(1)	23(1)
C(14)	5128(1)	2556(2)	5882(1)	22(1)
C(15)	5305(2)	1571(2)	5507(1)	39(1)
C(16)	5744(2)	1641(2)	4931(2)	53(1)
C(17)	6024(1)	2673(2)	4750(2)	40(1)
C(18)	5858(2)	3629(3)	5124(2)	81(1)
C(19)	5418(2)	3596(3)	5687(2)	85(1)
N(1)	5000	3243(2)	7500	18(1)
F(1)	3063(1)	-4172(1)	7880(1)	43(1)
P(1)	4534(1)	2461(1)	6607(1)	17(1)
Au(1)	4169(1)	648(1)	6941(1)	17(1)

Table A13. Bond lengths [Å] and angles [º] for wjw485.

C(1)-N(1)	1.480(3)	C(8)-C(9)	1.382(3)
C(1)-H(1A)	0.9800	C(8)-C(13)	1.401(2)
C(1)-H(1B)	0.9800	C(8)-P(1)	1.8070(19)
C(1)-H(1C)	0.9800	C(9)-C(10)	1.393(3)
C(2)-C(7)	1.382(3)	C(9)-H(9)	0.9500
C(2)-C(3)	1.393(3)	C(10)-C(11)	1.375(3)
C(2)-Au(1)	2.0689(19)	C(10)-H(10)	0.9500
C(3)-C(4)	1.393(3)	C(11)-C(12)	1.368(3)
C(3)-H(3)	0.9500	C(11)-H(11)	0.9500
C(4)-C(5)	1.364(3)	C(12)-C(13)	1.379(3)
C(4)-H(4)	0.9500	C(12)-H(12)	0.9500
C(5)-F(1)	1.369(2)	C(13)-H(13)	0.9500
C(5)-C(6)	1.373(3)	C(14)-C(15)	1.364(3)
C(6)-C(7)	1.384(3)	C(14)-C(19)	1.377(3)
C(6)-H(6)	0.9500	C(14)-P(1)	1.811(2)
C(7)-H(7)	0.9500	C(15)-C(16)	1.391(3)

C(15)-H(15)	0.9500	C(11)-C(10)-C(9)	118.8(2)
C(16)-C(17)	1.354(3)	C(11)-C(10)-H(10)	120.6
C(16)-H(16)	0.9500	C(9)-C(10)-H(10)	120.6
C(17)-C(18)	1.329(4)	C(12)-C(11)-C(10)	121.7(2)
C(17)-H(17)	0.9500	C(12)-C(11)-H(11)	119.2
C(18)-C(19)	1.373(4)	C(10)-C(11)-H(11)	119.2
C(18)-H(18)	0.9500	C(11)-C(12)-C(13)	119.6(2)
C(19)-H(19)	0.9500	C(11)-C(12)-H(12)	120.2
N(1)-P(1)	1.7040(13)	C(13)-C(12)-H(12)	120.2
N(1)-P(1)#1	1.7040(13)	C(12)-C(13)-C(8)	120.3(2)
P(1)-Au(1)	2.2953(5)	C(12)-C(13)-H(13)	119.9
Au(1)-Au(1)#1	3.0357(2)	C(8)-C(13)-H(13)	119.9
		C(15)-C(14)-C(19)	117.6(2)
N(1)-C(1)-H(1A)	109.5	C(15)-C(14)-P(1)	119.87(18)
N(1)-C(1)-H(1B)	109.5	C(19)-C(14)-P(1)	122.53(18)
H(1A)-C(1)-H(1B)	109.5	C(14)-C(15)-C(16)	120.2(2)
N(1)-C(1)-H(1C)	109.5	C(14)-C(15)-H(15)	119.9
H(1A)-C(1)-H(1C)	109.5	C(16)-C(15)-H(15)	119.9
H(1B)-C(1)-H(1C)	109.5	C(17)-C(16)-C(15)	121.2(2)
C(7)-C(2)-C(3)	116.69(18)	C(17)-C(16)-H(16)	119.4
C(7)-C(2)-Au(1)	124.57(14)	C(15)-C(16)-H(16)	119.4
C(3)-C(2)-Au(1)	118.73(14)	C(18)-C(17)-C(16)	118.4(2)
C(2)-C(3)-C(4)	122.25(19)	C(18)-C(17)-H(17)	120.8
C(2)-C(3)-H(3)	118.9	C(16)-C(17)-H(17)	120.8
C(4)-C(3)-H(3)	118.9	C(17)-C(18)-C(19)	122.0(3)
C(5)-C(4)-C(3)	118.4(2)	C(17)-C(18)-H(18)	119.0
C(5)-C(4)-H(4)	120.8	C(19)-C(18)-H(18)	119.0
C(3)-C(4)-H(4)	120.8	C(18)-C(19)-C(14)	120.6(3)
C(4)-C(5)-F(1)	118.6(2)	C(18)-C(19)-H(19)	119.7
C(4)-C(5)-C(6)	121.6(2)	C(14)-C(19)-H(19)	119.7
F(1)-C(5)-C(6)	119.9(2)	C(1)-N(1)-P(1)	121.79(7)
C(5)-C(6)-C(7)	118.9(2)	C(1)-N(1)-P(1)#1	121.79(7)
C(5)-C(6)-H(6)	120.5	P(1)-N(1)-P(1)#1	116.43(13)
C(7)-C(6)-H(6)	120.5	N(1)-P(1)-C(8)	104.93(8)
C(2)-C(7)-C(6)	122.2(2)	N(1)-P(1)-C(14)	106.01(7)
C(2)-C(7)-H(7)	118.9	C(8)-P(1)-C(14)	105.08(9)
C(6)-C(7)-H(7)	118.9	N(1)-P(1)-Au(1)	112.60(6)
C(9)-C(8)-C(13)	118.94(18)	C(8)-P(1)-Au(1)	108.99(6)
C(9)-C(8)-P(1)	119.54(14)	C(14)-P(1)-Au(1)	118.21(7)
C(13)-C(8)-P(1)	120.79(15)	C(2)-Au(1)-P(1)	175.82(5)
C(8)-C(9)-C(10)	120.7(2)	C(2)-Au(1)-Au(1)#1	103.05(5)
C(8)-C(9)-H(9)	119.7	P(1)-Au(1)-Au(1)#1	80.565(13)
C(10)-C(9)-H(9)	119.7		

Symmetry transformations used to generate equivalent atoms:
#1 -x+1,y,-z+3/2

Table A14. Anisotropic displacement parameters ($Å^2 x\ 10^3$)for wjw485. The anisotropic displacement factor exponent takes the form: $-2\pi^2[\ h^2 a^{*2} U^{11} + ... + 2\ h\ k\ a^*\ b^*\ U^{12}\ ]$

	U^{11}	U^{22}	U^{33}	U^{23}	U^{13}	U^{12}
C(1)	68(3)	15(2)	28(2)	0	-12(2)	0
C(2)	19(1)	14(1)	16(1)	3(1)	7(1)	1(1)
C(3)	19(1)	33(1)	28(1)	3(1)	11(1)	-2(1)
C(4)	29(1)	31(1)	32(1)	11(1)	13(1)	6(1)
C(5)	41(1)	18(1)	39(1)	3(1)	25(1)	-3(1)
C(6)	26(1)	28(1)	32(1)	-6(1)	13(1)	-5(1)
C(7)	28(1)	20(1)	20(1)	4(1)	10(1)	4(1)
C(8)	16(1)	17(1)	15(1)	2(1)	-1(1)	-7(1)
C(9)	19(1)	34(1)	21(1)	4(1)	3(1)	2(1)
C(10)	20(1)	46(2)	41(2)	5(1)	9(1)	3(1)
C(11)	24(1)	32(2)	35(1)	8(1)	-12(1)	-2(1)
C(12)	40(1)	26(1)	18(1)	11(1)	-4(1)	-3(1)
C(13)	29(1)	20(1)	16(1)	-1(1)	3(1)	-6(1)
C(14)	18(1)	28(1)	20(1)	-7(1)	6(1)	-6(1)
C(15)	61(2)	26(1)	34(1)	6(1)	24(1)	15(1)
C(16)	74(2)	46(2)	51(2)	10(1)	40(2)	31(2)
C(17)	26(1)	61(2)	37(1)	-2(1)	16(1)	5(1)
C(18)	117(3)	66(2)	98(3)	-45(2)	90(2)	-64(2)
C(19)	140(3)	42(2)	123(3)	-52(2)	115(3)	-52(2)
N(1)	21(1)	13(1)	13(1)	0	-4(1)	0
F(1)	56(1)	26(1)	56(1)	8(1)	29(1)	-8(1)
P(1)	17(1)	16(1)	16(1)	-2(1)	2(1)	-2(1)
Au(1)	17(1)	16(1)	15(1)	-1(1)	2(1)	-1(1)

Table A15. Hydrogen coordinates ($x\ 10^4$) and isotropic displacement parameters ($Å^2 x\ 10^3$) for wjw485.

	x	y	z	U(eq)
H(1A)	5297	4817	8069	64
H(1B)	4469	4817	7368	64
H(1C)	5234	4817	7062	64
H(3)	4714	-1308	8209	31
H(4)	4324	-3133	8573	36
H(6)	2327	-2793	6678	33
H(7)	2720	-975	6329	27
H(9)	3364	3563	7184	30
H(10)	2180	4460	6511	43
H(11)	1787	4648	5019	42
H(12)	2555	4014	4192	37
H(13)	3751	3180	4857	27
H(15)	5128	835	5640	46
H(16)	5849	952	4660	63
H(17)	6332	2713	4365	48
H(18)	6049	4358	4998	98

H(19)	5313	4297	5944	103

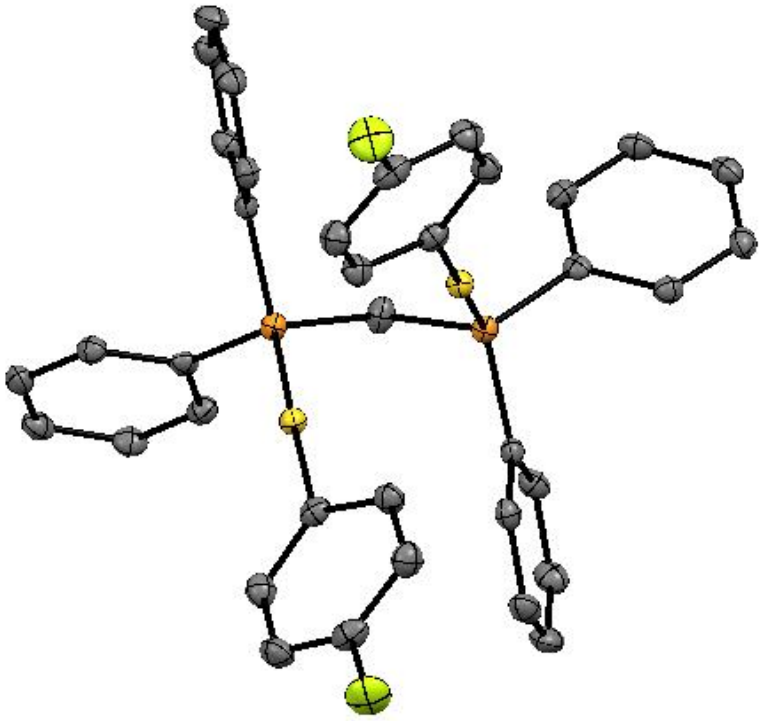

Figure A4. ORTEP representation of **8**. Thermal ellipsoids are set at 50% probability and hydrogen atoms are removed for clarity. Atoms are color-coded: carbon (grey), fluorine (yellow), gold (gold), phosphorus (orange), nitrogen (blue).

A colorless block 0.10 x 0.1 x 0.05 mm in size was mounted on a Cryoloop with Paratone oil. Data were collected in a nitrogen gas stream at 100(2) K using phi and omega scans. Crystal-to-detector distance was 60 mm and exposure time was 5 seconds per frame using a scan width of 0.4°. Data collection was 100.0% complete to 25.00° in θ. A total of 107338 reflections were collected covering the indices, -19<=h<=19, -10<=k<=12, -21<=l<=21. 2841 reflections were found to be symmetry independent, with an R_{int} of 0.0268. Indexing and unit cell refinement indicated a C-centered, monoclinic lattice. The space group was found to be C2/c (No. 15). The data were integrated using the Bruker SAINT software program and scaled using the SADABS software program. Solution by direct methods (SHELXL-97) produced a complete heavy-atom phasing model consistent with the proposed structure. All non-hydrogen atoms were refined anisotropically by full-matrix least-squares (SHELXL-97). The Crystallographic Information File (.cif) has been deposited in the Cambridge Structural Database; Reference Number CCDC 955221.

Table A16. Crystal data and structure refinement for msw02114.

Identification code	msw02114
Empirical formula	C_{37} H_{30} Au_2 F_2 P_2
Formula weight	968.48
Temperature	100(2) K
Wavelength	0.71073 Å
Crystal system	Monoclinic

Space group	C2/c	
Unit cell dimensions	a = 16.1721(8) Å	α= 90º.
	b = 10.6985(6) Å	β= 98.385(2)º.
	c = 18.0543(10) Å	γ = 90º.
Volume	3090.3(3) $Å^3$	
Z	4	
Density (calculated)	2.082 Mg/m^3	
Absorption coefficient	9.626 mm^{-1}	
F(000)	1832	
Crystal size	0.10 x 0.10 x 0.05 mm^3	
Theta range for data collection	2.28 to 25.40º.	
Index ranges	-19<=h<=19, -10<=k<=12, -21<=l<=21	
Reflections collected	24190	
Independent reflections	2841 [R(int) = 0.0268]	
Completeness to theta = 25.00º	100.0 %	
Absorption correction	Semi-empirical from equivalents	
Max. and min. transmission	0.6447 and 0.4461	
Refinement method	Full-matrix least-squares on F^2	
Data / restraints / parameters	2841 / 0 / 195	
Goodness-of-fit on F^2	1.081	
Final R indices [I>2sigma(I)]	R1 = 0.0117, wR2 = 0.0283	
R indices (all data)	R1 = 0.0124, wR2 = 0.0287	
Largest diff. peak and hole	0.752 and -0.379 $e.Å^{-3}$	

Table A17. Atomic coordinates (x 10^4) and equivalent isotropic displacement parameters ($Å^2$x 10^3) for msw02114. U(eq) is defined as one third of the trace of the orthogonalized U^{ij} tensor.

	x	y	z	U(eq)
C(1)	10000	23(3)	2500	21(1)
C(2)	10576(1)	4544(2)	3674(1)	19(1)
C(3)	10872(1)	5316(2)	3140(1)	21(1)
C(4)	11306(1)	6419(2)	3332(1)	24(1)
C(5)	11444(1)	6754(2)	4071(1)	24(1)
C(6)	11184(2)	6047(2)	4622(1)	24(1)
C(7)	10754(1)	4938(2)	4412(1)	22(1)
C(8)	8366(1)	1042(2)	2408(1)	16(1)
C(9)	8056(1)	2164(2)	2092(1)	18(1)
C(10)	7317(2)	2179(2)	1585(1)	23(1)
C(11)	6887(2)	1077(2)	1402(1)	25(1)
C(12)	7192(2)	-43(2)	1714(1)	24(1)
C(13)	7929(1)	-61(2)	2213(1)	20(1)
C(14)	9147(1)	36(2)	3817(1)	16(1)
C(15)	8472(1)	382(2)	4175(1)	18(1)
C(16)	8293(1)	-272(2)	4796(1)	21(1)
C(17)	8796(1)	-1260(2)	5079(1)	22(1)
C(18)	9479(1)	-1592(2)	4736(1)	22(1)
C(19)	9653(1)	-955(2)	4108(1)	20(1)
F(1)	11879(1)	7833(1)	4263(1)	36(1)
P(1)	9356(1)	998(1)	3035(1)	15(1)

Au(1)	9964(1)	2900(1)	3364(1)	15(1)

Table A18. Bond lengths [Å] and angles [º] for msw02114.

C(1)-P(1)#1	1.8436(19)	P(1)-C(1)-H(1B)	109.4
C(1)-P(1)	1.8436(19)	H(1A)-C(1)-H(1B)	108.0
C(1)-H(1A)	0.9900	C(7)-C(2)-C(3)	115.9(2)
C(1)-H(1B)	0.9900	C(7)-C(2)-Au(1)	123.13(17)
C(2)-C(7)	1.386(3)	C(3)-C(2)-Au(1)	120.94(17)
C(2)-C(3)	1.405(3)	C(4)-C(3)-C(2)	122.5(2)
C(2)-Au(1)	2.056(2)	C(4)-C(3)-H(3)	118.7
C(3)-C(4)	1.392(3)	C(2)-C(3)-H(3)	118.7
C(3)-H(3)	0.9500	C(5)-C(4)-C(3)	118.0(2)
C(4)-C(5)	1.367(3)	C(5)-C(4)-H(4)	121.0
C(4)-H(4)	0.9500	C(3)-C(4)-H(4)	121.0
C(5)-C(6)	1.365(4)	C(6)-C(5)-C(4)	122.8(2)
C(5)-F(1)	1.370(3)	C(6)-C(5)-F(1)	118.9(2)
C(6)-C(7)	1.399(3)	C(4)-C(5)-F(1)	118.2(2)
C(6)-H(6)	0.9500	C(5)-C(6)-C(7)	117.8(2)
C(7)-H(7)	0.9500	C(5)-C(6)-H(6)	121.1
C(8)-C(9)	1.391(3)	C(7)-C(6)-H(6)	121.1
C(8)-C(13)	1.394(3)	C(2)-C(7)-C(6)	123.0(2)
C(8)-P(1)	1.822(2)	C(2)-C(7)-H(7)	118.5
C(9)-C(10)	1.395(3)	C(6)-C(7)-H(7)	118.5
C(9)-H(9)	0.9500	C(9)-C(8)-C(13)	119.2(2)
C(10)-C(11)	1.385(3)	C(9)-C(8)-P(1)	120.60(17)
C(10)-H(10)	0.9500	C(13)-C(8)-P(1)	120.16(17)
C(11)-C(12)	1.385(4)	C(8)-C(9)-C(10)	120.2(2)
C(11)-H(11)	0.9500	C(8)-C(9)-H(9)	119.9
C(12)-C(13)	1.385(3)	C(10)-C(9)-H(9)	119.9
C(12)-H(12)	0.9500	C(11)-C(10)-C(9)	120.0(2)
C(13)-H(13)	0.9500	C(11)-C(10)-H(10)	120.0
C(14)-C(19)	1.395(3)	C(9)-C(10)-H(10)	120.0
C(14)-C(15)	1.397(3)	C(12)-C(11)-C(10)	120.2(2)
C(14)-P(1)	1.817(2)	C(12)-C(11)-H(11)	119.9
C(15)-C(16)	1.388(3)	C(10)-C(11)-H(11)	119.9
C(15)-H(15)	0.9500	C(11)-C(12)-C(13)	119.9(2)
C(16)-C(17)	1.386(3)	C(11)-C(12)-H(12)	120.0
C(16)-H(16)	0.9500	C(13)-C(12)-H(12)	120.0
C(17)-C(18)	1.388(3)	C(12)-C(13)-C(8)	120.6(2)
C(17)-H(17)	0.9500	C(12)-C(13)-H(13)	119.7
C(18)-C(19)	1.387(3)	C(8)-C(13)-H(13)	119.7
C(18)-H(18)	0.9500	C(19)-C(14)-C(15)	118.8(2)
C(19)-H(19)	0.9500	C(19)-C(14)-P(1)	123.90(17)
P(1)-Au(1)	2.2987(6)	C(15)-C(14)-P(1)	117.14(17)
Au(1)-Au(1)#1	3.1373(2)	C(16)-C(15)-C(14)	120.6(2)
		C(16)-C(15)-H(15)	119.7
P(1)#1-C(1)-P(1)	111.08(17)	C(14)-C(15)-H(15)	119.7
P(1)#1-C(1)-H(1A)	109.4	C(17)-C(16)-C(15)	120.2(2)
P(1)-C(1)-H(1A)	109.4	C(17)-C(16)-H(16)	119.9
P(1)#1-C(1)-H(1B)	109.4	C(15)-C(16)-H(16)	119.9

C(16)-C(17)-C(18)	119.5(2)	C(14)-P(1)-C(8)	104.48(10)
C(16)-C(17)-H(17)	120.2	C(14)-P(1)-C(1)	105.66(11)
C(18)-C(17)-H(17)	120.2	C(8)-P(1)-C(1)	101.61(7)
C(19)-C(18)-C(17)	120.6(2)	C(14)-P(1)-Au(1)	114.96(7)
C(19)-C(18)-H(18)	119.7	C(8)-P(1)-Au(1)	116.18(7)
C(17)-C(18)-H(18)	119.7	C(1)-P(1)-Au(1)	112.53(8)
C(18)-C(19)-C(14)	120.3(2)	C(2)-Au(1)-P(1)	176.46(6)
C(18)-C(19)-H(19)	119.9	C(2)-Au(1)-Au(1)#1	100.65(6)
C(14)-C(19)-H(19)	119.9	P(1)-Au(1)-Au(1)#1	79.647(14)

Symmetry transformations used to generate equivalent atoms:
#1 -x+2,y,-z+1/2

Table A19. Anisotropic displacement parameters ($Å^2 x\ 10^3$)for msw02114. The anisotropic displacement factor exponent takes the form: $-2\pi^2[\ h^2a^{*2}U^{11} + ... + 2\ h\ k\ a^*\ b^*\ U^{12}\ ]$

	U^{11}	U^{22}	U^{33}	U^{23}	U^{13}	U^{12}
C(1)	21(2)	16(2)	28(2)	0	10(1)	0
C(2)	16(1)	15(1)	24(1)	-1(1)	2(1)	2(1)
C(3)	23(1)	20(1)	20(1)	-3(1)	4(1)	-1(1)
C(4)	25(1)	22(1)	26(1)	2(1)	6(1)	-3(1)
C(5)	19(1)	16(1)	35(2)	-5(1)	1(1)	0(1)
C(6)	27(1)	26(1)	20(1)	-6(1)	1(1)	1(1)
C(7)	24(1)	21(1)	21(1)	4(1)	5(1)	2(1)
C(8)	17(1)	19(1)	14(1)	0(1)	5(1)	0(1)
C(9)	21(1)	16(1)	18(1)	-1(1)	7(1)	1(1)
C(10)	27(1)	23(1)	19(1)	4(1)	3(1)	7(1)
C(11)	24(1)	34(2)	16(1)	-2(1)	-3(1)	2(1)
C(12)	28(1)	24(1)	20(1)	-2(1)	1(1)	-5(1)
C(13)	26(1)	17(1)	17(1)	1(1)	2(1)	1(1)
C(14)	16(1)	14(1)	16(1)	-2(1)	0(1)	-4(1)
C(15)	18(1)	18(1)	19(1)	-1(1)	1(1)	1(1)
C(16)	22(1)	26(1)	17(1)	-4(1)	6(1)	-3(1)
C(17)	26(1)	24(1)	16(1)	3(1)	1(1)	-5(1)
C(18)	25(1)	20(1)	20(1)	4(1)	-1(1)	2(1)
C(19)	16(1)	20(1)	23(1)	-1(1)	2(1)	1(1)
F(1)	42(1)	24(1)	43(1)	-10(1)	4(1)	-13(1)
P(1)	15(1)	13(1)	17(1)	0(1)	3(1)	0(1)
Au(1)	16(1)	14(1)	16(1)	0(1)	3(1)	-1(1)

Table A20. Hydrogen coordinates ($x\ 10^4$) and isotropic displacement parameters ($Å^2 x\ 10^3$) for msw02114.

	x	y	z	U(eq)
H(1A)	10368	-521	2849	25
H(1B)	9632	-521	2151	25
H(3)	10771	5075	2629	25

H(4)	11500	6925	2961	29
H(6)	11291	6298	5132	29
H(7)	10575	4433	4791	26
H(9)	8348	2921	2221	22
H(10)	7109	2945	1366	28
H(11)	6380	1089	1061	30
H(12)	6896	-799	1586	29
H(13)	8138	-832	2425	24
H(15)	8131	1070	3991	22
H(16)	7825	-41	5028	25
H(17)	8675	-1707	5505	26
H(18)	9829	-2262	4933	27
H(19)	10119	-1195	3876	24

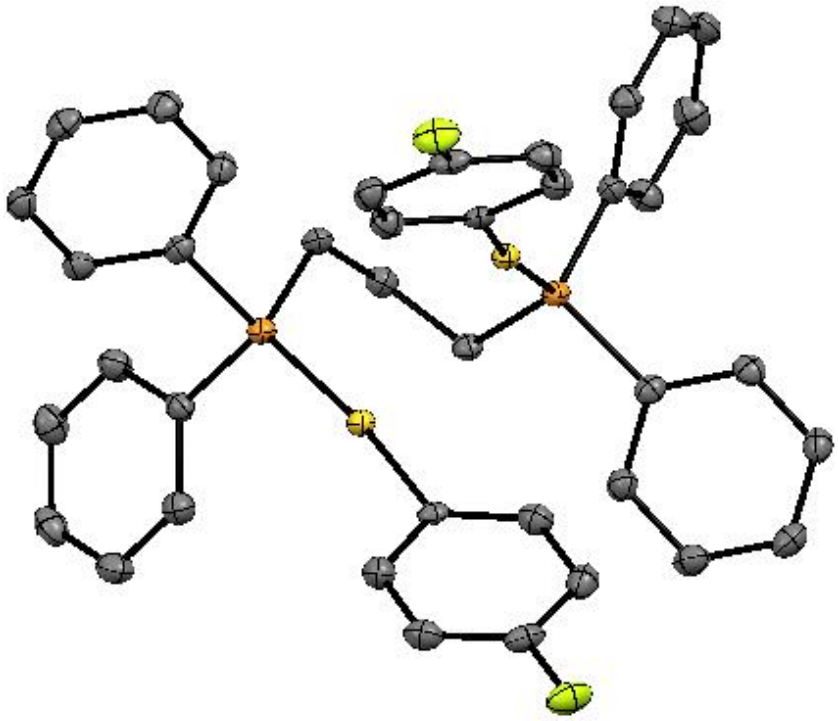

Figure A5. ORTEP representation of **11**. Thermal ellipsoids are set at 50% probability and hydrogen atoms are removed for clarity. Atoms are color-coded: carbon (grey), fluorine (yellow), gold (gold), phosphorus (orange), nitrogen (blue).

A colorless block 0.10 x 0.1 x 0.05 mm in size was mounted on a Cryoloop with Paratone oil. Data were collected in a nitrogen gas stream at 100(2) K using phi and omega scans. Crystal-to-detector distance was 40 mm and exposure time was 5 seconds per frame using a scan width of 0.4°. Data collection was 100.0% complete to 25.00° in θ. A total of 107338 reflections were collected covering the indices, -27<=h<=27, -11<=k<=11, -22<=l<=22. 3009 reflections were found to be symmetry independent, with an R_{int} of 0.0247. Indexing and unit cell refinement indicated a C-centered, monoclinic lattice. The space group was found to be C2/c (No. 15). The data were integrated using the Bruker SAINT software

program and scaled using the SADABS software program. Solution by direct methods (SHELXL-97) produced a complete heavy-atom phasing model consistent with the proposed structure. All non-hydrogen atoms were refined anisotropically by full-matrix least-squares (SHELXL-97). The Crystallographic Information File (.cif) has been deposited in the Cambridge Structural Database; Reference Number CCDC 955220.
CheckCIF alerts: A low-resolution (8.93 Å) reflection (0, 0, 2) was observed with a large ΔF^2/e.s.d. resulting in the B-level alert. The difference between the observed and predicted was not substantial enough to warrant deletion of the reflection.

Table A21. Crystal data and structure refinement for msw113.

Identification code	shelxl	
Empirical formula	$C_{19.50}H_{17}$ Au F P	
Formula weight	498.27	
Temperature	100(2) K	
Wavelength	0.71073 Å	
Crystal system	Monoclinic	
Space group	C2/c	
Unit cell dimensions	a = 23.0127(11) Å	α= 90º.
	b = 9.3100(5) Å	β= 126.3370(10)º.
	c = 19.0897(9) Å	γ = 90º.
Volume	3294.6(3) Å^3	
Z	8	
Density (calculated)	2.009 Mg/m^3	
Absorption coefficient	9.032 mm^{-1}	
F(000)	1896	
Crystal size	0.20 x 0.20 x 0.10 mm^3	
Theta range for data collection	2.20 to 25.33º.	
Index ranges	-27<=h<=27, -11<=k<=11, -22<=l<=22	
Reflections collected	35342	
Independent reflections	3009 [R(int) = 0.0247]	
Completeness to theta = 25.00º	100.0 %	
Absorption correction	Multi_scan	
Max. and min. transmission	0.4653 and 0.2653	
Refinement method	Full-matrix least-squares on F^2	
Data / restraints / parameters	3009 / 0 / 204	
Goodness-of-fit on F^2	1.213	
Final R indices [I>2sigma(I)]	R1 = 0.0122, wR2 = 0.0322	
R indices (all data)	R1 = 0.0123, wR2 = 0.0322	
Largest diff. peak and hole	0.355 and -0.780 e.Å^{-3}	

Table A22. Atomic coordinates (x 10^4) and equivalent isotropic displacement parameters (Å^{2}x 10^3) for msw113. U(eq) is defined as one third of the trace of the orthogonalized U^{ij} tensor.

	x	y	z	U(eq)
C(1)	9678(1)	5969(2)	3304(1)	14(1)
C(2)	9013(1)	5574(3)	2552(2)	22(1)
C(3)	8649(1)	4331(3)	2499(2)	23(1)
C(4)	8976(1)	3464(3)	3222(2)	22(1)
C(5)	9636(1)	3775(3)	3981(2)	23(1)
C(6)	9977(1)	5037(3)	4014(2)	22(1)

C(7)	11126(1)	10846(3)	4639(1)	18(1)
C(8)	10870(1)	10341(3)	5099(2)	22(1)
C(9)	11016(1)	11083(3)	5819(2)	27(1)
C(10)	11423(2)	12335(3)	6088(2)	26(1)
C(11)	11688(2)	12835(3)	5640(2)	26(1)
C(12)	11536(1)	12104(3)	4916(2)	23(1)
C(13)	11833(1)	9300(2)	4027(2)	17(1)
C(14)	12459(1)	9383(2)	4880(2)	20(1)
C(15)	13111(1)	8924(3)	5075(2)	22(1)
C(16)	13151(1)	8358(3)	4431(2)	23(1)
C(17)	12535(1)	8277(3)	3582(2)	24(1)
C(18)	11880(1)	8748(3)	3383(2)	21(1)
C(19)	10685(1)	11125(3)	2858(1)	17(1)
C(20)	10000	12004(4)	2500	19(1)
F(1)	8638(1)	2213(2)	3176(1)	29(1)
P(1)	10944(1)	9812(1)	3720(1)	15(1)
Au(1)	10226(1)	7823(1)	3415(1)	15(1)

Table A23. Bond lengths [Å] and angles [º] for msw113.

C(1)-C(2)	1.391(3)	C(16)-C(17)	1.385(3)
C(1)-C(6)	1.399(3)	C(16)-H(16)	0.9500
C(1)-Au(1)	2.073(2)	C(17)-C(18)	1.389(3)
C(2)-C(3)	1.397(4)	C(17)-H(17)	0.9500
C(2)-H(2)	0.9500	C(18)-H(18)	0.9500
C(3)-C(4)	1.376(4)	C(19)-C(20)	1.531(3)
C(3)-H(3)	0.9500	C(19)-P(1)	1.842(2)
C(4)-C(5)	1.371(4)	C(19)-H(19A)	0.9900
C(4)-F(1)	1.374(3)	C(19)-H(19B)	0.9900
C(5)-C(6)	1.394(3)	C(20)-C(19)#1	1.531(3)
C(5)-H(5)	0.9500	C(20)-H(20A)	0.9900
C(6)-H(6)	0.9500	C(20)-H(20B)	0.9900
C(7)-C(8)	1.397(3)	P(1)-Au(1)	2.3155(6)
C(7)-C(12)	1.397(3)	Au(1)-Au(1)#1	2.9969(2)
C(7)-P(1)	1.819(2)		
C(8)-C(9)	1.390(3)	C(2)-C(1)-C(6)	116.4(2)
C(8)-H(8)	0.9500	C(2)-C(1)-Au(1)	123.80(17)
C(9)-C(10)	1.389(4)	C(6)-C(1)-Au(1)	119.80(16)
C(9)-H(9)	0.9500	C(1)-C(2)-C(3)	122.7(2)
C(10)-C(11)	1.391(4)	C(1)-C(2)-H(2)	118.7
C(10)-H(10)	0.9500	C(3)-C(2)-H(2)	118.7
C(11)-C(12)	1.388(4)	C(4)-C(3)-C(2)	117.7(2)
C(11)-H(11)	0.9500	C(4)-C(3)-H(3)	121.1
C(12)-H(12)	0.9500	C(2)-C(3)-H(3)	121.1
C(13)-C(18)	1.393(3)	C(5)-C(4)-F(1)	118.5(2)
C(13)-C(14)	1.397(3)	C(5)-C(4)-C(3)	122.8(2)
C(13)-P(1)	1.827(2)	F(1)-C(4)-C(3)	118.7(2)
C(14)-C(15)	1.383(3)	C(4)-C(5)-C(6)	117.9(2)
C(14)-H(14)	0.9500	C(4)-C(5)-H(5)	121.1
C(15)-C(16)	1.391(3)	C(6)-C(5)-H(5)	121.1
C(15)-H(15)	0.9500	C(5)-C(6)-C(1)	122.6(2)

C(5)-C(6)-H(6)	118.7
C(1)-C(6)-H(6)	118.7
C(8)-C(7)-C(12)	119.1(2)
C(8)-C(7)-P(1)	119.08(19)
C(12)-C(7)-P(1)	121.76(18)
C(9)-C(8)-C(7)	120.6(2)
C(9)-C(8)-H(8)	119.7
C(7)-C(8)-H(8)	119.7
C(10)-C(9)-C(8)	119.9(2)
C(10)-C(9)-H(9)	120.1
C(8)-C(9)-H(9)	120.1
C(9)-C(10)-C(11)	119.9(2)
C(9)-C(10)-H(10)	120.0
C(11)-C(10)-H(10)	120.0
C(12)-C(11)-C(10)	120.3(2)
C(12)-C(11)-H(11)	119.9
C(10)-C(11)-H(11)	119.9
C(11)-C(12)-C(7)	120.2(2)
C(11)-C(12)-H(12)	119.9
C(7)-C(12)-H(12)	119.9
C(18)-C(13)-C(14)	119.0(2)
C(18)-C(13)-P(1)	118.09(17)
C(14)-C(13)-P(1)	122.89(18)
C(15)-C(14)-C(13)	120.0(2)
C(15)-C(14)-H(14)	120.0
C(13)-C(14)-H(14)	120.0
C(14)-C(15)-C(16)	120.6(2)
C(14)-C(15)-H(15)	119.7
C(16)-C(15)-H(15)	119.7
C(17)-C(16)-C(15)	119.8(2)
C(17)-C(16)-H(16)	120.1
C(15)-C(16)-H(16)	120.1
C(16)-C(17)-C(18)	119.7(2)
C(16)-C(17)-H(17)	120.2
C(18)-C(17)-H(17)	120.2
C(17)-C(18)-C(13)	120.9(2)
C(17)-C(18)-H(18)	119.5
C(13)-C(18)-H(18)	119.5
C(20)-C(19)-P(1)	117.23(14)
C(20)-C(19)-H(19A)	108.0
P(1)-C(19)-H(19A)	108.0
C(20)-C(19)-H(19B)	108.0
P(1)-C(19)-H(19B)	108.0
H(19A)-C(19)-H(19B)	107.2
C(19)#1-C(20)-C(19)	115.3(3)
C(19)#1-C(20)-H(20A)	108.4
C(19)-C(20)-H(20A)	108.4
C(19)#1-C(20)-H(20B)	108.4
C(19)-C(20)-H(20B)	108.4
H(20A)-C(20)-H(20B)	107.5
C(7)-P(1)-C(13)	104.80(10)
C(7)-P(1)-C(19)	106.11(11)
C(13)-P(1)-C(19)	99.70(10)
C(7)-P(1)-Au(1)	112.81(8)
C(13)-P(1)-Au(1)	111.65(8)
C(19)-P(1)-Au(1)	120.05(8)
C(1)-Au(1)-P(1)	172.80(6)
C(1)-Au(1)-Au(1)#1	96.36(6)
P(1)-Au(1)-Au(1)#1	89.766(14)

Symmetry transformations used to generate equivalent atoms:
#1 -x+2,y,-z+1/2

Table A24. Anisotropic displacement parameters ($Å^2 x\ 10^3$)for msw113. The anisotropic displacement factor exponent takes the form: $-2\pi^2[\ h^2 a^{*2} U^{11} + ... + 2\ h\ k\ a^*\ b^*\ U^{12}\ ]$

	U^{11}	U^{22}	U^{33}	U^{23}	U^{13}	U^{12}
C(1)	17(1)	14(1)	19(1)	-1(1)	14(1)	0(1)
C(2)	24(1)	21(1)	22(1)	2(1)	14(1)	2(1)
C(3)	19(1)	25(1)	24(1)	-6(1)	12(1)	-2(1)
C(4)	27(1)	17(1)	34(1)	-4(1)	25(1)	-4(1)
C(5)	28(1)	22(1)	24(1)	4(1)	19(1)	3(1)
C(6)	21(1)	24(1)	20(1)	-1(1)	12(1)	-1(1)
C(7)	18(1)	21(1)	15(1)	1(1)	10(1)	3(1)
C(8)	22(1)	25(1)	22(1)	-1(1)	14(1)	-2(1)
C(9)	28(1)	35(2)	24(1)	1(1)	19(1)	1(1)
C(10)	29(1)	30(1)	19(1)	-3(1)	13(1)	5(1)
C(11)	31(1)	21(1)	24(1)	-3(1)	14(1)	-2(1)
C(12)	26(1)	23(1)	22(1)	1(1)	16(1)	-1(1)
C(13)	17(1)	16(1)	21(1)	1(1)	12(1)	-1(1)
C(14)	22(1)	20(1)	20(1)	2(1)	14(1)	-1(1)
C(15)	18(1)	24(1)	19(1)	4(1)	9(1)	0(1)
C(16)	18(1)	22(1)	30(1)	2(1)	16(1)	2(1)
C(17)	23(1)	26(1)	27(1)	-5(1)	17(1)	-1(1)
C(18)	17(1)	23(1)	20(1)	-3(1)	10(1)	-1(1)
C(19)	17(1)	20(1)	18(1)	1(1)	12(1)	-2(1)
C(20)	22(2)	17(2)	19(2)	0	13(1)	0
F(1)	34(1)	22(1)	42(1)	-4(1)	29(1)	-7(1)
P(1)	15(1)	18(1)	15(1)	0(1)	10(1)	-1(1)
Au(1)	15(1)	17(1)	15(1)	0(1)	10(1)	0(1)

Table A25. Hydrogen coordinates ($x\ 10^4$) and isotropic displacement parameters ($Å^2 x\ 10^3$) for msw113.

	x	y	z	U(eq)
H(2)	8797	6175	2054	26
H(3)	8191	4093	1981	28
H(5)	9853	3150	4468	27
H(6)	10430	5274	4539	26
H(8)	10594	9483	4918	27
H(9)	10838	10735	6126	32
H(10)	11520	12850	6576	32
H(11)	11975	13681	5832	32
H(12)	11711	12461	4607	28
H(14)	12435	9756	5326	24
H(15)	13535	8996	5655	26
H(16)	13600	8029	4572	27

H(17)	12560	7900	3138	28
H(18)	11458	8694	2800	25
H(19A)	11091	11803	3086	21
H(19B)	10624	10602	2367	21
H(20A)	10083	12633	2970	22
H(20B)	9917	12633	2030	22

X-ray Crystallographic Data

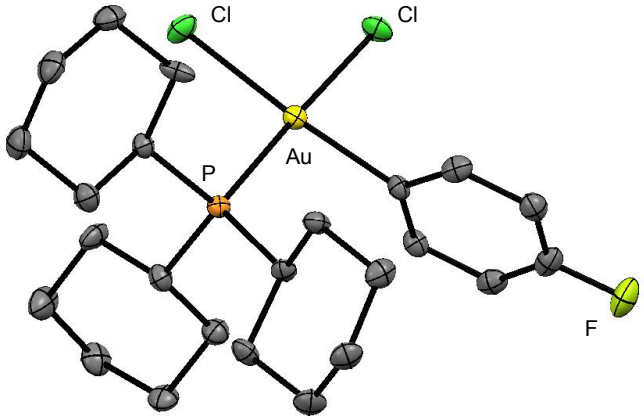

Figure A6. Thermal ellipsoid representation of *cis*-$Cy_3PAu(4\text{-}F\text{-}C_6H_4)Cl_2$ (**3.2**) at the 50% probability level. Hydrogen atoms and cocrystallized CH_2Cl_2 have been omitted for clarity. Atoms are color-coded: grey (carbon), green (chlorine), yellow (fluorine), gold (gold), orange (phosphorus).

Crystal Structure and Refinement Details for 3.2.

Table A26. Crystal data and structure refinement for **3.2.**

Identification code	WJW551	
Empirical formula	C25 H39 Au Cl4 F P	
Formula weight	728.30	
Temperature	100(2) K	
Wavelength	0.71073 Å	
Crystal system	Orthorhombic	
Space group	P2(1)2(1)2(1)	
Unit cell dimensions	a = 10.2268(5) Å	a= 90º.
	b = 14.9875(8) Å	b= 90º.
	c = 18.2383(9) Å	g = 90º.
Volume	2795.5(2) $Å^3$	
Z	4	
Density (calculated)	1.730 Mg/m^3	
Absorption coefficient	5.721 mm^{-1}	
F(000)	1440	

Crystal size	0.10 x 0.10 x 0.05 mm^3
Theta range for data collection	1.76 to 25.34∞.
Index ranges	-12<=h<=12, -18<=k<=18, -21<=l<=21
Reflections collected	58272
Independent reflections	5097 [R(int) = 0.0438]
Completeness to theta = 25.00º	100.0 %
Absorption correction	Multi_scan
Max. and min. transmission	0.7629 and 0.5985
Refinement method	Full-matrix least-squares on F^2
Data / restraints / parameters	5097 / 0 / 289
Goodness-of-fit on F^2	1.066
Final R indices [I>2sigma(I)]	R1 = 0.0208, wR2 = 0.0447
R indices (all data)	R1 = 0.0220, wR2 = 0.0454
Absolute structure parameter	-0.017(5)
Largest diff. peak and hole	1.431 and -0.880 e.$Å^{-3}$

Table A27. Atomic coordinates (x 10^4) and equivalent isotropic displacement parameters ($Å^2$x 10^3) for wjw551. U(eq) is defined as one third of the trace of the orthogonalized U^{ij} tensor.

	x	y	z	U(eq)
C(1)	743(5)	6755(3)	-36(2)	16(1)
C(2)	-443(4)	6510(3)	-351(2)	18(1)
C(3)	-451(4)	6071(3)	-1026(2)	21(1)
C(4)	732(5)	5911(3)	-1363(2)	22(1)
C(5)	1912(4)	6148(3)	-1064(2)	22(1)
C(6)	1908(4)	6582(3)	-386(2)	20(1)
C(7)	-805(4)	6104(3)	2003(2)	18(1)
C(8)	-1488(4)	6834(3)	2461(3)	25(1)
C(9)	-2773(4)	6462(3)	2770(3)	31(1)
C(10)	-3664(4)	6120(3)	2174(2)	25(1)
C(11)	-2976(4)	5420(3)	1709(2)	24(1)
C(12)	-1712(4)	5796(3)	1383(2)	21(1)
C(13)	1725(4)	6801(3)	2487(2)	15(1)
C(14)	3039(4)	7253(3)	2329(2)	20(1)
C(15)	3593(4)	7679(3)	3009(2)	25(1)
C(16)	3733(4)	6993(3)	3627(2)	27(1)
C(17)	2448(4)	6521(3)	3778(2)	27(1)
C(18)	1865(4)	6089(3)	3094(2)	22(1)
C(19)	1526(4)	5398(3)	1266(2)	16(1)
C(20)	3017(4)	5455(3)	1180(2)	18(1)
C(21)	3514(4)	4675(3)	726(2)	23(1)
C(22)	3124(4)	3787(3)	1059(2)	24(1)
C(23)	1651(4)	3738(3)	1181(2)	25(1)
C(24)	1146(4)	4513(3)	1641(2)	21(1)
C(25)	7135(6)	4214(4)	-171(4)	71(2)
F(1)	720(3)	5508(2)	-2037(1)	34(1)
P(1)	815(1)	6416(1)	1681(1)	14(1)
Cl(1)	648(2)	8733(1)	-15(1)	23(1)

Cl(2)	568(2)	8681(1)	1794(1)	24(1)
Cl(3)	8641(1)	3729(1)	-43(1)	62(1)
Cl(4)	5919(1)	3477(1)	-459(1)	40(1)
Au(1)	706(1)	7588(1)	855(1)	15(1)

Table A28. Bond lengths [Å] and angles [º] for wjw55

C(1)-C(6)	1.376(7)	C(16)-H(16B)	0.9900
C(1)-C(2)	1.391(6)	C(17)-C(18)	1.528(6)
C(1)-Au(1)	2.049(4)	C(17)-H(17A)	0.9900
C(2)-C(3)	1.396(6)	C(17)-H(17B)	0.9900
C(2)-H(2)	0.9500	C(18)-H(18A)	0.9900
C(3)-C(4)	1.377(6)	C(18)-H(18B)	0.9900
C(3)-H(3)	0.9500	C(19)-C(20)	1.535(6)
C(4)-F(1)	1.370(4)	C(19)-C(24)	1.542(5)
C(4)-C(5)	1.371(6)	C(19)-P(1)	1.851(4)
C(5)-C(6)	1.398(6)	C(19)-H(19)	1.0000
C(5)-H(5)	0.9500	C(20)-C(21)	1.521(5)
C(6)-H(6)	0.9500	C(20)-H(20A)	0.9900
C(7)-C(12)	1.533(6)	C(20)-H(20B)	0.9900
C(7)-C(8)	1.543(5)	C(21)-C(22)	1.517(6)
C(7)-P(1)	1.819(4)	C(21)-H(21A)	0.9900
C(7)-H(7)	1.0000	C(21)-H(21B)	0.9900
C(8)-C(9)	1.535(6)	C(22)-C(23)	1.524(6)
C(8)-H(8A)	0.9900	C(22)-H(22A)	0.9900
C(8)-H(8B)	0.9900	C(22)-H(22B)	0.9900
C(9)-C(10)	1.508(6)	C(23)-C(24)	1.523(6)
C(9)-H(9A)	0.9900	C(23)-H(23A)	0.9900
C(9)-H(9B)	0.9900	C(23)-H(23B)	0.9900
C(10)-C(11)	1.521(6)	C(24)-H(24A)	0.9900
C(10)-H(10A)	0.9900	C(24)-H(24B)	0.9900
C(10)-H(10B)	0.9900	C(25)-Cl(3)	1.718(6)
C(11)-C(12)	1.531(6)	C(25)-Cl(4)	1.745(6)
C(11)-H(11A)	0.9900	C(25)-H(25A)	0.9900
C(11)-H(11B)	0.9900	C(25)-H(25B)	0.9900
C(12)-H(12A)	0.9900	P(1)-Au(1)	2.3169(10)
C(12)-H(12B)	0.9900	Cl(1)-Au(1)	2.3378(9)
C(13)-C(14)	1.533(5)	Cl(2)-Au(1)	2.3750(10)
C(13)-C(18)	1.543(5)		
C(13)-P(1)	1.834(4)	C(6)-C(1)-C(2)	120.9(3)
C(13)-H(13)	1.0000	C(6)-C(1)-Au(1)	119.9(3)
C(14)-C(15)	1.504(5)	C(2)-C(1)-Au(1)	118.2(3)
C(14)-H(14A)	0.9900	C(1)-C(2)-C(3)	119.6(4)
C(14)-H(14B)	0.9900	C(1)-C(2)-H(2)	120.2
C(15)-C(16)	1.533(6)	C(3)-C(2)-H(2)	120.2
C(15)-H(15A)	0.9900	C(4)-C(3)-C(2)	118.0(4)
C(15)-H(15B)	0.9900	C(4)-C(3)-H(3)	121.0
C(16)-C(17)	1.518(6)	C(2)-C(3)-H(3)	121.0
C(16)-H(16A)	0.9900	F(1)-C(4)-C(5)	118.6(4)

F(1)-C(4)-C(3)	118.0(4)	C(15)-C(14)-H(14A)	109.4
C(5)-C(4)-C(3)	123.4(4)	C(13)-C(14)-H(14A)	109.4
C(4)-C(5)-C(6)	118.0(4)	C(15)-C(14)-H(14B)	109.4
C(4)-C(5)-H(5)	121.0	C(13)-C(14)-H(14B)	109.4
C(6)-C(5)-H(5)	121.0	H(14A)-C(14)-H(14B)	108.0
C(1)-C(6)-C(5)	120.0(4)	C(14)-C(15)-C(16)	111.0(3)
C(1)-C(6)-H(6)	120.0	C(14)-C(15)-H(15A)	109.4
C(5)-C(6)-H(6)	120.0	C(16)-C(15)-H(15A)	109.4
C(12)-C(7)-C(8)	109.8(4)	C(14)-C(15)-H(15B)	109.4
C(12)-C(7)-P(1)	112.9(3)	C(16)-C(15)-H(15B)	109.4
C(8)-C(7)-P(1)	113.9(3)	H(15A)-C(15)-H(15B)	108.0
C(12)-C(7)-H(7)	106.6	C(17)-C(16)-C(15)	111.4(4)
C(8)-C(7)-H(7)	106.6	C(17)-C(16)-H(16A)	109.4
P(1)-C(7)-H(7)	106.6	C(15)-C(16)-H(16A)	109.4
C(9)-C(8)-C(7)	109.2(3)	C(17)-C(16)-H(16B)	109.4
C(9)-C(8)-H(8A)	109.8	C(15)-C(16)-H(16B)	109.4
C(7)-C(8)-H(8A)	109.8	H(16A)-C(16)-H(16B)	108.0
C(9)-C(8)-H(8B)	109.8	C(16)-C(17)-C(18)	112.8(4)
C(7)-C(8)-H(8B)	109.8	C(16)-C(17)-H(17A)	109.0
H(8A)-C(8)-H(8B)	108.3	C(18)-C(17)-H(17A)	109.0
C(10)-C(9)-C(8)	112.0(4)	C(16)-C(17)-H(17B)	109.0
C(10)-C(9)-H(9A)	109.2	C(18)-C(17)-H(17B)	109.0
C(8)-C(9)-H(9A)	109.2	H(17A)-C(17)-H(17B)	107.8
C(10)-C(9)-H(9B)	109.2	C(17)-C(18)-C(13)	109.2(3)
C(8)-C(9)-H(9B)	109.2	C(17)-C(18)-H(18A)	109.8
H(9A)-C(9)-H(9B)	107.9	C(13)-C(18)-H(18A)	109.8
C(9)-C(10)-C(11)	110.9(4)	C(17)-C(18)-H(18B)	109.8
C(9)-C(10)-H(10A)	109.5	C(13)-C(18)-H(18B)	109.8
C(11)-C(10)-H(10A)	109.5	H(18A)-C(18)-H(18B)	108.3
C(9)-C(10)-H(10B)	109.5	C(20)-C(19)-C(24)	110.1(3)
C(11)-C(10)-H(10B)	109.5	C(20)-C(19)-P(1)	112.7(3)
H(10A)-C(10)-H(10B)	108.0	C(24)-C(19)-P(1)	115.3(3)
C(10)-C(11)-C(12)	110.6(4)	C(20)-C(19)-H(19)	106.0
C(10)-C(11)-H(11A)	109.5	C(24)-C(19)-H(19)	106.0
C(12)-C(11)-H(11A)	109.5	P(1)-C(19)-H(19)	106.0
C(10)-C(11)-H(11B)	109.5	C(21)-C(20)-C(19)	110.1(3)
C(12)-C(11)-H(11B)	109.5	C(21)-C(20)-H(20A)	109.6
H(11A)-C(11)-H(11B)	108.1	C(19)-C(20)-H(20A)	109.6
C(7)-C(12)-C(11)	109.5(3)	C(21)-C(20)-H(20B)	109.6
C(7)-C(12)-H(12A)	109.8	C(19)-C(20)-H(20B)	109.6
C(11)-C(12)-H(12A)	109.8	H(20A)-C(20)-H(20B)	108.1
C(7)-C(12)-H(12B)	109.8	C(22)-C(21)-C(20)	111.6(3)
C(11)-C(12)-H(12B)	109.8	C(22)-C(21)-H(21A)	109.3
H(12A)-C(12)-H(12B)	108.2	C(20)-C(21)-H(21A)	109.3
C(14)-C(13)-C(18)	111.0(3)	C(22)-C(21)-H(21B)	109.3
C(14)-C(13)-P(1)	115.7(3)	C(20)-C(21)-H(21B)	109.3
C(18)-C(13)-P(1)	113.9(3)	H(21A)-C(21)-H(21B)	108.0
C(14)-C(13)-H(13)	105.0	C(21)-C(22)-C(23)	111.1(3)
C(18)-C(13)-H(13)	105.0	C(21)-C(22)-H(22A)	109.4
P(1)-C(13)-H(13)	105.0	C(23)-C(22)-H(22A)	109.4
C(15)-C(14)-C(13)	111.3(3)	C(21)-C(22)-H(22B)	109.4

C(23)-C(22)-H(22B)	109.4	Cl(3)-C(25)-H(25B)	108.7
H(22A)-C(22)-H(22B)	108.0	Cl(4)-C(25)-H(25B)	108.7
C(22)-C(23)-C(24)	112.3(4)	H(25A)-C(25)-H(25B)	107.6
C(22)-C(23)-H(23A)	109.1	C(7)-P(1)-C(13)	106.50(18)
C(24)-C(23)-H(23A)	109.1	C(7)-P(1)-C(19)	106.16(18)
C(22)-C(23)-H(23B)	109.1	C(13)-P(1)-C(19)	112.82(19)
C(24)-C(23)-H(23B)	109.1	C(7)-P(1)-Au(1)	111.18(14)
H(23A)-C(23)-H(23B)	107.9	C(13)-P(1)-Au(1)	107.88(13)
C(23)-C(24)-C(19)	109.0(3)	C(19)-P(1)-Au(1)	112.19(13)
C(23)-C(24)-H(24A)	109.9	C(1)-Au(1)-P(1)	92.99(11)
C(19)-C(24)-H(24A)	109.9	C(1)-Au(1)-Cl(1)	84.85(10)
C(23)-C(24)-H(24B)	109.9	P(1)-Au(1)-Cl(1)	177.52(4)
C(19)-C(24)-H(24B)	109.9	C(1)-Au(1)-Cl(2)	173.41(12)
H(24A)-C(24)-H(24B)	108.3	P(1)-Au(1)-Cl(2)	93.26(3)
Cl(3)-C(25)-Cl(4)	114.4(3)	Cl(1)-Au(1)-Cl(2)	88.94(3)
Cl(3)-C(25)-H(25A)	108.7		
Cl(4)-C(25)-H(25A)	108.7		

Crystal Structure and Refinement Details for 3.3a

Table A29. Crystal data and structure refinement for **3.3a**.

Identification code	WJW5124	
Empirical formula	$C_{24}H_{37}AuF_4IP \cdot CH_2Cl_2$	
Formula weight	853.31	
Temperature	100(2) K	
Wavelength	0.71073 Å	
Crystal system	Monoclinic	
Space group	P2(1)/c	
Unit cell dimensions	a = 11.5448(4) Å	a= 90º.
	b = 18.1771(6) Å	b= 92.9300(10)º.
	c = 14.4575(5) Å	g = 90º.
Volume	3029.95(18) $Å^3$	
Z	4	
Density (calculated)	1.871 Mg/m^3	
Absorption coefficient	6.142 mm^{-1}	
F(000)	1648	
Crystal size	0.10 x 0.05 x 0.05 mm^3	
Theta range for data collection	1.77 to 25.40º.	
Index ranges	-13<=h<=13, -21<=k<=21, -17<=l<=17	
Reflections collected	60711	
Independent reflections	5533 [R(int) = 0.0244]	
Completeness to theta = 25.00º	99.9 %	
Absorption correction	Semi-empirical from equivalents	
Max. and min. transmission	0.7488 and 0.5787	
Refinement method	Full-matrix least-squares on F^2	
Data / restraints / parameters	5533 / 0 / 316	
Goodness-of-fit on F^2	1.036	
Final R indices [I>2sigma(I)]	R1 = 0.0216, wR2 = 0.0506	
R indices (all data)	R1 = 0.0232, wR2 = 0.0514	

Largest diff. peak and hole 1.415 and -1.571 $Å^{-3}$

Table A30. Atomic coordinates (x 10^4) and equivalent isotropic displacement parameters ($Å^2$x 10^3) for wjw5124. U(eq) is defined as one third of the trace of the orthogonalized U^{ij} tensor.

	x	y	z	U(eq)
C(2)	2824(3)	-386(2)	-407(2)	18(1)
C(3)	1976(3)	-898(2)	-214(2)	23(1)
C(4)	2241(4)	-1642(2)	-159(3)	26(1)
C(5)	3366(4)	-1857(2)	-272(2)	26(1)
C(6)	4230(3)	-1367(2)	-463(2)	22(1)
C(7)	3950(3)	-625(2)	-534(2)	19(1)
C(8)	2336(3)	-166(2)	-2582(2)	16(1)
C(9)	1184(3)	-573(2)	-2500(2)	19(1)
C(10)	1304(4)	-1379(2)	-2784(3)	29(1)
C(11)	1716(4)	-1431(2)	-3769(3)	35(1)
C(12)	2835(4)	-1008(2)	-3879(3)	29(1)
C(13)	2717(3)	-205(2)	-3587(2)	21(1)
C(14)	3525(3)	1260(2)	-2517(2)	15(1)
C(15)	4680(3)	894(2)	-2209(3)	22(1)
C(16)	5680(3)	1264(2)	-2684(3)	28(1)
C(17)	5720(3)	2085(2)	-2465(3)	28(1)
C(18)	4576(3)	2447(2)	-2760(3)	25(1)
C(19)	3557(3)	2085(2)	-2302(3)	22(1)
C(20)	980(3)	1261(2)	-2454(2)	15(1)
C(21)	768(3)	1303(2)	-3511(2)	18(1)
C(22)	-222(3)	1839(2)	-3750(3)	22(1)
C(23)	-1324(3)	1620(2)	-3277(3)	25(1)
C(24)	-1102(3)	1562(2)	-2232(3)	22(1)
C(25)	-127(3)	1018(2)	-1990(3)	19(1)
C(26)	2896(5)	999(4)	3747(4)	58(2)
F(1)	1471(3)	614(2)	1386(2)	71(1)
F(2)	3030(4)	49(2)	1411(2)	96(2)
F(3)	3034(4)	1189(2)	1475(2)	78(1)
F(4)	3636(2)	-2585(1)	-204(2)	36(1)
Cl(1)	1589(1)	628(1)	4073(1)	65(1)
Cl(2)	4068(2)	699(2)	4381(2)	159(2)
C(1)	2506(3)	633(2)	1064(3)	23(1)
P(4)	2291(1)	760(1)	-2055(1)	13(1)
I(2)	1770(1)	2110(1)	-229(1)	31(1)
Au(1)	2408(1)	712(1)	-405(1)	15(1)

Table A31. Bond lengths [Å] and angles [º] for wjw5124.

C(2)-C(7)	1.391(5)	C(3)-C(4)	1.388(6)
C(2)-C(3)	1.389(5)	C(3)-H(3)	0.9500
C(2)-Au(1)	2.054(4)	C(4)-C(5)	1.374(6)

C(4)-H(4)	0.9500	C(22)-H(22B)	0.9900
C(5)-F(4)	1.363(4)	C(23)-C(24)	1.523(5)
C(5)-C(6)	1.376(6)	C(23)-H(23A)	0.9900
C(6)-C(7)	1.390(5)	C(23)-H(23B)	0.9900
C(6)-H(6)	0.9500	C(24)-C(25)	1.525(5)
C(7)-H(7)	0.9500	C(24)-H(24A)	0.9900
C(8)-C(9)	1.532(5)	C(24)-H(24B)	0.9900
C(8)-C(13)	1.541(5)	C(25)-H(25A)	0.9900
C(8)-P(4)	1.849(3)	C(25)-H(25B)	0.9900
C(8)-H(8)	1.0000	C(26)-Cl(2)	1.686(6)
C(9)-C(10)	1.531(5)	C(26)-Cl(1)	1.740(6)
C(9)-H(9A)	0.9900	C(26)-H(26A)	0.9900
C(9)-H(9B)	0.9900	C(26)-H(26B)	0.9900
C(10)-C(11)	1.527(6)	F(1)-C(1)	1.304(5)
C(10)-H(10A)	0.9900	F(2)-C(1)	1.308(5)
C(10)-H(10B)	0.9900	F(3)-C(1)	1.308(5)
C(11)-C(12)	1.519(6)	C(1)-Au(1)	2.125(4)
C(11)-H(11A)	0.9900	P(4)-Au(1)	2.3847(8)
C(11)-H(11B)	0.9900	I(2)-Au(1)	2.6603(3)
C(12)-C(13)	1.527(5)		
C(12)-H(12A)	0.9900	C(7)-C(2)-C(3)	119.4(3)
C(12)-H(12B)	0.9900	C(7)-C(2)-Au(1)	121.6(3)
C(13)-H(13A)	0.9900	C(3)-C(2)-Au(1)	118.9(3)
C(13)-H(13B)	0.9900	C(4)-C(3)-C(2)	120.5(4)
C(14)-C(19)	1.531(5)	C(4)-C(3)-H(3)	119.7
C(14)-C(15)	1.536(5)	C(2)-C(3)-H(3)	119.7
C(14)-P(4)	1.843(3)	C(5)-C(4)-C(3)	118.5(4)
C(14)-H(14)	1.0000	C(5)-C(4)-H(4)	120.7
C(15)-C(16)	1.529(5)	C(3)-C(4)-H(4)	120.7
C(15)-H(15A)	0.9900	F(4)-C(5)-C(4)	118.9(4)
C(15)-H(15B)	0.9900	F(4)-C(5)-C(6)	118.5(4)
C(16)-C(17)	1.525(6)	C(4)-C(5)-C(6)	122.6(4)
C(16)-H(16A)	0.9900	C(5)-C(6)-C(7)	118.3(4)
C(16)-H(16B)	0.9900	C(5)-C(6)-H(6)	120.8
C(17)-C(18)	1.517(5)	C(7)-C(6)-H(6)	120.8
C(17)-H(17A)	0.9900	C(6)-C(7)-C(2)	120.6(3)
C(17)-H(17B)	0.9900	C(6)-C(7)-H(7)	119.7
C(18)-C(19)	1.528(5)	C(2)-C(7)-H(7)	119.7
C(18)-H(18A)	0.9900	C(9)-C(8)-C(13)	110.0(3)
C(18)-H(18B)	0.9900	C(9)-C(8)-P(4)	111.4(2)
C(19)-H(19A)	0.9900	C(13)-C(8)-P(4)	116.5(2)
C(19)-H(19B)	0.9900	C(9)-C(8)-H(8)	106.1
C(20)-C(25)	1.538(5)	C(13)-C(8)-H(8)	106.1
C(20)-C(21)	1.537(5)	P(4)-C(8)-H(8)	106.1
C(20)-P(4)	1.834(3)	C(10)-C(9)-C(8)	110.5(3)
C(20)-H(20)	1.0000	C(10)-C(9)-H(9A)	109.5
C(21)-C(22)	1.528(5)	C(8)-C(9)-H(9A)	109.5
C(21)-H(21A)	0.9900	C(10)-C(9)-H(9B)	109.5
C(21)-H(21B)	0.9900	C(8)-C(9)-H(9B)	109.5
C(22)-C(23)	1.527(5)	H(9A)-C(9)-H(9B)	108.1
C(22)-H(22A)	0.9900	C(11)-C(10)-C(9)	110.2(3)

C(11)-C(10)-H(10A)	109.6	C(19)-C(18)-H(18B)	109.3
C(9)-C(10)-H(10A)	109.6	H(18A)-C(18)-H(18B)	107.9
C(11)-C(10)-H(10B)	109.6	C(18)-C(19)-C(14)	110.2(3)
C(9)-C(10)-H(10B)	109.6	C(18)-C(19)-H(19A)	109.6
H(10A)-C(10)-H(10B)	108.1	C(14)-C(19)-H(19A)	109.6
C(12)-C(11)-C(10)	111.9(3)	C(18)-C(19)-H(19B)	109.6
C(12)-C(11)-H(11A)	109.2	C(14)-C(19)-H(19B)	109.6
C(10)-C(11)-H(11A)	109.2	H(19A)-C(19)-H(19B)	108.1
C(12)-C(11)-H(11B)	109.2	C(25)-C(20)-C(21)	110.7(3)
C(10)-C(11)-H(11B)	109.2	C(25)-C(20)-P(4)	114.3(2)
H(11A)-C(11)-H(11B)	107.9	C(21)-C(20)-P(4)	115.1(2)
C(11)-C(12)-C(13)	111.5(3)	C(25)-C(20)-H(20)	105.2
C(11)-C(12)-H(12A)	109.3	C(21)-C(20)-H(20)	105.2
C(13)-C(12)-H(12A)	109.3	P(4)-C(20)-H(20)	105.2
C(11)-C(12)-H(12B)	109.3	C(22)-C(21)-C(20)	109.6(3)
C(13)-C(12)-H(12B)	109.3	C(22)-C(21)-H(21A)	109.7
H(12A)-C(12)-H(12B)	108.0	C(20)-C(21)-H(21A)	109.7
C(12)-C(13)-C(8)	109.8(3)	C(22)-C(21)-H(21B)	109.7
C(12)-C(13)-H(13A)	109.7	C(20)-C(21)-H(21B)	109.7
C(8)-C(13)-H(13A)	109.7	H(21A)-C(21)-H(21B)	108.2
C(12)-C(13)-H(13B)	109.7	C(21)-C(22)-C(23)	111.3(3)
C(8)-C(13)-H(13B)	109.7	C(21)-C(22)-H(22A)	109.4
H(13A)-C(13)-H(13B)	108.2	C(23)-C(22)-H(22A)	109.4
C(19)-C(14)-C(15)	110.7(3)	C(21)-C(22)-H(22B)	109.4
C(19)-C(14)-P(4)	114.9(2)	C(23)-C(22)-H(22B)	109.4
C(15)-C(14)-P(4)	110.9(2)	H(22A)-C(22)-H(22B)	108.0
C(19)-C(14)-H(14)	106.6	C(24)-C(23)-C(22)	111.1(3)
C(15)-C(14)-H(14)	106.6	C(24)-C(23)-H(23A)	109.4
P(4)-C(14)-H(14)	106.6	C(22)-C(23)-H(23A)	109.4
C(16)-C(15)-C(14)	110.1(3)	C(24)-C(23)-H(23B)	109.4
C(16)-C(15)-H(15A)	109.6	C(22)-C(23)-H(23B)	109.4
C(14)-C(15)-H(15A)	109.6	H(23A)-C(23)-H(23B)	108.0
C(16)-C(15)-H(15B)	109.6	C(23)-C(24)-C(25)	111.0(3)
C(14)-C(15)-H(15B)	109.6	C(23)-C(24)-H(24A)	109.4
H(15A)-C(15)-H(15B)	108.2	C(25)-C(24)-H(24A)	109.4
C(17)-C(16)-C(15)	110.7(3)	C(23)-C(24)-H(24B)	109.4
C(17)-C(16)-H(16A)	109.5	C(25)-C(24)-H(24B)	109.4
C(15)-C(16)-H(16A)	109.5	H(24A)-C(24)-H(24B)	108.0
C(17)-C(16)-H(16B)	109.5	C(24)-C(25)-C(20)	109.5(3)
C(15)-C(16)-H(16B)	109.5	C(24)-C(25)-H(25A)	109.8
H(16A)-C(16)-H(16B)	108.1	C(20)-C(25)-H(25A)	109.8
C(18)-C(17)-C(16)	110.5(3)	C(24)-C(25)-H(25B)	109.8
C(18)-C(17)-H(17A)	109.6	C(20)-C(25)-H(25B)	109.8
C(16)-C(17)-H(17A)	109.6	H(25A)-C(25)-H(25B)	108.2
C(18)-C(17)-H(17B)	109.6	Cl(2)-C(26)-Cl(1)	114.2(3)
C(16)-C(17)-H(17B)	109.6	Cl(2)-C(26)-H(26A)	108.7
H(17A)-C(17)-H(17B)	108.1	Cl(1)-C(26)-H(26A)	108.7
C(17)-C(18)-C(19)	111.7(3)	Cl(2)-C(26)-H(26B)	108.7
C(17)-C(18)-H(18A)	109.3	Cl(1)-C(26)-H(26B)	108.7
C(19)-C(18)-H(18A)	109.3	H(26A)-C(26)-H(26B)	107.6
C(17)-C(18)-H(18B)	109.3	F(1)-C(1)-F(2)	104.8(4)

F(1)-C(1)-F(3)	105.8(4)	C(8)-P(4)-Au(1)	112.21(11)
F(2)-C(1)-F(3)	104.8(4)	C(2)-Au(1)-C(1)	86.27(14)
F(1)-C(1)-Au(1)	110.8(3)	C(2)-Au(1)-P(4)	91.99(9)
F(2)-C(1)-Au(1)	116.0(3)	C(1)-Au(1)-P(4)	178.15(10)
F(3)-C(1)-Au(1)	113.6(3)	C(2)-Au(1)-I(2)	173.91(10)
C(20)-P(4)-C(14)	106.37(15)	C(1)-Au(1)-I(2)	88.33(10)
C(20)-P(4)-C(8)	111.24(16)	P(4)-Au(1)-I(2)	93.39(2)
C(14)-P(4)-C(8)	105.16(16)		
C(20)-P(4)-Au(1)	109.62(11)		
C(14)-P(4)-Au(1)	112.04(11)		

Crystal Structure and Refinement Details for 3.3b

Table A32. Crystal data and structure refinement for **3.3b**

Identification code	shelx	
Empirical formula	C25 H36 Au F5 I P	
Formula weight	786.37	
Temperature	100(2) K	
Wavelength	0.71073 ≈	
Crystal system	Monoclinic	
Space group	P 21/n	
Unit cell dimensions	a = 9.6496(4) ≈	a= 90∞.
	b = 15.8469(7) ≈	b= 101.4020(10)∞.
	c = 17.6621(7) ≈	g = 90∞.
Volume	2647.52(19) $\approx^3$	
Z	4	
Density (calculated)	1.973 Mg/m^3	
Absorption coefficient	6.830 mm^{-1}	
F(000)	1512	
Crystal size	0.240 x 0.200 x 0.160 mm^3	
Theta range for data collection	1.742 to 25.352∞.	
Index ranges	-11<=h<=11, -19<=k<=18, -21<=l<=21	
Reflections collected	52522	
Independent reflections	4848 [R(int) = 0.0226]	
Completeness to theta = 25.000∞	99.8 %	
Absorption correction	Semi-empirical from equivalents	
Max. and min. transmission	0.205 and 0.111	
Refinement method	Full-matrix least-squares on F^2	
Data / restraints / parameters	4848 / 0 / 298	
Goodness-of-fit on F^2	1.172	
Final R indices [I>2sigma(I)]	R1 = 0.0175, wR2 = 0.0424	
R indices (all data)	R1 = 0.0177, wR2 = 0.0425	
Extinction coefficient	n/a	
Largest diff. peak and hole	1.674 and -1.016 e.$\approx^{-3}$	

Table A33. Atomic coordinates (x 10^4) and equivalent isotropic displacement parameters ($Å^2$x 10^3) for mkt_training_1_041014. U(eq) is defined as one third of the trace of the orthogonalized U^{ij} tensor.

	x	y	z	U(eq)
C(6)	7279(3)	3122(2)	440(2)	18(1)
C(7)	10339(3)	3513(2)	1999(2)	21(1)
C(8)	5012(3)	3531(2)	2464(2)	15(1)
C(9)	6319(3)	1995(2)	3296(2)	16(1)
C(10)	5124(3)	2013(2)	1562(2)	14(1)
C(11)	4994(3)	4103(2)	1757(2)	18(1)
C(12)	5354(3)	4050(2)	3214(2)	18(1)
C(13)	4943(3)	1601(2)	3457(2)	20(1)
C(14)	7504(3)	1327(2)	3400(2)	19(1)
C(15)	3506(3)	1995(2)	1472(2)	20(1)
C(16)	5696(3)	1115(2)	1506(2)	17(1)
C(33)	5210(4)	1253(2)	4282(2)	26(1)
C(34)	6417(4)	613(2)	4425(2)	28(1)
C(35)	7766(4)	984(2)	4228(2)	25(1)
C(36)	4265(4)	4761(2)	3186(2)	22(1)
C(37)	4245(4)	5335(2)	2487(2)	24(1)
C(38)	2832(3)	1581(2)	703(2)	24(1)
C(39)	3439(4)	714(2)	601(2)	25(1)
C(40)	5050(4)	749(2)	714(2)	21(1)
C(49)	3946(4)	4830(2)	1737(2)	22(1)
F(3)	11434(2)	3090(2)	2435(1)	30(1)
F(4)	10585(2)	3469(2)	1269(1)	32(1)
F(5)	10524(2)	4331(1)	2191(1)	32(1)
C(1)	8024(3)	2636(2)	1045(2)	14(1)
C(2)	8644(3)	1883(2)	890(2)	16(1)
C(3)	8486(3)	1619(2)	130(2)	17(1)
C(4)	7749(3)	2070(2)	-481(2)	20(1)
C(5)	7168(3)	2823(2)	-304(2)	20(1)
F(1)	9088(2)	880(1)	-15(1)	26(1)
F(2)	6459(2)	3297(1)	-892(1)	31(1)
P(4)	6133(1)	2601(1)	2392(1)	12(1)
I(2)	9143(1)	3517(1)	3620(1)	24(1)
Au(1)	8380(1)	3048(1)	2170(1)	12(1)

Table A34. Bond lengths [Å] and angles [º] for mkt_training_1_041014.

C(6)-C(5)	1.382(5)	C(9)-P(4)	1.841(3)
C(6)-C(1)	1.395(4)	C(9)-H(9)	1.0000
C(6)-H(6)	0.9500	C(10)-C(16)	1.536(4)
C(7)-F(5)	1.343(4)	C(10)-C(15)	1.538(4)
C(7)-F(3)	1.354(4)	C(10)-P(4)	1.843(3)
C(7)-F(4)	1.359(4)	C(10)-H(10)	1.0000
C(7)-Au(1)	2.106(3)	C(11)-C(49)	1.529(4)
C(8)-C(12)	1.539(4)	C(11)-H(11A)	0.9900
C(8)-C(11)	1.540(4)	C(11)-H(11B)	0.9900
C(8)-P(4)	1.847(3)	C(12)-C(36)	1.535(4)
C(8)-H(8)	1.0000	C(12)-H(12A)	0.9900
C(9)-C(14)	1.543(4)	C(12)-H(12B)	0.9900
C(9)-C(13)	1.543(4)	C(13)-C(33)	1.532(4)

C(13)-H(13A)	0.9900
C(13)-H(13B)	0.9900
C(14)-C(35)	1.534(4)
C(14)-H(14A)	0.9900
C(14)-H(14B)	0.9900
C(15)-C(38)	1.534(4)
C(15)-H(15A)	0.9900
C(15)-H(15B)	0.9900
C(16)-C(40)	1.529(4)
C(16)-H(16A)	0.9900
C(16)-H(16B)	0.9900
C(33)-C(34)	1.527(5)
C(33)-H(33A)	0.9900
C(33)-H(33B)	0.9900
C(34)-C(35)	1.530(5)
C(34)-H(34A)	0.9900
C(34)-H(34B)	0.9900
C(35)-H(35A)	0.9900
C(35)-H(35B)	0.9900
C(36)-C(37)	1.529(5)
C(36)-H(36A)	0.9900
C(36)-H(36B)	0.9900
C(37)-C(49)	1.525(5)
C(37)-H(37A)	0.9900
C(37)-H(37B)	0.9900
C(38)-C(39)	1.518(5)
C(38)-H(38A)	0.9900
C(38)-H(38B)	0.9900
C(39)-C(40)	1.528(5)
C(39)-H(39A)	0.9900
C(39)-H(39B)	0.9900
C(40)-H(40A)	0.9900
C(40)-H(40B)	0.9900
C(49)-H(49A)	0.9900
C(49)-H(49B)	0.9900
C(1)-C(2)	1.387(4)
C(1)-Au(1)	2.054(3)
C(2)-C(3)	1.385(4)
C(2)-H(2)	0.9500
C(3)-F(1)	1.355(4)
C(3)-C(4)	1.370(5)
C(4)-C(5)	1.379(5)
C(4)-H(4)	0.9500
C(5)-F(2)	1.353(4)
P(4)-Au(1)	2.3857(7)
I(2)-Au(1)	2.6286(2)

C(5)-C(6)-C(1)	118.0(3)
C(5)-C(6)-H(6)	121.0
C(1)-C(6)-H(6)	121.0
F(5)-C(7)-F(3)	106.5(3)
F(5)-C(7)-F(4)	104.4(3)
F(3)-C(7)-F(4)	104.5(3)
F(5)-C(7)-Au(1)	112.3(2)
F(3)-C(7)-Au(1)	111.6(2)
F(4)-C(7)-Au(1)	116.6(2)
C(12)-C(8)-C(11)	110.4(3)
C(12)-C(8)-P(4)	117.3(2)
C(11)-C(8)-P(4)	109.0(2)
C(12)-C(8)-H(8)	106.5
C(11)-C(8)-H(8)	106.5
P(4)-C(8)-H(8)	106.5
C(14)-C(9)-C(13)	110.2(3)
C(14)-C(9)-P(4)	113.8(2)
C(13)-C(9)-P(4)	115.5(2)
C(14)-C(9)-H(9)	105.4
C(13)-C(9)-H(9)	105.4
P(4)-C(9)-H(9)	105.4
C(16)-C(10)-C(15)	110.3(3)
C(16)-C(10)-P(4)	112.3(2)
C(15)-C(10)-P(4)	117.2(2)
C(16)-C(10)-H(10)	105.3
C(15)-C(10)-H(10)	105.3
P(4)-C(10)-H(10)	105.3
C(49)-C(11)-C(8)	111.4(3)
C(49)-C(11)-H(11A)	109.4
C(8)-C(11)-H(11A)	109.4
C(49)-C(11)-H(11B)	109.4
C(8)-C(11)-H(11B)	109.4
H(11A)-C(11)-H(11B)	108.0
C(36)-C(12)-C(8)	109.6(3)
C(36)-C(12)-H(12A)	109.7
C(8)-C(12)-H(12A)	109.7
C(36)-C(12)-H(12B)	109.7
C(8)-C(12)-H(12B)	109.7
H(12A)-C(12)-H(12B)	108.2
C(33)-C(13)-C(9)	109.4(3)
C(33)-C(13)-H(13A)	109.8
C(9)-C(13)-H(13A)	109.8
C(33)-C(13)-H(13B)	109.8
C(9)-C(13)-H(13B)	109.8
H(13A)-C(13)-H(13B)	108.2
C(35)-C(14)-C(9)	109.6(3)
C(35)-C(14)-H(14A)	109.8
C(9)-C(14)-H(14A)	109.8
C(35)-C(14)-H(14B)	109.8
C(9)-C(14)-H(14B)	109.8
H(14A)-C(14)-H(14B)	108.2
C(38)-C(15)-C(10)	110.0(3)
C(38)-C(15)-H(15A)	109.7
C(10)-C(15)-H(15A)	109.7
C(38)-C(15)-H(15B)	109.7

C(10)-C(15)-H(15B)	109.7
H(15A)-C(15)-H(15B)	108.2
C(40)-C(16)-C(10)	108.9(3)
C(40)-C(16)-H(16A)	109.9
C(10)-C(16)-H(16A)	109.9
C(40)-C(16)-H(16B)	109.9
C(10)-C(16)-H(16B)	109.9
H(16A)-C(16)-H(16B)	108.3
C(34)-C(33)-C(13)	112.0(3)
C(34)-C(33)-H(33A)	109.2
C(13)-C(33)-H(33A)	109.2
C(34)-C(33)-H(33B)	109.2
C(13)-C(33)-H(33B)	109.2
H(33A)-C(33)-H(33B)	107.9
C(33)-C(34)-C(35)	111.3(3)
C(33)-C(34)-H(34A)	109.4
C(35)-C(34)-H(34A)	109.4
C(33)-C(34)-H(34B)	109.4
C(35)-C(34)-H(34B)	109.4
H(34A)-C(34)-H(34B)	108.0
C(34)-C(35)-C(14)	111.4(3)
C(34)-C(35)-H(35A)	109.3
C(14)-C(35)-H(35A)	109.3
C(34)-C(35)-H(35B)	109.3
C(14)-C(35)-H(35B)	109.3
H(35A)-C(35)-H(35B)	108.0
C(37)-C(36)-C(12)	111.2(3)
C(37)-C(36)-H(36A)	109.4
C(12)-C(36)-H(36A)	109.4
C(37)-C(36)-H(36B)	109.4
C(12)-C(36)-H(36B)	109.4
H(36A)-C(36)-H(36B)	108.0
C(49)-C(37)-C(36)	111.0(3)
C(49)-C(37)-H(37A)	109.4
C(36)-C(37)-H(37A)	109.4
C(49)-C(37)-H(37B)	109.4
C(36)-C(37)-H(37B)	109.4
H(37A)-C(37)-H(37B)	108.0
C(39)-C(38)-C(15)	112.7(3)
C(39)-C(38)-H(38A)	109.0
C(15)-C(38)-H(38A)	109.0
C(39)-C(38)-H(38B)	109.0
C(15)-C(38)-H(38B)	109.0
H(38A)-C(38)-H(38B)	107.8
C(38)-C(39)-C(40)	110.9(3)
C(38)-C(39)-H(39A)	109.4
C(40)-C(39)-H(39A)	109.4
C(38)-C(39)-H(39B)	109.4
C(40)-C(39)-H(39B)	109.4
H(39A)-C(39)-H(39B)	108.0
C(39)-C(40)-C(16)	110.7(3)
C(39)-C(40)-H(40A)	109.5
C(16)-C(40)-H(40A)	109.5
C(39)-C(40)-H(40B)	109.5
C(16)-C(40)-H(40B)	109.5
H(40A)-C(40)-H(40B)	108.1
C(37)-C(49)-C(11)	111.4(3)
C(37)-C(49)-H(49A)	109.3
C(11)-C(49)-H(49A)	109.3
C(37)-C(49)-H(49B)	109.3
C(11)-C(49)-H(49B)	109.3
H(49A)-C(49)-H(49B)	108.0
C(2)-C(1)-C(6)	120.0(3)
C(2)-C(1)-Au(1)	118.0(2)
C(6)-C(1)-Au(1)	121.8(2)
C(3)-C(2)-C(1)	118.8(3)
C(3)-C(2)-H(2)	120.6
C(1)-C(2)-H(2)	120.6
F(1)-C(3)-C(4)	118.6(3)
F(1)-C(3)-C(2)	118.4(3)
C(4)-C(3)-C(2)	123.1(3)
C(3)-C(4)-C(5)	116.4(3)
C(3)-C(4)-H(4)	121.8
C(5)-C(4)-H(4)	121.8
F(2)-C(5)-C(4)	118.3(3)
F(2)-C(5)-C(6)	118.1(3)
C(4)-C(5)-C(6)	123.6(3)
C(9)-P(4)-C(10)	111.78(15)
C(9)-P(4)-C(8)	108.28(14)
C(10)-P(4)-C(8)	103.53(14)
C(9)-P(4)-Au(1)	111.18(10)
C(10)-P(4)-Au(1)	111.97(10)
C(8)-P(4)-Au(1)	109.76(10)
C(1)-Au(1)-C(7)	87.49(12)
C(1)-Au(1)-P(4)	94.65(8)
C(7)-Au(1)-P(4)	176.63(10)
C(1)-Au(1)-I(2)	173.28(8)
C(7)-Au(1)-I(2)	87.33(9)
P(4)-Au(1)-I(2)	90.727(19)

Crystal Structure and Refinement Details for 3.3c

Table A35. Crystal data and structure refinement for **3.3c**.

Identification code	shelx	
Empirical formula	$C_{25}H_{38}AuF_3IP$	
Formula weight	750.39	
Temperature	100(2) K	
Wavelength	0.71073 Å	
Crystal system	Monoclinic	
Space group	P 21/n	
Unit cell dimensions	a = 18.0923(9) Å	a= 90.
	b = 14.9606(7) Å	b= 107.340(2)º.
	c = 20.1354(11) Å	g = 90º.
Volume	5202.4(5) $Å^3$	
Z	8	
Density (calculated)	1.916 Mg/m^3	
Absorption coefficient	6.936 mm^{-1}	
F(000)	2896	
Crystal size	0.100 x 0.100 x 0.050 mm^3	
Theta range for data collection	1.725 to 28.392º.	
Index ranges	-24<=h<=24, -19<=k<=19, -26<=l<=26	
Reflections collected	93423	
Independent reflections	12974 [R(int) = 0.0323]	
Completeness to theta = 25.000∞	100.0 %	
Absorption correction	Semi-empirical from equivalents	
Max. and min. transmission	0.209 and 0.168	
Refinement method	Full-matrix least-squares on F^2	
Data / restraints / parameters	12974 / 0 / 559	
Goodness-of-fit on F^2	1.020	
Final R indices [I>2sigma(I)]	R1 = 0.0194, wR2 = 0.0377	
R indices (all data)	R1 = 0.0236, wR2 = 0.0388	
Extinction coefficient	n/a	
Largest diff. peak and hole	1.190 and -0.924 $e.Å^{-3}$	

Table A36. Atomic coordinates (x 10^4) and equivalent isotropic displacement parameters ($Å^2$x 10^3) for wjw633. U(eq) is defined as one third of the trace of the orthogonalized U^{ij} tensor.

	x	y	z	U(eq)
C(1)	3265(2)	1368(2)	6188(1)	21(1)
C(2)	2928(1)	3172(2)	6263(1)	14(1)
C(3)	3431(1)	3620(2)	6818(1)	17(1)
C(4)	3816(1)	4382(2)	6703(2)	21(1)
C(5)	3706(2)	4687(2)	6033(2)	24(1)
C(6)	3208(2)	4239(2)	5478(1)	23(1)
C(7)	2819(1)	3478(2)	5591(1)	18(1)
C(8)	1443(1)	4139(2)	6474(1)	12(1)
C(9)	1142(1)	4805(2)	6911(1)	16(1)

C(10)	1319(2)	5762(2)	6739(1)	18(1)
C(11)	986(2)	5970(2)	5966(1)	18(1)
C(12)	1267(2)	5295(2)	5531(1)	18(1)
C(13)	1077(1)	4338(2)	5694(1)	14(1)
C(14)	406(1)	2482(2)	6265(1)	12(1)
C(15)	-247(1)	2989(2)	6441(1)	15(1)
C(16)	-985(1)	2426(2)	6231(1)	19(1)
C(17)	-1206(1)	2170(2)	5464(1)	20(1)
C(18)	-544(1)	1715(2)	5277(1)	18(1)
C(19)	195(1)	2285(2)	5484(1)	15(1)
C(20)	1482(1)	2908(2)	7613(1)	12(1)
C(21)	2324(1)	3099(2)	8042(1)	15(1)
C(22)	2388(2)	3220(2)	8810(1)	19(1)
C(23)	2053(1)	2420(2)	9095(1)	19(1)
C(24)	1230(1)	2228(2)	8653(1)	18(1)
C(25)	1184(1)	2068(2)	7892(1)	16(1)
C(26)	5766(2)	-424(2)	7169(1)	22(1)
C(27)	6170(1)	912(2)	6371(1)	15(1)
C(28)	5480(2)	1040(2)	5853(1)	19(1)
C(29)	5459(2)	985(2)	5157(1)	26(1)
C(30)	6123(2)	781(2)	4981(2)	29(1)
C(31)	6809(2)	640(2)	5499(2)	28(1)
C(32)	6839(2)	704(2)	6196(1)	21(1)
C(33)	7672(1)	2436(2)	8066(1)	17(1)
C(34)	8110(1)	1765(2)	7756(2)	23(1)
C(35)	8987(2)	1829(2)	8104(2)	29(1)
C(36)	9191(2)	1747(2)	8891(2)	33(1)
C(37)	8752(2)	2416(2)	9192(2)	28(1)
C(38)	7881(1)	2318(2)	8858(1)	22(1)
C(39)	6162(1)	2963(2)	8192(1)	17(1)
C(40)	6406(2)	3946(2)	8336(2)	24(1)
C(41)	6145(2)	4277(2)	8950(2)	32(1)
C(42)	5278(2)	4163(2)	8813(2)	32(1)
C(43)	5020(2)	3204(2)	8620(1)	24(1)
C(44)	5282(1)	2867(2)	8007(1)	19(1)
C(45)	6459(2)	2988(2)	6787(1)	22(1)
C(46)	6917(2)	3820(2)	6761(2)	39(1)
C(47)	6771(2)	4107(3)	6000(2)	52(1)
C(48)	5899(2)	4247(3)	5645(2)	54(1)
C(49)	5444(2)	3437(2)	5690(2)	34(1)
C(50)	5593(1)	3154(2)	6439(1)	19(1)
F(1)	3323(1)	491(1)	6313(1)	35(1)
F(2)	3972(1)	1676(1)	6564(1)	47(1)
F(3)	3244(1)	1461(1)	5525(1)	49(1)
F(4)	5015(1)	-478(1)	7142(1)	41(1)
F(5)	6124(1)	-1033(1)	7645(1)	33(1)
F(6)	5797(2)	-785(1)	6568(1)	63(1)
P(1)	1376(1)	2935(1)	6676(1)	11(1)
P(6)	6621(1)	2382(1)	7611(1)	14(1)
I(1)	1641(1)	521(1)	6523(1)	20(1)
I(2)	6202(1)	640(1)	8715(1)	19(1)

Au(1)	2352(1)	2048(1)	6412(1)	11(1)
Au(2)	6183(1)	878(1)	7395(1)	14(1)

Table A37. Bond lengths [Å] and angles [º] for wjw633.

C(1)-F(3)	1.330(3)	C(17)-H(17B)	0.9900
C(1)-F(1)	1.335(3)	C(18)-C(19)	1.534(3)
C(1)-F(2)	1.358(3)	C(18)-H(18A)	0.9900
C(1)-Au(1)	2.099(3)	C(18)-H(18B)	0.9900
C(2)-C(3)	1.384(3)	C(19)-H(19A)	0.9900
C(2)-C(7)	1.386(3)	C(19)-H(19B)	0.9900
C(2)-Au(1)	2.047(2)	C(20)-C(21)	1.538(3)
C(3)-C(4)	1.391(3)	C(20)-C(25)	1.537(3)
C(3)-H(3)	0.9500	C(20)-P(1)	1.840(2)
C(4)-C(5)	1.382(4)	C(20)-H(20)	1.0000
C(4)-H(4)	0.9500	C(21)-C(22)	1.527(3)
C(5)-C(6)	1.382(4)	C(21)-H(21A)	0.9900
C(5)-H(5)	0.9500	C(21)-H(21B)	0.9900
C(6)-C(7)	1.392(4)	C(22)-C(23)	1.530(3)
C(6)-H(6)	0.9500	C(22)-H(22A)	0.9900
C(7)-H(7)	0.9500	C(22)-H(22B)	0.9900
C(8)-C(9)	1.533(3)	C(23)-C(24)	1.518(3)
C(8)-C(13)	1.540(3)	C(23)-H(23A)	0.9900
C(8)-P(1)	1.858(2)	C(23)-H(23B)	0.9900
C(8)-H(8)	1.0000	C(24)-C(25)	1.528(3)
C(9)-C(10)	1.530(3)	C(24)-H(24A)	0.9900
C(9)-H(9A)	0.9900	C(24)-H(24B)	0.9900
C(9)-H(9B)	0.9900	C(25)-H(25A)	0.9900
C(10)-C(11)	1.523(4)	C(25)-H(25B)	0.9900
C(10)-H(10A)	0.9900	C(26)-F(5)	1.342(3)
C(10)-H(10B)	0.9900	C(26)-F(6)	1.341(3)
C(11)-C(12)	1.520(3)	C(26)-F(4)	1.345(3)
C(11)-H(11A)	0.9900	C(26)-Au(2)	2.089(3)
C(11)-H(11B)	0.9900	C(27)-C(28)	1.381(4)
C(12)-C(13)	1.532(3)	C(27)-C(32)	1.393(3)
C(12)-H(12A)	0.9900	C(27)-Au(2)	2.055(2)
C(12)-H(12B)	0.9900	C(28)-C(29)	1.393(4)
C(13)-H(13A)	0.9900	C(28)-H(28)	0.9500
C(13)-H(13B)	0.9900	C(29)-C(30)	1.384(4)
C(14)-C(19)	1.531(3)	C(29)-H(29)	0.9500
C(14)-C(15)	1.531(3)	C(30)-C(31)	1.379(4)
C(14)-P(1)	1.834(2)	C(30)-H(30)	0.9500
C(14)-H(14)	1.0000	C(31)-C(32)	1.391(4)
C(15)-C(16)	1.529(3)	C(31)-H(31)	0.9500
C(15)-H(15A)	0.9900	C(32)-H(32)	0.9500
C(15)-H(15B)	0.9900	C(33)-C(34)	1.524(4)
C(16)-C(17)	1.523(4)	C(33)-C(38)	1.535(4)
C(16)-H(16A)	0.9900	C(33)-P(6)	1.850(2)
C(16)-H(16B)	0.9900	C(33)-H(33)	1.0000
C(17)-C(18)	1.520(4)	C(34)-C(35)	1.533(4)
C(17)-H(17A)	0.9900	C(34)-H(34A)	0.9900

C(34)-H(34B)	0.9900	I(2)-Au(2)	2.6720(2)
C(35)-C(36)	1.522(4)		
C(35)-H(35A)	0.9900	F(3)-C(1)-F(1)	105.6(2)
C(35)-H(35B)	0.9900	F(3)-C(1)-F(2)	105.4(2)
C(36)-C(37)	1.511(4)	F(1)-C(1)-F(2)	102.7(2)
C(36)-H(36A)	0.9900	F(3)-C(1)-Au(1)	112.04(17)
C(36)-H(36B)	0.9900	F(1)-C(1)-Au(1)	117.27(17)
C(37)-C(38)	1.525(3)	F(2)-C(1)-Au(1)	112.73(17)
C(37)-H(37A)	0.9900	C(3)-C(2)-C(7)	119.7(2)
C(37)-H(37B)	0.9900	C(3)-C(2)-Au(1)	121.38(18)
C(38)-H(38A)	0.9900	C(7)-C(2)-Au(1)	118.87(18)
C(38)-H(38B)	0.9900	C(2)-C(3)-C(4)	120.3(2)
C(39)-C(44)	1.530(3)	C(2)-C(3)-H(3)	119.9
C(39)-C(40)	1.537(3)	C(4)-C(3)-H(3)	119.9
C(39)-P(6)	1.841(3)	C(5)-C(4)-C(3)	119.9(2)
C(39)-H(39)	1.0000	C(5)-C(4)-H(4)	120.0
C(40)-C(41)	1.530(4)	C(3)-C(4)-H(4)	120.0
C(40)-H(40A)	0.9900	C(6)-C(5)-C(4)	119.9(2)
C(40)-H(40B)	0.9900	C(6)-C(5)-H(5)	120.0
C(41)-C(42)	1.518(4)	C(4)-C(5)-H(5)	120.0
C(41)-H(41A)	0.9900	C(5)-C(6)-C(7)	120.3(2)
C(41)-H(41B)	0.9900	C(5)-C(6)-H(6)	119.9
C(42)-C(43)	1.522(4)	C(7)-C(6)-H(6)	119.9
C(42)-H(42A)	0.9900	C(2)-C(7)-C(6)	119.8(2)
C(42)-H(42B)	0.9900	C(2)-C(7)-H(7)	120.1
C(43)-C(44)	1.533(4)	C(6)-C(7)-H(7)	120.1
C(43)-H(43A)	0.9900	C(9)-C(8)-C(13)	109.96(19)
C(43)-H(43B)	0.9900	C(9)-C(8)-P(1)	116.52(16)
C(44)-H(44A)	0.9900	C(13)-C(8)-P(1)	111.98(16)
C(44)-H(44B)	0.9900	C(9)-C(8)-H(8)	105.8
C(45)-C(46)	1.505(4)	C(13)-C(8)-H(8)	105.8
C(45)-C(50)	1.535(3)	P(1)-C(8)-H(8)	105.8
C(45)-P(6)	1.836(3)	C(10)-C(9)-C(8)	110.1(2)
C(45)-H(45)	1.0000	C(10)-C(9)-H(9A)	109.6
C(46)-C(47)	1.538(4)	C(8)-C(9)-H(9A)	109.6
C(46)-H(46A)	0.9900	C(10)-C(9)-H(9B)	109.6
C(46)-H(46B)	0.9900	C(8)-C(9)-H(9B)	109.6
C(47)-C(48)	1.540(5)	H(9A)-C(9)-H(9B)	108.1
C(47)-H(47A)	0.9900	C(11)-C(10)-C(9)	112.1(2)
C(47)-H(47B)	0.9900	C(11)-C(10)-H(10A)	109.2
C(48)-C(49)	1.483(4)	C(9)-C(10)-H(10A)	109.2
C(48)-H(48A)	0.9900	C(11)-C(10)-H(10B)	109.2
C(48)-H(48B)	0.9900	C(9)-C(10)-H(10B)	109.2
C(49)-C(50)	1.511(4)	H(10A)-C(10)-H(10B)	107.9
C(49)-H(49A)	0.9900	C(12)-C(11)-C(10)	110.8(2)
C(49)-H(49B)	0.9900	C(12)-C(11)-H(11A)	109.5
C(50)-H(50A)	0.9900	C(10)-C(11)-H(11A)	109.5
C(50)-H(50B)	0.9900	C(12)-C(11)-H(11B)	109.5
P(1)-Au(1)	2.3926(6)	C(10)-C(11)-H(11B)	109.5
P(6)-Au(2)	2.3818(6)	H(11A)-C(11)-H(11B)	108.1
I(1)-Au(1)	2.6639(2)	C(11)-C(12)-C(13)	111.2(2)

C(11)-C(12)-H(12A)	109.4
C(13)-C(12)-H(12A)	109.4
C(11)-C(12)-H(12B)	109.4
C(13)-C(12)-H(12B)	109.4
H(12A)-C(12)-H(12B)	108.0
C(12)-C(13)-C(8)	110.09(19)
C(12)-C(13)-H(13A)	109.6
C(8)-C(13)-H(13A)	109.6
C(12)-C(13)-H(13B)	109.6
C(8)-C(13)-H(13B)	109.6
H(13A)-C(13)-H(13B)	108.2
C(19)-C(14)-C(15)	111.07(19)
C(19)-C(14)-P(1)	116.52(16)
C(15)-C(14)-P(1)	114.41(16)
C(19)-C(14)-H(14)	104.4
C(15)-C(14)-H(14)	104.4
P(1)-C(14)-H(14)	104.4
C(16)-C(15)-C(14)	109.5(2)
C(16)-C(15)-H(15A)	109.8
C(14)-C(15)-H(15A)	109.8
C(16)-C(15)-H(15B)	109.8
C(14)-C(15)-H(15B)	109.8
H(15A)-C(15)-H(15B)	108.2
C(17)-C(16)-C(15)	111.2(2)
C(17)-C(16)-H(16A)	109.4
C(15)-C(16)-H(16A)	109.4
C(17)-C(16)-H(16B)	109.4
C(15)-C(16)-H(16B)	109.4
H(16A)-C(16)-H(16B)	108.0
C(18)-C(17)-C(16)	112.1(2)
C(18)-C(17)-H(17A)	109.2
C(16)-C(17)-H(17A)	109.2
C(18)-C(17)-H(17B)	109.2
C(16)-C(17)-H(17B)	109.2
H(17A)-C(17)-H(17B)	107.9
C(17)-C(18)-C(19)	111.8(2)
C(17)-C(18)-H(18A)	109.3
C(19)-C(18)-H(18A)	109.3
C(17)-C(18)-H(18B)	109.3
C(19)-C(18)-H(18B)	109.3
H(18A)-C(18)-H(18B)	107.9
C(14)-C(19)-C(18)	108.46(19)
C(14)-C(19)-H(19A)	110.0
C(18)-C(19)-H(19A)	110.0
C(14)-C(19)-H(19B)	110.0
C(18)-C(19)-H(19B)	110.0
H(19A)-C(19)-H(19B)	108.4
C(21)-C(20)-C(25)	110.08(19)
C(21)-C(20)-P(1)	110.71(16)
C(25)-C(20)-P(1)	116.86(16)
C(21)-C(20)-H(20)	106.2
C(25)-C(20)-H(20)	106.2
P(1)-C(20)-H(20)	106.2
C(22)-C(21)-C(20)	110.7(2)
C(22)-C(21)-H(21A)	109.5
C(20)-C(21)-H(21A)	109.5
C(22)-C(21)-H(21B)	109.5
C(20)-C(21)-H(21B)	109.5
H(21A)-C(21)-H(21B)	108.1
C(21)-C(22)-C(23)	111.7(2)
C(21)-C(22)-H(22A)	109.3
C(23)-C(22)-H(22A)	109.3
C(21)-C(22)-H(22B)	109.3
C(23)-C(22)-H(22B)	109.3
H(22A)-C(22)-H(22B)	107.9
C(24)-C(23)-C(22)	110.9(2)
C(24)-C(23)-H(23A)	109.5
C(22)-C(23)-H(23A)	109.5
C(24)-C(23)-H(23B)	109.5
C(22)-C(23)-H(23B)	109.5
H(23A)-C(23)-H(23B)	108.0
C(23)-C(24)-C(25)	111.6(2)
C(23)-C(24)-H(24A)	109.3
C(25)-C(24)-H(24A)	109.3
C(23)-C(24)-H(24B)	109.3
C(25)-C(24)-H(24B)	109.3
H(24A)-C(24)-H(24B)	108.0
C(24)-C(25)-C(20)	108.59(19)
C(24)-C(25)-H(25A)	110.0
C(20)-C(25)-H(25A)	110.0
C(24)-C(25)-H(25B)	110.0
C(20)-C(25)-H(25B)	110.0
H(25A)-C(25)-H(25B)	108.4
F(5)-C(26)-F(6)	103.2(2)
F(5)-C(26)-F(4)	104.8(2)
F(6)-C(26)-F(4)	104.6(2)
F(5)-C(26)-Au(2)	114.32(18)
F(6)-C(26)-Au(2)	117.50(17)
F(4)-C(26)-Au(2)	111.14(17)
C(28)-C(27)-C(32)	119.8(2)
C(28)-C(27)-Au(2)	119.95(18)
C(32)-C(27)-Au(2)	119.82(19)
C(27)-C(28)-C(29)	120.0(2)
C(27)-C(28)-H(28)	120.0
C(29)-C(28)-H(28)	120.0
C(30)-C(29)-C(28)	120.3(3)
C(30)-C(29)-H(29)	119.9
C(28)-C(29)-H(29)	119.9
C(31)-C(30)-C(29)	119.6(3)
C(31)-C(30)-H(30)	120.2
C(29)-C(30)-H(30)	120.2
C(30)-C(31)-C(32)	120.5(3)

C(30)-C(31)-H(31)	119.7	C(39)-C(40)-H(40B)	109.9
C(32)-C(31)-H(31)	119.7	H(40A)-C(40)-H(40B)	108.3
C(27)-C(32)-C(31)	119.7(3)	C(42)-C(41)-C(40)	111.6(2)
C(27)-C(32)-H(32)	120.2	C(42)-C(41)-H(41A)	109.3
C(31)-C(32)-H(32)	120.2	C(40)-C(41)-H(41A)	109.3
C(34)-C(33)-C(38)	110.6(2)	C(42)-C(41)-H(41B)	109.3
C(34)-C(33)-P(6)	110.59(17)	C(40)-C(41)-H(41B)	109.3
C(38)-C(33)-P(6)	114.09(17)	H(41A)-C(41)-H(41B)	108.0
C(34)-C(33)-H(33)	107.1	C(41)-C(42)-C(43)	112.0(2)
C(38)-C(33)-H(33)	107.1	C(41)-C(42)-H(42A)	109.2
P(6)-C(33)-H(33)	107.1	C(43)-C(42)-H(42A)	109.2
C(33)-C(34)-C(35)	111.4(2)	C(41)-C(42)-H(42B)	109.2
C(33)-C(34)-H(34A)	109.3	C(43)-C(42)-H(42B)	109.2
C(35)-C(34)-H(34A)	109.3	H(42A)-C(42)-H(42B)	107.9
C(33)-C(34)-H(34B)	109.3	C(42)-C(43)-C(44)	111.8(2)
C(35)-C(34)-H(34B)	109.3	C(42)-C(43)-H(43A)	109.3
H(34A)-C(34)-H(34B)	108.0	C(44)-C(43)-H(43A)	109.3
C(36)-C(35)-C(34)	111.5(2)	C(42)-C(43)-H(43B)	109.3
C(36)-C(35)-H(35A)	109.3	C(44)-C(43)-H(43B)	109.3
C(34)-C(35)-H(35A)	109.3	H(43A)-C(43)-H(43B)	107.9
C(36)-C(35)-H(35B)	109.3	C(39)-C(44)-C(43)	108.9(2)
C(34)-C(35)-H(35B)	109.3	C(39)-C(44)-H(44A)	109.9
H(35A)-C(35)-H(35B)	108.0	C(43)-C(44)-H(44A)	109.9
C(37)-C(36)-C(35)	111.8(2)	C(39)-C(44)-H(44B)	109.9
C(37)-C(36)-H(36A)	109.3	C(43)-C(44)-H(44B)	109.9
C(35)-C(36)-H(36A)	109.3	H(44A)-C(44)-H(44B)	108.3
C(37)-C(36)-H(36B)	109.3	C(46)-C(45)-C(50)	110.4(2)
C(35)-C(36)-H(36B)	109.3	C(46)-C(45)-P(6)	119.9(2)
H(36A)-C(36)-H(36B)	107.9	C(50)-C(45)-P(6)	111.06(17)
C(36)-C(37)-C(38)	110.8(2)	C(46)-C(45)-H(45)	104.7
C(36)-C(37)-H(37A)	109.5	C(50)-C(45)-H(45)	104.7
C(38)-C(37)-H(37A)	109.5	P(6)-C(45)-H(45)	104.7
C(36)-C(37)-H(37B)	109.5	C(45)-C(46)-C(47)	109.5(3)
C(38)-C(37)-H(37B)	109.5	C(45)-C(46)-H(46A)	109.8
H(37A)-C(37)-H(37B)	108.1	C(47)-C(46)-H(46A)	109.8
C(37)-C(38)-C(33)	110.5(2)	C(45)-C(46)-H(46B)	109.8
C(37)-C(38)-H(38A)	109.5	C(47)-C(46)-H(46B)	109.8
C(33)-C(38)-H(38A)	109.5	H(46A)-C(46)-H(46B)	108.2
C(37)-C(38)-H(38B)	109.5	C(48)-C(47)-C(46)	110.3(3)
C(33)-C(38)-H(38B)	109.5	C(48)-C(47)-H(47A)	109.6
H(38A)-C(38)-H(38B)	108.1	C(46)-C(47)-H(47A)	109.6
C(44)-C(39)-C(40)	110.7(2)	C(48)-C(47)-H(47B)	109.6
C(44)-C(39)-P(6)	115.81(17)	C(46)-C(47)-H(47B)	109.6
C(40)-C(39)-P(6)	114.47(18)	H(47A)-C(47)-H(47B)	108.1
C(44)-C(39)-H(39)	104.8	C(49)-C(48)-C(47)	111.8(3)
C(40)-C(39)-H(39)	104.8	C(49)-C(48)-H(48A)	109.3
P(6)-C(39)-H(39)	104.8	C(47)-C(48)-H(48A)	109.3
C(41)-C(40)-C(39)	108.8(2)	C(49)-C(48)-H(48B)	109.3
C(41)-C(40)-H(40A)	109.9	C(47)-C(48)-H(48B)	109.3
C(39)-C(40)-H(40A)	109.9	H(48A)-C(48)-H(48B)	107.9
C(41)-C(40)-H(40B)	109.9	C(48)-C(49)-C(50)	110.7(3)

C(48)-C(49)-H(49A)	109.5	C(45)-P(6)-C(33)	106.82(11)
C(50)-C(49)-H(49A)	109.5	C(39)-P(6)-C(33)	104.84(11)
C(48)-C(49)-H(49B)	109.5	C(45)-P(6)-Au(2)	110.25(9)
C(50)-C(49)-H(49B)	109.5	C(39)-P(6)-Au(2)	111.97(8)
H(49A)-C(49)-H(49B)	108.1	C(33)-P(6)-Au(2)	111.66(8)
C(49)-C(50)-C(45)	110.8(2)	C(2)-Au(1)-C(1)	84.24(9)
C(49)-C(50)-H(50A)	109.5	C(2)-Au(1)-P(1)	91.02(6)
C(45)-C(50)-H(50A)	109.5	C(1)-Au(1)-P(1)	175.15(7)
C(49)-C(50)-H(50B)	109.5	C(2)-Au(1)-I(1)	175.33(7)
C(45)-C(50)-H(50B)	109.5	C(1)-Au(1)-I(1)	91.92(7)
H(50A)-C(50)-H(50B)	108.1	P(1)-Au(1)-I(1)	92.859(15)
C(14)-P(1)-C(20)	104.33(10)	C(27)-Au(2)-C(26)	84.83(10)
C(14)-P(1)-C(8)	112.06(11)	C(27)-Au(2)-P(6)	93.66(7)
C(20)-P(1)-C(8)	104.62(11)	C(26)-Au(2)-P(6)	177.72(8)
C(14)-P(1)-Au(1)	111.43(8)	C(27)-Au(2)-I(2)	173.78(6)
C(20)-P(1)-Au(1)	111.00(8)	C(26)-Au(2)-I(2)	89.36(7)
C(8)-P(1)-Au(1)	112.86(8)	P(6)-Au(2)-I(2)	92.211(16)
C(45)-P(6)-C(39)	111.06(12)		

Crystal Structure and Refinement Details for 3.3d

Table A38. Crystal data and structure refinement for **3.3d**

Identification code	shelx	
Empirical formula	C_{26} H_{40} Au F_3 I P	
Formula weight	764.41	
Temperature	100(2) K	
Wavelength	0.71073 Å	
Crystal system	Triclinic	
Space group	P -1	
Unit cell dimensions	a = 11.4612(6) Å	a= 83.4800(10)º.
	b = 14.5201(8) Å	b= 76.1610(10)º.
	c = 18.0799(10) Å	g = 71.1950(10)º.
Volume	2763.4(3) $Å^3$	
Z	4	
Density (calculated)	1.837 Mg/m^3	
Absorption coefficient	6.531 mm^{-1}	
F(000)	1480	
Crystal size	0.200 x 0.200 x 0.100 mm^3	
Theta range for data collection	1.483 to 25.357º.	
Index ranges	-13<=h<=13, -17<=k<=17, -21<=l<=21	
Reflections collected	74826	
Independent reflections	10116 [R(int) = 0.0206]	
Completeness to theta = 25.000∞	99.8 %	
Absorption correction	Semi-empirical from equivalents	
Max. and min. transmission	0.092 and 0.046	
Refinement method	Full-matrix least-squares on F^2	
Data / restraints / parameters	10116 / 0 / 579	
Goodness-of-fit on F^2	1.067	

Final R indices [I>2sigma(I)]	R1 = 0.0164, wR2 = 0.0394
R indices (all data)	R1 = 0.0175, wR2 = 0.0402
Extinction coefficient	n/a
Largest diff. peak and hole	1.109 and -0.572 e.Å^{-3}

Table A39. Atomic coordinates (x 10^4) and equivalent isotropic displacement parameters (Å^{2}x 10^3) for msw3161a. U(eq) is defined as one third of the trace of the orthogonalized U^{ij} tensor.

	x	y	z	U(eq)
C(1)				
C(2)	7536(3)	5013(2)	5450(2)	21(1)
C(3)	8478(3)	5220(2)	5700(2)	24(1)
C(4)	8201(3)	6069(2)	6084(2)	30(1)
C(5)	6987(3)	6718(2)	6232(2)	33(1)
C(6)	6047(3)	6501(2)	5988(2)	33(1)
C(7)	6318(3)	5657(2)	5596(2)	28(1)
C(8)	6697(4)	7651(2)	6634(2)	48(1)
C(9)	7160(2)	3432(2)	6790(1)	19(1)
C(10)	7533(3)	2883(2)	7517(2)	26(1)
C(11)	6933(3)	3541(2)	8201(2)	34(1)
C(12)	5511(3)	3942(2)	8300(2)	41(1)
C(13)	5161(3)	4497(2)	7579(2)	37(1)
C(14)	5717(3)	3845(2)	6897(2)	26(1)
C(15)	9428(2)	1990(2)	6000(1)	18(1)
C(16)	10016(2)	1120(2)	5480(2)	23(1)
C(17)	11291(3)	518(2)	5648(2)	28(1)
C(18)	12183(3)	1127(2)	5529(2)	31(1)
C(19)	11624(3)	1995(2)	6040(2)	30(1)
C(20)	10320(2)	2613(2)	5906(2)	23(1)
C(21)	6997(2)	1901(2)	5836(1)	17(1)
C(22)	6861(2)	1204(2)	6537(2)	20(1)
C(23)	6433(3)	384(2)	6348(2)	24(1)
C(24)	5234(3)	765(2)	6029(2)	26(1)
C(25)	5347(2)	1506(2)	5366(2)	22(1)
C(26)	5737(2)	2339(2)	5583(2)	22(1)
C(27)	2543(3)	-825(2)	918(2)	31(1)
C(28)	2297(3)	230(2)	-496(2)	22(1)
C(29)	3533(3)	-128(2)	-915(2)	28(1)
C(30)	3762(3)	-457(2)	-1644(2)	30(1)
C(31)	2779(3)	-452(2)	-1971(2)	30(1)
C(32)	1552(3)	-94(2)	-1552(2)	28(1)
C(33)	1307(3)	245(2)	-820(2)	24(1)
C(34)	3036(4)	-815(3)	-2762(2)	44(1)
C(35)	1616(2)	2531(2)	-820(1)	19(1)
C(36)	856(3)	3499(2)	-1151(2)	26(1)
C(37)	1078(3)	3440(2)	-2020(2)	32(1)
C(38)	2472(3)	3180(2)	-2401(2)	32(1)
C(39)	3234(3)	2243(2)	-2052(2)	30(1)
C(40)	3030(2)	2312(2)	-1191(2)	23(1)
C(41)	2219(2)	2974(2)	621(2)	22(1)

C(42)	3640(2)	2443(2)	542(2)	25(1)
C(43)	4151(3)	2926(2)	1047(2)	33(1)
C(44)	3930(3)	4000(2)	830(2)	42(1)
C(45)	2528(3)	4531(2)	869(2)	40(1)
C(46)	1994(3)	4053(2)	370(2)	29(1)
C(47)	-318(2)	2974(2)	590(2)	19(1)
C(48)	-690(3)	3207(3)	1425(2)	41(1)
C(49)	-2102(3)	3760(2)	1658(2)	32(1)
C(50)	-2889(3)	3199(3)	1478(2)	44(1)
C(51)	-2530(3)	2986(4)	637(3)	70(2)
C(52)	-1123(3)	2423(3)	396(2)	42(1)
F(1)	8455(2)	5563(1)	3958(1)	41(1)
F(2)	6862(2)	5256(2)	3743(1)	66(1)
F(3)	8743(2)	4474(1)	3209(1)	56(1)
F(4)	2903(3)	-1467(1)	363(1)	79(1)
F(5)	1611(2)	-1076(1)	1411(1)	53(1)
F(6)	3519(2)	-1093(1)	1263(1)	44(1)
P(1)	7842(1)	2761(1)	5902(1)	15(1)
P(2)	1371(1)	2344(1)	223(1)	17(1)
I(1)	8405(1)	2415(1)	3851(1)	32(1)
I(2)	1715(1)	1035(1)	2050(1)	32(1)
Au(1)	7950(1)	3829(1)	4802(1)	18(1)
Au(2)	1999(1)	655(1)	595(1)	19(1)

Table A40. Bond lengths [Å] and angles [º] for msw3161a.

C(1)-F(2)	1.340(3)	C(10)-H(10B)	0.9900
C(1)-F(1)	1.342(3)	C(11)-C(12)	1.516(5)
C(1)-F(3)	1.351(3)	C(11)-H(11A)	0.9900
C(1)-Au(1)	2.087(3)	C(11)-H(11B)	0.9900
C(2)-C(7)	1.390(4)	C(12)-C(13)	1.520(5)
C(2)-C(3)	1.390(4)	C(12)-H(12A)	0.9900
C(2)-Au(1)	2.055(3)	C(12)-H(12B)	0.9900
C(3)-C(4)	1.393(4)	C(13)-C(14)	1.524(4)
C(3)-H(3)	0.9500	C(13)-H(13A)	0.9900
C(4)-C(5)	1.389(4)	C(13)-H(13B)	0.9900
C(4)-H(4)	0.9500	C(14)-H(14A)	0.9900
C(5)-C(6)	1.390(5)	C(14)-H(14B)	0.9900
C(5)-C(8)	1.514(4)	C(15)-C(16)	1.533(3)
C(6)-C(7)	1.394(4)	C(15)-C(20)	1.540(4)
C(6)-H(6)	0.9500	C(15)-P(1)	1.840(2)
C(7)-H(7)	0.9500	C(15)-H(15)	1.0000
C(8)-H(8A)	0.9800	C(16)-C(17)	1.523(4)
C(8)-H(8B)	0.9800	C(16)-H(16A)	0.9900
C(8)-H(8C)	0.9800	C(16)-H(16B)	0.9900
C(9)-C(10)	1.535(4)	C(17)-C(18)	1.520(4)
C(9)-C(14)	1.538(4)	C(17)-H(17A)	0.9900
C(9)-P(1)	1.845(2)	C(17)-H(17B)	0.9900
C(9)-H(9)	1.0000	C(18)-C(19)	1.521(4)
C(10)-C(11)	1.534(4)	C(18)-H(18A)	0.9900
C(10)-H(10A)	0.9900	C(18)-H(18B)	0.9900

C(19)-C(20)	1.535(4)	C(37)-H(37B)	0.9900
C(19)-H(19A)	0.9900	C(38)-C(39)	1.522(4)
C(19)-H(19B)	0.9900	C(38)-H(38A)	0.9900
C(20)-H(20A)	0.9900	C(38)-H(38B)	0.9900
C(20)-H(20B)	0.9900	C(39)-C(40)	1.526(4)
C(21)-C(26)	1.534(3)	C(39)-H(39A)	0.9900
C(21)-C(22)	1.541(3)	C(39)-H(39B)	0.9900
C(21)-P(1)	1.839(2)	C(40)-H(40A)	0.9900
C(21)-H(21)	1.0000	C(40)-H(40B)	0.9900
C(22)-C(23)	1.525(4)	C(41)-C(46)	1.537(4)
C(22)-H(22A)	0.9900	C(41)-C(42)	1.539(4)
C(22)-H(22B)	0.9900	C(41)-P(2)	1.832(3)
C(23)-C(24)	1.530(4)	C(41)-H(41)	1.0000
C(23)-H(23A)	0.9900	C(42)-C(43)	1.529(4)
C(23)-H(23B)	0.9900	C(42)-H(42A)	0.9900
C(24)-C(25)	1.528(4)	C(42)-H(42B)	0.9900
C(24)-H(24A)	0.9900	C(43)-C(44)	1.517(5)
C(24)-H(24B)	0.9900	C(43)-H(43A)	0.9900
C(25)-C(26)	1.535(4)	C(43)-H(43B)	0.9900
C(25)-H(25A)	0.9900	C(44)-C(45)	1.530(4)
C(25)-H(25B)	0.9900	C(44)-H(44A)	0.9900
C(26)-H(26A)	0.9900	C(44)-H(44B)	0.9900
C(26)-H(26B)	0.9900	C(45)-C(46)	1.532(4)
C(27)-F(6)	1.337(3)	C(45)-H(45A)	0.9900
C(27)-F(5)	1.338(4)	C(45)-H(45B)	0.9900
C(27)-F(4)	1.347(4)	C(46)-H(46A)	0.9900
C(27)-Au(2)	2.092(3)	C(46)-H(46B)	0.9900
C(28)-C(33)	1.388(4)	C(47)-C(48)	1.513(4)
C(28)-C(29)	1.397(4)	C(47)-C(52)	1.520(4)
C(28)-Au(2)	2.052(3)	C(47)-P(2)	1.845(3)
C(29)-C(30)	1.389(4)	C(47)-H(47)	1.0000
C(29)-H(29)	0.9500	C(48)-C(49)	1.534(4)
C(30)-C(31)	1.390(4)	C(48)-H(48A)	0.9900
C(30)-H(30)	0.9500	C(48)-H(48B)	0.9900
C(31)-C(32)	1.389(4)	C(49)-C(50)	1.503(4)
C(31)-C(34)	1.510(4)	C(49)-H(49A)	0.9900
C(32)-C(33)	1.399(4)	C(49)-H(49B)	0.9900
C(32)-H(32)	0.9500	C(50)-C(51)	1.518(5)
C(33)-H(33)	0.9500	C(50)-H(50A)	0.9900
C(34)-H(34A)	0.9800	C(50)-H(50B)	0.9900
C(34)-H(34B)	0.9800	C(51)-C(52)	1.534(5)
C(34)-H(34C)	0.9800	C(51)-H(51A)	0.9900
C(35)-C(36)	1.537(3)	C(51)-H(51B)	0.9900
C(35)-C(40)	1.540(4)	C(52)-H(52A)	0.9900
C(35)-P(2)	1.842(3)	C(52)-H(52B)	0.9900
C(35)-H(35)	1.0000	P(1)-Au(1)	2.3844(6)
C(36)-C(37)	1.538(4)	P(2)-Au(2)	2.3882(6)
C(36)-H(36A)	0.9900	I(1)-Au(1)	2.6688(2)
C(36)-H(36B)	0.9900	I(2)-Au(2)	2.6701(2)
C(37)-C(38)	1.521(4)		
C(37)-H(37A)	0.9900	F(2)-C(1)-F(1)	106.0(2)

F(2)-C(1)-F(3)	104.8(2)	C(13)-C(12)-H(12B)	109.5
F(1)-C(1)-F(3)	102.0(2)	H(12A)-C(12)-H(12B)	108.1
F(2)-C(1)-Au(1)	110.22(19)	C(12)-C(13)-C(14)	110.8(3)
F(1)-C(1)-Au(1)	116.37(18)	C(12)-C(13)-H(13A)	109.5
F(3)-C(1)-Au(1)	116.32(19)	C(14)-C(13)-H(13A)	109.5
C(7)-C(2)-C(3)	119.2(2)	C(12)-C(13)-H(13B)	109.5
C(7)-C(2)-Au(1)	119.8(2)	C(14)-C(13)-H(13B)	109.5
C(3)-C(2)-Au(1)	120.9(2)	H(13A)-C(13)-H(13B)	108.1
C(2)-C(3)-C(4)	120.2(3)	C(13)-C(14)-C(9)	110.5(2)
C(2)-C(3)-H(3)	119.9	C(13)-C(14)-H(14A)	109.6
C(4)-C(3)-H(3)	119.9	C(9)-C(14)-H(14A)	109.6
C(5)-C(4)-C(3)	121.1(3)	C(13)-C(14)-H(14B)	109.6
C(5)-C(4)-H(4)	119.5	C(9)-C(14)-H(14B)	109.6
C(3)-C(4)-H(4)	119.5	H(14A)-C(14)-H(14B)	108.1
C(4)-C(5)-C(6)	118.5(3)	C(16)-C(15)-C(20)	111.0(2)
C(4)-C(5)-C(8)	120.9(3)	C(16)-C(15)-P(1)	115.28(17)
C(6)-C(5)-C(8)	120.7(3)	C(20)-C(15)-P(1)	110.36(17)
C(5)-C(6)-C(7)	120.9(3)	C(16)-C(15)-H(15)	106.6
C(5)-C(6)-H(6)	119.6	C(20)-C(15)-H(15)	106.6
C(7)-C(6)-H(6)	119.6	P(1)-C(15)-H(15)	106.6
C(2)-C(7)-C(6)	120.3(3)	C(17)-C(16)-C(15)	109.8(2)
C(2)-C(7)-H(7)	119.9	C(17)-C(16)-H(16A)	109.7
C(6)-C(7)-H(7)	119.9	C(15)-C(16)-H(16A)	109.7
C(5)-C(8)-H(8A)	109.5	C(17)-C(16)-H(16B)	109.7
C(5)-C(8)-H(8B)	109.5	C(15)-C(16)-H(16B)	109.7
H(8A)-C(8)-H(8B)	109.5	H(16A)-C(16)-H(16B)	108.2
C(5)-C(8)-H(8C)	109.5	C(18)-C(17)-C(16)	111.1(2)
H(8A)-C(8)-H(8C)	109.5	C(18)-C(17)-H(17A)	109.4
H(8B)-C(8)-H(8C)	109.5	C(16)-C(17)-H(17A)	109.4
C(10)-C(9)-C(14)	111.1(2)	C(18)-C(17)-H(17B)	109.4
C(10)-C(9)-P(1)	116.24(17)	C(16)-C(17)-H(17B)	109.4
C(14)-C(9)-P(1)	110.11(18)	H(17A)-C(17)-H(17B)	108.0
C(10)-C(9)-H(9)	106.2	C(17)-C(18)-C(19)	110.6(2)
C(14)-C(9)-H(9)	106.2	C(17)-C(18)-H(18A)	109.5
P(1)-C(9)-H(9)	106.2	C(19)-C(18)-H(18A)	109.5
C(11)-C(10)-C(9)	110.3(2)	C(17)-C(18)-H(18B)	109.5
C(11)-C(10)-H(10A)	109.6	C(19)-C(18)-H(18B)	109.5
C(9)-C(10)-H(10A)	109.6	H(18A)-C(18)-H(18B)	108.1
C(11)-C(10)-H(10B)	109.6	C(18)-C(19)-C(20)	111.0(2)
C(9)-C(10)-H(10B)	109.6	C(18)-C(19)-H(19A)	109.4
H(10A)-C(10)-H(10B)	108.1	C(20)-C(19)-H(19A)	109.4
C(12)-C(11)-C(10)	111.6(3)	C(18)-C(19)-H(19B)	109.4
C(12)-C(11)-H(11A)	109.3	C(20)-C(19)-H(19B)	109.4
C(10)-C(11)-H(11A)	109.3	H(19A)-C(19)-H(19B)	108.0
C(12)-C(11)-H(11B)	109.3	C(19)-C(20)-C(15)	111.2(2)
C(10)-C(11)-H(11B)	109.3	C(19)-C(20)-H(20A)	109.4
H(11A)-C(11)-H(11B)	108.0	C(15)-C(20)-H(20A)	109.4
C(11)-C(12)-C(13)	110.7(2)	C(19)-C(20)-H(20B)	109.4
C(11)-C(12)-H(12A)	109.5	C(15)-C(20)-H(20B)	109.4
C(13)-C(12)-H(12A)	109.5	H(20A)-C(20)-H(20B)	108.0
C(11)-C(12)-H(12B)	109.5	C(26)-C(21)-C(22)	110.7(2)

C(26)-C(21)-P(1)	116.18(17)	C(32)-C(31)-C(34)	120.9(3)
C(22)-C(21)-P(1)	114.71(17)	C(30)-C(31)-C(34)	121.0(3)
C(26)-C(21)-H(21)	104.6	C(31)-C(32)-C(33)	121.2(3)
C(22)-C(21)-H(21)	104.6	C(31)-C(32)-H(32)	119.4
P(1)-C(21)-H(21)	104.6	C(33)-C(32)-H(32)	119.4
C(23)-C(22)-C(21)	109.8(2)	C(28)-C(33)-C(32)	120.2(3)
C(23)-C(22)-H(22A)	109.7	C(28)-C(33)-H(33)	119.9
C(21)-C(22)-H(22A)	109.7	C(32)-C(33)-H(33)	119.9
C(23)-C(22)-H(22B)	109.7	C(31)-C(34)-H(34A)	109.5
C(21)-C(22)-H(22B)	109.7	C(31)-C(34)-H(34B)	109.5
H(22A)-C(22)-H(22B)	108.2	H(34A)-C(34)-H(34B)	109.5
C(22)-C(23)-C(24)	112.4(2)	C(31)-C(34)-H(34C)	109.5
C(22)-C(23)-H(23A)	109.1	H(34A)-C(34)-H(34C)	109.5
C(24)-C(23)-H(23A)	109.1	H(34B)-C(34)-H(34C)	109.5
C(22)-C(23)-H(23B)	109.1	C(36)-C(35)-C(40)	110.0(2)
C(24)-C(23)-H(23B)	109.1	C(36)-C(35)-P(2)	118.43(18)
H(23A)-C(23)-H(23B)	107.8	C(40)-C(35)-P(2)	111.05(18)
C(25)-C(24)-C(23)	112.2(2)	C(36)-C(35)-H(35)	105.4
C(25)-C(24)-H(24A)	109.2	C(40)-C(35)-H(35)	105.4
C(23)-C(24)-H(24A)	109.2	P(2)-C(35)-H(35)	105.4
C(25)-C(24)-H(24B)	109.2	C(35)-C(36)-C(37)	109.3(2)
C(23)-C(24)-H(24B)	109.2	C(35)-C(36)-H(36A)	109.8
H(24A)-C(24)-H(24B)	107.9	C(37)-C(36)-H(36A)	109.8
C(24)-C(25)-C(26)	111.5(2)	C(35)-C(36)-H(36B)	109.8
C(24)-C(25)-H(25A)	109.3	C(37)-C(36)-H(36B)	109.8
C(26)-C(25)-H(25A)	109.3	H(36A)-C(36)-H(36B)	108.3
C(24)-C(25)-H(25B)	109.3	C(38)-C(37)-C(36)	112.0(2)
C(26)-C(25)-H(25B)	109.3	C(38)-C(37)-H(37A)	109.2
H(25A)-C(25)-H(25B)	108.0	C(36)-C(37)-H(37A)	109.2
C(21)-C(26)-C(25)	108.4(2)	C(38)-C(37)-H(37B)	109.2
C(21)-C(26)-H(26A)	110.0	C(36)-C(37)-H(37B)	109.2
C(25)-C(26)-H(26A)	110.0	H(37A)-C(37)-H(37B)	107.9
C(21)-C(26)-H(26B)	110.0	C(37)-C(38)-C(39)	111.4(2)
C(25)-C(26)-H(26B)	110.0	C(37)-C(38)-H(38A)	109.4
H(26A)-C(26)-H(26B)	108.4	C(39)-C(38)-H(38A)	109.4
F(6)-C(27)-F(5)	105.6(2)	C(37)-C(38)-H(38B)	109.4
F(6)-C(27)-F(4)	103.4(3)	C(39)-C(38)-H(38B)	109.4
F(5)-C(27)-F(4)	103.9(3)	H(38A)-C(38)-H(38B)	108.0
F(6)-C(27)-Au(2)	113.5(2)	C(38)-C(39)-C(40)	110.9(2)
F(5)-C(27)-Au(2)	111.9(2)	C(38)-C(39)-H(39A)	109.5
F(4)-C(27)-Au(2)	117.31(19)	C(40)-C(39)-H(39A)	109.5
C(33)-C(28)-C(29)	118.8(2)	C(38)-C(39)-H(39B)	109.5
C(33)-C(28)-Au(2)	121.9(2)	C(40)-C(39)-H(39B)	109.5
C(29)-C(28)-Au(2)	119.2(2)	H(39A)-C(39)-H(39B)	108.0
C(30)-C(29)-C(28)	120.4(3)	C(39)-C(40)-C(35)	109.9(2)
C(30)-C(29)-H(29)	119.8	C(39)-C(40)-H(40A)	109.7
C(28)-C(29)-H(29)	119.8	C(35)-C(40)-H(40A)	109.7
C(29)-C(30)-C(31)	121.2(3)	C(39)-C(40)-H(40B)	109.7
C(29)-C(30)-H(30)	119.4	C(35)-C(40)-H(40B)	109.7
C(31)-C(30)-H(30)	119.4	H(40A)-C(40)-H(40B)	108.2
C(32)-C(31)-C(30)	118.1(3)	C(46)-C(41)-C(42)	110.5(2)

C(46)-C(41)-P(2)	115.27(18)
C(42)-C(41)-P(2)	114.77(18)
C(46)-C(41)-H(41)	105.0
C(42)-C(41)-H(41)	105.0
P(2)-C(41)-H(41)	105.0
C(43)-C(42)-C(41)	108.6(2)
C(43)-C(42)-H(42A)	110.0
C(41)-C(42)-H(42A)	110.0
C(43)-C(42)-H(42B)	110.0
C(41)-C(42)-H(42B)	110.0
H(42A)-C(42)-H(42B)	108.4
C(44)-C(43)-C(42)	111.4(3)
C(44)-C(43)-H(43A)	109.3
C(42)-C(43)-H(43A)	109.3
C(44)-C(43)-H(43B)	109.3
C(42)-C(43)-H(43B)	109.3
H(43A)-C(43)-H(43B)	108.0
C(43)-C(44)-C(45)	111.1(3)
C(43)-C(44)-H(44A)	109.4
C(45)-C(44)-H(44A)	109.4
C(43)-C(44)-H(44B)	109.4
C(45)-C(44)-H(44B)	109.4
H(44A)-C(44)-H(44B)	108.0
C(44)-C(45)-C(46)	111.1(3)
C(44)-C(45)-H(45A)	109.4
C(46)-C(45)-H(45A)	109.4
C(44)-C(45)-H(45B)	109.4
C(46)-C(45)-H(45B)	109.4
H(45A)-C(45)-H(45B)	108.0
C(45)-C(46)-C(41)	109.2(2)
C(45)-C(46)-H(46A)	109.8
C(41)-C(46)-H(46A)	109.8
C(45)-C(46)-H(46B)	109.8
C(41)-C(46)-H(46B)	109.8
H(46A)-C(46)-H(46B)	108.3
C(48)-C(47)-C(52)	111.6(3)
C(48)-C(47)-P(2)	115.79(19)
C(52)-C(47)-P(2)	110.21(18)
C(48)-C(47)-H(47)	106.2
C(52)-C(47)-H(47)	106.2
P(2)-C(47)-H(47)	106.2
C(47)-C(48)-C(49)	111.1(2)
C(47)-C(48)-H(48A)	109.4
C(49)-C(48)-H(48A)	109.4
C(47)-C(48)-H(48B)	109.4
C(49)-C(48)-H(48B)	109.4
H(48A)-C(48)-H(48B)	108.0
C(50)-C(49)-C(48)	111.0(3)
C(50)-C(49)-H(49A)	109.4
C(48)-C(49)-H(49A)	109.4
C(50)-C(49)-H(49B)	109.4
C(48)-C(49)-H(49B)	109.4
H(49A)-C(49)-H(49B)	108.0
C(49)-C(50)-C(51)	110.7(3)
C(49)-C(50)-H(50A)	109.5
C(51)-C(50)-H(50A)	109.5
C(49)-C(50)-H(50B)	109.5
C(51)-C(50)-H(50B)	109.5
H(50A)-C(50)-H(50B)	108.1
C(50)-C(51)-C(52)	111.0(3)
C(50)-C(51)-H(51A)	109.4
C(52)-C(51)-H(51A)	109.4
C(50)-C(51)-H(51B)	109.4
C(52)-C(51)-H(51B)	109.4
H(51A)-C(51)-H(51B)	108.0
C(47)-C(52)-C(51)	110.6(3)
C(47)-C(52)-H(52A)	109.5
C(51)-C(52)-H(52A)	109.5
C(47)-C(52)-H(52B)	109.5
C(51)-C(52)-H(52B)	109.5
H(52A)-C(52)-H(52B)	108.1
C(21)-P(1)-C(15)	104.88(11)
C(21)-P(1)-C(9)	111.33(12)
C(15)-P(1)-C(9)	105.29(12)
C(21)-P(1)-Au(1)	111.86(8)
C(15)-P(1)-Au(1)	111.03(8)
C(9)-P(1)-Au(1)	112.02(8)
C(41)-P(2)-C(35)	111.43(12)
C(41)-P(2)-C(47)	105.24(12)
C(35)-P(2)-C(47)	105.21(12)
C(41)-P(2)-Au(2)	109.58(9)
C(35)-P(2)-Au(2)	111.64(8)
C(47)-P(2)-Au(2)	113.52(9)
C(2)-Au(1)-C(1)	84.33(11)
C(2)-Au(1)-P(1)	92.18(7)
C(1)-Au(1)-P(1)	176.51(8)
C(2)-Au(1)-I(1)	174.31(7)
C(1)-Au(1)-I(1)	90.40(8)
P(1)-Au(1)-I(1)	93.085(16)
C(28)-Au(2)-C(27)	87.06(11)
C(28)-Au(2)-P(2)	92.78(7)
C(27)-Au(2)-P(2)	179.76(9)
C(28)-Au(2)-I(2)	174.65(7)
C(27)-Au(2)-I(2)	87.67(8)
P(2)-Au(2)-I(2)	92.483(16)

Crystal Structure and Refinement Details for 3.5a

Table A41. Crystal data and structure refinement for **3.5a**.

Identification code	MSW3127	
Empirical formula	$C_{25}H_{19}AuF_4IP \cdot CH_2Cl_2$	
Formula weight	835.16	
Temperature	100(2) K	
Wavelength	0.71073 Å	
Crystal system	Monoclinic	
Space group	P2(1)	
Unit cell dimensions	a = 10.0238(6) Å	a= 90º.
	b = 11.7238(7) Å	b= 111.701(2)º.
	c = 12.1838(8) Å	g = 90º.
Volume	1330.33(14) $Å^3$	
Z	2	
Density (calculated)	2.085 Mg/m^3	
Absorption coefficient	6.993 mm^{-1}	
F(000)	788	
Crystal size	0.15 x 0.08 x 0.04 mm^3	
Theta range for data collection	1.80 to 26.07º.	
Index ranges	-12<=h<=12, -14<=k<=14, -15<=l<=15	
Reflections collected	47270	
Independent reflections	4864 [R(int) = 0.0326]	
Completeness to theta = 25.00º	99.9 %	
Absorption correction	Semi-empirical from equivalents	
Max. and min. transmission	0.7673 and 0.4202	
Refinement method	Full-matrix least-squares on F^2	
Data / restraints / parameters	4864 / 7 / 316	
Goodness-of-fit on F^2	1.087	
Final R indices [I>2sigma(I)]	R1 = 0.0134, wR2 = 0.0320	
R indices (all data)	R1 = 0.0135, wR2 = 0.0321	
Absolute structure parameter	0.026(3)	
Largest diff. peak and hole	1.090 and -0.580 $Å^{-3}$	

Table A42. Atomic coordinates (x 10^4) and equivalent isotropic displacement parameters ($Å^2$x 10^3) for msw3137. U(eq) is defined as one third of the trace of the orthogonalized U^{ij} tensor.

C(1)	8456(4)	7257(3)	4124(3)	14(1)
C(2)	11513(3)	7136(3)	5002(3)	14(1)
C(3)	11981(3)	7690(3)	6094(3)	19(1)
C(4)	12963(4)	7143(4)	7088(3)	22(1)
C(5)	13434(4)	6080(3)	6952(3)	22(1)
C(6)	12987(4)	5503(3)	5890(3)	22(1)
C(7)	12011(4)	6055(3)	4913(3)	17(1)

C(8)	13633(3)	8839(3)	4442(3)	11(1)
C(9)	13834(4)	9853(3)	5087(3)	12(1)
C(10)	14958(4)	9940(3)	6178(3)	14(1)
C(11)	15887(4)	9035(3)	6614(3)	18(1)
C(12)	15709(3)	8031(4)	5972(3)	17(1)
C(13)	14580(3)	7936(4)	4895(2)	14(1)
C(14)	11653(3)	10052(3)	2423(3)	11(1)
C(15)	12250(4)	10387(3)	1613(3)	15(1)
C(16)	11969(4)	11477(3)	1120(3)	18(1)
C(17)	11107(4)	12213(3)	1432(3)	17(1)
C(18)	10504(4)	11884(3)	2244(3)	16(1)
C(19)	10772(4)	10805(3)	2742(3)	13(1)
C(20)	12532(3)	7705(3)	2159(2)	9(1)
C(21)	13857(3)	7830(4)	2017(2)	13(1)
C(22)	14169(4)	7146(3)	1226(3)	15(1)
C(23)	13202(4)	6318(3)	578(3)	19(1)
C(24)	11910(4)	6181(3)	730(3)	18(1)
C(25)	11577(4)	6874(3)	1516(3)	16(1)
C(26)	2706(4)	10210(3)	8266(3)	25(1)
F(1)	8696(2)	6096(2)	4374(2)	26(1)
F(2)	8615(2)	7740(2)	5142(2)	26(1)
F(3)	7152(2)	7338(2)	3411(2)	27(1)
F(4)	14407(2)	5557(2)	7924(2)	34(1)
P(1)	12037(1)	8651(1)	3116(1)	9(1)
I(1)	8152(1)	8608(1)	1481(1)	16(1)
Cl(1)	3948(1)	9462(1)	9458(1)	32(1)
Cl(2)	918(1)	9808(1)	8022(1)	31(1)
Au(1)	10079(1)	7888(1)	3525(1)	9(1)

Table A43. Bond lengths [Å] and angles [º] for msw3137.

C(1)-F(3)	1.277(4)	C(9)-H(9)	0.9500
C(1)-F(2)	1.319(4)	C(10)-C(11)	1.382(5)
C(1)-F(1)	1.396(4)	C(10)-H(10)	0.9500
C(1)-Au(1)	2.146(3)	C(11)-C(12)	1.387(5)
C(2)-C(7)	1.382(5)	C(11)-H(11)	0.9500
C(2)-C(3)	1.397(5)	C(12)-C(13)	1.385(4)
C(2)-Au(1)	2.041(3)	C(12)-H(12)	0.9500
C(3)-C(4)	1.402(5)	C(13)-H(13)	0.9500
C(3)-H(3)	0.9500	C(14)-C(15)	1.387(5)
C(4)-C(5)	1.364(6)	C(14)-C(19)	1.401(5)
C(4)-H(4)	0.9500	C(14)-P(1)	1.821(3)
C(5)-F(4)	1.369(4)	C(15)-C(16)	1.395(5)
C(5)-C(6)	1.380(6)	C(15)-H(15)	0.9500
C(6)-C(7)	1.389(5)	C(16)-C(17)	1.370(5)
C(6)-H(6)	0.9500	C(16)-H(16)	0.9500
C(7)-H(7)	0.9500	C(17)-C(18)	1.391(5)
C(8)-C(13)	1.392(5)	C(17)-H(17)	0.9500
C(8)-C(9)	1.399(5)	C(18)-C(19)	1.386(5)
C(8)-P(1)	1.818(3)	C(18)-H(18)	0.9500
C(9)-C(10)	1.393(5)	C(19)-H(19)	0.9500

C(20)-C(25)	1.387(5)
C(20)-C(21)	1.409(4)
C(20)-P(1)	1.806(3)
C(21)-C(22)	1.376(5)
C(21)-H(21)	0.9500
C(22)-C(23)	1.392(5)
C(22)-H(22)	0.9500
C(23)-C(24)	1.383(5)
C(23)-H(23)	0.9500
C(24)-C(25)	1.388(5)
C(24)-H(24)	0.9500
C(25)-H(25)	0.9500
C(26)-Cl(1)	1.758(4)
C(26)-Cl(2)	1.769(4)
C(26)-H(26A)	0.9900
C(26)-H(26B)	0.9900
P(1)-Au(1)	2.3717(8)
I(1)-Au(1)	2.6623(3)

F(3)-C(1)-F(2)	110.2(3)
F(3)-C(1)-F(1)	105.8(3)
F(2)-C(1)-F(1)	105.2(3)
F(3)-C(1)-Au(1)	117.2(2)
F(2)-C(1)-Au(1)	109.2(2)
F(1)-C(1)-Au(1)	108.6(2)
C(7)-C(2)-C(3)	119.8(3)
C(7)-C(2)-Au(1)	119.0(2)
C(3)-C(2)-Au(1)	121.2(3)
C(2)-C(3)-C(4)	119.4(4)
C(2)-C(3)-H(3)	120.3
C(4)-C(3)-H(3)	120.3
C(5)-C(4)-C(3)	118.5(3)
C(5)-C(4)-H(4)	120.7
C(3)-C(4)-H(4)	120.7
C(4)-C(5)-F(4)	118.1(3)
C(4)-C(5)-C(6)	123.6(3)
F(4)-C(5)-C(6)	118.2(3)
C(5)-C(6)-C(7)	117.2(3)
C(5)-C(6)-H(6)	121.4
C(7)-C(6)-H(6)	121.4
C(2)-C(7)-C(6)	121.4(3)
C(2)-C(7)-H(7)	119.3
C(6)-C(7)-H(7)	119.3
C(13)-C(8)-C(9)	119.2(3)
C(13)-C(8)-P(1)	120.5(3)
C(9)-C(8)-P(1)	119.9(2)
C(10)-C(9)-C(8)	119.7(3)
C(10)-C(9)-H(9)	120.1
C(8)-C(9)-H(9)	120.1
C(11)-C(10)-C(9)	120.2(3)
C(11)-C(10)-H(10)	119.9
C(9)-C(10)-H(10)	119.9
C(10)-C(11)-C(12)	120.5(3)
C(10)-C(11)-H(11)	119.8
C(12)-C(11)-H(11)	119.8
C(13)-C(12)-C(11)	119.5(3)
C(13)-C(12)-H(12)	120.2
C(11)-C(12)-H(12)	120.2
C(12)-C(13)-C(8)	120.8(4)
C(12)-C(13)-H(13)	119.6
C(8)-C(13)-H(13)	119.6
C(15)-C(14)-C(19)	120.0(3)
C(15)-C(14)-P(1)	120.8(3)
C(19)-C(14)-P(1)	119.1(3)
C(14)-C(15)-C(16)	119.6(3)
C(14)-C(15)-H(15)	120.2
C(16)-C(15)-H(15)	120.2
C(17)-C(16)-C(15)	120.3(3)
C(17)-C(16)-H(16)	119.8
C(15)-C(16)-H(16)	119.8
C(16)-C(17)-C(18)	120.5(3)
C(16)-C(17)-H(17)	119.8
C(18)-C(17)-H(17)	119.8
C(19)-C(18)-C(17)	119.9(3)
C(19)-C(18)-H(18)	120.0
C(17)-C(18)-H(18)	120.0
C(18)-C(19)-C(14)	119.6(3)
C(18)-C(19)-H(19)	120.2
C(14)-C(19)-H(19)	120.2
C(25)-C(20)-C(21)	119.2(3)
C(25)-C(20)-P(1)	119.9(3)
C(21)-C(20)-P(1)	120.8(2)
C(22)-C(21)-C(20)	119.7(3)
C(22)-C(21)-H(21)	120.2
C(20)-C(21)-H(21)	120.2
C(21)-C(22)-C(23)	120.8(3)
C(21)-C(22)-H(22)	119.6
C(23)-C(22)-H(22)	119.6
C(24)-C(23)-C(22)	119.7(3)
C(24)-C(23)-H(23)	120.1
C(22)-C(23)-H(23)	120.1
C(23)-C(24)-C(25)	120.0(3)
C(23)-C(24)-H(24)	120.0
C(25)-C(24)-H(24)	120.0
C(20)-C(25)-C(24)	120.6(3)
C(20)-C(25)-H(25)	119.7
C(24)-C(25)-H(25)	119.7
Cl(1)-C(26)-Cl(2)	111.7(2)
Cl(1)-C(26)-H(26A)	109.3
Cl(2)-C(26)-H(26A)	109.3
Cl(1)-C(26)-H(26B)	109.3
Cl(2)-C(26)-H(26B)	109.3

H(26A)-C(26)-H(26B)	107.9	C(2)-Au(1)-C(1)	85.80(12)
C(20)-P(1)-C(8)	106.62(14)	C(2)-Au(1)-P(1)	88.88(9)
C(20)-P(1)-C(14)	108.43(15)	C(1)-Au(1)-P(1)	172.74(9)
C(8)-P(1)-C(14)	105.59(15)	C(2)-Au(1)-I(1)	172.82(10)
C(20)-P(1)-Au(1)	110.48(11)	C(1)-Au(1)-I(1)	92.76(8)
C(8)-P(1)-Au(1)	112.55(11)	P(1)-Au(1)-I(1)	93.12(2)
C(14)-P(1)-Au(1)	112.84(11)		

Crystal Structure and Refinement Details for 3.5b

Table A44. Crystal data and structure refinement for **3.5b**.

Identification code	shelx	
Empirical formula	C26 H22 Au F3 I P	
Formula weight	746.27	
Temperature	100(2) K	
Wavelength	0.71073 Å	
Crystal system	Monoclinic	
Space group	P 21/n	
Unit cell dimensions	a = 11.3296(18) Å	a= 90º.
	b = 16.648(3) Å	b= 92.676(7)º.
	c = 14.015(2) Å	g = 90º.
Volume	2640.4(7) Å^3	
Z	4	
Density (calculated)	1.877 Mg/m^3	
Absorption coefficient	6.833 mm^{-1}	
F(000)	1408	
Crystal size	0.100 x 0.100 x 0.050 mm^3	
Theta range for data collection	1.901 to 25.452º.	
Index ranges	-13<=h<=13, -20<=k<=20, -16<=l<=16	
Reflections collected	47100	
Independent reflections	4857 [R(int) = 0.0622]	
Completeness to theta = 25.000∞	100.0 %	
Absorption correction	Semi-empirical from equivalents	
Max. and min. transmission	0.092 and 0.057	
Refinement method	Full-matrix least-squares on F^2	
Data / restraints / parameters	4857 / 0 / 290	
Goodness-of-fit on F^2	1.063	
Final R indices [I>2sigma(I)]	R1 = 0.0189, wR2 = 0.0454	
R indices (all data)	R1 = 0.0210, wR2 = 0.0465	
Extinction coefficient	n/a	
Largest diff. peak and hole	1.003 and -0.711 e.Å^{-3}	

Table A45. Atomic coordinates (x 10^4) and equivalent isotropic displacement parameters (Å^{2}x 10^3) for msw3164. U(eq) is defined as one third of the trace of the orthogonalized U^{ij} tensor.

	x	y	z	U(eq)

C(1)	7410(3)	5820(2)	5337(2)	32(1)
C(2)	9547(3)	6495(2)	4818(2)	23(1)
C(3)	9129(3)	7164(2)	4333(2)	31(1)
C(4)	9510(3)	7333(2)	3427(3)	37(1)
C(5)	10300(3)	6837(2)	2994(2)	36(1)
C(6)	10719(3)	6166(2)	3490(3)	34(1)
C(7)	10361(3)	5995(2)	4396(2)	28(1)
C(8)	10709(4)	7019(3)	2006(3)	54(1)
C(9)	11940(3)	6811(2)	6198(2)	23(1)
C(10)	11987(3)	7377(2)	5465(2)	33(1)
C(11)	12944(3)	7394(2)	4896(3)	40(1)
C(12)	13854(3)	6849(2)	5038(3)	40(1)
C(13)	13822(3)	6299(2)	5759(3)	39(1)
C(14)	12869(3)	6278(2)	6342(2)	27(1)
C(15)	10356(3)	7801(2)	7210(2)	28(1)
C(16)	9206(3)	8094(2)	7224(3)	38(1)
C(17)	9004(4)	8892(2)	7445(3)	49(1)
C(18)	9938(4)	9404(2)	7642(3)	50(1)
C(19)	11069(4)	9120(2)	7639(3)	49(1)
C(20)	11291(3)	8321(2)	7427(3)	41(1)
C(21)	11045(3)	6204(2)	7960(2)	29(1)
C(22)	11054(3)	5372(2)	7908(3)	38(1)
C(23)	11317(4)	4913(3)	8721(3)	58(1)
C(24)	11575(5)	5304(4)	9581(3)	78(2)
C(25)	11583(5)	6118(4)	9627(3)	70(2)
C(26)	11316(3)	6595(3)	8822(2)	45(1)
F(1)	7641(2)	5446(1)	4511(2)	44(1)
F(2)	6697(2)	6440(1)	5091(2)	51(1)
F(3)	6721(2)	5289(2)	5779(2)	52(1)
P(1)	10630(1)	6767(1)	6893(1)	22(1)
I(1)	7904(1)	5946(1)	7768(1)	32(1)
Au(1)	8906(1)	6222(1)	6116(1)	21(1)

Table A46. Bond lengths [Å] and angles [º] for msw3164.

C(1)-F(2)	1.345(4)		
C(1)-F(3)	1.349(4)	C(8)-H(8A)	0.9800
C(1)-F(1)	1.351(4)	C(8)-H(8B)	0.9800
C(1)-Au(1)	2.082(3)	C(8)-H(8C)	0.9800
C(2)-C(3)	1.378(4)	C(9)-C(14)	1.384(5)
C(2)-C(7)	1.395(5)	C(9)-C(10)	1.397(4)
C(2)-Au(1)	2.040(3)	C(9)-P(1)	1.814(3)
C(3)-C(4)	1.388(5)	C(10)-C(11)	1.375(5)
C(3)-H(3)	0.9500	C(10)-H(10)	0.9500
C(4)-C(5)	1.380(5)	C(11)-C(12)	1.380(5)
C(4)-H(4)	0.9500	C(11)-H(11)	0.9500
C(5)-C(6)	1.387(5)	C(12)-C(13)	1.366(5)
C(5)-C(8)	1.512(5)	C(12)-H(12)	0.9500
C(6)-C(7)	1.380(5)	C(13)-C(14)	1.384(5)
C(6)-H(6)	0.9500	C(13)-H(13)	0.9500
C(7)-H(7)	0.9500	C(14)-H(14)	0.9500

C(15)-C(20)	1.390(5)
C(15)-C(16)	1.393(5)
C(15)-P(1)	1.809(3)
C(16)-C(17)	1.384(5)
C(16)-H(16)	0.9500
C(17)-C(18)	1.377(6)
C(17)-H(17)	0.9500
C(18)-C(19)	1.365(6)
C(18)-H(18)	0.9500
C(19)-C(20)	1.389(6)
C(19)-H(19)	0.9500
C(20)-H(20)	0.9500
C(21)-C(22)	1.387(5)
C(21)-C(26)	1.393(5)
C(21)-P(1)	1.808(3)
C(22)-C(23)	1.394(5)
C(22)-H(22)	0.9500
C(23)-C(24)	1.389(7)
C(23)-H(23)	0.9500
C(24)-C(25)	1.357(8)
C(24)-H(24)	0.9500
C(25)-C(26)	1.401(6)
C(25)-H(25)	0.9500
C(26)-H(26)	0.9500
P(1)-Au(1)	2.3724(8)
I(1)-Au(1)	2.6666(4)

F(2)-C(1)-F(3)	105.5(3)
F(2)-C(1)-F(1)	105.8(3)
F(3)-C(1)-F(1)	103.3(3)
F(2)-C(1)-Au(1)	110.6(2)
F(3)-C(1)-Au(1)	116.4(2)
F(1)-C(1)-Au(1)	114.3(2)
C(3)-C(2)-C(7)	119.5(3)
C(3)-C(2)-Au(1)	119.4(2)
C(7)-C(2)-Au(1)	121.0(2)
C(2)-C(3)-C(4)	120.1(3)
C(2)-C(3)-H(3)	120.0
C(4)-C(3)-H(3)	120.0
C(5)-C(4)-C(3)	121.1(3)
C(5)-C(4)-H(4)	119.4
C(3)-C(4)-H(4)	119.4
C(4)-C(5)-C(6)	118.3(3)
C(4)-C(5)-C(8)	121.1(4)
C(6)-C(5)-C(8)	120.6(4)
C(7)-C(6)-C(5)	121.3(3)
C(7)-C(6)-H(6)	119.3
C(5)-C(6)-H(6)	119.3
C(6)-C(7)-C(2)	119.7(3)
C(6)-C(7)-H(7)	120.2
C(2)-C(7)-H(7)	120.2
C(5)-C(8)-H(8A)	109.5
C(5)-C(8)-H(8B)	109.5
H(8A)-C(8)-H(8B)	109.5
C(5)-C(8)-H(8C)	109.5
H(8A)-C(8)-H(8C)	109.5
H(8B)-C(8)-H(8C)	109.5
C(14)-C(9)-C(10)	119.0(3)
C(14)-C(9)-P(1)	122.1(2)
C(10)-C(9)-P(1)	118.9(2)
C(11)-C(10)-C(9)	119.9(3)
C(11)-C(10)-H(10)	120.1
C(9)-C(10)-H(10)	120.1
C(12)-C(11)-C(10)	120.5(3)
C(12)-C(11)-H(11)	119.8
C(10)-C(11)-H(11)	119.8
C(13)-C(12)-C(11)	120.1(4)
C(13)-C(12)-H(12)	120.0
C(11)-C(12)-H(12)	120.0
C(12)-C(13)-C(14)	120.2(4)
C(12)-C(13)-H(13)	119.9
C(14)-C(13)-H(13)	119.9
C(9)-C(14)-C(13)	120.4(3)
C(9)-C(14)-H(14)	119.8
C(13)-C(14)-H(14)	119.8
C(20)-C(15)-C(16)	118.9(3)
C(20)-C(15)-P(1)	120.6(3)
C(16)-C(15)-P(1)	120.6(3)
C(17)-C(16)-C(15)	120.2(4)
C(17)-C(16)-H(16)	119.9
C(15)-C(16)-H(16)	119.9
C(18)-C(17)-C(16)	120.3(4)
C(18)-C(17)-H(17)	119.8
C(16)-C(17)-H(17)	119.8
C(19)-C(18)-C(17)	119.9(4)
C(19)-C(18)-H(18)	120.1
C(17)-C(18)-H(18)	120.1
C(18)-C(19)-C(20)	120.7(4)
C(18)-C(19)-H(19)	119.6
C(20)-C(19)-H(19)	119.6
C(19)-C(20)-C(15)	120.0(4)
C(19)-C(20)-H(20)	120.0
C(15)-C(20)-H(20)	120.0
C(22)-C(21)-C(26)	120.7(3)
C(22)-C(21)-P(1)	118.4(3)
C(26)-C(21)-P(1)	120.9(3)
C(21)-C(22)-C(23)	120.4(4)
C(21)-C(22)-H(22)	119.8
C(23)-C(22)-H(22)	119.8
C(24)-C(23)-C(22)	118.7(5)
C(24)-C(23)-H(23)	120.6
C(22)-C(23)-H(23)	120.6

C(25)-C(24)-C(23)	120.7(4)	C(15)-P(1)-C(9)	104.32(15)
C(25)-C(24)-H(24)	119.7	C(21)-P(1)-Au(1)	111.03(12)
C(23)-C(24)-H(24)	119.7	C(15)-P(1)-Au(1)	109.26(11)
C(24)-C(25)-C(26)	121.8(5)	C(9)-P(1)-Au(1)	116.45(10)
C(24)-C(25)-H(25)	119.1	C(2)-Au(1)-C(1)	85.40(13)
C(26)-C(25)-H(25)	119.1	C(2)-Au(1)-P(1)	90.23(9)
C(21)-C(26)-C(25)	117.7(4)	C(1)-Au(1)-P(1)	174.85(10)
C(21)-C(26)-H(26)	121.2	C(2)-Au(1)-I(1)	174.99(9)
C(25)-C(26)-H(26)	121.2	C(1)-Au(1)-I(1)	91.77(10)
C(21)-P(1)-C(15)	109.34(16)	P(1)-Au(1)-I(1)	92.39(2)
C(21)-P(1)-C(9)	106.10(15)		

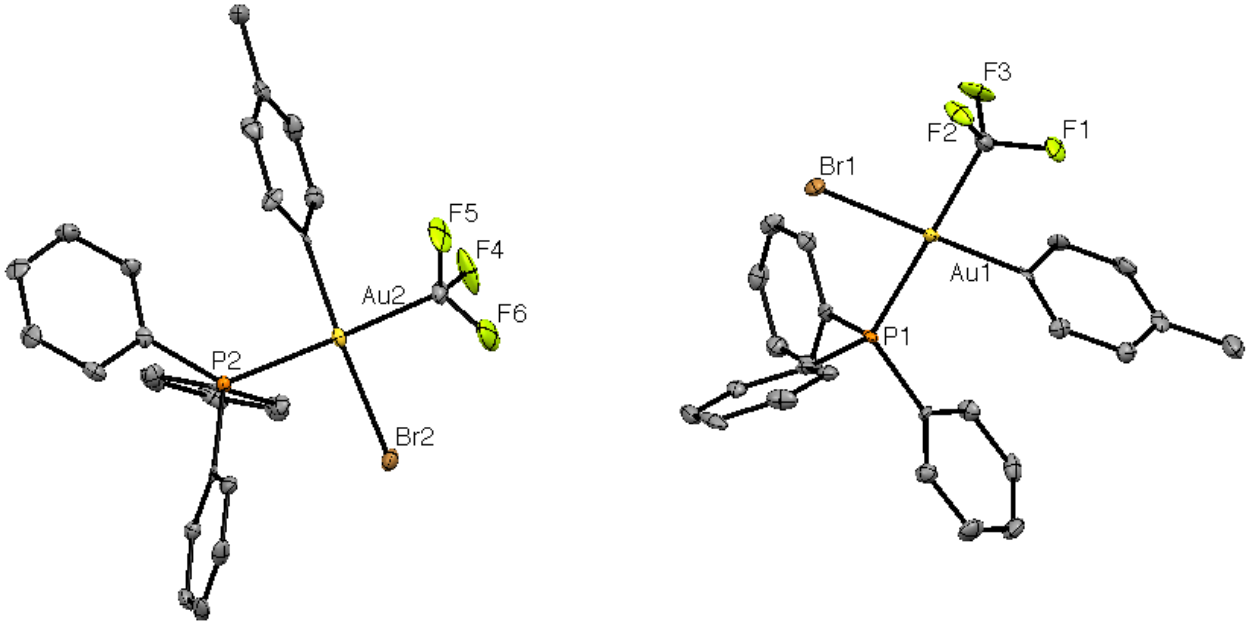

Figure A7. Thermal Ellipsoid Representation of **4.1-Br** at the 50% probability level and hydrogen atoms omitted for clarity.

Table A47. Crystal data and structure refinement for **4.1-Br**.

Identification code	shelx	
Empirical formula	C_{26} H_{22} Au Br F_3 P	
Formula weight	699.28	
Temperature	100(2) K	
Wavelength	0.71073 Å	
Crystal system	Triclinic	
Space group	P -1	
Unit cell dimensions	a = 9.8032(7) Å	α= 88.1550(10)º.
	b = 13.4073(9) Å	β= 89.724(2)º.
	c = 18.8219(13) Å	γ = 75.7450(10)º.
Volume	2396.4(3) $Å^3$	
Z	4	
Density (calculated)	1.938 Mg/m^3	
Absorption coefficient	7.908 mm^{-1}	
F(000)	1336	
Crystal size	0.200 x 0.100 x 0.080 mm^3	
Theta range for data collection	1.568 to 25.423º.	

Index ranges	-11<=h<=11, -16<=k<=16, 0<=l<=22
Reflections collected	8705
Independent reflections	8705 [R(int) = 0.0454]
Completeness to theta = 25.000∞	99.1 %
Absorption correction	Semi-empirical from equivalents
Max. and min. transmission	0.745212 and 0.632020
Refinement method	Full-matrix least-squares on F^2
Data / restraints / parameters	8705 / 18 / 580
Goodness-of-fit on F^2	1.060
Final R indices [I>2sigma(I)]	R1 = 0.0281, wR2 = 0.0724
R indices (all data)	R1 = 0.0298, wR2 = 0.0729
Extinction coefficient	n/a
Largest diff. peak and hole	1.395 and -1.826 e.$Å^{-3}$

Table A48. Atomic coordinates (x 10^4) and equivalent isotropic displacement parameters ($Å^2$x 10^3) for **4.1-Br**. U(eq) is defined as one third of the trace of the orthogonalized U^{ij} tensor.

	x	y	z	U(eq)
C(1)	7302(7)	9852(5)	3710(4)	17(2)
C(2)	7301(7)	8769(5)	5069(3)	11(1)
C(3)	8762(6)	8538(5)	5185(4)	14(2)
C(4)	9248(7)	8715(6)	5846(4)	20(2)
C(5)	8335(8)	9104(5)	6396(4)	17(2)
C(6)	6892(7)	9309(5)	6264(4)	16(2)
C(7)	6379(7)	9140(5)	5601(4)	14(1)
C(8)	8886(9)	9311(6)	7111(4)	29(2)
C(9)	7166(7)	5958(5)	4189(3)	13(1)
C(10)	7994(7)	6016(5)	3589(4)	14(1)
C(11)	8969(7)	5143(6)	3376(4)	17(2)
C(12)	9147(7)	4222(6)	3759(4)	19(2)
C(13)	8327(8)	4161(6)	4347(4)	20(2)
C(14)	7338(7)	5021(5)	4562(4)	17(2)
C(15)	4161(7)	7098(5)	4140(4)	13(1)
C(16)	3841(7)	6223(5)	3864(3)	15(1)
C(17)	2498(7)	6271(6)	3630(4)	21(2)
C(18)	1458(7)	7186(6)	3682(4)	22(2)
C(19)	1772(7)	8057(6)	3941(4)	22(2)
C(20)	3128(7)	8007(5)	4176(3)	15(2)
C(21)	5751(7)	6912(5)	5439(3)	11(1)
C(22)	4489(7)	7060(6)	5785(4)	16(2)
C(23)	4421(8)	6958(6)	6516(4)	23(2)
C(24)	5632(8)	6671(6)	6914(4)	22(2)
C(25)	6941(7)	6497(5)	6575(4)	20(2)
C(26)	7008(7)	6616(5)	5840(4)	16(2)
C(27)	2299(7)	4837(5)	1098(4)	18(2)
C(28)	2482(6)	3759(5)	-170(3)	11(1)
C(29)	3919(7)	3344(5)	-226(4)	17(2)
C(30)	4604(7)	3472(6)	-850(4)	20(2)

C(31)	3906(8)	4011(6)	-1436(4)	20(2)
C(32)	2466(7)	4418(6)	-1372(4)	21(2)
C(33)	1756(7)	4295(5)	-750(4)	16(1)
C(34)	4675(8)	4142(7)	-2115(4)	29(2)
C(35)	2235(6)	1042(5)	584(3)	12(1)
C(36)	3050(7)	1022(5)	1201(4)	14(1)
C(37)	4132(7)	189(6)	1356(4)	19(2)
C(38)	4436(7)	-648(6)	921(4)	20(2)
C(39)	3658(7)	-643(6)	313(4)	21(2)
C(40)	2554(7)	194(5)	145(4)	15(1)
C(41)	322(7)	2057(5)	-541(4)	12(1)
C(42)	1338(7)	2043(5)	-1069(4)	15(2)
C(43)	1026(8)	1907(6)	-1774(4)	21(2)
C(44)	-313(7)	1776(6)	-1944(4)	20(2)
C(45)	-1300(7)	1806(6)	-1432(4)	20(2)
C(46)	-1009(7)	1941(5)	-725(4)	15(1)
C(47)	-763(6)	1986(5)	875(3)	10(1)
C(48)	-1924(7)	2819(6)	909(3)	15(2)
C(49)	-3112(7)	2730(6)	1269(4)	18(2)
C(50)	-3133(7)	1820(6)	1628(4)	20(2)
C(51)	-1990(7)	984(5)	1610(4)	18(2)
C(52)	-793(7)	1068(5)	1226(4)	12(1)
F(1)	7478(5)	10501(3)	4210(2)	28(1)
F(2)	6488(4)	10441(3)	3211(2)	24(1)
F(3)	8574(4)	9494(3)	3410(3)	29(1)
F(4)	3672(4)	4495(4)	1266(3)	40(1)
F(5)	2207(6)	5595(3)	599(3)	39(1)
F(6)	1687(5)	5323(4)	1657(3)	39(1)
P(1)	5884(2)	7084(1)	4485(1)	9(1)
P(2)	779(2)	2148(1)	387(1)	10(1)
Br(1)	5637(1)	8385(1)	2867(1)	15(1)
Br(2)	575(1)	3377(1)	1982(1)	17(1)
Au(1)	6551(1)	8585(1)	4077(1)	9(1)
Au(2)	1510(1)	3610(1)	772(1)	11(1)

Table A49. Bond lengths [Å] and angles [º] for **1-Br**

C(1)-F(2)	1.339(8)	C(23)-H(23)	0.9500
C(1)-F(1)	1.343(8)	C(24)-C(25)	1.401(10)
C(1)-F(3)	1.349(8)	C(24)-H(24)	0.9500
C(1)-Au(1)	2.108(7)	C(25)-C(26)	1.390(10)
C(2)-C(7)	1.367(9)	C(25)-H(25)	0.9500
C(2)-C(3)	1.406(9)	C(26)-H(26)	0.9500
C(2)-Au(1)	2.055(6)	C(27)-F(6)	1.319(8)
C(3)-C(4)	1.382(10)	C(27)-F(4)	1.346(8)
C(3)-H(3)	0.9500	C(27)-F(5)	1.347(8)
C(4)-C(5)	1.393(10)	C(27)-Au(2)	2.093(7)
C(4)-H(4)	0.9500	C(28)-C(33)	1.385(9)
C(5)-C(6)	1.395(10)	C(28)-C(29)	1.386(9)
C(5)-C(8)	1.511(10)	C(28)-Au(2)	2.036(6)
C(6)-C(7)	1.394(10)	C(29)-C(30)	1.376(10)
C(6)-H(6)	0.9500	C(29)-H(29)	0.9500
C(7)-H(7)	0.9500	C(30)-C(31)	1.387(11)
C(8)-H(8A)	0.9800	C(30)-H(30)	0.9500
C(8)-H(8B)	0.9800	C(31)-C(32)	1.389(10)
C(8)-H(8C)	0.9800	C(31)-C(34)	1.507(10)
C(9)-C(14)	1.392(10)	C(32)-C(33)	1.385(10)
C(9)-C(10)	1.400(9)	C(32)-H(32)	0.9500
C(9)-P(1)	1.812(7)	C(33)-H(33)	0.9500
C(10)-C(11)	1.385(9)	C(34)-H(34A)	0.9800
C(10)-H(10)	0.9500	C(34)-H(34B)	0.9800
C(11)-C(12)	1.383(10)	C(34)-H(34C)	0.9800
C(11)-H(11)	0.9500	C(35)-C(40)	1.399(9)
C(12)-C(13)	1.377(10)	C(35)-C(36)	1.408(9)
C(12)-H(12)	0.9500	C(35)-P(2)	1.817(7)
C(13)-C(14)	1.381(10)	C(36)-C(37)	1.363(9)
C(13)-H(13)	0.9500	C(36)-H(36)	0.9500
C(14)-H(14)	0.9500	C(37)-C(38)	1.382(10)
C(15)-C(20)	1.382(9)	C(37)-H(37)	0.9500
C(15)-C(16)	1.403(9)	C(38)-C(39)	1.377(11)
C(15)-P(1)	1.809(7)	C(38)-H(38)	0.9500
C(16)-C(17)	1.377(9)	C(39)-C(40)	1.384(9)
C(16)-H(16)	0.9500	C(39)-H(39)	0.9500
C(17)-C(18)	1.395(10)	C(40)-H(40)	0.9500
C(17)-H(17)	0.9500	C(41)-C(46)	1.398(9)
C(18)-C(19)	1.383(10)	C(41)-C(42)	1.401(9)
C(18)-H(18)	0.9500	C(41)-P(2)	1.820(7)
C(19)-C(20)	1.388(9)	C(42)-C(43)	1.390(10)
C(19)-H(19)	0.9500	C(42)-H(42)	0.9500
C(20)-H(20)	0.9500	C(43)-C(44)	1.406(10)
C(21)-C(22)	1.369(9)	C(43)-H(43)	0.9500
C(21)-C(26)	1.413(9)	C(44)-C(45)	1.357(10)
C(21)-P(1)	1.811(7)	C(44)-H(44)	0.9500
C(22)-C(23)	1.381(10)	C(45)-C(46)	1.388(10)
C(22)-H(22)	0.9500	C(45)-H(45)	0.9500
C(23)-C(24)	1.373(10)	C(46)-H(46)	0.9500

C(47)-C(52)	1.384(9)
C(47)-C(48)	1.387(9)
C(47)-P(2)	1.820(7)
C(48)-C(49)	1.374(9)
C(48)-H(48)	0.9500
C(49)-C(50)	1.379(10)
C(49)-H(49)	0.9500
C(50)-C(51)	1.377(10)
C(50)-H(50)	0.9500
C(51)-C(52)	1.402(9)
C(51)-H(51)	0.9500
C(52)-H(52)	0.9500
P(1)-Au(1)	2.3682(16)
P(2)-Au(2)	2.3812(16)
Br(1)-Au(1)	2.4973(7)
Br(2)-Au(2)	2.4907(7)

F(2)-C(1)-F(1)	105.4(6)
F(2)-C(1)-F(3)	106.4(6)
F(1)-C(1)-F(3)	106.4(5)
F(2)-C(1)-Au(1)	113.9(4)
F(1)-C(1)-Au(1)	115.6(5)
F(3)-C(1)-Au(1)	108.5(4)
C(7)-C(2)-C(3)	120.8(6)
C(7)-C(2)-Au(1)	119.8(5)
C(3)-C(2)-Au(1)	119.3(5)
C(4)-C(3)-C(2)	118.5(6)
C(4)-C(3)-H(3)	120.7
C(2)-C(3)-H(3)	120.7
C(3)-C(4)-C(5)	122.0(6)
C(3)-C(4)-H(4)	119.0
C(5)-C(4)-H(4)	119.0
C(4)-C(5)-C(6)	117.9(6)
C(4)-C(5)-C(8)	121.2(6)
C(6)-C(5)-C(8)	120.9(7)
C(7)-C(6)-C(5)	121.1(7)
C(7)-C(6)-H(6)	119.4
C(5)-C(6)-H(6)	119.4
C(2)-C(7)-C(6)	119.6(6)
C(2)-C(7)-H(7)	120.2
C(6)-C(7)-H(7)	120.2
C(5)-C(8)-H(8A)	109.5
C(5)-C(8)-H(8B)	109.5
H(8A)-C(8)-H(8B)	109.5
C(5)-C(8)-H(8C)	109.5
H(8A)-C(8)-H(8C)	109.5
H(8B)-C(8)-H(8C)	109.5
C(14)-C(9)-C(10)	119.2(6)
C(14)-C(9)-P(1)	120.0(5)
C(10)-C(9)-P(1)	120.8(5)
C(11)-C(10)-C(9)	119.6(7)
C(11)-C(10)-H(10)	120.2
C(9)-C(10)-H(10)	120.2
C(12)-C(11)-C(10)	120.5(7)
C(12)-C(11)-H(11)	119.7
C(10)-C(11)-H(11)	119.7
C(13)-C(12)-C(11)	120.0(7)
C(13)-C(12)-H(12)	120.0
C(11)-C(12)-H(12)	120.0
C(12)-C(13)-C(14)	120.2(7)
C(12)-C(13)-H(13)	119.9
C(14)-C(13)-H(13)	119.9
C(13)-C(14)-C(9)	120.4(7)
C(13)-C(14)-H(14)	119.8
C(9)-C(14)-H(14)	119.8
C(20)-C(15)-C(16)	120.0(6)
C(20)-C(15)-P(1)	117.5(5)
C(16)-C(15)-P(1)	122.4(5)
C(17)-C(16)-C(15)	119.8(7)
C(17)-C(16)-H(16)	120.1
C(15)-C(16)-H(16)	120.1
C(16)-C(17)-C(18)	119.6(7)
C(16)-C(17)-H(17)	120.2
C(18)-C(17)-H(17)	120.2
C(19)-C(18)-C(17)	120.8(6)
C(19)-C(18)-H(18)	119.6
C(17)-C(18)-H(18)	119.6
C(18)-C(19)-C(20)	119.4(7)
C(18)-C(19)-H(19)	120.3
C(20)-C(19)-H(19)	120.3
C(15)-C(20)-C(19)	120.3(7)
C(15)-C(20)-H(20)	119.9
C(19)-C(20)-H(20)	119.9
C(22)-C(21)-C(26)	118.9(6)
C(22)-C(21)-P(1)	122.9(5)
C(26)-C(21)-P(1)	118.3(5)
C(21)-C(22)-C(23)	121.5(7)
C(21)-C(22)-H(22)	119.3
C(23)-C(22)-H(22)	119.3
C(24)-C(23)-C(22)	120.4(7)
C(24)-C(23)-H(23)	119.8
C(22)-C(23)-H(23)	119.8
C(23)-C(24)-C(25)	119.5(7)
C(23)-C(24)-H(24)	120.3
C(25)-C(24)-H(24)	120.3
C(26)-C(25)-C(24)	120.1(6)
C(26)-C(25)-H(25)	120.0
C(24)-C(25)-H(25)	120.0
C(25)-C(26)-C(21)	119.7(6)
C(25)-C(26)-H(26)	120.2
C(21)-C(26)-H(26)	120.2
F(6)-C(27)-F(4)	106.1(6)

F(6)-C(27)-F(5)	103.7(6)	C(43)-C(42)-H(42)	120.0
F(4)-C(27)-F(5)	106.7(6)	C(41)-C(42)-H(42)	120.0
F(6)-C(27)-Au(2)	115.9(5)	C(42)-C(43)-C(44)	119.0(7)
F(4)-C(27)-Au(2)	109.7(5)	C(42)-C(43)-H(43)	120.5
F(5)-C(27)-Au(2)	114.1(5)	C(44)-C(43)-H(43)	120.5
C(33)-C(28)-C(29)	119.0(6)	C(45)-C(44)-C(43)	120.7(7)
C(33)-C(28)-Au(2)	121.8(5)	C(45)-C(44)-H(44)	119.6
C(29)-C(28)-Au(2)	119.2(5)	C(43)-C(44)-H(44)	119.6
C(30)-C(29)-C(28)	120.0(7)	C(44)-C(45)-C(46)	121.1(6)
C(30)-C(29)-H(29)	120.0	C(44)-C(45)-H(45)	119.4
C(28)-C(29)-H(29)	120.0	C(46)-C(45)-H(45)	119.4
C(29)-C(30)-C(31)	122.2(6)	C(45)-C(46)-C(41)	119.3(6)
C(29)-C(30)-H(30)	118.9	C(45)-C(46)-H(46)	120.4
C(31)-C(30)-H(30)	118.9	C(41)-C(46)-H(46)	120.4
C(30)-C(31)-C(32)	117.0(7)	C(52)-C(47)-C(48)	119.5(6)
C(30)-C(31)-C(34)	121.5(7)	C(52)-C(47)-P(2)	121.9(5)
C(32)-C(31)-C(34)	121.5(7)	C(48)-C(47)-P(2)	118.6(5)
C(33)-C(32)-C(31)	121.7(7)	C(49)-C(48)-C(47)	120.5(7)
C(33)-C(32)-H(32)	119.2	C(49)-C(48)-H(48)	119.7
C(31)-C(32)-H(32)	119.2	C(47)-C(48)-H(48)	119.7
C(32)-C(33)-C(28)	120.1(6)	C(48)-C(49)-C(50)	119.9(7)
C(32)-C(33)-H(33)	119.9	C(48)-C(49)-H(49)	120.0
C(28)-C(33)-H(33)	119.9	C(50)-C(49)-H(49)	120.0
C(31)-C(34)-H(34A)	109.5	C(51)-C(50)-C(49)	120.8(6)
C(31)-C(34)-H(34B)	109.5	C(51)-C(50)-H(50)	119.6
H(34A)-C(34)-H(34B)	109.5	C(49)-C(50)-H(50)	119.6
C(31)-C(34)-H(34C)	109.5	C(50)-C(51)-C(52)	119.2(7)
H(34A)-C(34)-H(34C)	109.5	C(50)-C(51)-H(51)	120.4
H(34B)-C(34)-H(34C)	109.5	C(52)-C(51)-H(51)	120.4
C(40)-C(35)-C(36)	118.8(6)	C(47)-C(52)-C(51)	120.0(6)
C(40)-C(35)-P(2)	121.6(5)	C(47)-C(52)-H(52)	120.0
C(36)-C(35)-P(2)	119.6(5)	C(51)-C(52)-H(52)	120.0
C(37)-C(36)-C(35)	119.9(6)	C(15)-P(1)-C(21)	105.3(3)
C(37)-C(36)-H(36)	120.1	C(15)-P(1)-C(9)	110.1(3)
C(35)-C(36)-H(36)	120.1	C(21)-P(1)-C(9)	106.1(3)
C(36)-C(37)-C(38)	121.0(7)	C(15)-P(1)-Au(1)	109.6(2)
C(36)-C(37)-H(37)	119.5	C(21)-P(1)-Au(1)	116.3(2)
C(38)-C(37)-H(37)	119.5	C(9)-P(1)-Au(1)	109.3(2)
C(39)-C(38)-C(37)	120.2(6)	C(35)-P(2)-C(47)	108.8(3)
C(39)-C(38)-H(38)	119.9	C(35)-P(2)-C(41)	106.1(3)
C(37)-C(38)-H(38)	119.9	C(47)-P(2)-C(41)	104.2(3)
C(38)-C(39)-C(40)	119.9(7)	C(35)-P(2)-Au(2)	106.0(2)
C(38)-C(39)-H(39)	120.1	C(47)-P(2)-Au(2)	111.1(2)
C(40)-C(39)-H(39)	120.1	C(41)-P(2)-Au(2)	120.2(2)
C(39)-C(40)-C(35)	120.3(7)	C(2)-Au(1)-C(1)	88.3(3)
C(39)-C(40)-H(40)	119.8	C(2)-Au(1)-P(1)	90.77(18)
C(35)-C(40)-H(40)	119.8	C(1)-Au(1)-P(1)	175.67(19)
C(46)-C(41)-C(42)	119.8(6)	C(2)-Au(1)-Br(1)	179.24(18)
C(46)-C(41)-P(2)	120.4(5)	C(1)-Au(1)-Br(1)	91.0(2)
C(42)-C(41)-P(2)	119.7(5)	P(1)-Au(1)-Br(1)	89.94(4)
C(43)-C(42)-C(41)	120.1(6)	C(28)-Au(2)-C(27)	85.8(3)

C(28)-Au(2)-P(2)	92.07(18)	C(27)-Au(2)-P(2)	176.0(2)
C(28)-Au(2)-Br(2)	173.91(17)		
C(27)-Au(2)-Br(2)	91.5(2)		
P(2)-Au(2)-Br(2)	90.27(5)		

Table A50. Anisotropic displacement parameters ($Å^2$x 10^3)for **1-Br**. The anisotropic displacement factor exponent takes the form: $-2\pi^2[h^2a^{*2}U^{11} + ... + 2 h k a^* b^* U^{12}]$

	U^{11}	U^{22}	U^{33}	U^{23}	U^{13}	U^{12}
C(1)	21(4)	14(4)	20(4)	-2(3)	5(3)	-9(3)
C(2)	11(2)	10(2)	11(2)	0(1)	0(1)	-4(1)
C(3)	8(3)	19(4)	18(4)	-3(3)	5(3)	-5(3)
C(4)	14(3)	29(4)	21(4)	8(3)	-5(3)	-14(3)
C(5)	29(4)	10(4)	15(4)	5(3)	-6(3)	-10(3)
C(6)	19(4)	13(4)	15(4)	-3(3)	3(3)	-3(3)
C(7)	14(3)	12(4)	15(3)	0(3)	2(3)	-1(3)
C(8)	40(5)	28(4)	25(4)	1(4)	-4(4)	-22(4)
C(9)	10(3)	18(4)	12(4)	-2(3)	-2(3)	-7(3)
C(10)	14(3)	11(3)	17(4)	0(3)	0(3)	-2(3)
C(11)	11(3)	23(4)	16(4)	-1(3)	1(3)	-1(3)
C(12)	19(4)	17(4)	19(4)	-4(3)	-3(3)	1(3)
C(13)	25(4)	17(4)	19(4)	0(3)	2(3)	-7(3)
C(14)	11(3)	16(4)	24(4)	0(3)	3(3)	-3(3)
C(15)	12(3)	16(4)	11(3)	2(3)	3(3)	-6(3)
C(16)	20(3)	13(3)	12(3)	3(3)	-1(3)	-5(3)
C(17)	25(4)	25(4)	19(4)	4(3)	-5(3)	-17(3)
C(18)	18(4)	31(4)	21(4)	18(3)	-9(3)	-15(3)
C(19)	13(3)	25(4)	25(4)	9(3)	1(3)	-1(3)
C(20)	18(4)	16(4)	12(4)	3(3)	4(3)	-7(3)
C(21)	18(3)	12(3)	4(3)	-1(3)	1(3)	-7(3)
C(22)	14(3)	20(4)	15(4)	1(3)	0(3)	-4(3)
C(23)	25(4)	24(4)	18(4)	-6(3)	10(3)	-3(3)
C(24)	33(4)	24(4)	9(4)	1(3)	0(3)	-10(3)
C(25)	23(4)	14(4)	21(4)	-1(3)	-10(3)	-3(3)
C(26)	12(3)	17(4)	18(4)	3(3)	-2(3)	-3(3)
C(27)	27(4)	11(4)	16(4)	-2(3)	-2(3)	-7(3)
C(28)	11(2)	10(2)	12(2)	-1(1)	0(1)	-4(1)
C(29)	19(4)	16(4)	16(4)	-2(3)	-3(3)	-5(3)
C(30)	12(3)	21(4)	26(4)	-8(3)	-1(3)	-3(3)
C(31)	26(4)	18(4)	21(4)	-6(3)	2(3)	-15(3)
C(32)	24(4)	15(4)	24(4)	3(3)	-5(3)	-8(3)
C(33)	16(3)	15(4)	12(4)	2(3)	-3(3)	2(3)
C(34)	42(5)	37(5)	18(4)	-10(4)	10(4)	-28(4)
C(35)	11(3)	14(3)	13(4)	3(3)	5(3)	-8(3)
C(36)	17(3)	14(3)	10(4)	2(3)	-4(3)	-3(3)
C(37)	13(3)	22(4)	22(4)	4(3)	-6(3)	-4(3)
C(38)	10(3)	10(4)	39(5)	8(3)	0(3)	-1(3)
C(39)	13(3)	18(4)	34(5)	-5(3)	5(3)	-6(3)
C(40)	12(3)	13(3)	19(4)	-5(3)	2(3)	0(3)
C(41)	13(3)	7(3)	13(4)	0(3)	-2(3)	0(3)

C(42)	13(3)	16(4)	18(4)	-3(3)	5(3)	-4(3)
C(43)	21(4)	25(4)	20(4)	-2(3)	7(3)	-10(3)
C(44)	27(4)	21(4)	10(4)	6(3)	-5(3)	-5(3)
C(45)	21(4)	26(4)	15(4)	5(3)	-9(3)	-9(3)
C(46)	12(3)	12(3)	22(4)	4(3)	1(3)	-3(3)
C(47)	10(2)	11(2)	10(2)	-1(1)	-1(1)	-3(1)
C(48)	15(3)	22(4)	9(3)	0(3)	-1(3)	-7(3)
C(49)	10(3)	23(4)	20(4)	-12(3)	3(3)	0(3)
C(50)	12(3)	29(4)	23(4)	-14(3)	5(3)	-10(3)
C(51)	24(4)	14(4)	18(4)	-3(3)	-1(3)	-12(3)
C(52)	13(3)	12(3)	12(3)	-2(3)	0(3)	-2(3)
F(1)	48(3)	17(2)	25(3)	-1(2)	-1(2)	-21(2)
F(2)	22(2)	17(2)	34(3)	13(2)	-9(2)	-7(2)
F(3)	14(2)	24(2)	48(3)	4(2)	16(2)	-6(2)
F(4)	19(2)	28(3)	73(4)	-16(3)	-21(2)	-5(2)
F(5)	76(4)	13(2)	36(3)	5(2)	-14(3)	-24(2)
F(6)	50(3)	29(3)	48(3)	-24(2)	16(2)	-24(2)
P(1)	10(1)	8(1)	10(1)	2(1)	0(1)	-5(1)
P(2)	10(1)	9(1)	11(1)	-2(1)	0(1)	-4(1)
Br(1)	18(1)	16(1)	10(1)	2(1)	-1(1)	-5(1)
Br(2)	22(1)	19(1)	12(1)	-4(1)	-1(1)	-6(1)
Au(1)	9(1)	9(1)	10(1)	0(1)	2(1)	-3(1)
Au(2)	10(1)	8(1)	14(1)	-1(1)	-2(1)	-2(1)

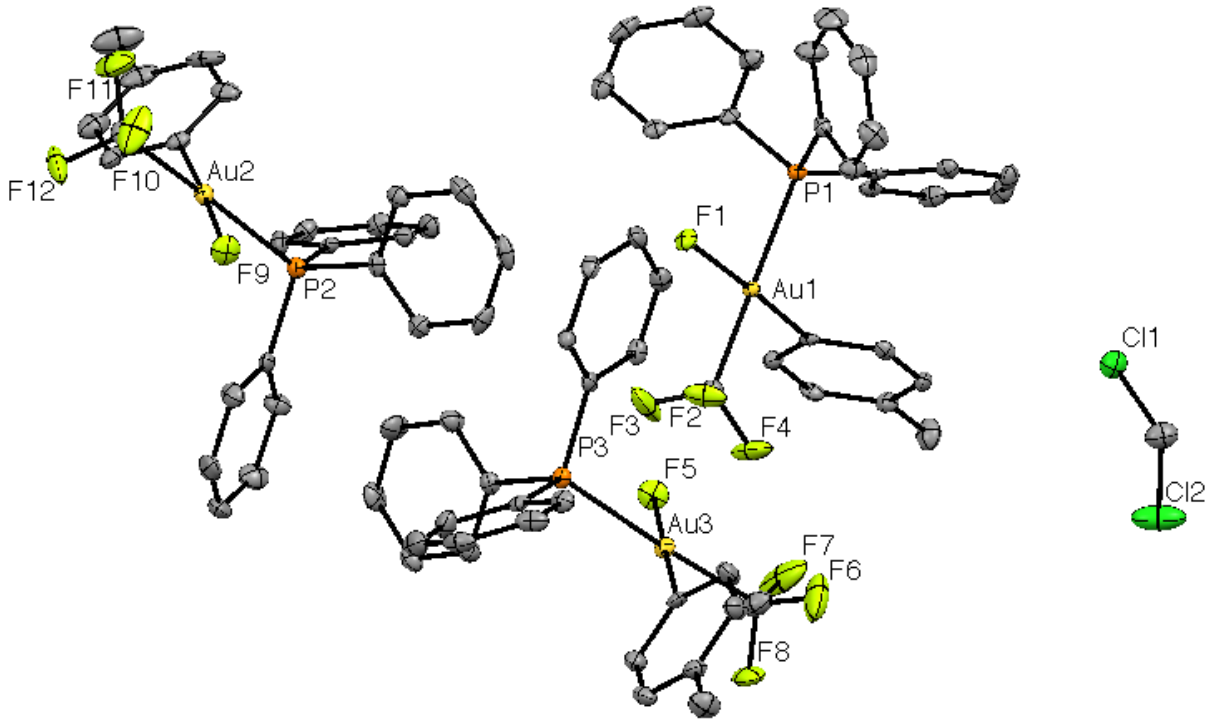

Figure A8. Thermal Ellipsoid Representation of **4.1-F** at the 50% Probability Level; hydrogen atoms omitted for clarity.

Table A51. Crystal data and structure refinement for **4.1-F**.

Identification code	shelx	
Empirical formula	$C_{26.33}$ $H_{22.67}$ Au $Cl_{0.67}$ F_4 P	
Formula weight	666.68	
Temperature	100(2) K	
Wavelength	0.71073 Å	
Crystal system	Triclinic	
Space group	P -1	
Unit cell dimensions	a = 12.8381(10) Å	α= 84.519(3)º.
	b = 13.7456(10) Å	β= 80.511(3)º.
	c = 23.3799(16) Å	γ = 64.036(3)º.
Volume	3657.4(5) $Å^3$	
Z	6	
Density (calculated)	1.816 Mg/m^3	
Absorption coefficient	6.215 mm^{-1}	
F(000)	1932	
Crystal size	0.100 x 0.060 x 0.040 mm^3	
Theta range for data collection	0.883 to 25.400º.	
Index ranges	-15<=h<=15, -16<=k<=16, -28<=l<=28	
Reflections collected	95920	
Independent reflections	13408 [R(int) = 0.0448]	
Completeness to theta = 25.000∞	99.9 %	
Absorption correction	Multi_scan	
Max. and min. transmission	0.7452 and 0.6140	
Refinement method	Full-matrix least-squares on F^2	
Data / restraints / parameters	13408 / 0 / 895	
Goodness-of-fit on F^2	1.019	
Final R indices [I>2sigma(I)]	R1 = 0.0218, wR2 = 0.0396	
R indices (all data)	R1 = 0.0300, wR2 = 0.0419	
Extinction coefficient	n/a	
Largest diff. peak and hole	0.874 and -0.994 $e.Å^{-3}$	

Table A52. Atomic coordinates (x 10^4) and equivalent isotropic displacement parameters ($Å^2$x 10^3) for **1-F**. U(eq) is defined as one third of the trace of the orthogonalized U^{ij} tensor.

	x	y	z	U(eq)
C(1)	7118(3)	4802(3)	791(1)	15(1)
C(2)	4687(3)	5340(2)	1117(1)	10(1)
C(3)	4643(3)	5013(3)	1699(1)	15(1)
C(4)	3978(3)	4457(3)	1920(1)	16(1)
C(5)	3347(3)	4219(3)	1576(1)	16(1)
C(6)	3404(3)	4546(3)	993(1)	14(1)
C(7)	4066(3)	5101(3)	769(1)	13(1)
C(8)	2601(3)	3647(3)	1827(2)	28(1)
C(9)	2546(3)	7669(2)	885(1)	12(1)
C(10)	2054(3)	7389(3)	1418(1)	14(1)
C(11)	1094(3)	7170(3)	1440(2)	19(1)
C(12)	639(3)	7200(3)	939(2)	21(1)
C(13)	1133(3)	7470(3)	411(2)	19(1)
C(14)	2082(3)	7707(3)	383(1)	14(1)
C(15)	3677(3)	8689(3)	1430(1)	13(1)
C(16)	2558(3)	9448(3)	1648(1)	19(1)
C(17)	2428(3)	10099(3)	2098(2)	24(1)
C(18)	3386(4)	10003(3)	2333(2)	25(1)
C(19)	4489(3)	9258(3)	2118(1)	22(1)
C(20)	4642(3)	8597(3)	1668(1)	16(1)
C(21)	4024(3)	8564(3)	168(1)	13(1)
C(22)	4584(3)	7973(3)	-330(1)	21(1)
C(23)	4698(3)	8505(3)	-854(2)	26(1)
C(24)	4274(3)	9609(3)	-876(2)	28(1)
C(25)	3746(4)	10203(3)	-382(2)	32(1)
C(26)	3613(3)	9679(3)	141(2)	26(1)
C(27)	10589(3)	9155(3)	3532(2)	21(1)
C(28)	8749(3)	8853(3)	4273(1)	16(1)
C(29)	7568(3)	9495(3)	4281(2)	23(1)
C(30)	6885(4)	9931(3)	4810(2)	32(1)
C(31)	7376(4)	9714(3)	5322(2)	32(1)
C(32)	8554(4)	9077(3)	5297(2)	30(1)
C(33)	9241(3)	8653(3)	4783(2)	21(1)
C(34)	6636(4)	10194(4)	5890(2)	51(1)
C(35)	7598(3)	7116(3)	3986(1)	12(1)
C(36)	6652(3)	7148(3)	3757(1)	15(1)
C(37)	5667(3)	7198(3)	4123(2)	20(1)
C(38)	5622(3)	7224(3)	4715(2)	19(1)
C(39)	6546(3)	7211(3)	4949(2)	20(1)
C(40)	7536(3)	7158(3)	4586(1)	16(1)
C(41)	8662(3)	6930(3)	2788(1)	14(1)
C(42)	8873(3)	5991(3)	2518(1)	16(1)
C(43)	8552(3)	6051(3)	1973(1)	21(1)
C(44)	8018(3)	7045(3)	1697(2)	22(1)
C(45)	7825(3)	7980(3)	1956(2)	23(1)
C(46)	8149(3)	7927(3)	2499(1)	18(1)

C(47)	9980(3)	5548(3)	3693(1)	14(1)
C(48)	9629(3)	4868(3)	4078(2)	20(1)
C(49)	10439(3)	3832(3)	4203(2)	27(1)
C(50)	11590(3)	3460(3)	3952(2)	26(1)
C(51)	11937(3)	4127(3)	3568(2)	26(1)
C(52)	11145(3)	5169(3)	3439(2)	22(1)
C(53)	5127(3)	1293(3)	3001(2)	28(1)
C(54)	7107(3)	1562(3)	2465(1)	16(1)
C(55)	6844(3)	1938(3)	1912(2)	23(1)
C(56)	7670(3)	1491(3)	1433(2)	24(1)
C(57)	8758(3)	656(3)	1489(2)	18(1)
C(58)	9009(3)	274(3)	2045(2)	20(1)
C(59)	8194(3)	727(3)	2531(2)	18(1)
C(60)	9636(3)	201(3)	958(2)	29(1)
C(61)	8155(3)	3176(3)	2949(1)	14(1)
C(62)	8283(3)	3216(3)	2343(2)	18(1)
C(63)	9375(3)	3022(3)	2030(2)	23(1)
C(64)	10309(3)	2795(3)	2313(2)	26(1)
C(65)	10187(3)	2761(3)	2909(2)	27(1)
C(66)	9112(3)	2951(3)	3230(2)	23(1)
C(67)	5739(3)	4794(3)	3153(1)	13(1)
C(68)	4531(3)	5136(3)	3300(1)	16(1)
C(69)	3767(3)	6179(3)	3142(1)	19(1)
C(70)	4197(3)	6872(3)	2846(2)	21(1)
C(71)	5394(3)	6540(3)	2704(1)	17(1)
C(72)	6162(3)	5504(3)	2855(1)	15(1)
C(73)	6866(3)	3350(3)	4099(1)	14(1)
C(74)	6521(3)	4277(3)	4413(1)	21(1)
C(75)	6705(3)	4193(3)	4985(2)	27(1)
C(76)	7241(3)	3179(3)	5244(2)	24(1)
C(77)	7582(3)	2259(3)	4936(2)	21(1)
C(78)	7393(3)	2340(3)	4366(1)	17(1)
C(79)	1080(4)	3457(3)	248(2)	28(1)
F(1)	6552(2)	7078(2)	595(1)	17(1)
F(2)	7909(2)	4809(2)	334(1)	34(1)
F(3)	7650(2)	4651(2)	1257(1)	50(1)
F(4)	7054(2)	3865(2)	742(1)	41(1)
F(5)	4710(2)	2938(2)	3847(1)	25(1)
F(6)	4903(3)	1357(2)	2445(1)	63(1)
F(7)	4082(2)	1574(2)	3305(2)	70(1)
F(8)	5738(2)	233(2)	3097(1)	38(1)
F(9)	10888(2)	7390(2)	2835(1)	25(1)
F(10)	11101(2)	9275(2)	3002(1)	50(1)
F(11)	9906(2)	10172(2)	3696(1)	49(1)
F(12)	11446(2)	8770(2)	3862(1)	48(1)
P(1)	3879(1)	7839(1)	841(1)	11(1)
P(2)	8954(1)	6913(1)	3520(1)	13(1)
P(3)	6728(1)	3416(1)	3338(1)	12(1)
Au(1)	5598(1)	6208(1)	831(1)	10(1)
Au(2)	9786(1)	8138(1)	3545(1)	13(1)
Au(3)	5922(1)	2245(1)	3156(1)	14(1)

Cl(1)	563(1)	4510(1)	747(1)	26(1)
Cl(2)	1313(1)	2210(1)	608(1)	52(1)

Table A53. Bond lengths [Å] and angles [º] for **1-F**.

C(1)-F(3)	1.333(4)	C(21)-C(22)	1.388(5)
C(1)-F(4)	1.343(4)	C(21)-P(1)	1.807(3)
C(1)-F(2)	1.350(4)	C(22)-C(23)	1.387(5)
C(1)-Au(1)	2.054(3)	C(22)-H(22)	0.9500
C(2)-C(7)	1.378(5)	C(23)-C(24)	1.368(5)
C(2)-C(3)	1.391(4)	C(23)-H(23)	0.9500
C(2)-Au(1)	2.012(3)	C(24)-C(25)	1.377(5)
C(3)-C(4)	1.390(5)	C(24)-H(24)	0.9500
C(3)-H(3)	0.9500	C(25)-C(26)	1.383(5)
C(4)-C(5)	1.381(5)	C(25)-H(25)	0.9500
C(4)-H(4)	0.9500	C(26)-H(26)	0.9500
C(5)-C(6)	1.393(5)	C(27)-F(12)	1.332(4)
C(5)-C(8)	1.506(5)	C(27)-F(11)	1.336(4)
C(6)-C(7)	1.388(4)	C(27)-F(10)	1.336(4)
C(6)-H(6)	0.9500	C(27)-Au(2)	2.065(4)
C(7)-H(7)	0.9500	C(28)-C(29)	1.379(5)
C(8)-H(8A)	0.9800	C(28)-C(33)	1.389(5)
C(8)-H(8B)	0.9800	C(28)-Au(2)	2.014(3)
C(8)-H(8C)	0.9800	C(29)-C(30)	1.406(5)
C(9)-C(14)	1.388(5)	C(29)-H(29)	0.9500
C(9)-C(10)	1.402(4)	C(30)-C(31)	1.390(6)
C(9)-P(1)	1.811(3)	C(30)-H(30)	0.9500
C(10)-C(11)	1.383(5)	C(31)-C(32)	1.371(6)
C(10)-H(10)	0.9500	C(31)-C(34)	1.518(5)
C(11)-C(12)	1.381(5)	C(32)-C(33)	1.378(5)
C(11)-H(11)	0.9500	C(32)-H(32)	0.9500
C(12)-C(13)	1.388(5)	C(33)-H(33)	0.9500
C(12)-H(12)	0.9500	C(34)-H(34A)	0.9800
C(13)-C(14)	1.383(5)	C(34)-H(34B)	0.9800
C(13)-H(13)	0.9500	C(34)-H(34C)	0.9800
C(14)-H(14)	0.9500	C(35)-C(36)	1.388(5)
C(15)-C(20)	1.391(5)	C(35)-C(40)	1.397(4)
C(15)-C(16)	1.400(5)	C(35)-P(2)	1.818(3)
C(15)-P(1)	1.805(3)	C(36)-C(37)	1.383(5)
C(16)-C(17)	1.388(5)	C(36)-H(36)	0.9500
C(16)-H(16)	0.9500	C(37)-C(38)	1.379(5)
C(17)-C(18)	1.378(5)	C(37)-H(37)	0.9500
C(17)-H(17)	0.9500	C(38)-C(39)	1.377(5)
C(18)-C(19)	1.377(5)	C(38)-H(38)	0.9500
C(18)-H(18)	0.9500	C(39)-C(40)	1.385(5)
C(19)-C(20)	1.389(5)	C(39)-H(39)	0.9500
C(19)-H(19)	0.9500	C(40)-H(40)	0.9500
C(20)-H(20)	0.9500	C(41)-C(42)	1.390(5)
C(21)-C(26)	1.384(5)	C(41)-C(46)	1.395(5)

C(41)-P(2)	1.806(3)	C(65)-H(65)	0.9500
C(42)-C(43)	1.386(5)	C(66)-H(66)	0.9500
C(42)-H(42)	0.9500	C(67)-C(72)	1.394(4)
C(43)-C(44)	1.383(5)	C(67)-C(68)	1.401(5)
C(43)-H(43)	0.9500	C(67)-P(3)	1.818(3)
C(44)-C(45)	1.379(5)	C(68)-C(69)	1.392(5)
C(44)-H(44)	0.9500	C(68)-H(68)	0.9500
C(45)-C(46)	1.386(5)	C(69)-C(70)	1.378(5)
C(45)-H(45)	0.9500	C(69)-H(69)	0.9500
C(46)-H(46)	0.9500	C(70)-C(71)	1.388(5)
C(47)-C(52)	1.395(5)	C(70)-H(70)	0.9500
C(47)-C(48)	1.401(5)	C(71)-C(72)	1.383(5)
C(47)-P(2)	1.812(3)	C(71)-H(71)	0.9500
C(48)-C(49)	1.385(5)	C(72)-H(72)	0.9500
C(48)-H(48)	0.9500	C(73)-C(78)	1.388(5)
C(49)-C(50)	1.377(5)	C(73)-C(74)	1.390(5)
C(49)-H(49)	0.9500	C(73)-P(3)	1.807(3)
C(50)-C(51)	1.383(5)	C(74)-C(75)	1.382(5)
C(50)-H(50)	0.9500	C(74)-H(74)	0.9500
C(51)-C(52)	1.385(5)	C(75)-C(76)	1.386(5)
C(51)-H(51)	0.9500	C(75)-H(75)	0.9500
C(52)-H(52)	0.9500	C(76)-C(77)	1.376(5)
C(53)-F(7)	1.319(4)	C(76)-H(76)	0.9500
C(53)-F(8)	1.335(4)	C(77)-C(78)	1.380(5)
C(53)-F(6)	1.365(5)	C(77)-H(77)	0.9500
C(53)-Au(3)	2.065(4)	C(78)-H(78)	0.9500
C(54)-C(59)	1.387(5)	C(79)-Cl(2)	1.759(4)
C(54)-C(55)	1.385(5)	C(79)-Cl(1)	1.768(4)
C(54)-Au(3)	2.007(3)	C(79)-H(79A)	0.9900
C(55)-C(56)	1.386(5)	C(79)-H(79B)	0.9900
C(55)-H(55)	0.9500	F(1)-Au(1)	2.0419(18)
C(56)-C(57)	1.384(5)	F(5)-Au(3)	2.0269(18)
C(56)-H(56)	0.9500	F(9)-Au(2)	2.0237(18)
C(57)-C(58)	1.388(5)	P(1)-Au(1)	2.3586(9)
C(57)-C(60)	1.508(5)	P(2)-Au(2)	2.3658(9)
C(58)-C(59)	1.395(5)	P(3)-Au(3)	2.3626(9)
C(58)-H(58)	0.9500		
C(59)-H(59)	0.9500	F(3)-C(1)-F(4)	104.6(3)
C(60)-H(60A)	0.9800	F(3)-C(1)-F(2)	105.4(3)
C(60)-H(60B)	0.9800	F(4)-C(1)-F(2)	103.4(3)
C(60)-H(60C)	0.9800	F(3)-C(1)-Au(1)	111.8(2)
C(61)-C(66)	1.391(5)	F(4)-C(1)-Au(1)	118.2(2)
C(61)-C(62)	1.398(5)	F(2)-C(1)-Au(1)	112.3(2)
C(61)-P(3)	1.808(3)	C(7)-C(2)-C(3)	119.0(3)
C(62)-C(63)	1.395(5)	C(7)-C(2)-Au(1)	122.9(2)
C(62)-H(62)	0.9500	C(3)-C(2)-Au(1)	118.1(2)
C(63)-C(64)	1.366(5)	C(2)-C(3)-C(4)	120.0(3)
C(63)-H(63)	0.9500	C(2)-C(3)-H(3)	120.0
C(64)-C(65)	1.374(5)	C(4)-C(3)-H(3)	120.0
C(64)-H(64)	0.9500	C(5)-C(4)-C(3)	121.5(3)
C(65)-C(66)	1.385(5)	C(5)-C(4)-H(4)	119.2

C(3)-C(4)-H(4)	119.2	C(15)-C(20)-H(20)	120.0
C(4)-C(5)-C(6)	117.9(3)	C(26)-C(21)-C(22)	119.7(3)
C(4)-C(5)-C(8)	120.9(3)	C(26)-C(21)-P(1)	122.0(3)
C(6)-C(5)-C(8)	121.2(3)	C(22)-C(21)-P(1)	118.3(3)
C(7)-C(6)-C(5)	120.9(3)	C(23)-C(22)-C(21)	119.8(3)
C(7)-C(6)-H(6)	119.6	C(23)-C(22)-H(22)	120.1
C(5)-C(6)-H(6)	119.6	C(21)-C(22)-H(22)	120.1
C(2)-C(7)-C(6)	120.7(3)	C(24)-C(23)-C(22)	119.8(3)
C(2)-C(7)-H(7)	119.6	C(24)-C(23)-H(23)	120.1
C(6)-C(7)-H(7)	119.6	C(22)-C(23)-H(23)	120.1
C(5)-C(8)-H(8A)	109.5	C(23)-C(24)-C(25)	120.9(3)
C(5)-C(8)-H(8B)	109.5	C(23)-C(24)-H(24)	119.5
H(8A)-C(8)-H(8B)	109.5	C(25)-C(24)-H(24)	119.5
C(5)-C(8)-H(8C)	109.5	C(24)-C(25)-C(26)	119.5(4)
H(8A)-C(8)-H(8C)	109.5	C(24)-C(25)-H(25)	120.2
H(8B)-C(8)-H(8C)	109.5	C(26)-C(25)-H(25)	120.2
C(14)-C(9)-C(10)	120.0(3)	C(25)-C(26)-C(21)	120.2(3)
C(14)-C(9)-P(1)	120.0(2)	C(25)-C(26)-H(26)	119.9
C(10)-C(9)-P(1)	119.7(3)	C(21)-C(26)-H(26)	119.9
C(11)-C(10)-C(9)	119.4(3)	F(12)-C(27)-F(11)	106.1(3)
C(11)-C(10)-H(10)	120.3	F(12)-C(27)-F(10)	105.0(3)
C(9)-C(10)-H(10)	120.3	F(11)-C(27)-F(10)	103.7(3)
C(12)-C(11)-C(10)	120.5(3)	F(12)-C(27)-Au(2)	112.1(2)
C(12)-C(11)-H(11)	119.8	F(11)-C(27)-Au(2)	116.9(2)
C(10)-C(11)-H(11)	119.8	F(10)-C(27)-Au(2)	112.2(2)
C(11)-C(12)-C(13)	120.0(3)	C(29)-C(28)-C(33)	119.6(3)
C(11)-C(12)-H(12)	120.0	C(29)-C(28)-Au(2)	121.9(3)
C(13)-C(12)-H(12)	120.0	C(33)-C(28)-Au(2)	118.5(3)
C(14)-C(13)-C(12)	120.3(3)	C(28)-C(29)-C(30)	119.0(4)
C(14)-C(13)-H(13)	119.9	C(28)-C(29)-H(29)	120.5
C(12)-C(13)-H(13)	119.9	C(30)-C(29)-H(29)	120.5
C(13)-C(14)-C(9)	119.8(3)	C(31)-C(30)-C(29)	121.3(4)
C(13)-C(14)-H(14)	120.1	C(31)-C(30)-H(30)	119.4
C(9)-C(14)-H(14)	120.1	C(29)-C(30)-H(30)	119.4
C(20)-C(15)-C(16)	119.6(3)	C(32)-C(31)-C(30)	118.2(4)
C(20)-C(15)-P(1)	119.9(3)	C(32)-C(31)-C(34)	120.7(4)
C(16)-C(15)-P(1)	120.5(3)	C(30)-C(31)-C(34)	121.0(4)
C(17)-C(16)-C(15)	119.4(3)	C(31)-C(32)-C(33)	121.4(4)
C(17)-C(16)-H(16)	120.3	C(31)-C(32)-H(32)	119.3
C(15)-C(16)-H(16)	120.3	C(33)-C(32)-H(32)	119.3
C(18)-C(17)-C(16)	120.7(3)	C(32)-C(33)-C(28)	120.5(4)
C(18)-C(17)-H(17)	119.6	C(32)-C(33)-H(33)	119.7
C(16)-C(17)-H(17)	119.6	C(28)-C(33)-H(33)	119.7
C(19)-C(18)-C(17)	120.0(3)	C(31)-C(34)-H(34A)	109.5
C(19)-C(18)-H(18)	120.0	C(31)-C(34)-H(34B)	109.5
C(17)-C(18)-H(18)	120.0	H(34A)-C(34)-H(34B)	109.5
C(18)-C(19)-C(20)	120.4(3)	C(31)-C(34)-H(34C)	109.5
C(18)-C(19)-H(19)	119.8	H(34A)-C(34)-H(34C)	109.5
C(20)-C(19)-H(19)	119.8	H(34B)-C(34)-H(34C)	109.5
C(19)-C(20)-C(15)	119.9(3)	C(36)-C(35)-C(40)	119.5(3)
C(19)-C(20)-H(20)	120.0	C(36)-C(35)-P(2)	120.6(2)

C(40)-C(35)-P(2)	119.6(3)	C(47)-C(52)-H(52)	120.1
C(37)-C(36)-C(35)	120.0(3)	F(7)-C(53)-F(8)	107.1(3)
C(37)-C(36)-H(36)	120.0	F(7)-C(53)-F(6)	102.6(3)
C(35)-C(36)-H(36)	120.0	F(8)-C(53)-F(6)	103.6(3)
C(36)-C(37)-C(38)	120.0(3)	F(7)-C(53)-Au(3)	113.0(3)
C(36)-C(37)-H(37)	120.0	F(8)-C(53)-Au(3)	115.0(3)
C(38)-C(37)-H(37)	120.0	F(6)-C(53)-Au(3)	114.5(3)
C(39)-C(38)-C(37)	120.7(3)	C(59)-C(54)-C(55)	119.1(3)
C(39)-C(38)-H(38)	119.6	C(59)-C(54)-Au(3)	121.2(3)
C(37)-C(38)-H(38)	119.6	C(55)-C(54)-Au(3)	119.7(3)
C(38)-C(39)-C(40)	119.7(3)	C(56)-C(55)-C(54)	120.0(3)
C(38)-C(39)-H(39)	120.1	C(56)-C(55)-H(55)	120.0
C(40)-C(39)-H(39)	120.1	C(54)-C(55)-H(55)	120.0
C(39)-C(40)-C(35)	120.1(3)	C(55)-C(56)-C(57)	121.8(3)
C(39)-C(40)-H(40)	120.0	C(55)-C(56)-H(56)	119.1
C(35)-C(40)-H(40)	120.0	C(57)-C(56)-H(56)	119.1
C(42)-C(41)-C(46)	119.2(3)	C(56)-C(57)-C(58)	117.8(3)
C(42)-C(41)-P(2)	122.1(3)	C(56)-C(57)-C(60)	120.2(3)
C(46)-C(41)-P(2)	118.6(3)	C(58)-C(57)-C(60)	122.0(3)
C(43)-C(42)-C(41)	120.1(3)	C(57)-C(58)-C(59)	121.0(3)
C(43)-C(42)-H(42)	119.9	C(57)-C(58)-H(58)	119.5
C(41)-C(42)-H(42)	119.9	C(59)-C(58)-H(58)	119.5
C(44)-C(43)-C(42)	120.2(3)	C(54)-C(59)-C(58)	120.2(3)
C(44)-C(43)-H(43)	119.9	C(54)-C(59)-H(59)	119.9
C(42)-C(43)-H(43)	119.9	C(58)-C(59)-H(59)	119.9
C(45)-C(44)-C(43)	120.1(3)	C(57)-C(60)-H(60A)	109.5
C(45)-C(44)-H(44)	119.9	C(57)-C(60)-H(60B)	109.5
C(43)-C(44)-H(44)	119.9	H(60A)-C(60)-H(60B)	109.5
C(44)-C(45)-C(46)	120.0(3)	C(57)-C(60)-H(60C)	109.5
C(44)-C(45)-H(45)	120.0	H(60A)-C(60)-H(60C)	109.5
C(46)-C(45)-H(45)	120.0	H(60B)-C(60)-H(60C)	109.5
C(45)-C(46)-C(41)	120.3(3)	C(66)-C(61)-C(62)	119.7(3)
C(45)-C(46)-H(46)	119.9	C(66)-C(61)-P(3)	122.5(3)
C(41)-C(46)-H(46)	119.9	C(62)-C(61)-P(3)	117.8(3)
C(52)-C(47)-C(48)	119.3(3)	C(63)-C(62)-C(61)	119.2(3)
C(52)-C(47)-P(2)	119.3(3)	C(63)-C(62)-H(62)	120.4
C(48)-C(47)-P(2)	121.4(3)	C(61)-C(62)-H(62)	120.4
C(49)-C(48)-C(47)	119.8(3)	C(64)-C(63)-C(62)	120.3(3)
C(49)-C(48)-H(48)	120.1	C(64)-C(63)-H(63)	119.9
C(47)-C(48)-H(48)	120.1	C(62)-C(63)-H(63)	119.9
C(50)-C(49)-C(48)	120.8(4)	C(63)-C(64)-C(65)	120.7(3)
C(50)-C(49)-H(49)	119.6	C(63)-C(64)-H(64)	119.6
C(48)-C(49)-H(49)	119.6	C(65)-C(64)-H(64)	119.6
C(49)-C(50)-C(51)	119.6(3)	C(64)-C(65)-C(66)	120.2(4)
C(49)-C(50)-H(50)	120.2	C(64)-C(65)-H(65)	119.9
C(51)-C(50)-H(50)	120.2	C(66)-C(65)-H(65)	119.9
C(52)-C(51)-C(50)	120.8(4)	C(65)-C(66)-C(61)	119.8(3)
C(52)-C(51)-H(51)	119.6	C(65)-C(66)-H(66)	120.1
C(50)-C(51)-H(51)	119.6	C(61)-C(66)-H(66)	120.1
C(51)-C(52)-C(47)	119.8(3)	C(72)-C(67)-C(68)	119.6(3)
C(51)-C(52)-H(52)	120.1	C(72)-C(67)-P(3)	121.1(3)

C(68)-C(67)-P(3)	119.3(3)	Cl(1)-C(79)-H(79B)	109.4
C(69)-C(68)-C(67)	119.6(3)	H(79A)-C(79)-H(79B)	108.0
C(69)-C(68)-H(68)	120.2	C(15)-P(1)-C(21)	107.89(15)
C(67)-C(68)-H(68)	120.2	C(15)-P(1)-C(9)	106.93(15)
C(70)-C(69)-C(68)	120.3(3)	C(21)-P(1)-C(9)	107.56(15)
C(70)-C(69)-H(69)	119.9	C(15)-P(1)-Au(1)	112.56(11)
C(68)-C(69)-H(69)	119.9	C(21)-P(1)-Au(1)	107.00(11)
C(69)-C(70)-C(71)	120.4(3)	C(9)-P(1)-Au(1)	114.61(11)
C(69)-C(70)-H(70)	119.8	C(41)-P(2)-C(47)	107.72(15)
C(71)-C(70)-H(70)	119.8	C(41)-P(2)-C(35)	105.70(15)
C(72)-C(71)-C(70)	119.9(3)	C(47)-P(2)-C(35)	104.93(15)
C(72)-C(71)-H(71)	120.0	C(41)-P(2)-Au(2)	107.84(11)
C(70)-C(71)-H(71)	120.0	C(47)-P(2)-Au(2)	110.44(11)
C(71)-C(72)-C(67)	120.3(3)	C(35)-P(2)-Au(2)	119.62(11)
C(71)-C(72)-H(72)	119.9	C(61)-P(3)-C(73)	105.98(16)
C(67)-C(72)-H(72)	119.9	C(61)-P(3)-C(67)	106.72(15)
C(78)-C(73)-C(74)	119.4(3)	C(73)-P(3)-C(67)	108.23(15)
C(78)-C(73)-P(3)	118.5(3)	C(61)-P(3)-Au(3)	117.00(11)
C(74)-C(73)-P(3)	122.0(3)	C(73)-P(3)-Au(3)	110.09(11)
C(75)-C(74)-C(73)	120.3(3)	C(67)-P(3)-Au(3)	108.49(11)
C(75)-C(74)-H(74)	119.8	C(2)-Au(1)-F(1)	176.28(10)
C(73)-C(74)-H(74)	119.8	C(2)-Au(1)-C(1)	89.30(13)
C(74)-C(75)-C(76)	119.6(3)	F(1)-Au(1)-C(1)	89.86(11)
C(74)-C(75)-H(75)	120.2	C(2)-Au(1)-P(1)	92.19(9)
C(76)-C(75)-H(75)	120.2	F(1)-Au(1)-P(1)	88.76(6)
C(77)-C(76)-C(75)	120.3(3)	C(1)-Au(1)-P(1)	177.73(9)
C(77)-C(76)-H(76)	119.8	C(28)-Au(2)-F(9)	177.42(12)
C(75)-C(76)-H(76)	119.8	C(28)-Au(2)-C(27)	88.66(14)
C(76)-C(77)-C(78)	120.2(3)	F(9)-Au(2)-C(27)	90.48(12)
C(76)-C(77)-H(77)	119.9	C(28)-Au(2)-P(2)	94.56(10)
C(78)-C(77)-H(77)	119.9	F(9)-Au(2)-P(2)	86.28(6)
C(77)-C(78)-C(73)	120.1(3)	C(27)-Au(2)-P(2)	176.70(10)
C(77)-C(78)-H(78)	119.9	C(54)-Au(3)-F(5)	179.32(11)
C(73)-C(78)-H(78)	119.9	C(54)-Au(3)-C(53)	86.97(14)
Cl(2)-C(79)-Cl(1)	111.1(2)	F(5)-Au(3)-C(53)	92.60(12)
Cl(2)-C(79)-H(79A)	109.4	C(54)-Au(3)-P(3)	95.21(10)
Cl(1)-C(79)-H(79A)	109.4	F(5)-Au(3)-P(3)	85.19(6)
Cl(2)-C(79)-H(79B)	109.4	C(53)-Au(3)-P(3)	176.82(11)

Table A54. Anisotropic displacement parameters ($Å^2 x\ 10^3$)for **1-F**. The anisotropic displacement factor exponent takes the form: $-2\pi^2[\ h^2a^{*2}U^{11} + ... + 2\ h\ k\ a^*\ b^*\ U^{12}\ ]$

	U^{11}	U^{22}	U^{33}	U^{23}	U^{13}	U^{12}
C(1)	15(2)	16(2)	13(2)	0(1)	0(2)	-7(2)
C(2)	7(2)	6(2)	14(2)	-1(1)	2(1)	-2(1)
C(3)	16(2)	13(2)	15(2)	-1(1)	-2(2)	-6(2)
C(4)	16(2)	14(2)	16(2)	6(1)	-2(2)	-5(2)
C(5)	14(2)	14(2)	21(2)	2(2)	0(2)	-8(2)
C(6)	14(2)	14(2)	17(2)	-3(1)	-4(1)	-7(2)

C(7)	11(2)	14(2)	9(2)	-2(1)	1(1)	-2(2)
C(8)	28(2)	35(2)	28(2)	5(2)	-5(2)	-22(2)
C(9)	13(2)	5(2)	15(2)	-3(1)	2(1)	-1(2)
C(10)	14(2)	10(2)	14(2)	-3(1)	0(1)	-2(2)
C(11)	17(2)	15(2)	23(2)	-3(2)	7(2)	-8(2)
C(12)	16(2)	22(2)	27(2)	-7(2)	4(2)	-11(2)
C(13)	18(2)	23(2)	17(2)	-7(2)	-3(2)	-8(2)
C(14)	12(2)	15(2)	14(2)	-3(1)	2(1)	-4(2)
C(15)	18(2)	11(2)	12(2)	2(1)	-2(1)	-8(2)
C(16)	17(2)	17(2)	21(2)	-4(2)	2(2)	-8(2)
C(17)	27(2)	17(2)	25(2)	-7(2)	10(2)	-11(2)
C(18)	44(3)	23(2)	16(2)	-7(2)	6(2)	-23(2)
C(19)	29(2)	27(2)	16(2)	2(2)	-2(2)	-20(2)
C(20)	20(2)	13(2)	15(2)	2(1)	0(2)	-9(2)
C(21)	10(2)	16(2)	12(2)	4(1)	-3(1)	-7(2)
C(22)	24(2)	17(2)	18(2)	1(2)	-1(2)	-7(2)
C(23)	25(2)	33(2)	15(2)	3(2)	0(2)	-9(2)
C(24)	33(2)	36(3)	19(2)	14(2)	-7(2)	-20(2)
C(25)	46(3)	19(2)	32(2)	11(2)	-8(2)	-15(2)
C(26)	30(2)	18(2)	23(2)	4(2)	0(2)	-6(2)
C(27)	21(2)	26(2)	16(2)	7(2)	-3(2)	-13(2)
C(28)	21(2)	13(2)	16(2)	-1(1)	2(2)	-9(2)
C(29)	22(2)	14(2)	30(2)	5(2)	-1(2)	-7(2)
C(30)	25(2)	10(2)	51(3)	-4(2)	11(2)	-4(2)
C(31)	50(3)	18(2)	28(2)	-2(2)	11(2)	-19(2)
C(32)	47(3)	25(2)	21(2)	0(2)	-2(2)	-19(2)
C(33)	27(2)	15(2)	22(2)	-1(2)	-3(2)	-12(2)
C(34)	70(4)	29(3)	39(3)	-9(2)	24(2)	-17(3)
C(35)	12(2)	8(2)	15(2)	-2(1)	1(1)	-4(2)
C(36)	16(2)	13(2)	16(2)	-1(1)	-2(2)	-4(2)
C(37)	13(2)	23(2)	26(2)	-5(2)	-2(2)	-7(2)
C(38)	17(2)	19(2)	21(2)	-4(2)	5(2)	-9(2)
C(39)	27(2)	22(2)	13(2)	-3(2)	2(2)	-13(2)
C(40)	16(2)	20(2)	16(2)	2(2)	-5(2)	-11(2)
C(41)	10(2)	23(2)	11(2)	-1(2)	1(1)	-10(2)
C(42)	15(2)	18(2)	16(2)	-1(2)	0(2)	-8(2)
C(43)	25(2)	28(2)	16(2)	-12(2)	5(2)	-17(2)
C(44)	12(2)	43(3)	15(2)	1(2)	-1(2)	-14(2)
C(45)	15(2)	29(2)	20(2)	7(2)	-4(2)	-6(2)
C(46)	15(2)	18(2)	20(2)	1(2)	-2(2)	-7(2)
C(47)	15(2)	15(2)	13(2)	-3(1)	-6(1)	-5(2)
C(48)	19(2)	19(2)	18(2)	2(2)	-1(2)	-6(2)
C(49)	36(3)	23(2)	21(2)	5(2)	-7(2)	-10(2)
C(50)	27(2)	15(2)	35(2)	2(2)	-19(2)	-2(2)
C(51)	13(2)	26(2)	39(2)	-6(2)	-8(2)	-5(2)
C(52)	19(2)	22(2)	30(2)	5(2)	-6(2)	-12(2)
C(53)	25(2)	23(2)	37(2)	-7(2)	4(2)	-13(2)
C(54)	19(2)	10(2)	19(2)	-5(1)	-2(2)	-7(2)
C(55)	19(2)	21(2)	22(2)	-3(2)	-8(2)	0(2)
C(56)	29(2)	21(2)	17(2)	-2(2)	-9(2)	-5(2)

C(57)	20(2)	13(2)	22(2)	-3(2)	-2(2)	-6(2)
C(58)	16(2)	14(2)	25(2)	4(2)	-4(2)	-3(2)
C(59)	19(2)	15(2)	19(2)	2(2)	-5(2)	-6(2)
C(60)	28(2)	28(2)	22(2)	-4(2)	0(2)	-5(2)
C(61)	13(2)	10(2)	20(2)	-2(1)	3(2)	-7(2)
C(62)	17(2)	18(2)	21(2)	2(2)	-1(2)	-10(2)
C(63)	22(2)	16(2)	24(2)	0(2)	9(2)	-7(2)
C(64)	15(2)	15(2)	41(3)	-3(2)	8(2)	-6(2)
C(65)	17(2)	24(2)	42(3)	-5(2)	-4(2)	-9(2)
C(66)	20(2)	28(2)	24(2)	-9(2)	-1(2)	-12(2)
C(67)	15(2)	15(2)	9(2)	-3(1)	-3(1)	-6(2)
C(68)	16(2)	23(2)	12(2)	-1(2)	1(1)	-12(2)
C(69)	15(2)	23(2)	16(2)	-5(2)	-1(2)	-6(2)
C(70)	23(2)	18(2)	19(2)	0(2)	-11(2)	-4(2)
C(71)	23(2)	20(2)	15(2)	4(2)	-7(2)	-14(2)
C(72)	16(2)	16(2)	14(2)	1(1)	-5(1)	-8(2)
C(73)	12(2)	18(2)	11(2)	-1(1)	0(1)	-6(2)
C(74)	24(2)	18(2)	17(2)	0(2)	-5(2)	-5(2)
C(75)	38(3)	22(2)	16(2)	-7(2)	-5(2)	-7(2)
C(76)	27(2)	31(2)	10(2)	1(2)	-6(2)	-9(2)
C(77)	21(2)	25(2)	19(2)	6(2)	-7(2)	-10(2)
C(78)	14(2)	16(2)	20(2)	-3(2)	-2(2)	-6(2)
C(79)	33(2)	23(2)	24(2)	-2(2)	3(2)	-11(2)
F(1)	16(1)	16(1)	22(1)	0(1)	0(1)	-12(1)
F(2)	23(1)	21(1)	39(1)	3(1)	16(1)	-1(1)
F(3)	35(2)	53(2)	37(1)	-13(1)	-24(1)	13(1)
F(4)	21(1)	13(1)	82(2)	-7(1)	11(1)	-6(1)
F(5)	19(1)	32(1)	19(1)	-1(1)	9(1)	-12(1)
F(6)	86(2)	76(2)	67(2)	22(2)	-45(2)	-66(2)
F(7)	32(2)	47(2)	139(3)	-46(2)	31(2)	-31(1)
F(8)	34(1)	12(1)	71(2)	2(1)	-14(1)	-11(1)
F(9)	24(1)	32(1)	17(1)	-6(1)	6(1)	-12(1)
F(10)	78(2)	76(2)	27(1)	7(1)	-1(1)	-66(2)
F(11)	41(2)	24(1)	87(2)	-9(1)	1(1)	-20(1)
F(12)	56(2)	49(2)	67(2)	35(1)	-50(1)	-40(1)
P(1)	11(1)	9(1)	11(1)	-1(1)	0(1)	-4(1)
P(2)	12(1)	15(1)	11(1)	0(1)	-1(1)	-6(1)
P(3)	12(1)	15(1)	11(1)	-1(1)	0(1)	-7(1)
Au(1)	9(1)	9(1)	10(1)	0(1)	0(1)	-4(1)
Au(2)	13(1)	15(1)	12(1)	2(1)	-2(1)	-8(1)
Au(3)	13(1)	14(1)	17(1)	0(1)	0(1)	-8(1)
Cl(1)	25(1)	29(1)	25(1)	-4(1)	-1(1)	-13(1)
Cl(2)	58(1)	23(1)	54(1)	3(1)	22(1)	-8(1)

Table 4.11. Hydrogen coordinates (x 10^4) and isotropic displacement parameters (Å^{2}x 10^3) for **4.1-F**.

	x	y	z	U(eq)

H(3)	5068	5169	1944	18
H(4)	3956	4236	2318	19
H(6)	2984	4386	746	17
H(7)	4092	5320	371	15
H(8A)	2923	3195	2162	41
H(8B)	2592	3190	1532	41
H(8C)	1801	4183	1949	41
H(10)	2376	7350	1762	17
H(11)	745	6998	1802	23
H(12)	-12	7036	957	25
H(13)	817	7492	67	22
H(14)	2415	7895	21	17
H(16)	1894	9517	1489	22
H(17)	1670	10617	2245	29
H(18)	3287	10449	2642	30
H(19)	5149	9197	2279	26
H(20)	5404	8083	1524	19
H(22)	4888	7206	-311	25
H(23)	5069	8104	-1197	32
H(24)	4345	9971	-1237	34
H(25)	3475	10967	-401	39
H(26)	3238	10085	482	31
H(29)	7221	9641	3936	28
H(30)	6073	10384	4817	38
H(32)	8904	8926	5642	36
H(33)	10057	8221	4777	25
H(34A)	6948	9693	6212	76
H(34B)	5827	10316	5881	76
H(34C)	6655	10885	5943	76
H(36)	6681	7135	3349	18
H(37)	5022	7214	3966	24
H(38)	4946	7252	4965	23
H(39)	6503	7238	5357	24
H(40)	8175	7149	4745	19
H(42)	9239	5306	2706	20
H(43)	8699	5407	1790	25
H(44)	7783	7084	1327	27
H(45)	7470	8661	1762	27
H(46)	8022	8571	2675	21
H(48)	8838	5118	4254	24
H(49)	10199	3372	4464	33
H(50)	12141	2751	4042	32
H(51)	12728	3868	3391	31
H(52)	11395	5623	3179	27
H(55)	6098	2501	1860	28
H(56)	7483	1766	1056	28
H(58)	9747	-304	2095	24
H(59)	8384	461	2908	21
H(60A)	9234	161	645	44
H(60B)	10217	-527	1050	44

H(60C)	10030	671	833	44
H(62)	7633	3372	2147	22
H(63)	9471	3047	1618	27
H(64)	11050	2659	2096	31
H(65)	10841	2607	3100	33
H(66)	9029	2927	3642	27
H(68)	4234	4660	3505	19
H(69)	2947	6414	3240	23
H(70)	3671	7581	2737	25
H(71)	5686	7023	2504	21
H(72)	6981	5276	2755	18
H(74)	6156	4970	4233	25
H(75)	6466	4827	5199	32
H(76)	7374	3118	5637	28
H(77)	7949	1567	5117	26
H(78)	7624	1703	4156	20
H(79A)	502	3627	-23	34
H(79B)	1822	3404	17	34

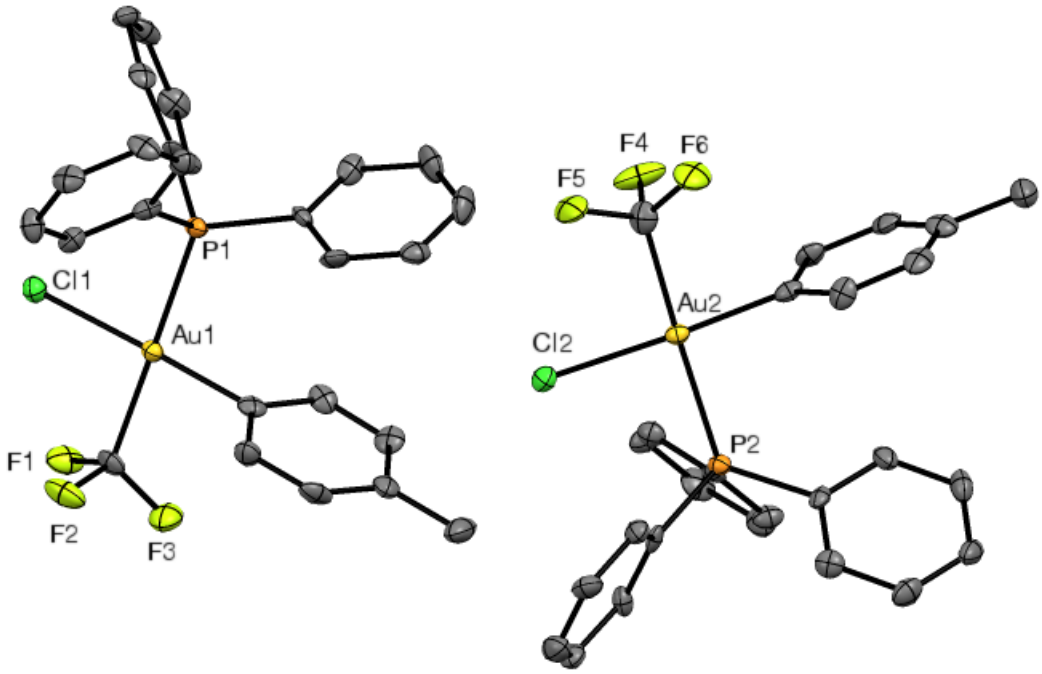

Figure A9. ORTEP of **4.1-Cl** with ellipsoids set to the 50 % probability level and hydrogen atoms omitted for clarity.

Table A55. Crystal data and structure refinement for **4.1-Cl**.

Identification code	shelx
Empirical formula	C_{26} H_{22} Au Cl F_3 P
Formula weight	654.82
Temperature	100(2) K
Wavelength	0.71073 Å

Crystal system	Triclinic	
Space group	P -1	
Unit cell dimensions	a = 9.7809(5) Å	α= 88.6390(10)º.
	b = 13.4014(7) Å	β= 89.9450(10)º.
	c = 18.6278(10) Å	γ = 75.5390(10)º.
Volume	2363.6(2) $Å^3$	
Z	4	
Density (calculated)	1.840 Mg/m^3	
Absorption coefficient	6.440 mm^{-1}	
F(000)	1264	
Crystal size	0.120 x 0.080 x 0.060 mm^3	
Theta range for data collection	1.570 to 25.617º.	
Index ranges	-11<=h<=11, -16<=k<=16, 0<=l<=22	
Reflections collected	8677	
Independent reflections	8677 [R(int) = 0.0728]	
Completeness to theta = 25.000∞	99.9 %	
Absorption correction	Semi-empirical from equivalents	
Max. and min. transmission	0.745 and 0.564	
Refinement method	Full-matrix least-squares on F^2	
Data / restraints / parameters	8677 / 12 / 580	
Goodness-of-fit on F^2	1.070	
Final R indices [I>2sigma(I)]	R1 = 0.0412, wR2 = 0.0894	
R indices (all data)	R1 = 0.0585, wR2 = 0.0994	
Extinction coefficient	n/a	
Largest diff. peak and hole	3.567 and -1.120 e.$Å^{-3}$	

Table A56. Atomic coordinates (x 10^4) and equivalent isotropic displacement parameters ($Å^2$x 10^3) for **4.1-Cl**. U(eq) is defined as one third of the trace of the orthogonalized U^{ij} tensor.

	x	y	z	U(eq)
C(1)	7250(10)	4868(7)	3718(5)	21(2)
C(2)	7352(10)	3774(7)	5066(4)	19(2)
C(3)	8803(10)	3503(8)	5166(5)	22(2)
C(4)	9364(10)	3651(8)	5836(5)	24(2)
C(5)	8504(10)	4055(7)	6391(4)	23(2)
C(6)	7061(11)	4315(7)	6284(5)	23(2)
C(7)	6482(10)	4163(7)	5627(4)	21(2)
C(8)	9137(12)	4201(8)	7122(5)	35(3)
C(9)	5718(9)	1913(7)	5463(4)	16(2)
C(10)	6939(10)	1691(7)	5881(5)	24(2)
C(11)	6845(10)	1564(7)	6613(5)	23(2)
C(12)	5552(12)	1664(8)	6939(5)	33(3)
C(13)	4358(11)	1881(8)	6525(5)	32(2)
C(14)	4417(11)	2020(7)	5788(4)	23(2)
C(15)	4191(9)	2069(7)	4128(4)	16(2)
C(16)	3122(9)	2995(7)	4139(4)	17(2)
C(17)	1798(10)	2999(8)	3886(5)	26(2)
C(18)	1531(10)	2108(8)	3618(5)	29(2)
C(19)	2566(10)	1206(8)	3590(4)	23(2)

C(20)	3899(10)	1187(7)	3855(4)	20(2)
C(21)	7206(9)	972(7)	4203(4)	18(2)
C(22)	7456(9)	45(7)	4592(4)	21(2)
C(23)	8458(10)	-818(7)	4364(5)	23(2)
C(24)	9207(10)	-755(7)	3734(5)	24(2)
C(25)	8978(10)	156(7)	3342(4)	24(2)
C(26)	7985(10)	1004(7)	3579(4)	20(2)
C(27)	7763(10)	132(8)	8853(5)	26(2)
C(28)	7527(10)	1243(7)	10119(4)	18(2)
C(29)	8250(10)	721(7)	10708(4)	22(2)
C(30)	7524(11)	626(7)	11342(5)	26(2)
C(31)	6103(11)	1031(7)	11410(5)	24(2)
C(32)	5387(11)	1542(7)	10817(5)	23(2)
C(33)	6063(10)	1656(8)	10174(5)	21(2)
C(34)	5343(12)	948(8)	12103(5)	32(2)
C(35)	10781(9)	2982(7)	9106(4)	16(2)
C(36)	11912(9)	2126(7)	9080(4)	19(2)
C(37)	13155(10)	2186(8)	8733(5)	24(2)
C(38)	13237(11)	3112(8)	8416(5)	29(2)
C(39)	12093(10)	3981(7)	8429(4)	22(2)
C(40)	10869(9)	3916(7)	8783(4)	18(2)
C(41)	9569(10)	2976(7)	10519(4)	17(2)
C(42)	10883(10)	3087(7)	10723(5)	21(2)
C(43)	11149(11)	3246(8)	11450(5)	26(2)
C(44)	10074(11)	3291(7)	11941(4)	26(2)
C(45)	8785(11)	3164(7)	11744(5)	26(2)
C(46)	8528(10)	3002(7)	11026(4)	22(2)
C(47)	7753(9)	3970(7)	9341(4)	16(2)
C(48)	7396(10)	4816(7)	9771(5)	21(2)
C(49)	6278(10)	5656(8)	9576(5)	27(2)
C(50)	5582(12)	5633(8)	8936(5)	31(2)
C(51)	5914(10)	4795(7)	8501(5)	21(2)
C(52)	7011(10)	3944(7)	8703(4)	20(2)
F(1)	6443(6)	5431(4)	3197(3)	32(1)
F(2)	8538(6)	4518(5)	3422(3)	36(1)
F(3)	7382(7)	5550(4)	4204(3)	34(1)
F(4)	6376(6)	442(4)	8681(4)	42(2)
F(5)	8376(7)	-327(5)	8263(3)	41(2)
F(6)	7856(7)	-631(4)	9341(3)	38(2)
P(1)	5887(2)	2091(2)	4494(1)	15(1)
P(2)	9192(2)	2853(2)	9569(1)	15(1)
Cl(1)	5636(2)	3402(2)	2930(1)	21(1)
Cl(2)	9454(2)	1569(2)	8030(1)	22(1)
Au(1)	6531(1)	3598(1)	4085(1)	15(1)
Au(2)	8499(1)	1375(1)	9178(1)	15(1)

Table A57. Bond lengths [Å] and angles [º] for **4.1-Cl**.

C(1)-F(3)	1.331(10)	C(1)-F(2)	1.352(10)
C(1)-F(1)	1.343(11)	C(1)-Au(1)	2.098(9)

C(2)-C(7)	1.376(12)	C(26)-H(26)	0.9500
C(2)-C(3)	1.385(13)	C(27)-F(5)	1.338(11)
C(2)-Au(1)	2.039(9)	C(27)-F(6)	1.339(11)
C(3)-C(4)	1.403(13)	C(27)-F(4)	1.352(11)
C(3)-H(3)	0.9500	C(27)-Au(2)	2.076(10)
C(4)-C(5)	1.366(13)	C(28)-C(29)	1.383(12)
C(4)-H(4)	0.9500	C(28)-C(33)	1.405(13)
C(5)-C(6)	1.380(14)	C(28)-Au(2)	2.018(8)
C(5)-C(8)	1.534(12)	C(29)-C(30)	1.397(13)
C(6)-C(7)	1.389(13)	C(29)-H(29)	0.9500
C(6)-H(6)	0.9500	C(30)-C(31)	1.367(14)
C(7)-H(7)	0.9500	C(30)-H(30)	0.9500
C(8)-H(8A)	0.9800	C(31)-C(32)	1.381(13)
C(8)-H(8B)	0.9800	C(31)-C(34)	1.504(13)
C(8)-H(8C)	0.9800	C(32)-C(33)	1.392(13)
C(9)-C(14)	1.385(13)	C(32)-H(32)	0.9500
C(9)-C(10)	1.392(12)	C(33)-H(33)	0.9500
C(9)-P(1)	1.828(8)	C(34)-H(34A)	0.9800
C(10)-C(11)	1.376(13)	C(34)-H(34B)	0.9800
C(10)-H(10)	0.9500	C(34)-H(34C)	0.9800
C(11)-C(12)	1.380(14)	C(35)-C(36)	1.382(12)
C(11)-H(11)	0.9500	C(35)-C(40)	1.397(13)
C(12)-C(13)	1.366(14)	C(35)-P(2)	1.821(9)
C(12)-H(12)	0.9500	C(36)-C(37)	1.396(13)
C(13)-C(14)	1.383(13)	C(36)-H(36)	0.9500
C(13)-H(13)	0.9500	C(37)-C(38)	1.381(14)
C(14)-H(14)	0.9500	C(37)-H(37)	0.9500
C(15)-C(20)	1.392(12)	C(38)-C(39)	1.401(13)
C(15)-C(16)	1.410(12)	C(38)-H(38)	0.9500
C(15)-P(1)	1.801(8)	C(39)-C(40)	1.387(12)
C(16)-C(17)	1.378(13)	C(39)-H(39)	0.9500
C(16)-H(16)	0.9500	C(40)-H(40)	0.9500
C(17)-C(18)	1.389(14)	C(41)-C(46)	1.384(12)
C(17)-H(17)	0.9500	C(41)-C(42)	1.386(13)
C(18)-C(19)	1.371(14)	C(41)-P(2)	1.827(8)
C(18)-H(18)	0.9500	C(42)-C(43)	1.409(13)
C(19)-C(20)	1.388(13)	C(42)-H(42)	0.9500
C(19)-H(19)	0.9500	C(43)-C(44)	1.384(13)
C(20)-H(20)	0.9500	C(43)-H(43)	0.9500
C(21)-C(22)	1.391(13)	C(44)-C(45)	1.364(14)
C(21)-C(26)	1.395(12)	C(44)-H(44)	0.9500
C(21)-P(1)	1.810(9)	C(45)-C(46)	1.392(13)
C(22)-C(23)	1.390(13)	C(45)-H(45)	0.9500
C(22)-H(22)	0.9500	C(46)-H(46)	0.9500
C(23)-C(24)	1.396(13)	C(47)-C(48)	1.376(13)
C(23)-H(23)	0.9500	C(47)-C(52)	1.398(12)
C(24)-C(25)	1.375(13)	C(47)-P(2)	1.822(9)
C(24)-H(24)	0.9500	C(48)-C(49)	1.401(13)
C(25)-C(26)	1.378(13)	C(48)-H(48)	0.9500
C(25)-H(25)	0.9500	C(49)-C(50)	1.379(14)

C(49)-H(49)	0.9500	C(13)-C(12)-C(11)	119.2(8)
C(50)-C(51)	1.372(14)	C(13)-C(12)-H(12)	120.4
C(50)-H(50)	0.9500	C(11)-C(12)-H(12)	120.4
C(51)-C(52)	1.401(13)	C(12)-C(13)-C(14)	121.4(10)
C(51)-H(51)	0.9500	C(12)-C(13)-H(13)	119.3
C(52)-H(52)	0.9500	C(14)-C(13)-H(13)	119.3
P(1)-Au(1)	2.369(2)	C(13)-C(14)-C(9)	119.3(9)
P(2)-Au(2)	2.377(2)	C(13)-C(14)-H(14)	120.4
Cl(1)-Au(1)	2.368(2)	C(9)-C(14)-H(14)	120.4
Cl(2)-Au(2)	2.3666(19)	C(20)-C(15)-C(16)	119.8(8)
		C(20)-C(15)-P(1)	123.1(7)
F(3)-C(1)-F(1)	104.6(7)	C(16)-C(15)-P(1)	117.1(6)
F(3)-C(1)-F(2)	106.6(7)	C(17)-C(16)-C(15)	118.8(8)
F(1)-C(1)-F(2)	105.4(7)	C(17)-C(16)-H(16)	120.6
F(3)-C(1)-Au(1)	117.0(5)	C(15)-C(16)-H(16)	120.6
F(1)-C(1)-Au(1)	113.8(6)	C(16)-C(17)-C(18)	120.4(9)
F(2)-C(1)-Au(1)	108.5(6)	C(16)-C(17)-H(17)	119.8
C(7)-C(2)-C(3)	119.8(8)	C(18)-C(17)-H(17)	119.8
C(7)-C(2)-Au(1)	120.7(7)	C(19)-C(18)-C(17)	121.5(9)
C(3)-C(2)-Au(1)	119.5(6)	C(19)-C(18)-H(18)	119.2
C(2)-C(3)-C(4)	119.3(9)	C(17)-C(18)-H(18)	119.2
C(2)-C(3)-H(3)	120.3	C(18)-C(19)-C(20)	118.7(9)
C(4)-C(3)-H(3)	120.3	C(18)-C(19)-H(19)	120.6
C(5)-C(4)-C(3)	121.1(9)	C(20)-C(19)-H(19)	120.6
C(5)-C(4)-H(4)	119.5	C(19)-C(20)-C(15)	120.8(9)
C(3)-C(4)-H(4)	119.5	C(19)-C(20)-H(20)	119.6
C(4)-C(5)-C(6)	118.9(8)	C(15)-C(20)-H(20)	119.6
C(4)-C(5)-C(8)	120.3(9)	C(22)-C(21)-C(26)	117.9(9)
C(6)-C(5)-C(8)	120.8(9)	C(22)-C(21)-P(1)	120.7(7)
C(5)-C(6)-C(7)	121.0(9)	C(26)-C(21)-P(1)	121.4(7)
C(5)-C(6)-H(6)	119.5	C(23)-C(22)-C(21)	120.7(8)
C(7)-C(6)-H(6)	119.5	C(23)-C(22)-H(22)	119.6
C(2)-C(7)-C(6)	119.9(9)	C(21)-C(22)-H(22)	119.6
C(2)-C(7)-H(7)	120.0	C(22)-C(23)-C(24)	119.6(9)
C(6)-C(7)-H(7)	120.0	C(22)-C(23)-H(23)	120.2
C(5)-C(8)-H(8A)	109.5	C(24)-C(23)-H(23)	120.2
C(5)-C(8)-H(8B)	109.5	C(25)-C(24)-C(23)	120.6(9)
H(8A)-C(8)-H(8B)	109.5	C(25)-C(24)-H(24)	119.7
C(5)-C(8)-H(8C)	109.5	C(23)-C(24)-H(24)	119.7
H(8A)-C(8)-H(8C)	109.5	C(24)-C(25)-C(26)	118.9(8)
H(8B)-C(8)-H(8C)	109.5	C(24)-C(25)-H(25)	120.5
C(14)-C(9)-C(10)	119.7(8)	C(26)-C(25)-H(25)	120.5
C(14)-C(9)-P(1)	122.0(7)	C(25)-C(26)-C(21)	122.3(9)
C(10)-C(9)-P(1)	118.3(6)	C(25)-C(26)-H(26)	118.8
C(11)-C(10)-C(9)	119.7(9)	C(21)-C(26)-H(26)	118.8
C(11)-C(10)-H(10)	120.2	F(5)-C(27)-F(6)	105.3(8)
C(9)-C(10)-H(10)	120.2	F(5)-C(27)-F(4)	104.5(7)
C(10)-C(11)-C(12)	120.8(9)	F(6)-C(27)-F(4)	104.9(8)
C(10)-C(11)-H(11)	119.6	F(5)-C(27)-Au(2)	115.0(6)
C(12)-C(11)-H(11)	119.6	F(6)-C(27)-Au(2)	115.8(6)

F(4)-C(27)-Au(2)	110.3(6)	C(44)-C(43)-H(43)	120.7
C(29)-C(28)-C(33)	118.6(8)	C(42)-C(43)-H(43)	120.7
C(29)-C(28)-Au(2)	121.9(7)	C(45)-C(44)-C(43)	122.0(8)
C(33)-C(28)-Au(2)	119.4(6)	C(45)-C(44)-H(44)	119.0
C(28)-C(29)-C(30)	119.8(9)	C(43)-C(44)-H(44)	119.0
C(28)-C(29)-H(29)	120.1	C(44)-C(45)-C(46)	119.4(9)
C(30)-C(29)-H(29)	120.1	C(44)-C(45)-H(45)	120.3
C(31)-C(30)-C(29)	122.6(9)	C(46)-C(45)-H(45)	120.3
C(31)-C(30)-H(30)	118.7	C(41)-C(46)-C(45)	120.1(9)
C(29)-C(30)-H(30)	118.7	C(41)-C(46)-H(46)	119.9
C(30)-C(31)-C(32)	117.1(9)	C(45)-C(46)-H(46)	119.9
C(30)-C(31)-C(34)	122.0(9)	C(48)-C(47)-C(52)	120.4(8)
C(32)-C(31)-C(34)	120.8(9)	C(48)-C(47)-P(2)	122.1(7)
C(31)-C(32)-C(33)	122.4(9)	C(52)-C(47)-P(2)	117.5(7)
C(31)-C(32)-H(32)	118.8	C(47)-C(48)-C(49)	120.2(8)
C(33)-C(32)-H(32)	118.8	C(47)-C(48)-H(48)	119.9
C(32)-C(33)-C(28)	119.5(8)	C(49)-C(48)-H(48)	119.9
C(32)-C(33)-H(33)	120.3	C(50)-C(49)-C(48)	118.7(9)
C(28)-C(33)-H(33)	120.3	C(50)-C(49)-H(49)	120.6
C(31)-C(34)-H(34A)	109.5	C(48)-C(49)-H(49)	120.6
C(31)-C(34)-H(34B)	109.5	C(51)-C(50)-C(49)	121.9(10)
H(34A)-C(34)-H(34B)	109.5	C(51)-C(50)-H(50)	119.0
C(31)-C(34)-H(34C)	109.5	C(49)-C(50)-H(50)	119.0
H(34A)-C(34)-H(34C)	109.5	C(50)-C(51)-C(52)	119.3(8)
H(34B)-C(34)-H(34C)	109.5	C(50)-C(51)-H(51)	120.3
C(36)-C(35)-C(40)	120.4(8)	C(52)-C(51)-H(51)	120.3
C(36)-C(35)-P(2)	118.2(7)	C(47)-C(52)-C(51)	119.3(9)
C(40)-C(35)-P(2)	121.5(7)	C(47)-C(52)-H(52)	120.3
C(35)-C(36)-C(37)	120.3(9)	C(51)-C(52)-H(52)	120.3
C(35)-C(36)-H(36)	119.8	C(15)-P(1)-C(21)	109.6(4)
C(37)-C(36)-H(36)	119.8	C(15)-P(1)-C(9)	104.9(4)
C(38)-C(37)-C(36)	119.1(9)	C(21)-P(1)-C(9)	105.9(4)
C(38)-C(37)-H(37)	120.5	C(15)-P(1)-Au(1)	110.0(3)
C(36)-C(37)-H(37)	120.5	C(21)-P(1)-Au(1)	108.9(3)
C(37)-C(38)-C(39)	121.2(9)	C(9)-P(1)-Au(1)	117.4(3)
C(37)-C(38)-H(38)	119.4	C(35)-P(2)-C(47)	108.9(4)
C(39)-C(38)-H(38)	119.4	C(35)-P(2)-C(41)	104.5(4)
C(40)-C(39)-C(38)	119.2(9)	C(47)-P(2)-C(41)	105.4(4)
C(40)-C(39)-H(39)	120.4	C(35)-P(2)-Au(2)	110.7(3)
C(38)-C(39)-H(39)	120.4	C(47)-P(2)-Au(2)	106.9(3)
C(39)-C(40)-C(35)	119.8(9)	C(41)-P(2)-Au(2)	119.9(3)
C(39)-C(40)-H(40)	120.1	C(2)-Au(1)-C(1)	87.7(3)
C(35)-C(40)-H(40)	120.1	C(2)-Au(1)-Cl(1)	178.4(3)
C(46)-C(41)-C(42)	120.2(8)	C(1)-Au(1)-Cl(1)	91.1(3)
C(46)-C(41)-P(2)	120.1(7)	C(2)-Au(1)-P(1)	91.4(2)
C(42)-C(41)-P(2)	119.6(7)	C(1)-Au(1)-P(1)	175.9(3)
C(41)-C(42)-C(43)	119.7(9)	Cl(1)-Au(1)-P(1)	89.75(7)
C(41)-C(42)-H(42)	120.1	C(28)-Au(2)-C(27)	86.2(3)
C(43)-C(42)-H(42)	120.1	C(28)-Au(2)-Cl(2)	175.4(3)
C(44)-C(43)-C(42)	118.5(9)	C(27)-Au(2)-Cl(2)	91.9(3)

C(28)-Au(2)-P(2)	91.6(3)	Cl(2)-Au(2)-P(2)	90.01(7)
C(27)-Au(2)-P(2)	176.4(3)		

Symmetry transformations used to generate equivalent atoms:

Table A58. Anisotropic displacement parameters ($Å^2 x\ 10^3$)for twin4. The anisotropic displacement factor exponent takes the form: $-2\pi^2[\ h^2a^{*2}U^{11} + ... + 2\ h\ k\ a^*\ b^*\ U^{12}\ ]$

	U^{11}	U^{22}	U^{33}	U^{23}	U^{13}	U^{12}
C(1)	16(5)	22(5)	25(4)	0(4)	9(4)	-5(4)
C(2)	23(4)	11(4)	24(3)	5(3)	-1(3)	-6(3)
C(3)	18(5)	29(6)	21(4)	0(4)	1(4)	-9(4)
C(4)	16(5)	31(6)	28(4)	14(4)	-10(4)	-13(4)
C(5)	31(6)	18(5)	21(4)	3(4)	3(4)	-12(4)
C(6)	30(5)	9(5)	27(4)	-1(4)	0(4)	0(4)
C(7)	23(5)	12(5)	25(4)	4(4)	3(4)	2(4)
C(8)	56(7)	32(6)	27(5)	3(4)	-10(5)	-28(6)
C(9)	19(5)	13(5)	16(4)	2(3)	7(3)	-6(4)
C(10)	25(4)	28(4)	27(3)	1(3)	-7(3)	-19(3)
C(11)	27(5)	16(5)	26(4)	4(4)	-5(4)	-9(4)
C(12)	52(7)	28(6)	14(4)	4(4)	-2(4)	-4(5)
C(13)	32(6)	35(6)	25(5)	-2(4)	16(4)	-2(5)
C(14)	31(5)	15(5)	20(4)	3(4)	-8(4)	0(4)
C(15)	12(4)	27(5)	12(3)	1(3)	-1(3)	-13(4)
C(16)	15(5)	17(5)	19(4)	2(4)	2(3)	-6(4)
C(17)	19(5)	24(5)	31(5)	7(4)	-2(4)	0(4)
C(18)	19(5)	42(6)	29(4)	17(5)	-8(4)	-15(5)
C(19)	29(5)	25(5)	21(4)	2(4)	-7(4)	-17(5)
C(20)	28(5)	11(5)	21(4)	6(4)	1(4)	-4(4)
C(21)	17(5)	13(5)	23(4)	-1(4)	-6(4)	-4(4)
C(22)	19(5)	24(5)	21(4)	-3(4)	0(4)	-6(4)
C(23)	24(5)	11(5)	34(5)	6(4)	4(4)	-2(4)
C(24)	22(5)	14(5)	35(5)	-7(4)	5(4)	0(4)
C(25)	25(5)	25(6)	18(4)	3(4)	1(4)	2(4)
C(26)	21(5)	19(5)	20(4)	-3(4)	-3(4)	-5(4)
C(27)	21(5)	26(6)	27(4)	-3(4)	3(4)	1(4)
C(28)	19(5)	12(5)	23(4)	-4(4)	-4(4)	-3(4)
C(29)	19(5)	19(5)	23(4)	-4(4)	-1(4)	5(4)
C(30)	43(6)	11(5)	24(4)	2(4)	-6(4)	-8(5)
C(31)	29(6)	11(5)	32(5)	0(4)	1(4)	-6(4)
C(32)	26(5)	19(5)	28(4)	-11(4)	0(4)	-10(4)
C(33)	14(5)	23(5)	25(4)	-4(4)	-6(4)	-4(4)
C(34)	45(7)	33(6)	23(4)	-3(4)	6(4)	-19(5)
C(35)	16(5)	21(5)	9(3)	-4(3)	-4(3)	-1(4)
C(36)	23(5)	16(5)	18(4)	-4(4)	2(3)	-5(4)
C(37)	20(5)	24(5)	30(4)	-5(4)	-2(4)	-10(4)
C(38)	27(6)	34(6)	30(5)	-10(4)	9(4)	-15(5)

C(39)	32(5)	16(5)	19(4)	-4(4)	2(4)	-8(4)
C(40)	17(5)	24(5)	12(3)	2(4)	1(3)	-1(4)
C(41)	29(5)	9(4)	13(4)	-1(3)	-2(3)	-6(4)
C(42)	18(5)	17(5)	26(4)	0(4)	0(4)	0(4)
C(43)	28(5)	25(5)	24(4)	-1(4)	-9(4)	-6(4)
C(44)	45(7)	24(5)	15(4)	2(4)	-5(4)	-19(5)
C(45)	37(6)	21(5)	17(4)	-1(4)	8(4)	-3(5)
C(46)	31(5)	19(5)	21(4)	-1(4)	8(4)	-12(4)
C(47)	11(4)	19(5)	20(4)	-2(4)	5(3)	-9(4)
C(48)	21(5)	15(5)	27(4)	1(4)	-5(4)	-4(4)
C(49)	32(6)	20(5)	27(4)	0(4)	4(4)	-5(4)
C(50)	37(6)	22(5)	32(5)	15(4)	-5(4)	-5(5)
C(51)	21(5)	18(5)	23(4)	1(4)	-7(4)	-4(4)
C(52)	17(5)	20(5)	24(4)	0(4)	1(4)	-4(4)
F(1)	36(3)	23(3)	38(3)	13(3)	-11(3)	-11(3)
F(2)	26(3)	28(3)	54(3)	4(3)	15(3)	-8(3)
F(3)	52(4)	22(3)	33(3)	-1(3)	-2(3)	-17(3)
F(4)	26(3)	21(3)	77(4)	-12(3)	-20(3)	-4(3)
F(5)	57(4)	33(4)	43(3)	-25(3)	20(3)	-26(3)
F(6)	57(4)	19(3)	40(3)	8(3)	-3(3)	-17(3)
P(1)	15(1)	14(1)	17(1)	0(1)	2(1)	-5(1)
P(2)	14(1)	13(1)	17(1)	-2(1)	2(1)	-4(1)
Cl(1)	24(1)	21(1)	17(1)	1(1)	0(1)	-6(1)
Cl(2)	26(1)	21(1)	19(1)	-4(1)	2(1)	-7(1)
Au(1)	15(1)	13(1)	16(1)	0(1)	2(1)	-4(1)
Au(2)	15(1)	12(1)	18(1)	-1(1)	-1(1)	-3(1)

Table A59. Hydrogen coordinates (x 10^4) and isotropic displacement parameters ($Å^2$x 10^3) for **4.1-Cl**.

	x	y	z	U(eq)
H(3)	9411	3220	4784	27
H(4)	10358	3467	5906	29
H(6)	6455	4602	6665	27
H(7)	5486	4328	5566	25
H(8A)	9352	3546	7395	53
H(8B)	8458	4722	7389	53
H(8C)	10007	4427	7050	53
H(10)	7834	1627	5662	29
H(11)	7681	1406	6898	27
H(12)	5492	1583	7445	39
H(13)	3468	1937	6747	38
H(14)	3575	2188	5509	27
H(16)	3312	3605	4318	20
H(17)	1063	3615	3895	31
H(18)	609	2123	3450	35
H(19)	2375	607	3394	28
H(20)	4621	563	3849	24

H(22)	6937	0	5017	25
H(23)	8633	-1446	4636	28
H(24)	9882	-1346	3573	29
H(25)	9495	199	2916	29
H(26)	7826	1631	3307	24
H(29)	9239	428	10681	27
H(30)	8039	266	11741	31
H(32)	4397	1826	10849	28
H(33)	5539	2010	9775	25
H(34A)	5687	252	12312	48
H(34B)	4327	1083	12009	48
H(34C)	5519	1454	12439	48
H(36)	11842	1493	9298	22
H(37)	13934	1599	8714	29
H(38)	14086	3160	8185	34
H(39)	12153	4608	8198	26
H(40)	10092	4504	8807	22
H(42)	11603	3056	10376	26
H(43)	12045	3321	11599	31
H(44)	10237	3413	12430	32
H(45)	8070	3186	12093	31
H(46)	7636	2908	10885	27
H(48)	7910	4830	10201	25
H(49)	6004	6231	9880	32
H(50)	4851	6214	8791	37
H(51)	5406	4792	8067	25
H(52)	7248	3355	8410	25